

University of Warwick institutional repository: <http://go.warwick.ac.uk/wrap>

A Thesis Submitted for the Degree of PhD at the University of Warwick

<http://go.warwick.ac.uk/wrap/72927>

This thesis is made available online and is protected by original copyright.

Please scroll down to view the document itself.

Please refer to the repository record for this item for information to help you to cite it. Our policy information is available from the repository home page.

MATERIALS EVALUATION USING ULTRASONIC SURFACE WAVES

by

W. WESTON-BARTHOLOMEW, M.Sc.

This thesis is submitted for the degree of Doctor of
Philosophy, University of Warwick, Coventry, England.

November 1972

BEST COPY

AVAILABLE

Variable print quality

ABSTRACT

The investigation reported in this thesis was prompted by the desire to develop an easy and reliable nondestructive method of testing to monitor changes in elastic properties of metals when they are subjected to creep, fatigue, and case hardening.

The possibilities of the useful application of such a test will be invaluable to the aircraft industry. It was therefore suggested that the specimens used should be made from the type of materials used in the aircraft industry. These were made of high strength alloys.

The method of nondestructive testing was to excite ultrasonic surface waves on the surface of the specimens, and measuring the changes in surface wave velocity, when the material (specimens) are subjected to creep, fatigue, and case hardening. An ultrasonic goniometer was designed and constructed and, using the goniometer, critical angle reflectometry was used to excite the surface waves on the surface of the specimens.

For the measurements during fatigue, specimens were fatigued at high stress levels and low cycles. Constant amplitude alternating stresses with the specimen remaining in tension during the whole program type of loading was used. Most of the specimens were made of titanium (Ti230) but some work was also done on mild steel.

The specimens used for creep were made from C263 Nickel alloy and Titanium 230. Each specimen was subjected to creep to a certain degree. The case hardened specimens were made of steel with carburized case.

It was found that using ultrasonic surface waves it was possible

to determine the depth of case hardening. Using a calibration curve drawn from the results obtained of the change in surface wave velocity for specimens with known case depths, it was possible to predict the case depths of specimens of unknown case depths by measuring their surface wave velocities. Also, a frequency effect was observed whereby lower frequencies were found to be better for detecting larger case depths.

When specimens which were subjected to creep were considered, it was found that ultrasonic surface waves can detect early stages of creep. This was the case for both materials studied. A difference was observed in the response to the surface waves for the two materials studied. In both cases a frequency effect was observed in that higher frequencies were better for detecting early creep.

For both materials studied during fatigue, most of the change in surface wave velocity occurred during the very early stages of fatigue life. During the latter stages of fatigue life the rate of change was very much lower. No pattern was observed for the change in surface wave velocity with the number of fatigue cycles for either material.

Lastly, measurements were done on brass, copper, aluminium, stainless steel and mild steel bar specimens, at the critical angle of incidence. For all the specimens it was found that the surface wave velocity changed with frequency.

ACKNOWLEDGEMENTS

The author is indebted to:-

- (i) The Ministry of Technology for their financial support throughout the project, and the Department of Engineering, Warwick University, head, Professor J.A.Shercliff where the work was conducted.
- (ii) Rolls Royce Ltd., Derby, and especially to Mr.J.Hislop and Mr.B.Wood for supplying the specimens and for their interest shown in the work.
- (iii) The University of Warwick workshop, head, Mr.A.J.McIntyre, Mr.L.Whittingham, foreman, and Mr.F.Holloway, technician, for manufacturing the ultrasonic goniometer. Also to Mr.D.G.Wood for advice on drawings.
- (iv) All the research students with whom he had helpful discussions, Mr.L.Baker for his help on electronic matters, Mr.A.Redhead and Mr.J.Hawkins for their assistance in the fatigue program.
- (v) Lastly, Dr.D.I.Crecraft my supervisor, whose helpful advice, discussions and encouragements were invaluable throughout the project. Also to Mr.M.K.McPhun and Dr.H.V.Shurmer who were helpful during the early and latter stages of the work respectively.

ABSTRACT

ACKNOWLEDGEMENTS

| | | |
|-----------|--|----|
| CHAPTER 1 | <u>INTRODUCTION</u> | 1 |
| 1.1 | Purpose of study | |
| 1.2 | Fatigue | |
| 1.3 | Creep | |
| 1.4 | Case hardening | |
| 1.5 | Surface waves ability to detect surface conditions | |
| 1.6 | Preferred orientation | |
| 1.7 | Surface residual stress | |
| CHAPTER 2 | <u>REVIEW OF TESTING FOR CASE DEPTH, CREEP AND FATIGUE</u> | 13 |
| 2.1 | Case depth | |
| 2.1.1 | Measuring of case depth(Destructive methods) | |
| 2.1.2 | Measuring of case depth(Nondestructive methods) | |
| 2.2 | Creep | |
| 2.2.1 | Creep measurements | |
| 2.3 | Fatigue | |
| 2.3.1 | Measuring of cumulative damage by Hypothesis | |
| 2.3.2 | Nondestructive methods | |
| CHAPTER 3 | <u>ULTRASONIC SURFACE WAVES</u> | 30 |
| 3.1 | Surface wave testing and reason for choosing method | |
| 3.1.1 | Surface wave generators | |
| 3.1.2 | Surface wave propagation | |
| 3.1.3 | The ultrasonic goniometer | |
| 3.1.4 | The corner reflection method(Liquid-solid interface) | |

| | | |
|-----------|---|----|
| 3.2 | Theory of ultrasonic surface wave propagation | |
| 3.2.1 | Theory of critical angle reflectometry | |
| 3.3 | Historical review of critical angle reflectometry | |
| CHAPTER 4 | <u>DESIGN OF ULTRASONIC GONIOMETER</u> | 58 |
| 4.1 | The system | |
| 4.2 | The ultrasonic goniometer | |
| 4.2.1 | The reflector block | |
| 4.2.2 | Accuracy | |
| 4.2.3 | Specimen holders | |
| 4.3 | The medium | 64 |
| 4.3.1 | Temperature considerations | |
| 4.3.2 | Depth considerations | |
| 4.3.3 | Distance consideration | |
| 4.3.4 | Beam directivity | 69 |
| 4.3.5 | Beam deviation | |
| 4.3.6 | Effect of skip distance or interference due to reradiated wave. | |
| 4.4 | The transducers | |
| CHAPTER 5 | <u>ELECTRONIC INSTRUMENTATION</u> | 72 |
| 5.1 | Astable multivibrator | |
| 5.2 | Monostable multivibrator | |
| 5.3 | The sinusoidal oscillator | |
| 5.4 | The signal used | |
| CHAPTER 6 | <u>THE SPECIMENS</u> | 76 |
| 6.1 | Case hardened specimens | |
| 6.2 | Creep specimens | |
| 6.3 | Fatigue specimens | |
| 6.4 | Other specimens | |

| | | |
|------------|---|------|
| CHAPTER 7 | <u>DATA COLLECTION AND EXPERIMENTAL RESULTS</u> | 79 |
| 7.1 | <u>Case depth</u> | |
| 7.1.1 | Data collection | |
| 7.1.2 | Results and data analysis | |
| 7.1.3 | Discussion of results and conclusions | |
| 7.2 | <u>Creep</u> | 83 |
| 7.2.1 | Data collection | |
| 7.2.2 | Results and data analysis | |
| 7.2.3 | Discussion of results and conclusions | 90 |
| 7.3 | <u>Fatigue</u> | 106 |
| 7.3.1 | Data collection | |
| 7.3.2 | Results and data analysis | |
| 7.3.3 | Discussion of results and conclusions | 108 |
| 7.4 | <u>Measurements of critical angle in some other materials</u> | 113 |
| 7.4.1 | Data collection | |
| 7.4.2 | Results and data analysis | |
| 7.4.3 | Discussion of results and conclusions | 115 |
| CHAPTER 8 | <u>SUGGESTION FOR FURTHER WORK</u> | 121 |
| CHAPTER 9 | <u>PAPERS</u> | 123 |
| CHAPTER 10 | <u>REFERENCES</u> | 124 |
| APPENDIX 1 | Transducer manufacture | 134 |
| 2 | Frequency spectrum of a pulsed continuous wave | 138 |
| 3 | Creep test on C263 Nickel alloy | 139a |
| 4 | Drawing of goniometer | 139c |
| 5 | Theory of skip distance | 140 |
| 6 | Suggested receive side | 143 |
| 7 | Theory of dislocations | 144 |

1. INTRODUCTION

1.1. Purpose of study.

The results of the study of the behaviour of engineering materials under various loading conditions are very important to the design engineer. Components manufactured from these materials are often designed to the closest limits. If detailed knowledge is available about these materials and their behaviour it will reduce the element of risk in the designs. Cost can be minimised and the materials used to their fullest.

Because some industries, like the aircraft industry, use very high strength alloys, components made from these alloys can withstand very high stresses, which is necessary for aircraft operation. Special heat resistant alloys are also employed in the manufacture of compressor and turbine blades. Sometimes it is sufficient to increase the component's strength by case-hardening the manufactured component, which has been manufactured from a lower strength material.

The cost of failure of any of these components is extremely high. It may result in the loss of human lives and the loss of the whole aircraft, costing millions of pounds.

Components under service loading conditions can be subjected to many types of stresses viz. tensile, bending, compressive, torsional, and thermal. Combinations of all these are not uncommon. Due to these loading conditions, combined with the variations in component behaviour (scatter), premature failure can occur. Due to these loading conditions also, the exact service life of a component is very difficult to predict.

At present there is no method of predicting the exact life cycle of components under service loading conditions, and it would be invaluable to industry if some type of nondestructive test can be devised to monitor the life cycle of a component in service.

Additionally, if a nondestructive test can be devised to measure the depth of casehardening of a component, which has inherent accuracy and is easy to apply, its use would be very beneficial to industry.

The purpose of this study therefore, is to investigate whether such a test can be devised.

1.2 Fatigue.

When a metal is subjected to many applications of the same load, fracture can occur at a much lower load than would be required for failure in a tensile load test. This failure due to alternating stresses is called fatigue.

Fatigue cracks always start at the surface. These cracks nucleate at the surface and grow under repeated load applications. As the crack grows, the load carrying cross section of the member is reduced and the stress is increased. When the remaining cross section is not strong enough to carry the load, the crack spreads causing failure. The study of the nature of crack propagation is a well established method of predicting fatigue failure.

Almost all materials have a fatigue limit. This is the stress (determined experimentally) below which failure will not occur regardless of the number of load cycles applied. This implies that components can be designed for working stresses below the fatigue limit. This however is very uneconomical from the design viewpoint. Surface finish also has an effect on fatigue life. A rough surface caused by machining, can reduce fatigue life, whilst if a specimen surface is highly polished, fatigue life is extended considerably.

Well before the appearance of a crack, a specimen when subjected to repeated loads will undergo many changes at the atomic level. It is known that slip and twinning are plastic deformation processes that occur without thermal activation. Slip bands are observed in polycrystalline metals well before fracture. These slip lines can become visible at any number of load

cycles. Depending upon the material they can be simple or multiple glide. Slip therefore can occur well below the fatigue limit. The number and extent of the slip bands will depend upon the amplitude of the applied stresses. Higher stresses give larger values of slip.

Dislocations are also considered to explain the early mechanism of fatigue. The movement of dislocations causes small deformations called extrusions to occur in the slip bands. An extrusion is a small ribbon of metal which is apparently extruded from the surface of the slip band. The opposite of extrusions are intrusions which are crevices, and these have been observed. These surface disturbances are about 0.1 to 1 μm high and appear as early as one tenth of the total fatigue life of the specimen. As the number of cycles increases small fissures open up in the slip bands in the disturbed regions.

Since these fissures are confined to the length of the slip segments, they are not actual cracks. However, as the number of cycles is increased, a macroscopic crack can be propagated from one fissure to another. This eventually leads to breakdown.

1.3 Creep

At room temperature the tensile properties of most engineering materials are independent of time, for all practical purposes. Furthermore, the anelastic behaviour of these materials at room temperature is of little consequence. At elevated temperatures however, the strength is very much dependent upon strain rate and time of exposure. Many metals behave like viscoelastic solids under these conditions. A metal subjected to a constant tensile load in an elevated temperature environment will creep and undergo a time dependent change in length.

When the temperature of a plastically deformed metal is raised, new crystals grow at the expense of the old ones. This is called

recrystallization. If the temperature is too low for recrystallization, plastic deformation, often called cold-work, will increase the critical stress necessary for further plastic strain. This process is called strain hardening. At this temperature, called the recrystallization temperature, changes in material properties take place. After recrystallization, the strength and hardness of the material is reduced and the ductility is increased. There is a complete release of internal stress in the material. At temperatures below the recrystallization temperature, a process of stress relief called recovery takes place. The mechanical properties of the metal are much less affected by recovery than by recrystallization. It therefore follows that the strain hardening that can be produced in a metal is dependent on temperature.

Creep is low in high melting-point solids, because of the high recrystallization temperatures. Alloying to raise the recrystallization temperature will increase creep resistance.

There are three stages of creep. When load is first applied to a metal there is an immediate elastic deformation, which is followed by a primary stage of creep. In this stage the creep rate is reduced to a minimum. Next, there is a secondary stage in which the strain rate slowly increases. Then follows the tertiary stage in which the strain rate increases rapidly, and eventually leading to failure.

The main deformation processes at elevated temperatures are slip, subgrain formation, grain boundary sliding and lattice rotation, in large-grained specimens. High temperature deformation is characterized by extreme inhomogeneity. Measurements of local creep elongation at various locations in a creep specimen have shown that the local strain undergoes many periodic changes with time, which ^{are} are not recorded in the changes in strain in the total length of the specimen.

Many secondary deformation processes have been observed in metals at elevated temperatures. e.g. multiple slip, the formation of extremely coarse slip bands, kink bands, fold formation at grain boundaries, and grain boundary migration.

Since the deformation is inhomogeneous, there are many opportunities for lattice bending to occur. It is known that kink bands, deformation bands, and local bending near grain boundaries can occur during creep. Polygonization can take place concurrently with lattice bending, since dislocations can climb readily at high temperatures. As creep progresses, large subgrains or cells are produced. The size of the subgrains depends upon the stress and the temperature.

Grain boundary processes observed during creep at high temperature are grain boundary sliding, grain boundary migration, and fold formation. It is not conclusive whether the sliding occurs along the grain boundaries, as a bulk movement of the two grains or in a softened area of each grain, adjacent to the grain boundary. Although the exact mechanism is not known, grain boundary sliding is not a simple viscous sliding of one grain past one another.

Grain boundary migration may be considered to be a stress induced grain growth. It is a creep recovery process which allowed the distorted material adjacent to the grain boundary to undergo further deformation. During high temperature creep due to inhomogeneous deformation of grain boundaries, wavy grain boundaries are usually observed.

A special class of complex materials called high temperature alloys (superalloys) have been developed for specific use in the aircraft industry. Ferritic alloys were developed first to meet increased temperature requirements in steam power plants. Essentially they are carbon steels which resist softening when certain proportions of chromium and molybdenum are added. These alloys extended the useful stress-bearing range from 1000°F to 1200°F, due to the increased oxidation resistance of austenitic steel.

For jet-engine applications, the superalloys used are based on either Nickel or Cobalt austenitic alloys, or a combination of the two. Generally, they contain appreciable chromium for oxidation resistance. Superalloys are creep resistant and they derive their strength from a dispersion of stable second phase particles.

1.4 Case hardening

In industrial applications many high load-bearing components are required to be very hard. The surfaces are required to be tough and wear-resistant. There are many metallurgical processes that can be conducted to achieve these aims. The easiest of these is that of heat treatment or tempering. This process however has a major disadvantage. There are two properties to be optimised, namely, toughness and surface hardness. Unfortunately, these two criteria cannot be met in the process of heat treatment. Treating a component for maximum hardness makes it too brittle, whilst treating for maximum surface toughness will make it less hard, i.e. it will not be hard enough.

To achieve this combination several processes were developed, namely carburizing, cyaniding, carbonitriding, nitriding, and localised surface hardening. From the first three processes, the surface hardness is dependent upon heat treatment after the composition of the case has been altered. In nitriding, the case composition is altered forming an inherently hard layer.

Carburizing

Case hardening is to obtain hard exteriors with tough interiors; low carbon steels are used. Any process which can increase the carbon content of the low carbon steel (.15% C) to the eutectoid proportions will achieve the desired results, provided the steel is properly heat treated.

There are three types of carburizing, which depend upon the carburizing medium. When solid carburizing material is used it is called solid or pack carburizing. When suitable hydrogen gases are used it is called gas carburizing. When fused baths of carburizing salt is used, it is called liquid carburizing.

Pack carburizing.

In this process parts to be carburized are packed in a container with a carburizing medium. The essential part of this medium or compound is some form of carbon. e.g. charcoal. The parts are placed in a furnace and heated to a temperature to form austenite. They are kept at this temperature until the required case depth is reached. Uniform penetration is not achieved ~~since~~ parts near the outer of the container reach the carburizing temperature before those at the centre. This process therefore is rarely used for case depth greater than .025 in. This process has been superseded by gas carburizing.

Gas carburizing.

The principal source of carbon used in this process is methane. Pressurised air-tight furnaces are used. Temperature is evenly distributed in the furnace. The furnace is brought up to the carburizing temperature, 1700 or 1750°F, and a dew point of 20 or 25°F, then purged with endothermic gas.

When the furnace temperature has recovered to the carburizing temperature, the carbon potential of the furnace is increased by adding some more methane. (5 to 10%). After about 50 to 75% of the total time cycle has elapsed, then no more methane is added. This creates equilibrium of the surface with the carrier potential.

If the temperature and the composition of the atmosphere can be controlled effectively, the depth of the case hardening can be controlled.

Liquid carburizing.

This process is applied to low case depth deposition, which can be produced at a lower cost than pack or gas carburizing. The fused baths are normally composed of sodium cyanide and alkaline earth salts. The salt reacts with the cyanide to form a cyanide of alkaline and earth metal, which reacts with the iron. A small amount of nitrogen is liberated and also absorbed. The parts are placed in molten salt for a desired time then quenched. Results from this process are similar to that obtained from gas or pack carburizing. The advantages are rapid heat transfer through the liquid, low distortion, negligible surface oxidation or decarburization and rapid absorption of carbon and nitrogen.

Heat treatment.

The process which is applied to carburized steels. The steel is cooled slowly from the carburizing temperature. The surface hardness of the steel is then low enough to permit machining.

Cyaniding.

Cyaniding is similar to liquid carburizing except that the bath used is generally fused sodium cyanide. Thin case depths less than 0.010 ins. can be made with this process. The steel is immersed in the molten bath of sodium cyanide at a temperature between 1475°F and 1600°F for between 30 min. and 3 hours, depending upon the case depth required.

Carbonitriding.

This is a modification of the gas carburizing process, which causes both carbon and nitrogen to be added to the surface through absorption.

Ammonia gas is added to the furnace atmosphere. This process is also called dry cyaniding, nitrocarburizing, gas cyaniding or ni-carbing.

Nitriding.

This is the process by which the surface hardness of certain alloy steels may be increased by heating, in contact with a nitrogenous medium without the necessity for quenching. The process involves the formation of hard wear-resistant nitrogen compounds on the surface of the steel by absorption of the nitrogen.

Other surface coatings.

Many other types of surface coatings are employed in industry. Some however, are used only for ornamental value, whilst others are for corrosion resistant, to protect against wear or to rebuild worn parts. Electroplating is one of these processes.

1.5 Surface wave ability to detect surface conditions.

Ultrasonic bulk wave testing is not easily applicable to detect surface or near surface defects. Reflections from the surface can mask the reflections from these defects.

A method that does not have the limitations of bulk waves is the application of ultrasonic surface waves. These waves are propagated on the material, penetrating a layer between one and two wavelengths thick. Materials of various shapes can be tested. These waves are usually called Rayleigh waves, and can be propagated for longer distances than either of the two bulk waves, since their acoustic attenuation with distance is less than for bulk waves. Therefore materials with high acoustic attenuation to bulk waves can be tested more easily with surface waves.

Rayleigh waves can be used in the immersion mode of testing. Both transducer and specimen are immersed in a liquid bath. Dilatational waves are propagated in the liquid and mode conversion takes place at the surface of the specimen. As the launching angle of the wave is varied, there will be a critical angle for the excitation of surface waves. The immersion method overcomes the problem of testing specimens of various shapes, since the problem of interfacing the transducer to the specimen is eliminated.

Rayleigh waves can be used for the locating and measuring of surface defects in specimens of almost any configuration. These include rods, beams, springs, wires, solid and hollow parts. All kinds of surface layer defects e.g. cracks, surface pitting, voids, inclusion of foreign impurities, to a depth of about one wavelength can be detected.

The Rayleigh wave method of testing is especially useful for the detection of microcracks which appear on the surface of metals during fatigue. Measuring the change in surface wave velocity could determine the change in surface wave elastic modulus. This change in elastic modulus could be due to residual stress, changes in dislocation densities near the surface, changes in point defects, or changes in planar defects.

Changes in hardness, grain size and grain orientation can also be responsible for this effect.

Measuring the changes in attenuation can be very useful for the determination of grain size changes that occur due to different mechanical processes. This change can be measured quite effectively by changing the

wavelength.

During high temperature creep changes in grain size take place in most metals. Surface waves can be used to measure the progressive change in grain size, due to recrystallization. Because grain size is a function of the hardness of the material it provides a useful method of nondestructive testing where surface waves can be used.

1.6 Preferred orientation.

A metal which has undergone severe deformation as in rolling or wire drawing will develop preferred orientation or texture in which certain crystallographic planes tends to orient themselves in a preferred direction of maximum strain.

In a polycrystalline aggregate, as distinct from a single crystal, the process is very complex. Individual grains cannot rotate freely and lattice bending and fragmentation thus occur. Preferred orientation may be measured by X-ray technique, and can also be measured by bulk ultrasonic shear waves,¹ which is more sensitive.

Formation of strong preferred orientation will result in an anisotropy of mechanical properties of the material. Although each individual grain is anisotropic, the aggregate tends to be isotropic, because of the random orientation of the grains. The elastic property of the **polycrystalline** solid is strongly dependent upon the degree of orientation.

Each grain has a given elastic modulus for a given orientation. If the aggregate is homogeneous each grain will have the same value of elastic modulus.

For all practical purposes a polycrystalline aggregate with preferred orientation is considered as being homogeneous but anisotropic. It thus follows that the wave velocities, which are dependent upon the properties of the material vary with the direction of propagation.

1.7 Surface residual stress

Many important technological processes produce high surface residual stresses which attain their maximum value either at the surface or just below the surface. Sometimes there are localised residual stresses on the surface of metals which can confuse measurements to determine surface elastic properties of materials. These can be compressive or tensile.

Because these stresses form a gradient from the surface, there will be an uneven effect on the depth of the disturbance caused by the surface wave. It is well known that the velocity of bulk waves changes with residual stress. Similar effects will take place with surface wave testing.

CHAPTER 2

REVIEW OF TESTING FOR CASE DEPTH, CREEP, AND FATIGUE.

2.1 CASE DEPTH

Introduction

Following the application of a case hardening technique, the depth of the case must be determined. This is necessary at an early stage in the process in order to avoid redundant processing. Once it is known that the processing conditions can produce the required case depth, many specimens are then case hardened.

Temperature and time are important factors in all the case hardening processes and if one of them changes the case depth of the surface also changes.

2.1.1 Measuring of case depth (Destructive method)

At present the accepted method for measuring the case depth of case hardened specimens, is a destructive one.² The specimen is cross sectioned and its hardness is measured.

Case depths may be classified as follows:-

Thin - Less than 0.020 in.

Medium - 0.020 to 0.040 in.

Medium heavy - 0.040 to 0.060 in.

2.1.2 Measuring of case depth (Nondestructive methods)

(a) Ultrasonic method.

Egorov^{2.1} reported on the feasibility of applying an ultrasonic reflection technique to the study of the elastic properties of surface consolidated layers. The test sample was submerged in the water and an ultrasonic radiation was produced by the free flexural wave reflected from the opposite end of the sample.

It was established that for surface consolidated layers, formed as a result of cementation and hardening, the change in elastic properties was very small. The damping of the ultrasonic waves depended largely on the distance between the layers being investigated, and the surface ones. With increase in distance up to the surface, the damping increased.

(b) Magnetic hysteresis method.

The test reported by Blitz et al³, is used for ferromagnetic materials. The materials were subjected to magnetic hysteresis. This method measured the difference in permeability, conductivity, or dimension between two specimens. Two identical coils were placed at right angles to each other. An amplifier followed by an oscilloscope was used to detect the signal. The coils were fed through a transformer in such a way that there was 180 degrees phase difference between them.

Signals from the two coils were superimposed on each other. With no test sample in, there was a phase cancellation and a straight line was obtained, since the coils were connected to the Y-plates of the

oscilloscope. When a test sample was placed in one of the coils, magnetic hysteresis occurred due to the loop being modified by the action of induced eddy currents. The straight line now changes to a pattern which is characteristic of the electrical conductivity, magnetic permeability and dimension of the sample. If an identical specimen is placed in the other coil, so that both specimens are in the same relative position, in the coils, a straight line is obtained once again. However if the other specimen has a different permeability, conductivity or dimension, the trace will change to a pattern which is characteristic of this difference.

2.2 CREEP

Introduction

The most serious limiting factor in creep testing is the inability to make full life tests of materials, particularly those intended for long life service under working conditions. Results from relatively short tests have to be extrapolated to indicate the probable long term behaviour.

This is a very risky and uncertain business, and there are many pitfalls, particularly in the possibilities in the unexpected development of tertiary creep. It is not conclusive to use a set of results from a single test made under different conditions as an indication of the creep behaviour of the material under investigation. There is also scatter in the results, and this scatter should be analysed.

Creep is the name given to slow deformation of solid materials over extended periods under loads. Normally creep is associated with high temperatures. However the important factor to consider is the application, and not the temperature. In some instances room temperature can introduce enough creep to cause severe deformation. This is possible in the case of large structures. Fig 2.1 shows the relationship between deformation and time for a constant applied load to a rod specimen.

The upward curving part of the curve (tertiary) usually precedes failure. It has been found that if the load is relieved during the test, some of the strain recovers. It therefore follows that the creep phenomenon contains both permanent and recoverable strains. The permanent effects are analogous to the plastic flow at high strain rates which characterizes for example, metal working processes.

Vicat⁴ was the first to make quantitative statements about creep. He investigated the reasons for the unpredicted behaviour of the cables for suspension bridges. He observed the first part of curve 2.1. Webster⁵ detected reversible creep in silk fibres. Boltzman⁶ attempted to study theoretically the 'memory' effect of the atomic processes involved in the deformation of metals. Tresca⁷ used the theory of viscous flow in liquids to formulate laws of plastic flow in solids. Many other workers contributed to the study of creep. (Ref.8 - 21)

With the advent of the steam turbine, jet aircraft and guided missiles, it became necessary to develop many new superalloys. Under service conditions these materials can be subjected to very high stresses at very high temperatures. There is therefore a need for detailed creep data on these materials.

2.2.1 Creep measurements.

(a) Measuring strain

A creep testing machine is employed to strain the material and thus to produce creep. Facilities are provided in this type of machine to control the temperature and the applied stress. Most tests are conducted in the tensile load application mode, which usually has an accuracy ranging from $\pm 0.5\%$ to $\pm 1.0\%$.

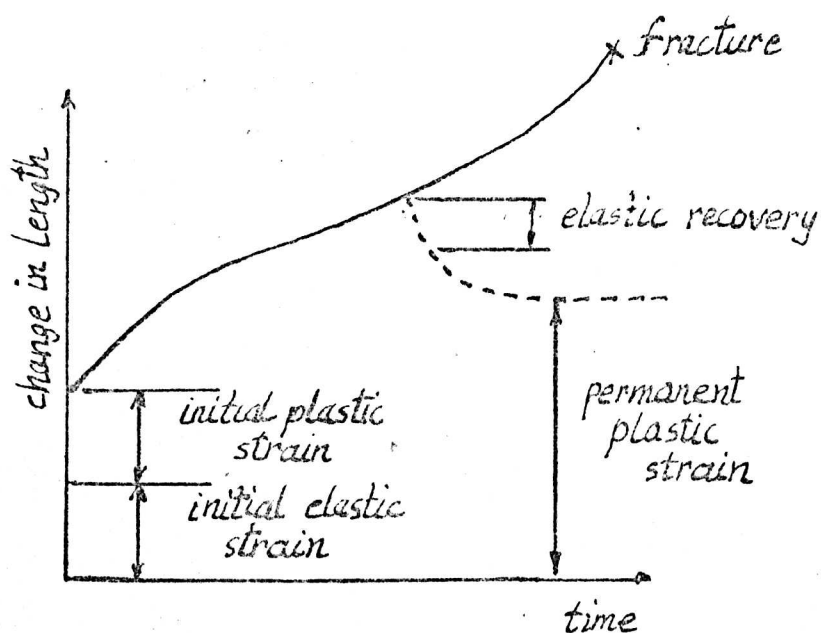


Fig 2.1 Creep Curve (dashed line shows behaviour on unloading)

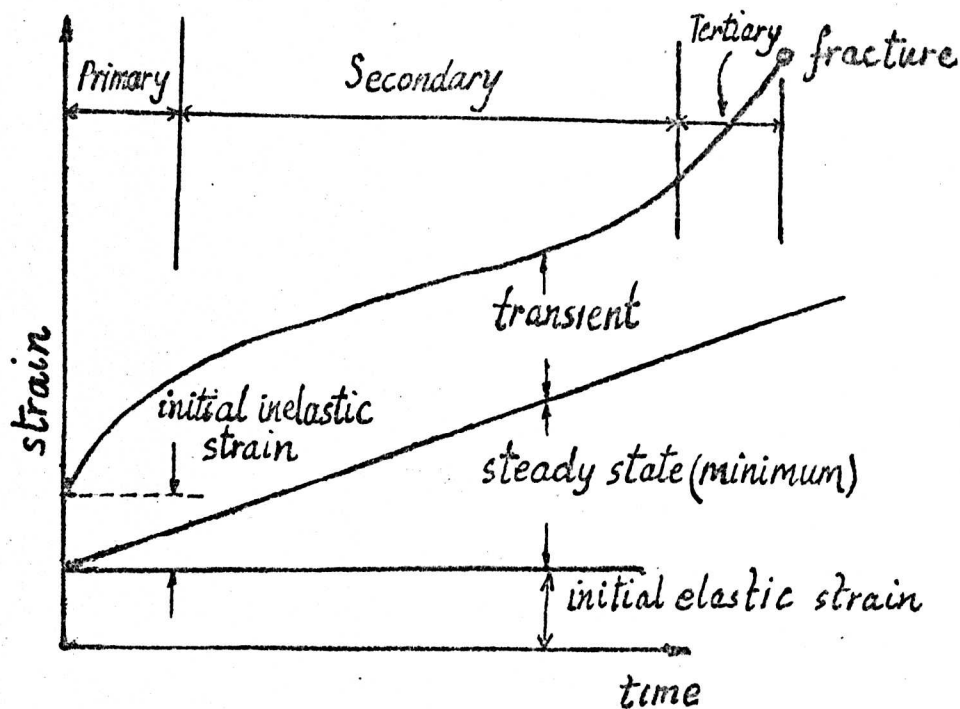


Fig 2.2 Typical creep curve showing the separation into stages for analytical convenience

These machines are fitted with accurately controlled temperature furnaces.

These furnaces are very carefully designed so that there is no thermal stress gradient on the surface of the specimen. For measuring the extensions, dial gauges and micrometers are fitted. For small specimens high accuracy is necessary. Sometimes to increase the accuracy, extensometers are mounted on the specimen gauge length. The extensometers are fitted with heat resisting arms for elevated temperature operations. They also have resetting adaptors for taking into account deflections that carry readings outside the normal range of the visible scale of the reading device.

Strain measurements as a function of time were first presented by Andrade^{14,22}. It was shown that for pure metals and alloys a typical creep curve can be plotted. See fig.2.2. It was proposed that the upward curvature of the tertiary stage was due to reduction in area at large strains. This however, was proved to be incorrect, by Sully²³ and Kanter²⁴. Andrade postulated a function to fit the creep curve. In recent years many workers²⁵ have postulated many functions to fit the creep curve.

Special superalloys and other metals had to be studied separately. With the superalloys, various pretreatments can cause drastic changes in the creep behaviour. Also, a large fraction of their creep life may consist of ~~of~~ primary creep in that the period of minimum rate is rather short. Dorn²⁶ is a foremost worker in this field. Chaudhuri²⁷ recently reported

on experimental work and curve fitting functions for Nickel-Base high temperature alloys.

Most of the work reported in the literature was done for high purity or slightly alloyed single or polycrystals.

Kornilov²⁸ measured the activation energy during creep for pure titanium, and found that the creep behaviour in this metal was different from metals belonging to the VIIth and VIIIth group of the periodic table. This may be due to the process of age hardening reported by Blenkinsop and Goosey²⁹. They found that the hardness increased initially with time at high temperatures, then **fell** off slowly with time. This study was done on titanium-2 $\frac{1}{2}$ %Cu., over a 24 hour period. If the creep tests were conducted on cold rolled sheets the creep measurements could **have** been affected by the effect of cold work³⁰ on the structure and property of the titanium.

(b) Xray methods.

Xray diffraction methods are used to determine local crystal orientation, near the subgrains which are discovered by microscope. Guiner³¹ and Barret³² have shown that the metallographically revealed lines or veins, separate crystal regions differing in orientation by as little as 10 seconds of arc. Guiner used the focussing method using transmission through thin plates. In a perfect single crystal well defined spots are observed. As strain is introduced, the points individually broaden into streaks of irregular density. Upon annealing the spots break up into striations, each representing coherent lattice regions of slightly differing orientations.

The Xray microscope has been used to study the changes in orientation within grains of Nickel and its alloys by Ancker³³, and Weissman³⁴. This was at up to 700°C. They found that creep brought out

characteristic small parallel boundaries which developed very early in the creep tensile tests.

(c) Other methods.

Resistivity and internal friction methods have been reported by Broom³⁵ and Nowick³⁵. Radioactive tracers are also used to measure the rate of chemical reaction in the study of segregation, and to monitor various recovery and diffusion process in the solid state.³⁷

(d) Metallographic methods.

This is a destructive test method. The specimens are sectioned, polished and etched. Parameters such as dislocation densities, velocity of dislocations motion, and crack propagation may be measured. Gilman and Johnston³⁸ reported on this type of work. Heslop³⁹ reported on work done on Nimonic alloys. The method was used to classify the types of fracture which lead to failure during creep.

(e) Ultrasonic methods.

Granato and De Rosset⁴⁰ have done ultrasonic studies of creep in single crystals of sodium chloride. Attenuation and velocity changes of a 10MHz ultrasonic shear wave were measured, during creep. From these measurements quantitative determinations of dislocation density, and average dislocation segment length were made. Comparisons were made with macroscopic strain measurements, and etch pit studies.

It was found that as creep increased somewhat exponentially with time, the change in the elastic modulus for the shear wave appeared

to follow the same pattern. The dislocation density increased nearly exponentially with time, whilst the loop length increased initially and then fell off with time. In this experiment, however, hardening mechanisms set in early and creep rate decayed exponentially with time. Hikata and Tutumi⁴¹ have found qualitatively that ultrasonic attenuation behaves like strain rates in aluminium.

2.3 FATIGUE

Introduction

The fatigue mechanism can be divided into two distinct stages. namely:- (a) The crack initiation stage, and,
(b) The crack propagation stage which eventually leads to failure.

However, prior to the crack nucleation, there are many mechanisms that are active at the atomic or *the microscopic levels*. Some or all of these mechanisms can cause changes in hardness, in yield point, and changes in electrical resistivity.

The level of the applied stress in relation to the yield stress of the material, will determine the nature of these early mechanisms. After about 1000 cycles of stress, in excess of the microscopic yield stress slip lines appear in most ductile metals. This is independent of the stress cycling rate. Bullen et al⁴² found that the hardness of polycrystalline copper increased rapidly with the number of cycles, and then levelled off to a near constant value. This value was maintained for all subsequent fatigue cycling. They thought that very early in the fatigue life, there was general plastic deformation throughout the whole specimen, followed

by work hardening. It was found that the damping rate and hysteresis were initially large but levelled off to a lower value with increased cycling. Bullen suggested that there are two processes that contribute to crack formation. These are local work hardening and, to a much greater extent, gradual movement of slip planes. Most workers have reported that strain hardening always exists prior to fracture.

When the stress level is lower than the yield stress, which is often the case in service loading conditions, the findings of Bullen et al⁴² are not applicable. Slip bands which are always associated with plastic flow, do not always appear in very early stages of fatigue, at these lower stress levels. In fact, for these lower stress levels a very large number of cycles is necessary before they appear. Therefore with this type of stress condition, the early fatigue mechanism is different. Later in the fatigue life the hardness levels off, as it does under the high stress loading conditions.

Palakowski and Palchouduri⁴³ found however, that for certain cold worked materials i.e. copper, nickel, aluminium and steel there was a distinct strain softening with cyclic loading. It was not clear if the incidence of strain softening was associated with cyclic stresses in excess of the fatigue limit, or for cyclic stresses below the fatigue limit.

After this hardening or softening stage crack nucleation and crack propagation takes place. Extensive studies have been done on this later stage of fatigue damage. Many studies have been done on the nature and velocity of crack propagation. For instance it is well established that, polishing the surface of a fatigue specimen, delays the formation of macro-cracks, which eventually leads to failure.

Most of the fatigue tests have been done under constant

stress amplitude conditions. In service conditions however, components can be subjected to many types of loading conditions. Random loading conditions have been studied by Swanson⁴⁴ and Fisher⁴⁵. The stress conditions can determine the nature of the conclusions that can be drawn from any fatigue studies.

Since there are so many mechanisms active in fatigue damage, one term 'cumulative damage' is used to describe the damage caused by different loading conditions. In all fatigue tests, there is a large element of scatter, and if two specimens are subjected to the same test conditions, there is very little certainty that they will ^{fail} at the same number of stress reversals. If it were possible to determine accurately the change in some material property, directly related to the fatigue life, then, the problem of scatter would be much less serious.

2.3.1 Measuring of cumulative damage by Hypothesis.

Miner⁴⁶ fatigued aluminium alloys at two stress levels to failure and from the results postulated that damage is linearly related to the number of stress cycles. Mathematically this means that:-

$$\sum \frac{N_i}{N_{Fi}} = 1 \quad \text{where } N_i = \text{Number of stress cycles at stress level } S_i, \text{ and,}$$

$$N_{Fi} = \text{Total fatigue life at stress } S_i.$$

Palmgren⁴⁷ and Serensen⁴⁸ also proposed the same theory. Other workers however, Swanson⁴⁹, proposed a nonlinear damage accumulation theory for high and low stress levels, but a linear one for medium stress levels. Marsh⁵⁰, found that the linear law is true only for sawtooth loadings above 80 percent of fatigue limit.

Corten and Dolan⁵¹ found that the damage was related

primarily to the maximum stress in the stressing program. Henry⁵² said that fatigue damage progressively lowers the fatigue limit until at failure the limit is zero. Other workers in the field including Richart and Newmark,⁵³ Grover, Bishop and Jackson,⁵⁴ Rey⁵⁵, Erickson and Work⁵⁶ have shown that for two-level cycling, damage was much higher when the high stress was followed by the low stress rather than vice versa.

2.3.2 Nondestructive Methods

(a) Measuring the apparent dynamic modulus and damping, during fatigue

Brook and Parry⁵⁷ measured the change in overall dynamic modulus and damping of a test specimen, during fatigue. Their objective was to try to provide some reliable information on the problem of cumulative damage. These parameters were measured during the fatigue tests without stopping the machine. Their assumption was that if the remaining life in the specimen at one stress level can be accurately estimated before it is tested to failure at a second stress amplitude, the problem of scatter would be largely overcome.

A series of these two-stress levels tests were conducted. They tried to plot the lines of equal damage on a diagram of stress amplitude plotted against the remaining life. The validity of these lines of equal damage could then be proved by subjecting a number of specimens to complicated programs of multilevel stress cycling and comparing the estimated lives with the experimental results.

(b) Measure of the change in Young's Modulus and damping.

Lazan and Wu⁵⁸, and Lazan and Demer⁵⁹, studied the change in Young's modulus and damping during fatigue. They measured the displacement of the free end of mild steel rotating-bend test pieces. They found that the initial damping change was quite rapid, flattening off as the stress continued. For low stress levels in mild steel, i.e. 28 and 29×10^3 lb/in², there was an increase in damping at a low number of cycles and a tendency to level off for the remaining fatigue life. The higher the stress level, the earlier this levelling off takes place. They found that above 34×10^3 lb/in², the energy change occurred predominantly in about the first one percent of fatigue life. This was very pronounced at 42×10^3 lb/in². The fatigue limit of the material used was 35×10^3 lb/in².

(c) Measure of stress-strain loops.

Morrow⁶⁰ studied stress-strain loops during strain cycling for fatigue lives up to half a million cycles. He showed that the plastic strain amplitude was related to the number of cycles to failure. Thompson, Coogan and Rider⁶¹ showed that the reduction in the area of the stress strain hysteresis loop changes with number of cycles.

(d) Measurement of magnetic hysteresis

Ueda and Tanaka⁶² measured the change in magnetic hysteresis during fatigue in 0.8 percent carbon steel. They found that for specimens having fibrous structures due to drawing, fatigue was little developed

below a certain number of cycles. There was a sudden increase in the magnetic hysteresis prior to fracture.

(e) Eddy current methods

The eddy current method was used to predict the fatigue life of samples by Nyukhalov et al.⁶³ The eddy current responses (disbalance voltage) was measured for many specimens. This was measured at various stress levels and for various number of cycles.

They mentioned that there was a critical disbalance voltage that had to be reached before the final mechanism sets in. For high stress levels, this critical value is reached very quickly, whilst for lower stresses the disbalance voltage never reaches this critical value. A standard virgin specimen was used as reference. A differential circuit was used to detect signals of induced eddy currents in both specimens. The result of the study on steel specimens was that, as the number of cycles increases, in the first stage of fatigue life, there is a sharp change in the disbalance voltage.

However, with increasing number of cycles, the intensity of the increment diminishes, and only in the final stages of fatigue development is there a renewed sharp increase in disbalance voltage.

(f) X-ray methods

Bullen⁴² used x-ray technique to study the changes in orientation due to fatigue. The x-ray diffraction patterns display discrete spots if there is no orientation change i.e. no disorientation in the lattice.

He found that a critical cycling rate was required to prevent the occurrence of disorientation. Once the cycling rate exceeded this value and a certain number of cycles had been reached, he found that by the x-ray method, fine slip lines were seen for low cycling rates; and for high cycling rates, the number of slip lines was very much smaller, and were observed in broad bands far apart. The lines often originated from points lying inside the grains and terminate at points also lying within the grains.

(g) Ultrasonic methods

Rasmussen⁶⁴ used ultrasonic surface waves to detect crack formation during fatigue. The surface waves were excited on both surfaces of the specimen, using contact probes (wedge type). The specimens were subjected to reverse bending loads, and the ultrasonic test frequency was 4 MHz.

It was found that microcracks appear very early in fatigue life. A figure of 39 to 44 percent was quoted for dynamic loading. The fatigue test was stopped and the specimens measured (a) Whilst in tension, and (b) "Off-machine." The first condition was similar to that obtained during dynamic loading, but with the second condition cracks appear at about 60 percent of the fatigue life. In both cases this percentage seems to be independent of stress level chosen. However, a dependence on surface treatment was observed. In this test program, high cycle, low stress level fatigue was used. The same measuring technique was used by the same author⁶⁵ to detect early flaws in turbine and compressor blades.

(h) Measure of magnetic permeability and magnetic viscosity

Shagaev⁶⁶ used electromagnetic methods to study the fatigue mechanism. He measured the magnetic permeability and the magnetic viscosity.

As the metal is fatigued, internal structural changes takes place which cause the magnetic properties to change. Steel specimens were used.

The permeability was measured using the e.m.f change of a measuring coil which is proportional to the differential magnetic permeability. The magnetic viscosity was measured using a standard equipment. The sample and the reference were magnetically shortcircuited. Coils were wound around both samples. Samples were demagnetized before making the measurement. Both samples were then magnetized.

Change in the field strengths produced a change in magnetic flux which is proportional to the magnetic viscosity. This change in viscosity is measured on a ballistic galvanometer after an interval of 2 secs. He tried to explain the fatigue mechanism in terms of dislocation theory. He found that the permeability increases with the number of stress cycles, to a peak then falls off, with cycles. It then increases to another peak then falls off again.

Viscosity was constant with number of cycles up to a certain number of cycles, then there was a gradual increase with number of cycles. It was thought that initially, during fatigue, there was a build up of microscopic plastic strain of the shear type, resulting from an increase in the density of the mobile dislocations in the ferrite grains oriented unfavourably with respect to the applied stress. As the dislocation moved, vacancies were generated around obstacles and the new dislocation appeared. The elastic stresses in the metal then increased and the motion of the dislocations was impeded, thus leading to hardness.

(i) Acoustic emission method

This is a process in which the intensity of sound radiated in materials undergoing strain is measured. Changes in the acoustic emission with crack growth can then be measured.

Mitchell⁶⁷ measured acoustic emission prior to crack initiation and propagation in steel specimens and the subsequent fatigue of each specimen was recorded. Analysis was done on the data. This showed that there was a burst of emission near failure. It was found that there was no correlation to fatigue life. It was proposed that the rate of emission was due to plastic deformation at or near the upper yield point.

Mitchell and Frederick⁶⁸ measured the acoustic emission from 175 specimens prior to fatiguing and during fatigue, but no parameter of the emission was found to correlate significantly with fatigue life. They reported on the high rate of emission which occurs at the yield stress, and proposed that this could be used to determine the yield stress in materials.

CHAPTER 3

ULTRASONIC SURFACE WAVES

3.1 SURFACE WAVE TESTING AND REASON FOR CHOOSING METHOD

3.1.1 Surface wave generators.

(a) "Corner" method

If an X cut longitudinal wave transducer is placed on the edge of a plate⁷⁰, surface waves will be excited. Optimum excitation will be obtained when the plate is inclined at 45° to the material surface, as shown in Fig.3.1(a).

(b) "Piston" source

This is a method used by Firestone and Frederick⁷¹. Either a longitudinal or a shear wave transducer is bonded to the surface by a thin layer of oil. Under these conditions, see Fig.3.1(b), surface waves are excited in all directions travelling away from the crystal. For a circular transducer, the amplitude has a maximum value when $\frac{D}{t} \approx 7$, where D is the diameter of the transducer, and t is the thickness of the transducer. This method is not very useful because there is a low conversion factor to surface waves.

(c) Wedge method

72

The wedge method proposed by Vinogradov is very widely used. A plastic prism or wedge is acoustically coupled through one of its faces

to a solid. A piezoelectric plate is placed on the sloping face of the wedge, the angle of which is chosen for optimum excitation using the expression $\sin \theta = \frac{C_1}{C_2}$ where C_1 is the velocity of the longitudinal wave in the wedge material and C_2 is the surface wave velocity in the solid. With the wedge method, essentially only one surface wave is generated. The level of the bulk waves excited is about 20 to 30db lower. The wedge is usually made of perspex because the longitudinal wave velocity in that material is lower than the shear wave velocity in most materials to be tested. This is the main consideration in this type of testing. The longitudinal wave velocity in perspex is 2700m/sec. The shear wave velocity in steel is 3235m/sec. The angle of optimum excitation is then $\theta = \sin^{-1}(2700/3235) \approx 34$ degrees. Fig.3.1(c) is a drawing of the wedge showing the optimum angle.

(d) Modified wedge

Shraiber⁷³ proposed a modified wedge. Instead of having mode conversion of the longitudinal wave, he used mode conversion of the shear wave at the surface. The advantage of this method is that instead of perspex, a wedge made of metal can be used. The relationship above will hold except that C_1 now represents the transverse wave velocity in the wedge.

(e) "Comb" transducer

This a method proposed by Sokolinskii.⁷⁴ A comb-like structure is used to generate a set of normal mode perturbations on the surface of the solid. The spatial period of the perturbation is the wavelength of the surface wave. Usually the structure is a metal plate with corrugations separated in space by $\lambda/2$. A longitudinal transducer is placed on this comblike structure and when placed on the surface of the material, surface waves can be generated as shown in Fig.3.1(d). This method has a disadvantage in that many unwanted bulk modes are produced.

Fig 3-1 Surface wave transducers

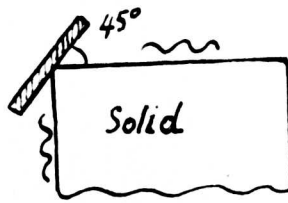


Fig 3-1(a) Corner method

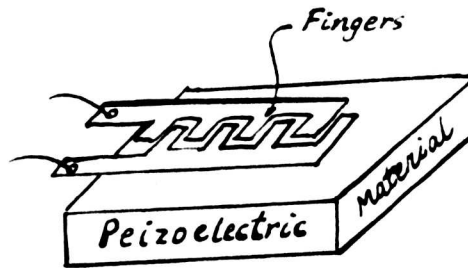


Fig 3-1(e) Interdital transducer

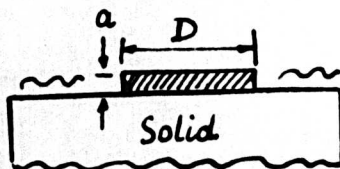


Fig 3-1(b) Piston source method

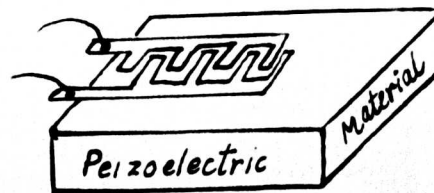


Fig 3-1(f) Wideband interdigital transducer

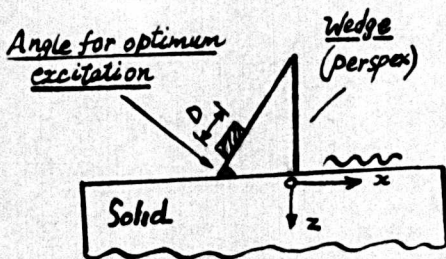


Fig 3-1(c) Wedge method

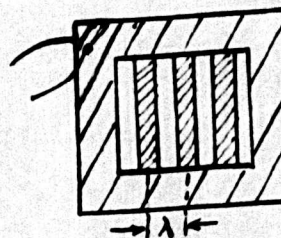


Fig 3-1(g) Window frame transducer

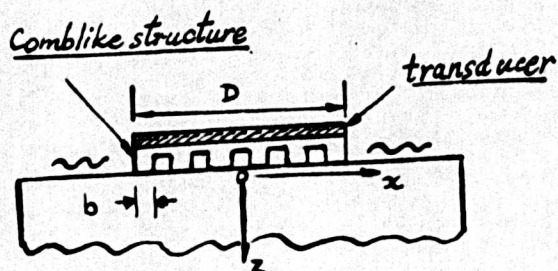


Fig 3-1(h) Comb transducer

(f) Interdigital structures

In recent years many workers have proposed methods of generating surface waves on piezoelectric materials and on ferroelectric ceramics (e.g. LiNbO_3). The interdigital transducer which comprises of electrode 'fingers', which are electrically excited and hence a surface wave is generated. The principle on which it works has been described by Bonnel et al.⁷⁵ In general the theory is that elastic strains can be directly generated at an electric field discontinuity in a piezoelectric medium.

The elastic strain is produced by coupling directly to the suitable piezoelectric moduli. de Klerk⁷⁶ showed how these waves are generated. Coquin and Tiersten⁷⁷ did an analysis of the excitation and detection of these surface waves in quartz. Some workers call these waves 'piezoelectric surface waves'. Fig.3.1(e) shows the type of transducer used. If the spacing between successive pairs of fingers is varied, (Fig.3.1(f)) the bandwidth can be increased. The grid responds to the high frequencies at the low dimension end, and to the lower frequencies at the high dimension end. This type of transducer is at present used in microwave work.

(g) The window frame transducer

Arzt⁷⁹ proposed the window frame transducer as shown in Fig.3.1(g), which is similar to the comb-like structure. It consists of equally spaced parallel conducting strips, connected at both ends. These strips are deposited on the surface of a piezoelectric plate, the other side of which is metalized and earthed, and supplied by an a.c. field. The electric fields of the strips are in phase with one another and the plate thickness determines the conversion loss. The assembly resonates at a frequency for which the spacing between the strips is one Rayleigh wavelength.

(b) Mode conversion

With this method (Bradfield(82)), a transducer can transmit dilatational waves in the liquid. (See Fig.3.2)). The waves are directed to the surface of the specimen, which is immersed in the liquid.

Energy reflected from the surface of the solid is detected by another transducer, which is also immersed in the liquid.

At one particular angle of incidence the wave entering the specimen is refracted into the surface, and becomes a surface wave propagating along the surface of the solid.

This is the method used by the author, and will be explained in greater detail later.

3.1.3 Surface wave propagation

Ultrasonic surface waves are confined to a surface layer of approximately one to two Rayleigh wavelengths. The attenuation of these waves is lower than bulk waves of the same frequency because they spread only in one plane, and thus be propagated for longer distances over the surface.

There are a number of factors to be considered before any surface wave method of testing can be used. e.g.

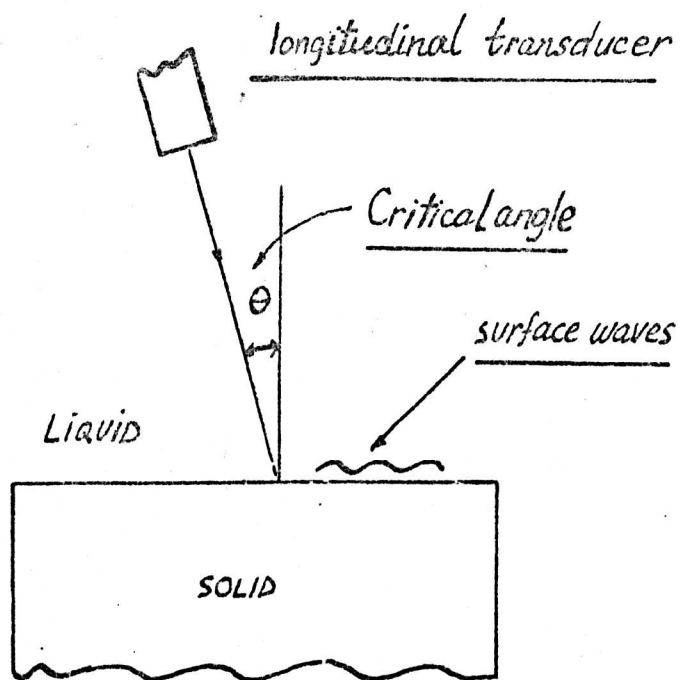


Fig 3.2 Mode conversion at a liquid-solid interface

(a) Dispersion

The problem of dispersion was studied by Daniel and deKlerk⁸³. They found that at high frequencies above 130 MHz, the surface wave velocity fell off with increase of frequency. This was for a two-layered system. Other workers Bogdanov et al⁸⁴, measured dispersion in a three-layered system, for frequencies of 4 to 16 MHz. They predicted dispersion in all three-layered systems.

(b) Surface defects

Viktorov and Kakaeina⁸⁶ reported on scattering of surface waves from models of surface and near surface defects. They developed models to simulate the type of defects that can exist on the surface. e.g. scratches, fissures and holes. They also did experiments with models of hemispherical indentations of various diameters and depths perpendicular to the surface. Similar experiments were done for cylindrical holes of various diameters.

In the work reported in this thesis, investigation was restricted to the case where there were no cracks on the surface.

(c) Surface irregularities.

The other problem is that of surface irregularities. These cause scattering of the surface waves and hence attenuation. Brekhovskikh⁸⁵ presented some theoretical studies on the effects of these irregularities on the surface waves. A further analysis for a periodic roughened surface has been done by Sabine⁸⁷. He presented some corrections to the Brekhovskikh equation for attenuation of Rayleigh waves propagating on a periodically roughened surface.

Generally the theory is that when Rayleigh waves travel over a rough surface, some of ~~their~~ energy is used to propagate bulk waves. Because the surface roughness is periodic, the attenuation will be a function of frequency. Certain assumptions were made:- i.e.

- (a) The height of the surface roughness is much less than the Rayleigh wavelength.
- (b) The slope of the uneven surface with respect to the average height is small.
- (c) The scattered wave's amplitude is small compared to the incident surface wave.

It was found that, for a certain frequency, and given degree of roughness, the only parameter required to determine the attenuation⁷⁸ was the Poisson's ratio. Thus at a given frequency, the attenuation will vary for different materials having the same surface conditions. It was shown that attenuation is dependent on the elastic modulus of the medium. In a plot of attenuation versus height, of the surface roughness, high and narrow peaks were obtained for materials with low values of Poisson's ratio, whilst lower and broader peaks were obtained for materials with higher values of Poisson's ratio. Elementary grating theory⁸⁹ was used to derive an expression for the angle for bulk waves radiation. An expression relating the surface roughness was derived. i.e.

$$\sin \alpha_B = (\lambda_B / \lambda_R) + m(\lambda_B / \lambda) \quad \text{where } \lambda_B \text{ is the}$$
wavelength of either the shear or dilatational bulk wave, α_B is the angle of surface corrugation, measured from the surface. λ_R is the Rayleigh wavelength, and λ is the period of the corrugation.

It follows that since $(\lambda_B / \lambda_R) > 1$, attenuation takes place only when $m = -1$.

It was calculated that no attenuation of bulk waves occurred

at very high and low frequencies when $n^2 > 1 > q$ where $n = \left(\frac{\lambda_s}{\lambda_r}\right) + m\left(\frac{\lambda_s}{\lambda}\right)$, and $q = \left(\frac{\lambda_s}{\lambda_L}\right)^2$

At medium frequencies, two conditions existed whereby, in one instance, ($q < n^2 < 1$), attenuation was due to scattering in the shear bulk waves. In the other instance, ($n^2 < q < 1$), attenuation was due to scattering in both shear and longitudinal bulk waves.

This theory was used by Humphreys and Ash⁸⁸ to convert bulk waves to surface waves, and vice versa. If bulk waves are incident at a surface on which there is periodic corrugation, surface waves will be generated. Using a surface wave transducer e.g. interdigital transducer, diffraction takes place and the bulk waves are produced on striking the corrugations.

It was proposed that with this method, surface waves can be transferred from one surface to another by means of mode conversion from surface to bulk waves.

3.1.3 The Ultrasonic Goniometer.

Critical angle reflectometry is used at a liquid-solid interface to propagate surface waves along the surface of the solid. A longitudinal wave transducer is used for producing compressional waves in the liquid. When incident at the surface of the specimen they are reflected. The reflected waves are received by the longitudinal wave transducer. (see fig 3.3). Both transducers are mounted so that they make equal angles with the normal and then rotated in opposite directions. The amplitude of the wave reflected from the surface is measured.

At a given critical angle, a dip is observed in the amplitude of the reflected wave. The surface wave velocity is then calculated from this angle by using the expression:-

$$C_R = \frac{C_w}{\sin \theta_R} \dots\dots\dots 3.1$$

where C_w is the dilatational wave velocity in the fluid, and, θ_R is the measured Rayleigh angle (critical angle).

This velocity varies for different materials, and for a given material in different mechanical states.

Surface waves travel along the surface of the solid at a velocity C_R which is determined by the elastic properties of the solid. i.e. the shear modulus, the Poisson's ratio and the density. Bradfield⁹¹ measured the elastic constant of the surface wave for most materials by this method.

If the elastic constant for the surface wave is G_{SR} then:-

$$C_R = \sqrt{\frac{G_{SR}}{\rho}}$$

where G_{SR} is used by analogy with C_{11} the elastic constant for longitudinal waves, and C_{44} the elastic constant for shear waves in solids. Using the generalised Hooke's law, C_{11} and C_{44} can be expressed as simple proportionalities of engineering stress (σ) to engineering strains (ϵ) in the absence of any other strains. i.e. $C_{11} = \frac{\sigma_{11}}{\epsilon_{11}}$ and $C_{44} = \frac{\sigma_{13}}{\epsilon_{13}}$ for stresses only in the xz plane.

With G_{SR} however, this is not the case because both the stress and strain distributions are made up of tensile and shear components.

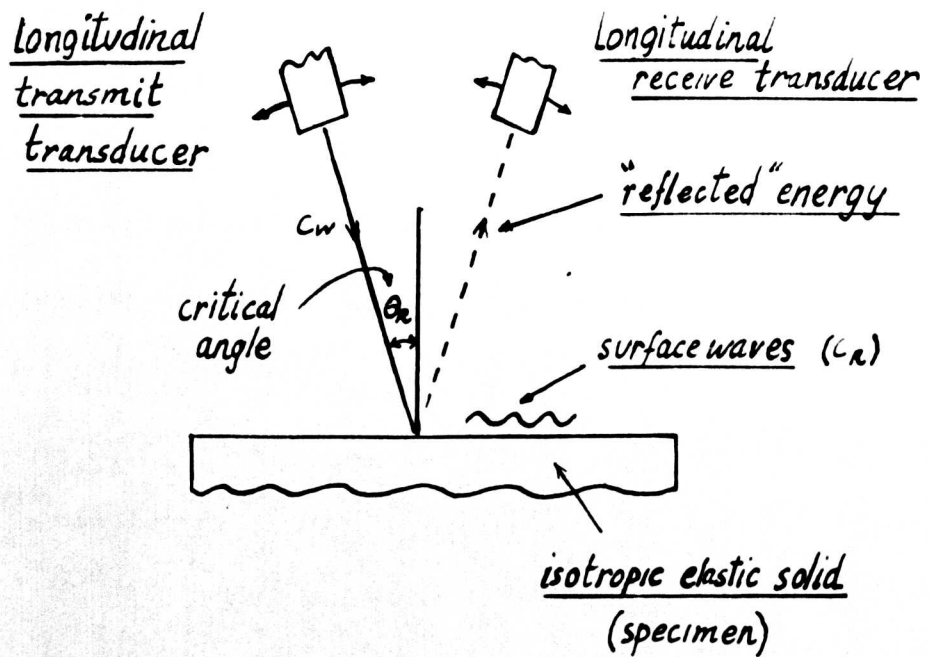


Fig 3.3 A two-probe Ultrasonic Goniometer (WHOLE SYSTEM immersed in Liquid.)

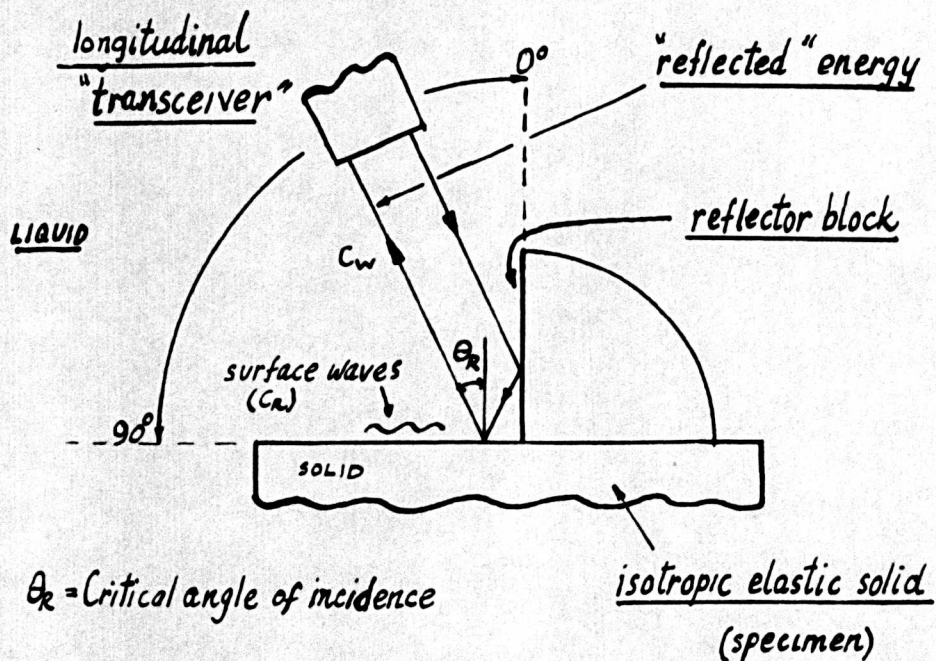


Fig 3.4 The "corner" reflector single-probe Ultrasonic Goniometer

Substituting for C_R in the above equation 3.1 we get:-

$$G_{SR} = \frac{\rho c_w^2}{\sin^2 \theta_R} \dots \dots \dots 3.3$$

Where ρ is the density of the solid.

With this type of testing the whole surface of the specimen can be tested, and the surface inhomogeneity can be detected.

If the specimen is rotated and the critical angle measured for all directions of surface wave propagation, then a measure of the preferred orientation can be obtained.

Let $C_{R\parallel}$ be the surface wave velocity along the direction of rolling, and $C_{R\perp}$ be the corresponding velocity in the direction normal to the direction of rolling, then the orientation factor can be calculated. i.e.

$$\beta = [C_{R\parallel} \sim C_{R\perp}] \dots \dots \dots 3.4$$

therefore substituting in equation 3.4 using equation 3.1 we get:-

$$\beta = c_w \left[\frac{1}{\sin \theta_{R\parallel}} \sim \frac{1}{\sin \theta_{R\perp}} \right] \dots \dots \dots 3.5$$

If the specimen has been fatigued or subjected to creep then it may be possible to separate out the effects of these processes.

Consider equation 3.5. Let β_0 be the measurements on the "as received" specimen, and β_1 be any value calculated from equation 3.5 using measured values of $\theta_{R\parallel}$ and $\theta_{R\perp}$ for a fatigued specimen. Then, if γ is the change in surface wave velocity due to the mechanical process, we have:-

$$\gamma = \beta_1 \sim \beta_0 \dots \dots \dots 3.6$$

If the frequency of the compressional wave is varied, then the critical angle can be measured at different frequencies, and a plot of frequency against critical angle thus obtained.

Another parameter that can be measured is the reflection factor. The exact division of energy at normal incidence is dependent upon the impedance mismatch at the boundary, and the amplitude ratio of the reflected and incident waves is given as follows:-

$$\frac{\text{Reflected Amplitude}}{\text{Incident amplitude}} = \frac{\rho_2 c_2 - \rho_1 c_1}{\rho_2 c_2 + \rho_1 c_1}$$

where $\rho_1 c_1$ and $\rho_2 c_2$ are the acoustic impedances of the liquid and the solid, respectively.

At the Rayleigh angle, however, a very complex mechanism is involved which determines the percentage of energy reflected from the surface. When this parameter is measured at different frequencies an indication of the best testing frequency can be obtained. Most materials appear to have some frequency at which most of the energy is converted to the surface wave. At frequencies above and below this value it seems that the conversion factor is lower. Therefore, it is useful to discover this frequency of least reflection, for the material under test.

Advantages of the test method

The advantages of this test method are:-

- (a) Since the ultrasonic beam is localised, tests can be conducted over the whole area of the specimen. Local surface properties can be detected.
- (b) A greater accuracy over short distances is obtained using this method than with the "through transmission" method. This is because the surface wave velocity in a localised area is measured at the critical angle.

- (c) Because the immersion mode of testing is employed, easy and consistent coupling is obtained between transducer and specimen.

3.1.4 The corner reflection method (Liquid-solid interface)

This is the method of surface wave testing employed in this investigation. It is a modification of the reflection method whereby one transducer is used as a transceiver. The method was first reported by Rollins.⁹² (see fig.3.4). The angle of incidence is measured and, as before, the surface wave velocity is calculated.

The reasons for choosing this method were:-

- (a) A quick and easy method of testing was required, and,
- (b) In this method only one transducer is used, therefore, the problem of transmitter and receiver transducer alignment is avoided.

3.2 Theory of ultrasonic surface wave propagation

Introduction

In 1885 Rayleigh⁹³ proposed to investigate the behaviour of waves upon a free surface of an infinite homogeneous isotropic elastic solid, their character being such that the disturbance is confined to a superficial layer of thickness comparable to a wavelength. This case was analogous to deep water waves, the difference being that the potential energy depended upon elastic resilience instead of gravity.

Lamb⁹⁴ conducted analytical studies on an elastic sphere from which Rayleigh's work was a special case. Rayleigh deduced that at the surface of an infinite solid the particles described elliptical orbits in the plane normal to the surface and parallel to the direction of propagation. He proposed that these surface waves played an important part in earthquakes. It was observed that these waves are nondispersive, and their amplitude decays exponentially with depth.

It was also shown that the propagation velocity was slightly slower than that for bulk shear waves. This type of surface wave is called the Rayleigh wave.

Most of the studies on surface waves were made by seismologists, e.g. Ewing et al⁹⁵ and it was only recently that Viktorov⁹⁷ considered the possibility of using ultrasonic surface waves for flaw detection, where bulk waves are not suitable. The advent of microwave acoustics has stimulated large scale research in the physics of elastic surface waves. Other types of waves are the "Generalized surface wave" (Tursanov⁹⁸), and Love waves (Love¹⁰¹). Recently Lim and Farnell¹⁰⁰ have used such terms as "leaky surface waves" or "pseudo surface waves" to describe special types of waves. Other workers (ref. 102 to 105) have contributed to the study of these waves.

Theory

Let us consider wave propagation on an infinite solid medium.

(see fig.3.5).

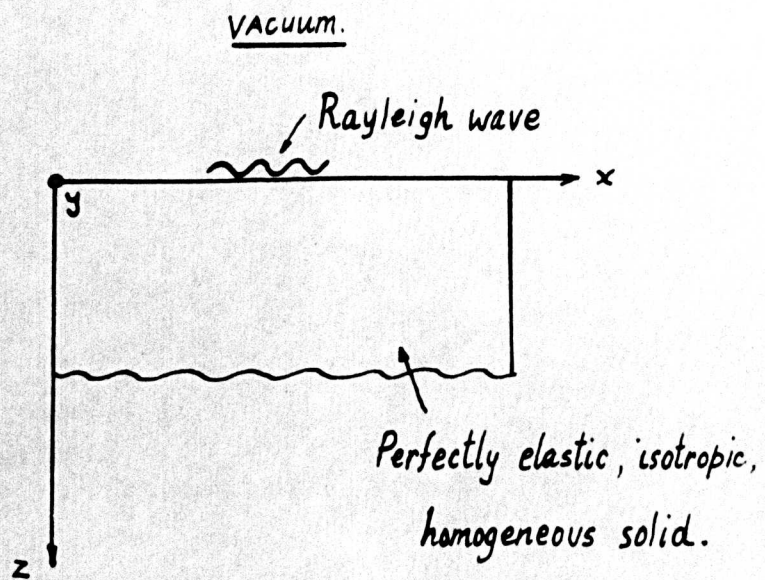


Fig 3.5 A vacuum - solid interface

Assume that:-

- (a) The medium is isotropic, elastic and homogeneous.
- (b) The wave is a plane harmonic wave propagating in the x direction.
- (c) Stress normal to the surface is zero, and stress in the plane of wave propagation is zero.

Under these conditions a Rayleigh wave can exist. The displacement vector of this wave will be $u = u_x i + u_y j + u_z k$. where,
 $u_x = u_{x0} \exp j(\omega t + \alpha)$, $u_y = u_{y0} \exp j(\omega t + \beta)$, $u_z = u_{z0} \exp j(\omega t + \gamma)$; and α, β , and γ are relative phase angles.

The force on the medium can then be written as:-

$$C_{11} \nabla \phi + C_{44} \nabla \times \psi = \rho \ddot{u} \quad \dots\dots\dots 3.7$$

where:-

$$C_{11} = \lambda + 2\mu, \text{ and } C_{44} = \mu.$$

ϕ = The tensile strain in the medium. i.e ($\nabla \cdot u$)

ψ = The shear strain in the medium. i.e ($\nabla \times u$)

ρ = Density of the medium.

Expanding equation 3.7, and equating terms, the following two terms are derived.

$$\begin{aligned} C_{11} \frac{\partial \phi}{\partial x} - C_{44} \frac{\partial \psi}{\partial z} &= \rho \omega^2 u_x \quad \dots\dots\dots 3.8 \\ C_{11} \frac{\partial \phi}{\partial z} + C_{44} \frac{\partial \psi}{\partial x} &= \rho \omega^2 u_z \end{aligned}$$

It follows therefore that the particle displacement is made up of two parts i.e.

$$\begin{aligned} u_x &= \frac{\partial \phi}{\partial x} - \frac{\partial \psi}{\partial z} \quad \dots\dots\dots 3.9 \\ u_z &= \frac{\partial \phi}{\partial z} + \frac{\partial \psi}{\partial x} \end{aligned}$$

Assume $\phi = A e^{-qz} e^{j(kx - \omega t)}$ and,

$$\psi = B e^{-sz} e^{j(kx - \omega t)} \quad \dots\dots\dots 3.10$$

where q and s are damping factors in the z plane for ϕ and ψ respectively.

Considering the condition when $\sigma_{xz} = 0$. In wave number terms, after substituting equation 3.9, we get:-

$$\sigma_{xz} = 2\mu k q \phi + 2\mu k^2 \psi + 2\mu s^2 \psi. \text{ then,}$$

$$\phi = -\left(\frac{k^2 + s^2}{2kq}\right)\psi \dots\dots\dots 3.11$$

Substituting 3.10 and 3.11 into 3.9, the following equations for the wave amplitudes are derived. viz.

$$u_x = Ak_R \left(e^{-q_R z} - \frac{2q_R s_R}{(k_R^2 + s_R^2)} e^{-s_R z} \right) \sin(k_R x - \omega t)$$

..... 3.12

$$u_z = Ak_R \left(e^{-q_R z} - \frac{2k_R^2}{(k_R^2 + s_R^2)} e^{-s_R z} \right) \cos(k_R x - \omega t)$$

These are the Rayleigh wave amplitudes, which can be seen to decay with depth. If there are losses in the solid they will also decay with distance in the x direction of propagation.

It can also be seen that the total particle displacement describes an elliptical orbit whilst the waves travel along the surface.

It has been calculated that the ellipses change direction of rotation at a depth of approximately 0.2 wavelengths (λ_R). The rotation becomes anticlockwise beyond this depth. (see fig 3.8). The eccentricity of the ellipse is a function of the depth from the surface and the Poisson's ratio of the solid.

Fig 3.6 is a plot of the calculated values of u_x and u_z . These are normalized to displacement amplitude on the surface. It can be seen that u_x becomes negative at approximately $0.2\lambda_R$. It also demonstrates that about one wavelength deep in the solid the vertical axis of the ellipse is only about 0.2 of its maximum value just below the surface.

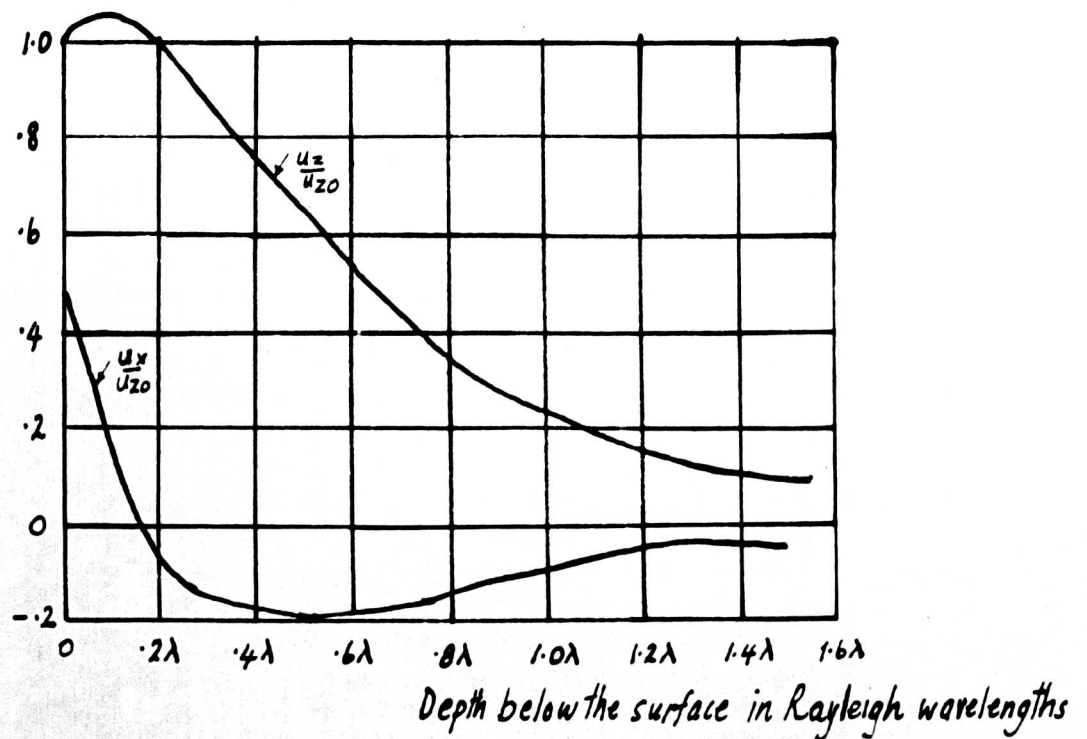


Fig 3-6 Variations of particle displacement with depth (after Viktorov⁹⁷)

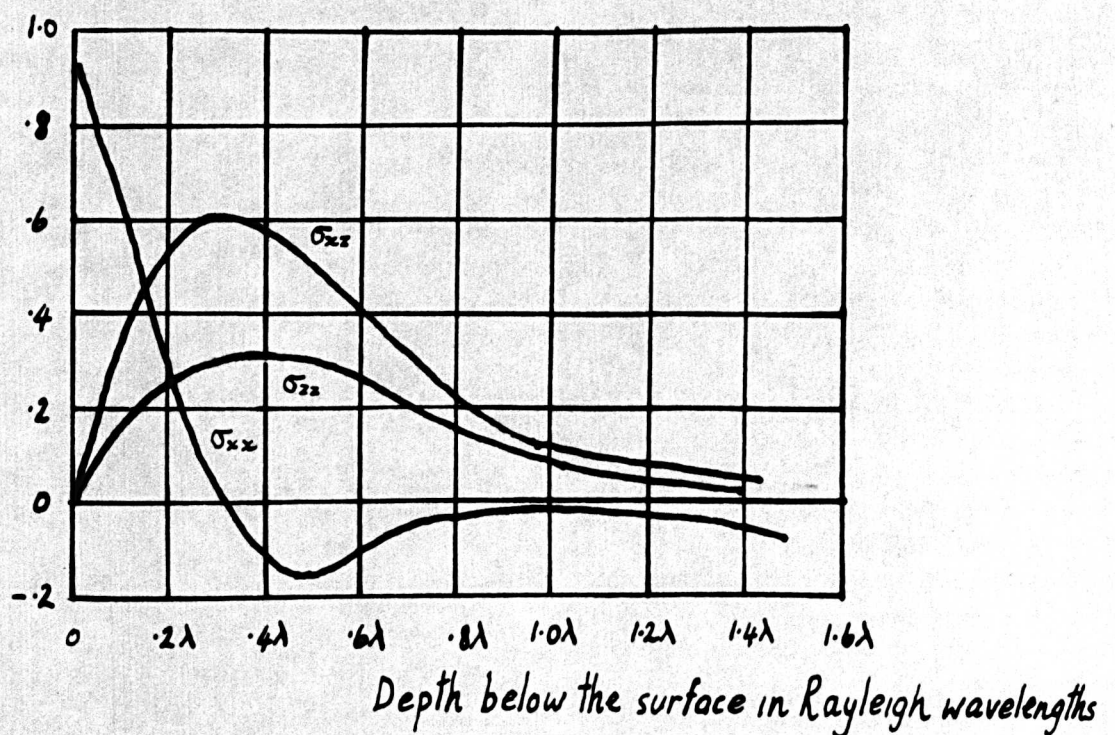


Fig 3-7 Variations of stress with depth (after Viktorov⁹⁷)

Fig3.7 is a plot of the stress distribution in the layer of the half space, in which the wave propagates. It shows how at the surface σ_{zz} and σ_{xz} are zero. Both these two graphs are useful to demonstrate the fundamental theory of surface wave propagation.

Fig.3.8 gives a picture of particle motion below the surface. It shows how the ellipses change directions and how the particle displacement amplitude decays with depth.

For the condition when the stress normal to the surface σ_{zz} is zero, the Rayleigh wave equation can be derived. In wave number terms the stress σ_{zz} can be written after substituting equation 3.9 as:-

$$(\lambda k^2 - \lambda q^2 - 2\mu q^2)\phi - 2\mu k s \psi = 0$$

Substituting eqn.3.11 into this equation the characteristic equation of the Rayleigh wave can be derived. i.e.

$$4k^2 q s - (s^2 + k^2)^2 = 0 \dots\dots\dots 3.13$$

Viktorov⁹⁷ gave the transformation of this equation. The result was:-

$$R^6 - 8R^4 + 8(3 - 2B^2)R^2 - 16(1 - B^2) = 0 \dots\dots\dots 3.13(a)$$

where:- $R = \frac{k_t}{k} = \frac{c}{c_t}$ and $B = \frac{k_1}{k_t} = \frac{c_t}{c_1}$.

This is called the Rayleigh equation. The approximate solution of this equation is given by Bergmann¹⁰⁷ and Viktorov¹⁰⁸ i.e.

$$n_R = \frac{0.87 + 1.12\nu}{1 + \nu} \dots\dots\dots 3.14$$

where ν is the Poisson's ratio of the material.

n_R ranges from 0.87 to 0.96 for Poisson's ratio of 0 to 0.5. This is the range of Poisson's ratio for most materials.

| $\frac{u_x}{u_{z_0}}$ | $\frac{u_z}{u_{z_0}}$ |
|-----------------------|-----------------------|
| 0.6 | 1.0 |
| 0.3 | 1.1 |
| 0 | 1.0 |
| -0.2 | 0.7 |
| -0.1 | 0.3 |
| -0.13 | 0.2 |
| -0.05 | 0.15 |
| -0.01 | 0.05 |

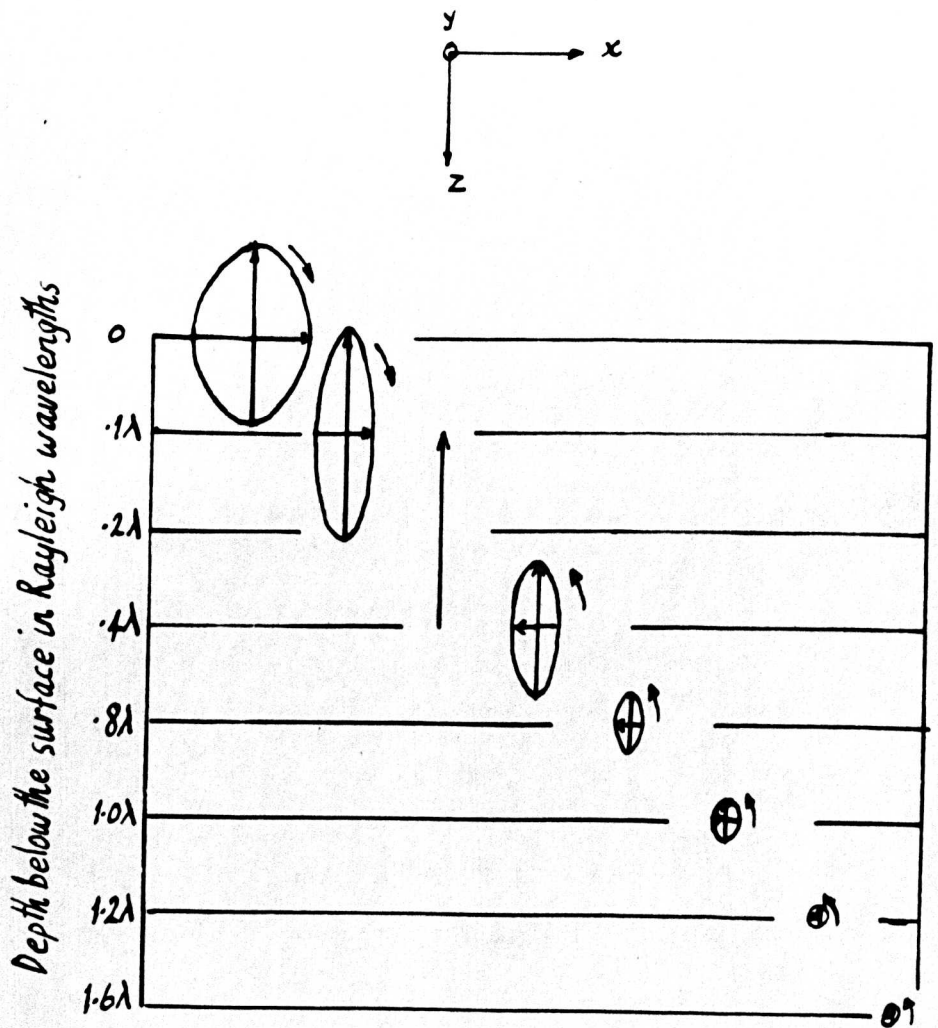


Fig 3.8 Variations of particle displacement with depth below the surface. (due to Author)

3.2.1 Theory of critical angle reflectometry

It follows from the general theory of surface waves given in the previous section that surface waves can propagate at a boundary between a solid and a liquid. In this case the vacuum is replaced by a liquid.

Consider Fig.3.9. A dilatational wave is transmitted in a liquid towards a liquid-solid boundary. Assume that:-

- (a) The liquid layer is semi-infinite, and is a perfect fluid.
- (b) The solid layer is semi-infinite, perfectly elastic, isotropic, and homogeneous.

Then at the interface, the energy in the dilatational wave will be used in general, for generating a longitudinal and a shear wave in the solid. The remainder of the energy will be reflected.

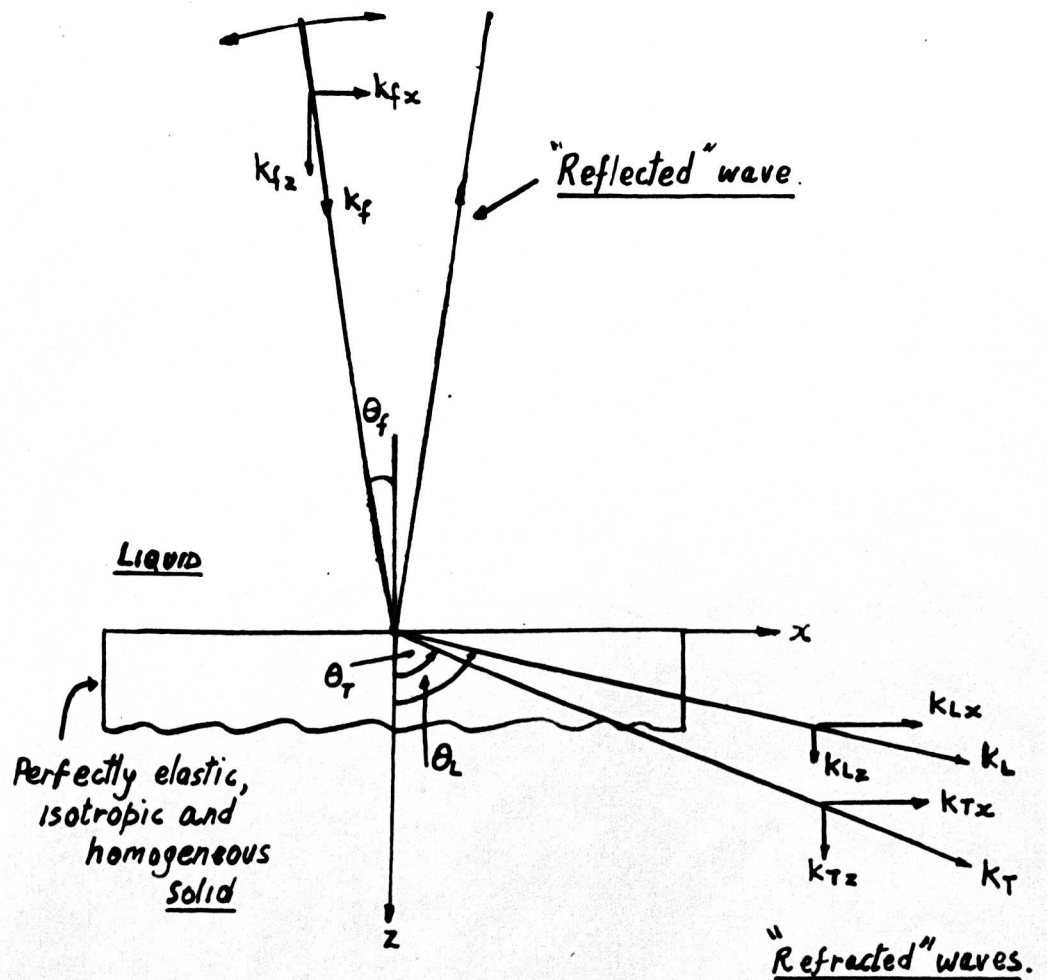
At this boundary the phase velocities of all three waves are equal. Therefore:-

$$k_{fx} = k_{Tx} = k_{Lx}$$

$$\text{or} \quad k_f \sin \theta_f = k_T \sin \theta_T = k_L \sin \theta_L \dots \dots \dots 3.15$$

This is the same as Snell's law. θ_f is the angle of incidence in the fluid. θ_T and θ_L are angles of refraction for the shear and the longitudinal waves in the solid respectively.

If the angle of incidence is varied, the energy reflected from the surface of the solid, if measured, will follow a plot as given in Fig.3.10. This plot is called a goniogram. The goniogram shown here is for a water-steel interface. As can be seen there are three main features in the plot.



k_L is the wavenumber of the longitudinal wave in the solid.
 k_T is the wavenumber of the transverse wave in the solid.
 k_f is the wavenumber of the longitudinal wave in the fluid.
 θ_f is the angle of incidence.

Fig 3.9 A liquid - solid interface

- (a) There is an angle where the dilatational wave in the solid is at grazing incidence. The amplitude reaches a peak, and theoretically all the energy is reflected back into the water. The critical angle of the dilatational wave in the solid is calculated from eqn.3.15, then:-

$$k_f \sin \theta_{iL} = k_L \sin 90$$

or

$$\theta_{iL} = \sin^{-1} \frac{C_f}{C_L} \approx \sin^{-1} \frac{1.5}{6.0} \dots\dots\dots 3.16$$

$$\approx 15^\circ \text{ for water/steel.}$$

- (b) There is an angle where the shear wave becomes critical, and a peak is observed on the goniogram. This shear criticality can be derived also from eqn.3.15, then:-

$$k_f \sin \theta_{iT} = k_T \sin 90$$

or

$$\theta_{iT} = \sin^{-1} \frac{C_f}{C_T} \approx \sin^{-1} \frac{1.5}{3.0} \dots\dots\dots 3.17$$

$$\approx 30^\circ \text{ for water/steel.}$$

- (c) Immediately beyond this point there is an angle where mode conversion takes place at the boundary. Most of the incident energy in the dilatational wave in the fluid, is converted into a surface wave. This angle is only slightly greater than the shear criticality angle, because the surface wave velocity is only slightly less than the shear wave velocity. This is represented by a sharp dip in the goniogram. Beyond this point, the energy is recovered to a high value.

The surface wave critical angle or Rayleigh angle can

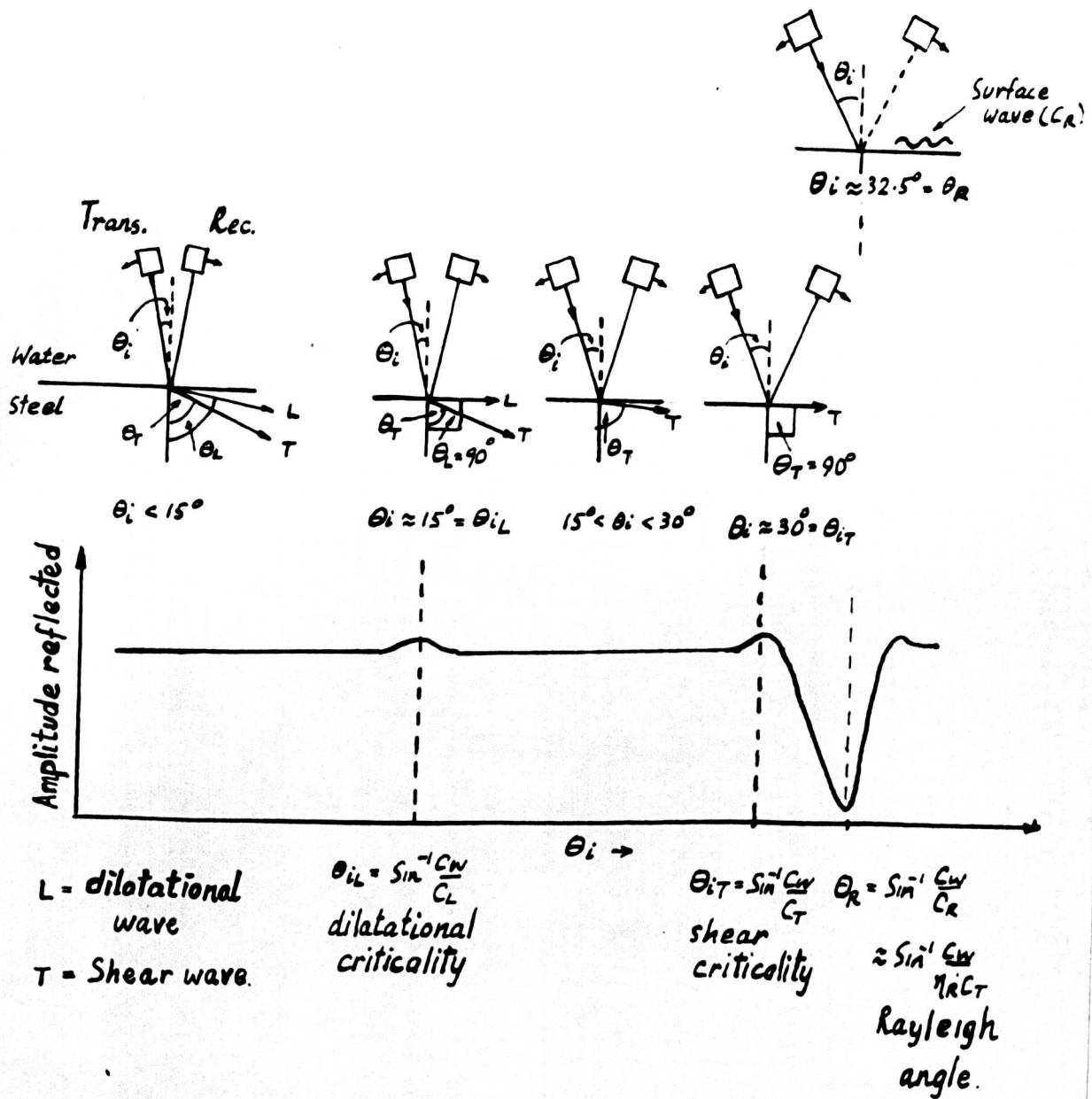


Fig3.10 Simplified "state diagrams" of conventional
two-probe reflectometry. (due to Author)
Water-steel interface

be derived again from eqn.3.15, then:-

$$k_f \sin \theta_R = k_R$$

or

$$\theta_R = \sin^{-1} \frac{C_f}{C_R} \dots\dots\dots 3.18$$

an approximate value of C_R is normally used when only the Poisson's ratio and the shear wave velocity of the material are known.i.e.

$$C_R \approx n_R C_T, \text{ where } n_R \text{ is as given in eqn.3.14.}$$

Then eqn3.18 above can be written as:-

$$\theta_R = \sin^{-1} \frac{C_f}{n_R C_T} \dots\dots\dots 3.19$$

$$\approx \sin^{-1} \frac{1.5}{0.95 \times 3.0} \approx 32.5^\circ \text{ for water/steel.}$$

At this angle the surface waves propagated are called "Leaky" Rayleigh waves. They are called "Leaky" because they radiate energy into the fluid as they propagate along the surface of the solid. They are attenuated more than free surface waves, and are propagated along the surface over shorter distances.

The theoretical explanation given for this type of wave is that the wave number is complex, which represents a wave which is radiating energy into the liquid as it propagates along the surface. As in the previous section, a characteristic equation can be derived for this type of interface, the previous one being for a vacuum-solid interface. The characteristic equation for this liquid-solid interface is similar to that for the vacuum-solid interface except that the effect of the fluid is taken into consideration.

The equation, which was derived by Viktorov⁹⁷ is:-

$$4k^2_{qs} - (s^2 + k^2) = -j \frac{\rho_f q k_T^4}{\rho \sqrt{k_f^2 - k^2}} \dots\dots\dots 3.20$$

This equation has only one real root corresponding to a surface wave travelling along the boundary of the interface. The expression leads to a complex value for the wave number(k) of the surface waves.

A new method of analysing different types of interface was recently devised by Oliner¹⁰⁹. He presented analogous electrical networks for many types of interface and compared them with the analytical results given by Viktorov.⁹⁷ His results were similar to those of Viktorov.

The reflection factor

At this critical angle, the reflection factor has to be taken into consideration. Becker and Richardson¹¹⁰ did some theoretical analysis and deduced that the reflection factor can be written as:-

$$\frac{z_{112}}{z_{111}} = \frac{\cos^2 \delta_{22} + \frac{c_{22}^2}{c_{12}^2} \sin^2 \delta_{12} \sin^2 \delta_{22} + \frac{\rho_1 c_{11} \sin \delta_{12}}{\rho_2 c_{12} \sin \delta_{11}}}{\cos^2 \delta_{22} + \frac{c_{22}^2}{c_{12}^2} \sin^2 \delta_{12} \sin^2 \delta_{22} - \frac{\rho_1 c_{11} \sin \delta_{12}}{\rho_2 c_{12} \sin \delta_{11}}} \dots\dots\dots 3.20$$

where:-

z_{111} = incident wave amplitude.

z_{112} = reflected wave amplitude.

δ_{11} = angle of incidence of longitudinal wave in water.

δ_{12} = angle of refraction of the longitudinal wave in the solid.

δ_{22} = angle of refraction of the shear wave in the solid.

C_{11} = longitudinal wave velocity in the liquid.

C_{12} = longitudinal wave velocity in the solid.

C_{22} = shear wave velocity in the solid.

If the test frequency is varied and the reflection factor at the critical angle measured, there will be a frequency where the reflection is a minimum. Fig. 3.19 is a plot due to Richardson and Becker¹¹⁰ showing theoretical and experimental values for a water-stainless steel interface.

Lateral beam displacement.

Schoch¹¹¹ reported that at the critical angle of incidence Rayleigh wave travels along the boundary on the surface of the solid before emerging again into the liquid. (see Fig. 3.12). Schoch calculated the value of this "skip distance" to be:-

$$\Delta = \lambda \frac{2}{\pi} \frac{\rho_s}{\rho_f} \frac{\sqrt{r(r-s)}}{s(s-1)} \left(\frac{1 + 6s^2(1-q) - 2s(3-2q)}{s-q} \right) \dots \dots 3.22$$

where:-

λ = wavelength in the liquid.

ρ_f = density of the liquid.

ρ_s = density of the solid.

$q = \left(\frac{C_T}{C_L} \right)^2$ where C_T and C_L are shear and longitudinal waves velocities in the solid.

$r = \left(\frac{C_T}{C_1} \right)^2$ where C_1 is the velocity of the longitudinal wave in the liquid.

$s = \left(\frac{C_T}{C_R} \right)^2$ where C_R is the velocity of the Rayleigh wave in the solid.

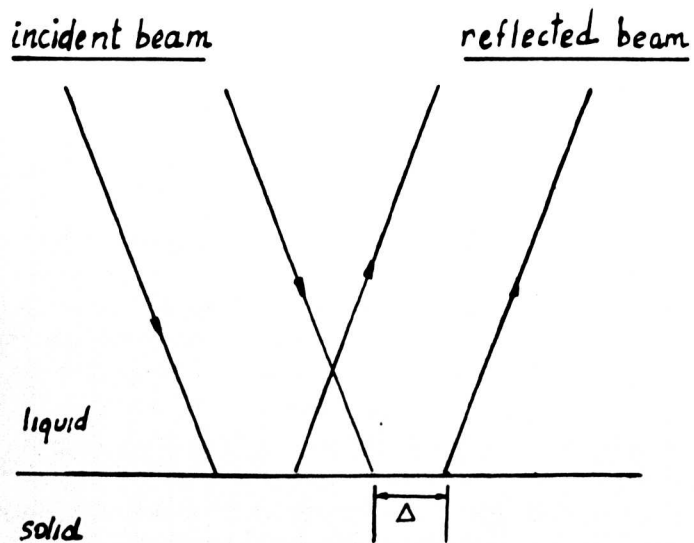


Fig 3-11 Showing the "skip distance" (Δ) at critical angle

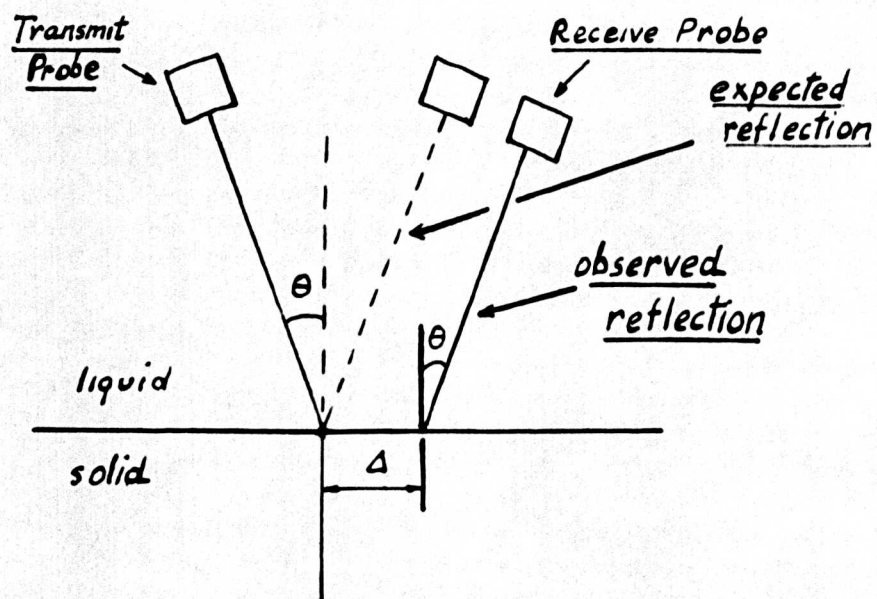


Fig 3-12 Showing the "skip distance" and the position to
locate receive probe for maximum
reflected energy

The derivation of this equation is given in Appendix(5). For a water-aluminium interface Δ was calculated to be 24.4λ .

Recently however it was observed by Curtis¹¹² that it appears that the reradiated wave mentioned before was interfering with the reflected wave, and so giving an uneven distribution of intensity across the wavefront.

Due to this interference he found that the highest intensity in the wavefront (water-glass interface), was not on the axis of the receiving transducer, but some distance away. (see fig.3.12). This phenomena could be the "skip distance" mentioned by Schoch.¹¹¹

The phenomenon was demonstrated by Curtis using Schlieren photographs. A microdensometer plot made by Curtis¹¹² across the wavefront of the reflected wave at the critical angle is shown in Fig.3.15. As can be seen the peak optical density is not on the axis of the receiving transducer.

Phase change at critical angle

It has been reported¹¹⁰ that at the critical angle there is a phase change of the received energy at the Rayleigh trough. It was suggested that if this phase change could be measured, then very early changes in material properties can be detected. Fig.3.14 is a curve showing this change at the critical angle.

3.3 Historical review of critical angle reflectometry.

Ultrasonic critical angle reflectometry was found to be useful for the measuring of changes in surface and near surface properties of materials.

The existence of this critical angle was found experimentally (fig.3.16). Brekhovskikh's¹¹⁴ theory for non-attenuative waves could not predict it.

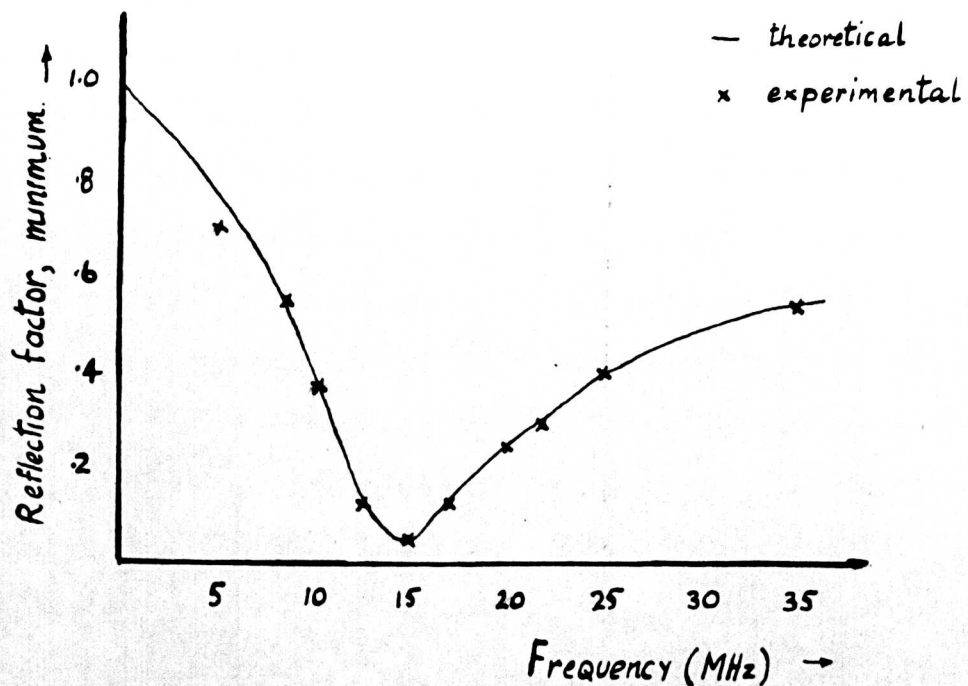


Fig 3-13 Plot of minimum critical angle reflection versus frequency
for a water-stainless steel interface. (due to Richardson and
 Becker (110))

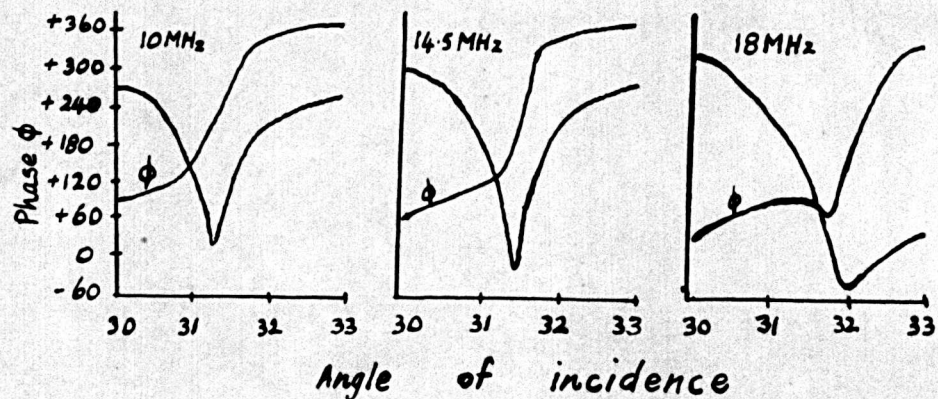


Fig 3-14 Showing phase change at critical angle for
different frequencies (due to Becker¹¹³)

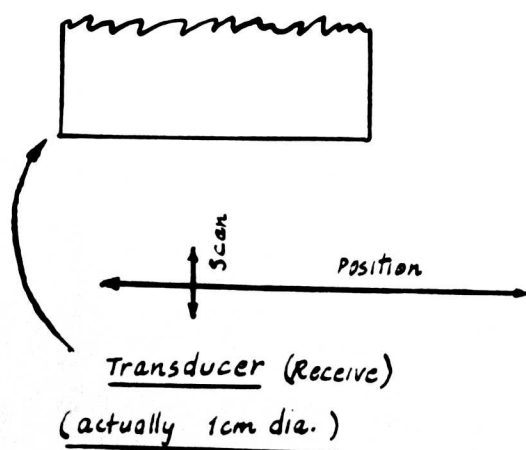
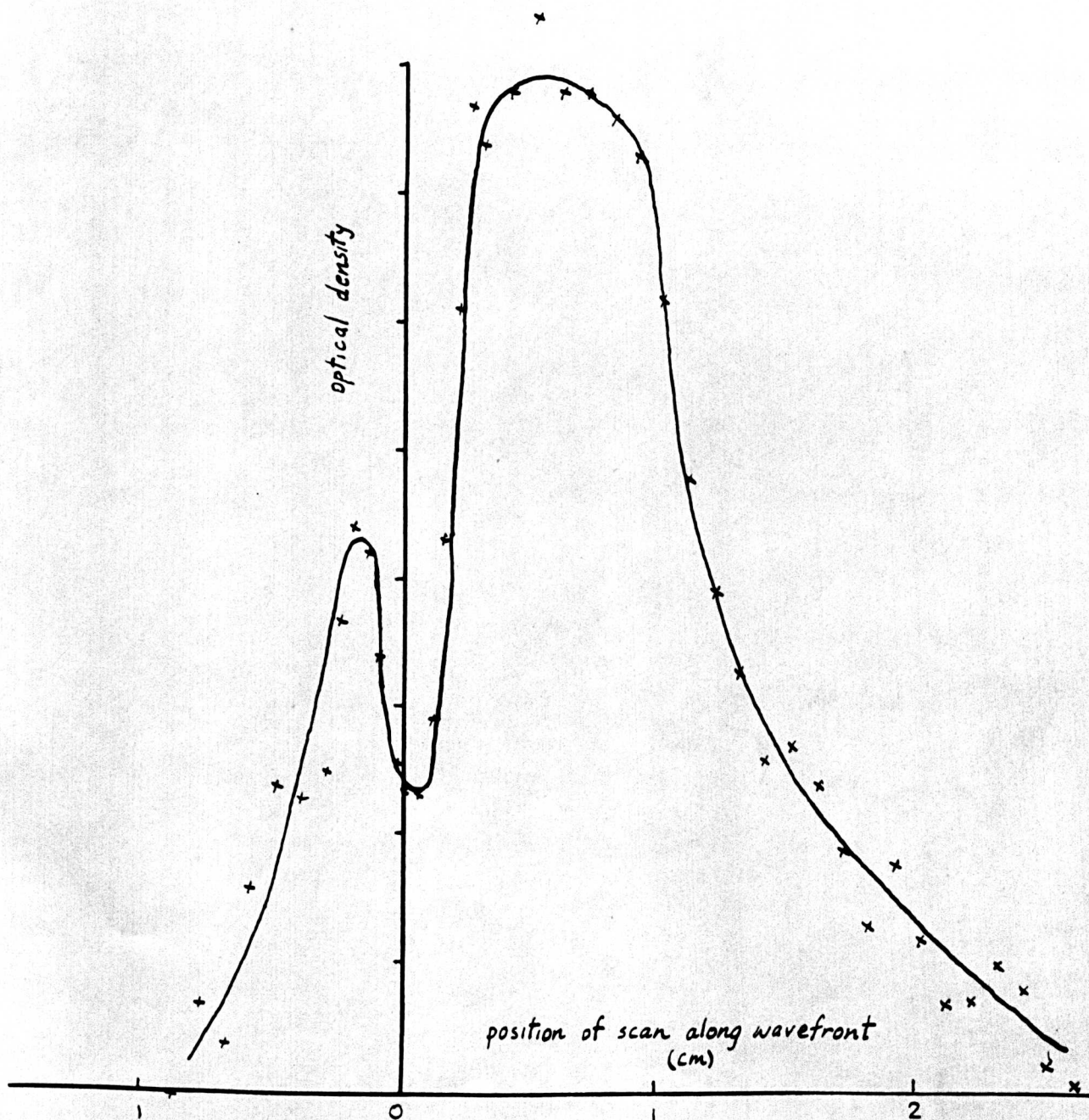


Fig 3.15 Microdensometer plot
across first wavefront
at critical angle.¹¹²



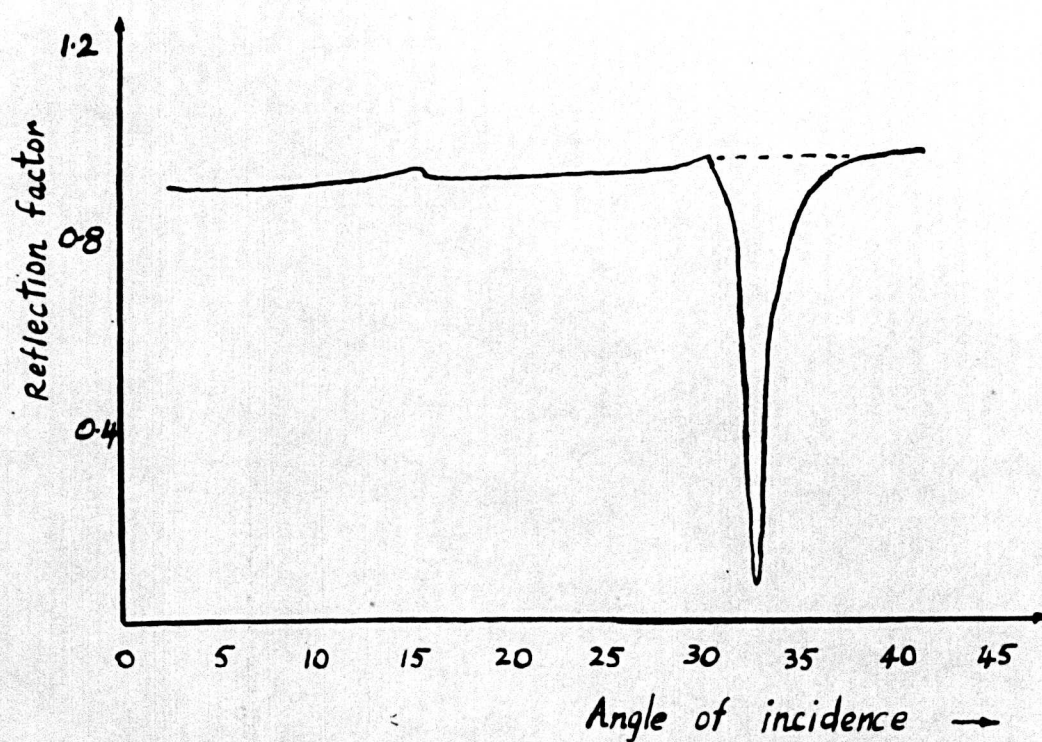


Fig 3.16 Reflected energy at a water-stainless interface
---- theoretical, — observed

The effect of plastic strain was studied. Brass in two states was measured. It was found that a frequency of 15MHz gave the lowest reflection. Higher reflections were obtained at 25 and 45MHz. This was for the "as received" state. For the 60% cold rolled brass, the frequency which gave the lowest reflection was 65MHz. The reflected amplitude increased as the frequency was lowered. The critical angle increased with frequency.

Another interesting phenomena was observed when measurements on the "as received" brass parallel and perpendicular to the rolling directions. Measurements were also made for cold rolled brass. They showed a 5 degree difference in critical angle for the cold rolled brass but only a 25mins difference for the "as received" brass.

The reflection dip is also dependent upon localised cold working, like grinding or milling. Even hand polishing has an effect on the critical angle. When steel (4340) was heated to above the austenization temperature and then quenched in oil, there was no reflection dip at the frequency of least reflection for the "as received" specimen. This was similar to what Papadakis^{121,122} reported on the attenuation characteristics for bulk waves in martensite formed by quick quenching from above the austenization temperature.

Rollins¹²³ studied single crystals of copper and reported on the pseudo surface wave¹⁰⁰. Measuring the critical angle in the (100) direction of the crystal one dip was observed in the reflection goniogram. This was the Rayleigh angle. However for a plane of incidence 30° to the (100) direction two dips were observed. The angle for the excitation of the pseudo surface wave was lower. This means that the velocity of the pseudo surface wave was lower than that for the Rayleigh wave.

Polycrystalline copper was also studied. Critical angles for various states of cold rolled copper were measured. From these measurements the

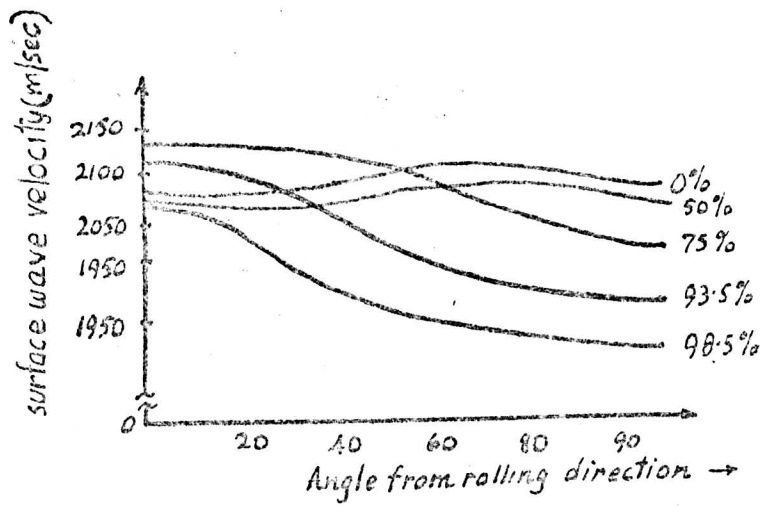


Fig 3.17 Surface wave velocity versus orientation for different states of cold rolling in polycrystalline copper (Rollins¹²³)

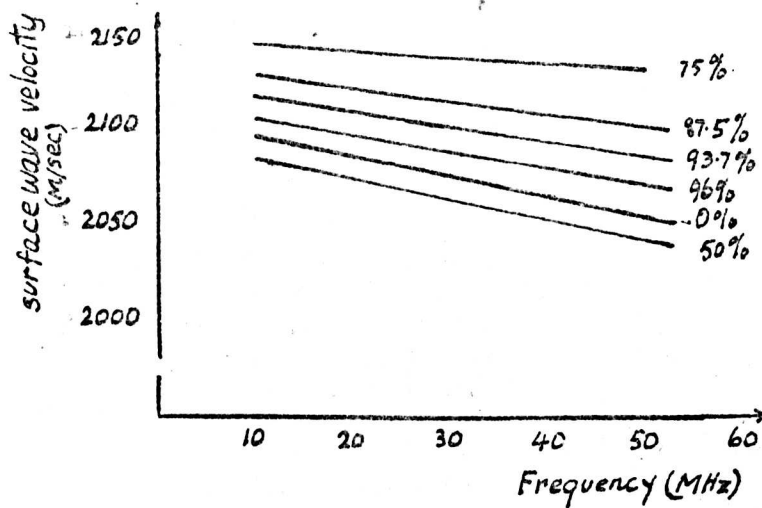


Fig 3.18 Surface wave velocity versus frequency for different states of cold rolling in polycrystalline copper (Rollins¹²³)

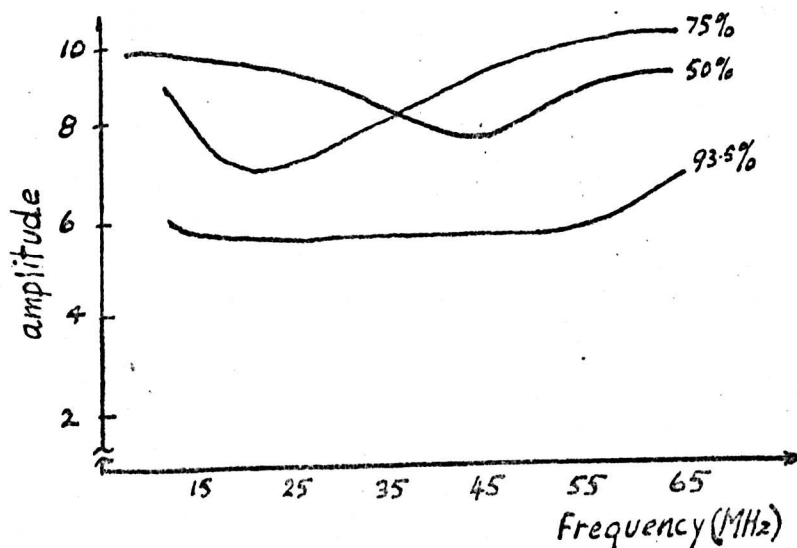


Fig 3.19 Amplitude of reflection dip versus frequency for polycrystalline cold rolled copper. (Rollins¹²³)

surface wave velocities were calculated. Fig.3.17 shows how the surface wave velocity varies with angle from rolling direction for different states of cold roll. An attempt was made to explain the cause of the velocity change. It was concluded that the change was due mainly to orientation, since studying an isotropic material (aluminium) the velocity change was very small due to cold rolling. Eighty percent cold roll caused only 0.5% change in surface wave velocity. Copper becomes very anisotropic when rolled. The velocity variations were compared with results obtained for single crystals¹²⁴ and were found to be similar.

The other that was studied is the manner in which the velocity changes with frequency is shown in fig.3.18. The only consistent trend observed was that in all cases, velocity fell off with frequency. The amplitude of the reflection dip was measured at different frequencies. (see fig.3.19).

Rollins¹²⁵ used the reflection method to evaluate the elastic constants of isotropic and slightly anisotropic materials. He compared results for Young's modulus in titanium rolled plate with stress-strain results and found good agreement. Curtis¹¹² reported on experimental work done for a liquid-polymer interface using the critical angle method. He showed that for certain liquid-solid interfaces the longitudinal peak is very clearly defined, whereas the Rayleigh trough is very ill-defined. The shear peak was not well defined. He also reported that the resin richness of epoxy resin matrix could be estimated using the reflection method.

CHAPTER 4

DESIGN OF THE ULTRASONIC GONIOMETER

Introduction

The corner reflection technique described by Rollins⁹² was used to excite the surface waves. Many factors had to be taken into consideration when designing this type of Goniometer. A reflector block was used to return the signal to the transducer. Therefore, the complement of the critical angle of the reflector block had to be far removed from the critical angle of the specimen being tested.

A typical goniogram for a water-steel interface using this type of goniometer can be seen in Fig.4.1. The reflector block used is made of stainless steel. Observe the two critical angles i.e. specimen and reflector block. The first trough is at the critical angle of the specimen, and the other one is at the complement of the critical angle of the block. The surface of the reflector block had to be level so as to prevent scattering of the incident waves.

With the goniometer the immersion mode of testing was used. It was thus important that the temperature of the fluid remained constant. Temperature control was necessary so that repeatability of measurements is not affected by variations in acoustic velocity in the coupling fluid.

There was also the problem of transducer near and far-field in this type of testing. This determined the distance between the transducer and the test object.

Another problem was that of corrosion when water was used as the liquid medium. Another problem was that of transducer alignment.

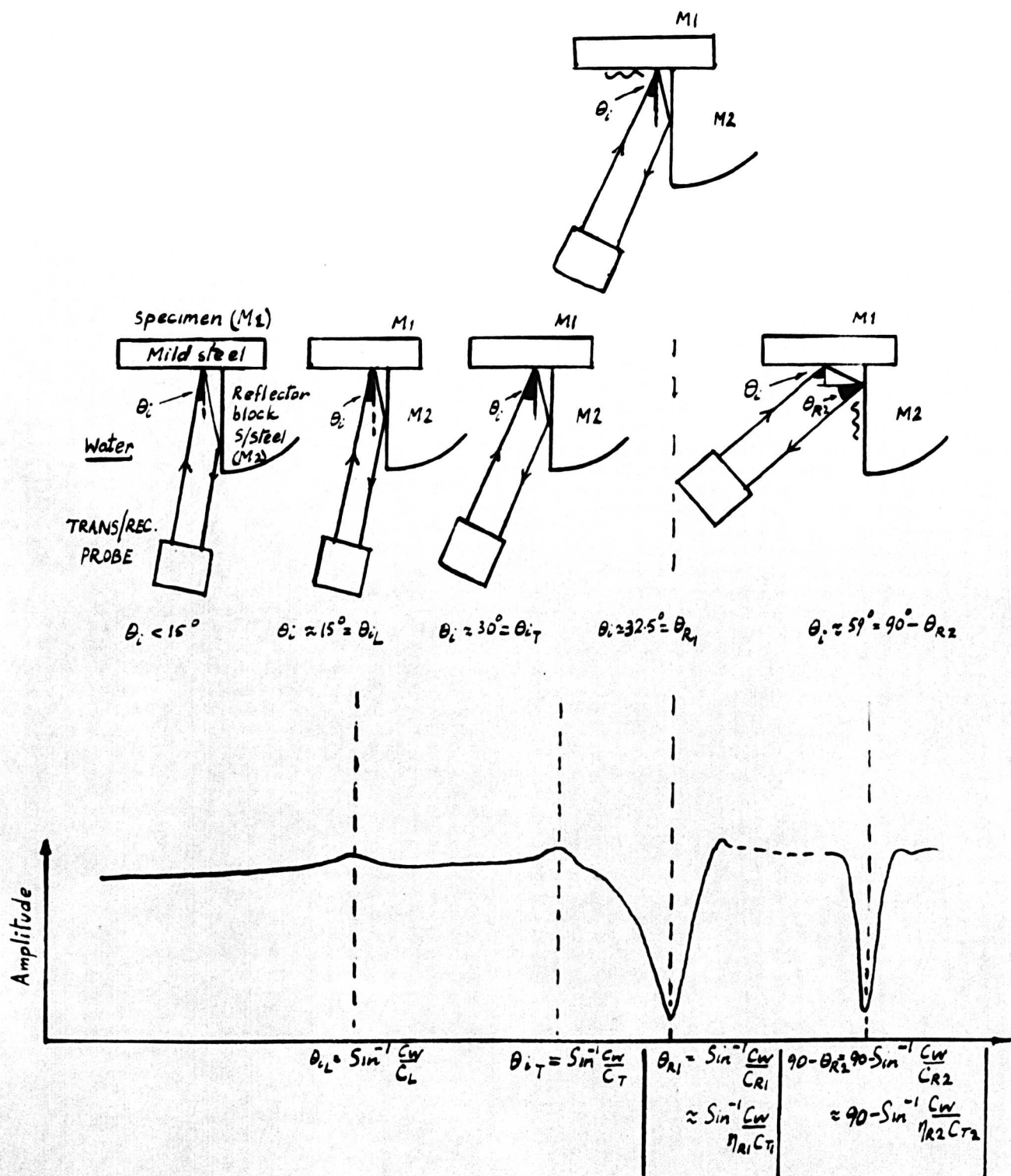


Fig 4-1 Simplified "state diagrams" for the corner reflector single probe reflectometry (dueto Author)

The axis of the transducer had to be in line with the corner, and using the corner as centre, the transducer had to be able to rotate through 90 degrees, at a fixed radius and height.

Since the test specimen had to be mounted behind the reflector block, the problem of specimen mounting had to be solved. Additionally, it would have been very useful if the specimen could be rotated in order to launch surface waves along different directions on the surface of the specimens. The width of the specimens had to be traversed and accurate measurements of the depth of testing had to be obtained.

4.1 The system

A drawing of the whole system used can be seen in Fig.4.2. The system description is as follows. A pulse generator was used to pulse a continuous-wave sinusoidal oscillator. This gave an output as shown in the figure. This signal was passed to the transducer via a 25dB variable attenuator. The echo received from the specimen via the reflector block was amplified then displayed on an oscilloscope. In the "delayed" sweep the echo pulse was viewed in detail. A photograph of the whole system can be seen in Fig.4.3.

4.2 The ultrasonic goniometer

General

The ultrasonic goniometer was designed by the author, (see appendix 4), and built in the University workshops. A photograph of the goniometer in its final form can be seen in Fig.4.4.

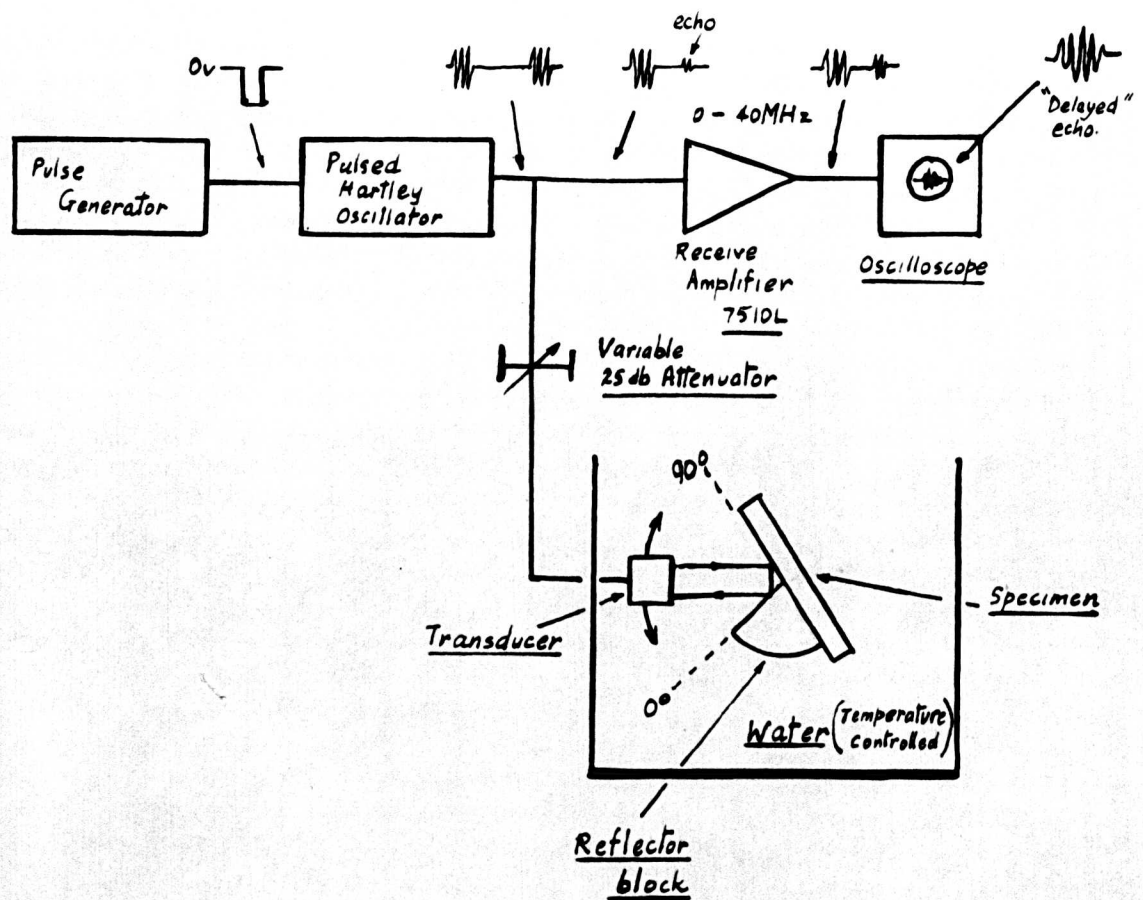
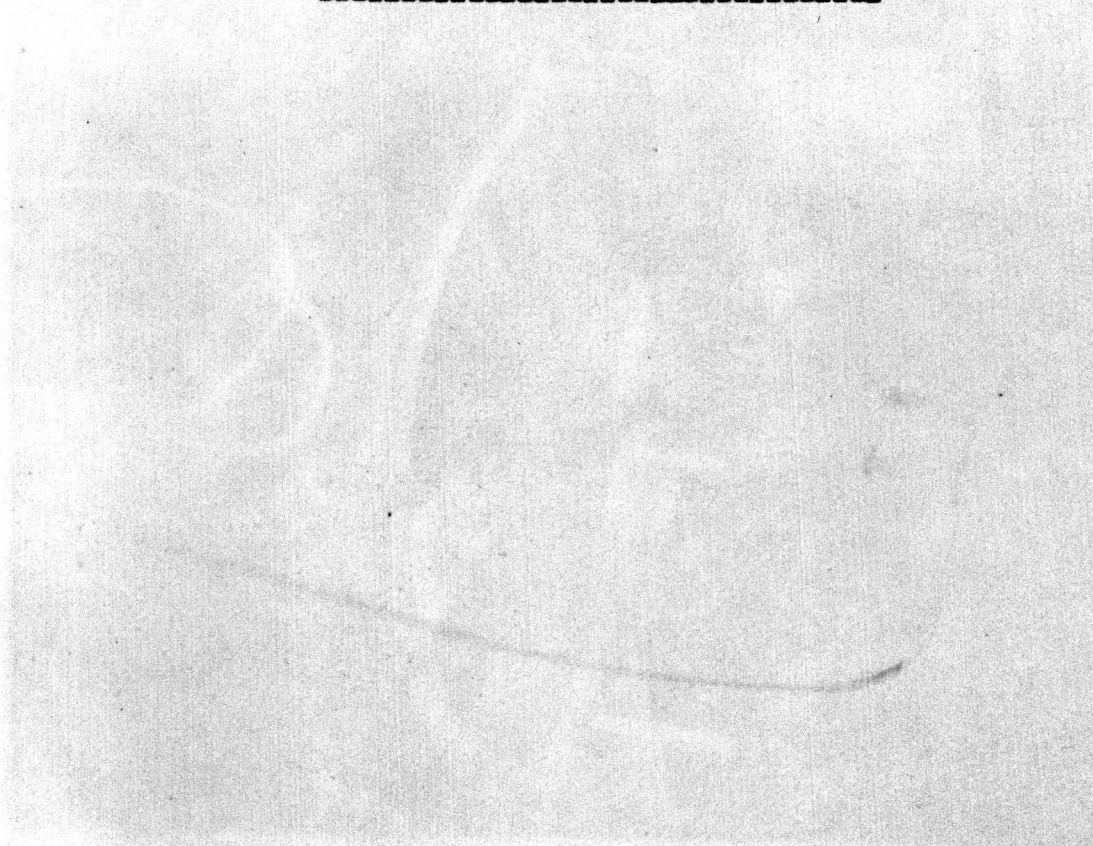
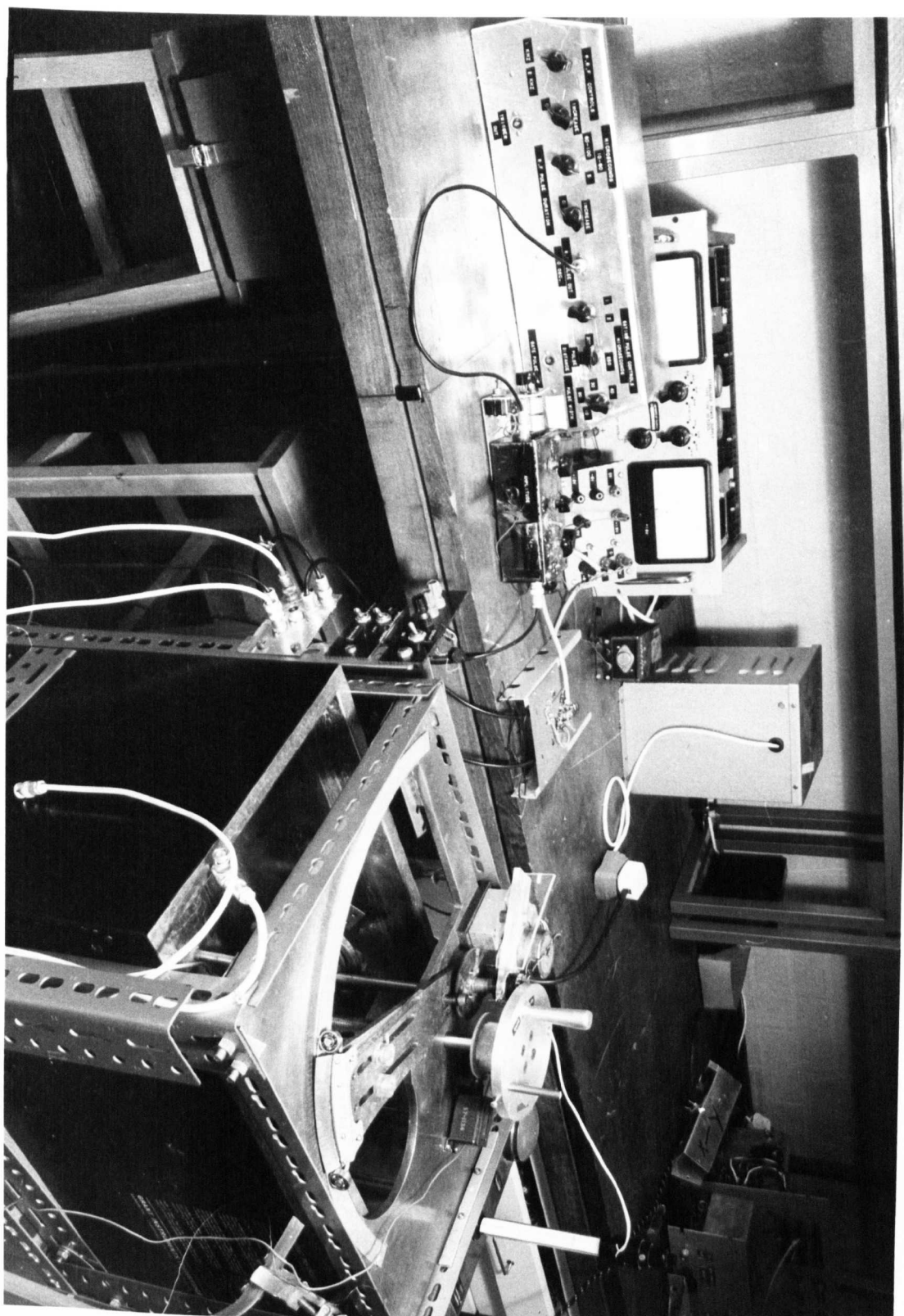


Fig 4.2 Schematic of System used

FIG. 4.3

PHOTOGRAPH OF THE WHOLE SYSTEM





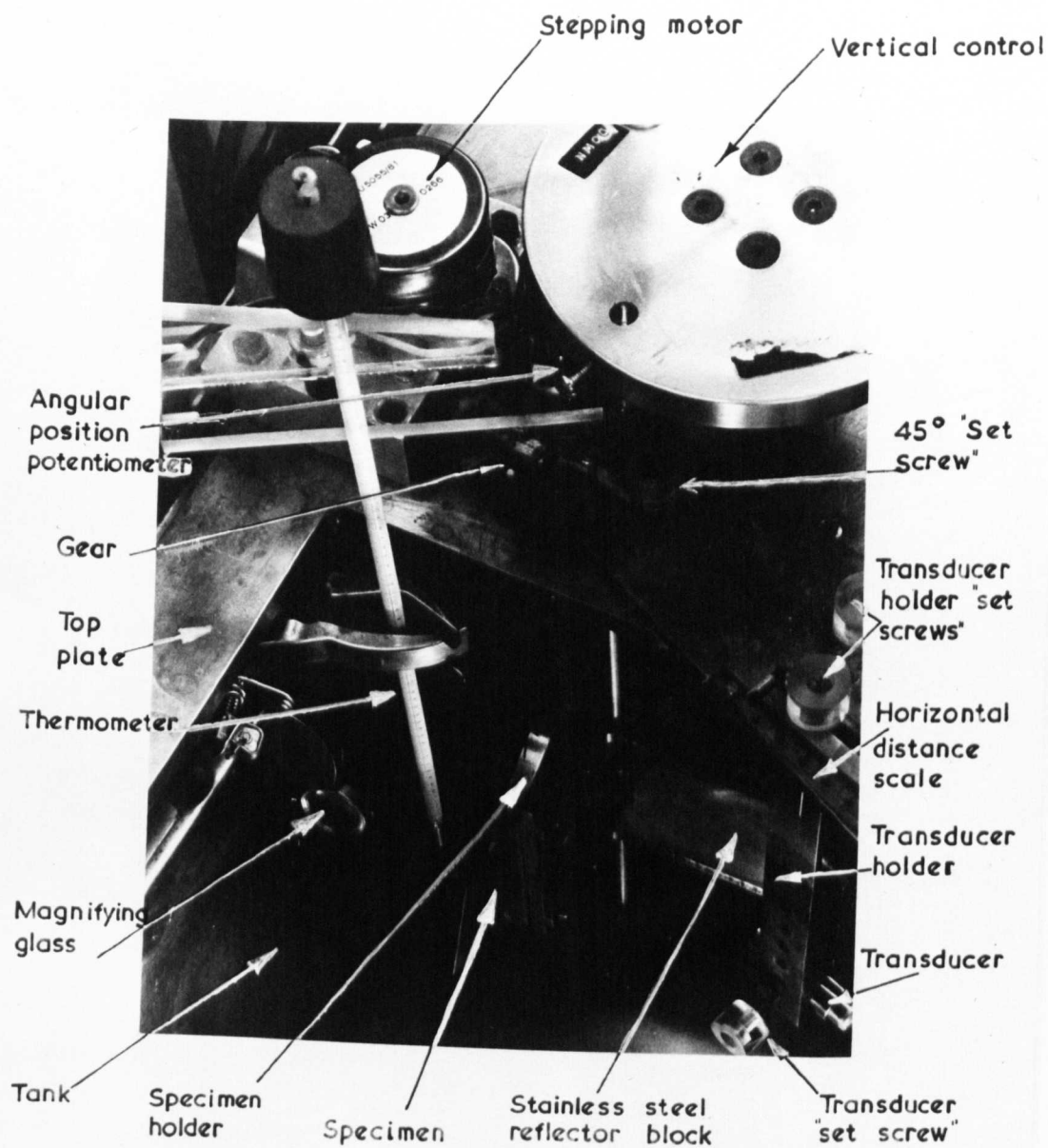


Fig. 4.4.

ULTRASONIC

GONIOMETER

As can be seen the reflector block, the vertical guides and vertical drive were made of stainless steel. All other parts of the goniometer were made of brass. Facilities were provided for varying:-

- (a) The depth of measurement.
- (b) The distance between specimen and transducer.
- (c) The angle of incidence.
- (d) The type of reflector block.
- (e) The orientation of the specimen.

Also there was continuous control in the z direction and in the angle of orientation of the specimen. A vernier scale was included for accurate reading of the main scale. The reflecting surface was highly polished for high frequency measurements. In order to obtain constant dilatational wave velocity in the liquid, a temperature controller was used. A stepping motor was used in some experiments to drive the transducer holder and arm over the top plate. Rollers were fitted to the transducer holder and arm so as to facilitate easy movement on the surface.

A depth gauge was fitted to measure the depth of testing. The gauge indicated the exact position on the specimen being examined along its width. The reflector drive was 15 threads per inch and the gauge read 0.1 revolution. It was therefore possible to locate any position on the specimen to about $\pm 7 \times 10^{-3}$ in.

4.2.1 The reflector block

There were three design considerations in designing the reflector block.

- (a) The surface roughness of the reflecting surface must be negligible.

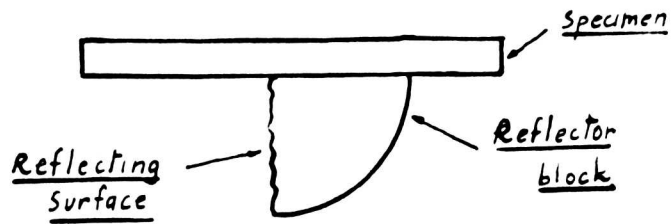


Fig 4.5 Showing surface roughness(S)

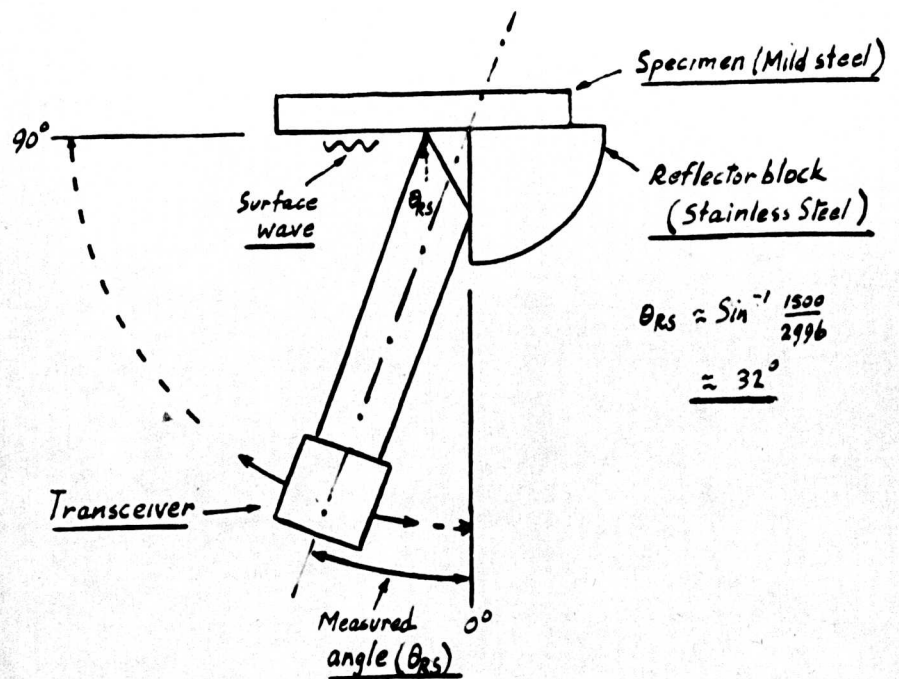


Fig 4.8 Critical angle of Specimen

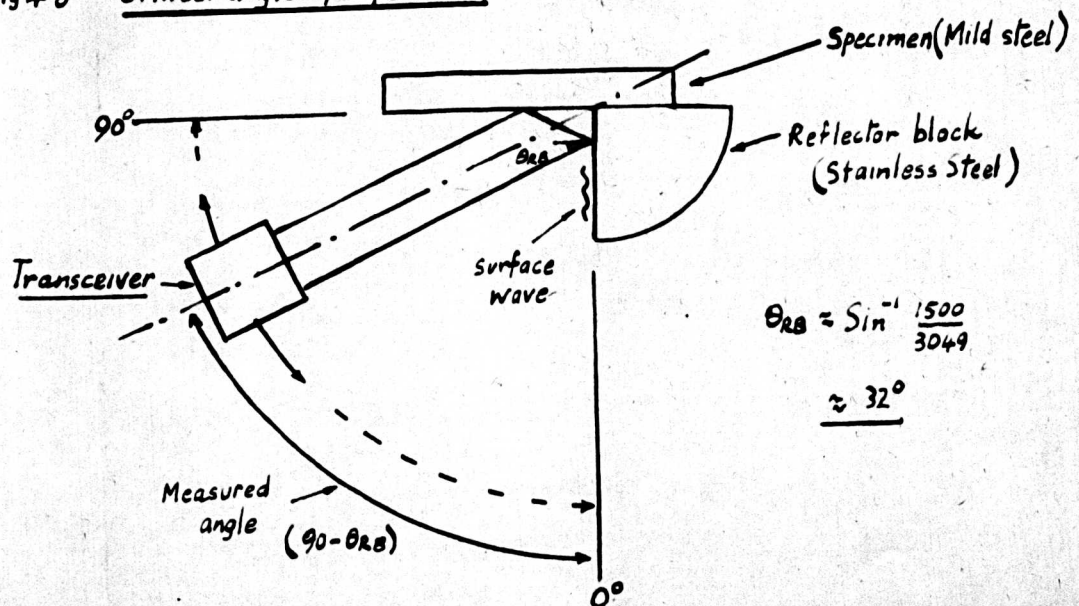


Fig 4.9 Critical angle of reflector

- (b) The critical angle of the block should be far removed from the critical angle of the specimen.
- (c) The block should be made from a non-corrosive material.

For consideration (a), a frequency of 100MHz was considered as being the highest usable frequency. Surface roughness permissible at this frequency was calculated. At this frequency the wavelength in steel is approximately 30 μ m ($C_T \approx 3000$ m/sec.). Therefore for the surface roughness(S) to be less than one wavelength, it should satisfy the condition $-15\mu\text{m} \leq S \leq +15\mu\text{m}$. The surface of the block was polished to get a good surface finish. (see Fig. 4.5). A plot of the surface roughness of the block used can be seen in Fig. 4.5(a).

For consideration (b), a block made of brass was first designed. Figs. 4.6 and 4.7. are results for different types of interfaces using the brass block. On Fig. 4.7 a plot due to Rollins¹²⁶ for a water-aluminium interface is superimposed. As can be seen from the graphs, the complement of the critical angle of the brass block was too close to the critical angle of the specimen. Since most of the tests were to be done on steel or similar specimens it was decided to use a duralumin block. There was a problem of corrosion with this block however, and finally a stainless steel block was used. The critical angle of steel is approximately 32° calculated from $\theta_R = \sin^{-1} \frac{C_f}{C_R}$ (see eqn. 3.18). C_f is the velocity of the dilatational wave in the water, and C_R is the velocity of the surface wave in the specimen.

Corresponding values from Bradfield¹²⁷ are, $C_L \approx 1500$ m/sec for water, $C_R \approx 1964$ m/sec for brass, $C_R \approx 2700$ m/sec for steel. The approximate value for the critical angle for brass is 51° and the complement of this angle is 39°. Therefore when testing steel this angle is not far removed from

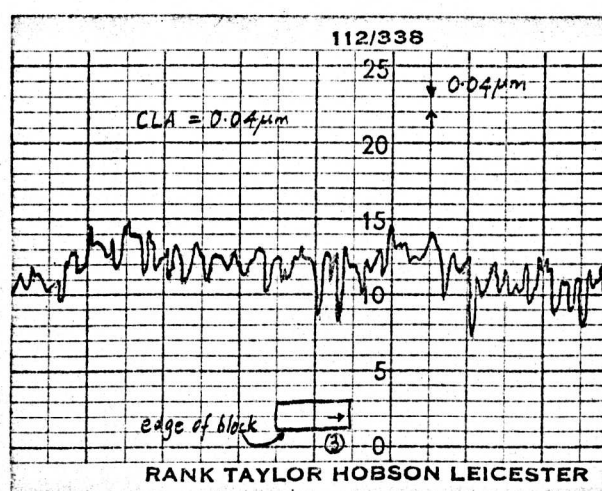
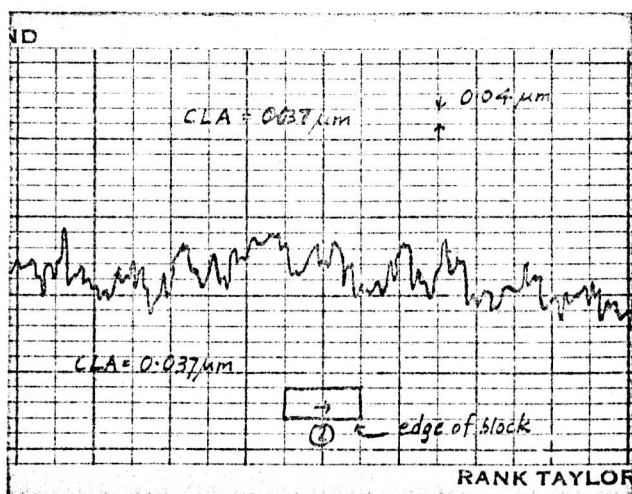
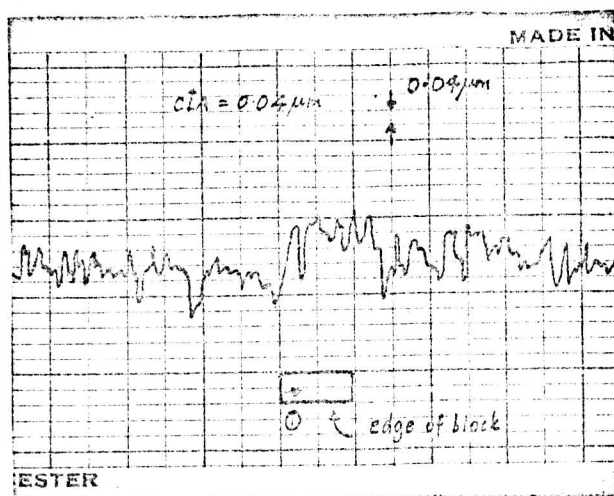


Fig 4.5(a) Showing surface roughness of corner reflector
block (stainless steel) (Tolerance = $\pm 15 \mu m$)

Fig 4.6 Goniogram for a water/brass interface (Room temperature) 4.7 MHz

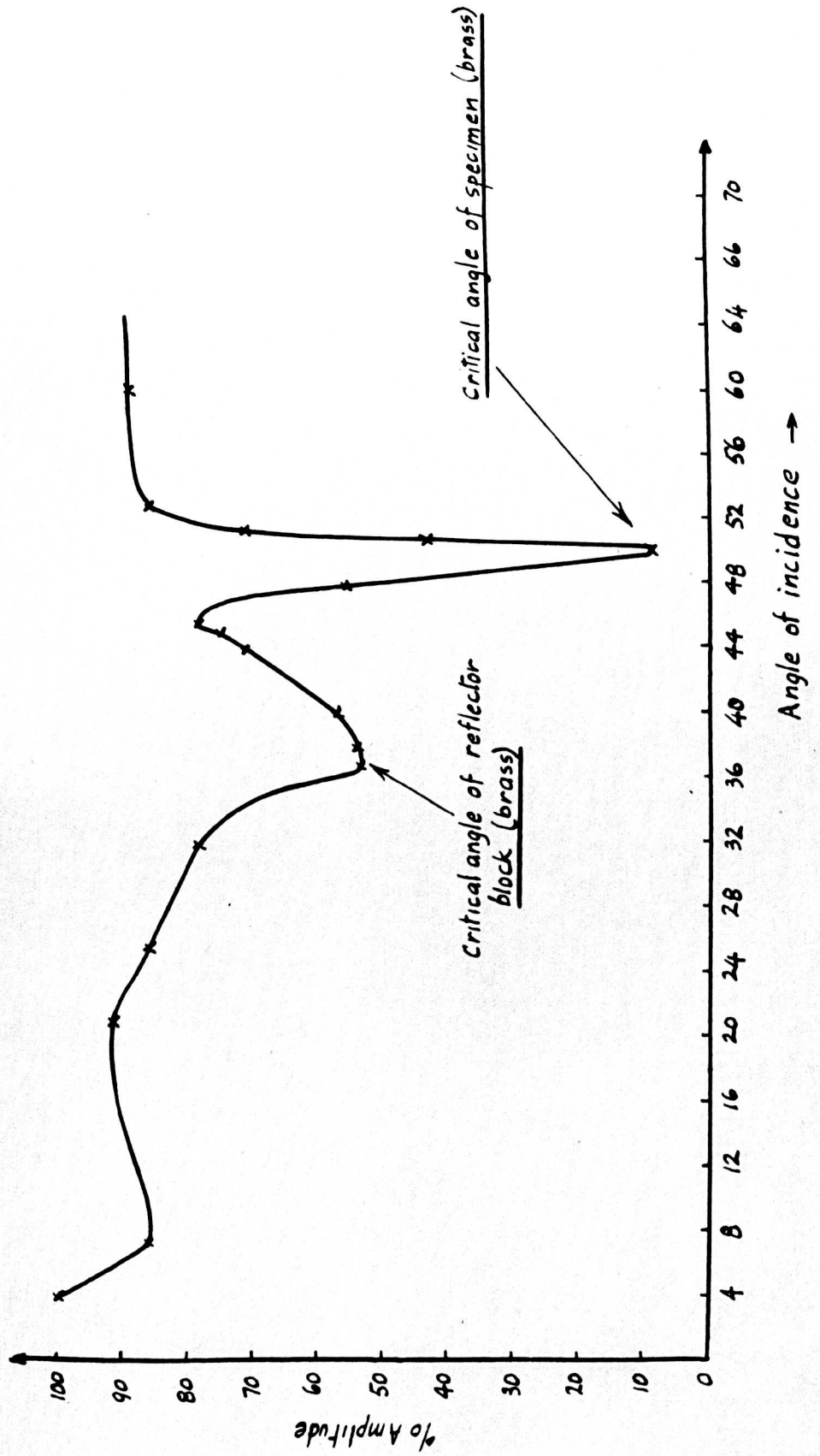
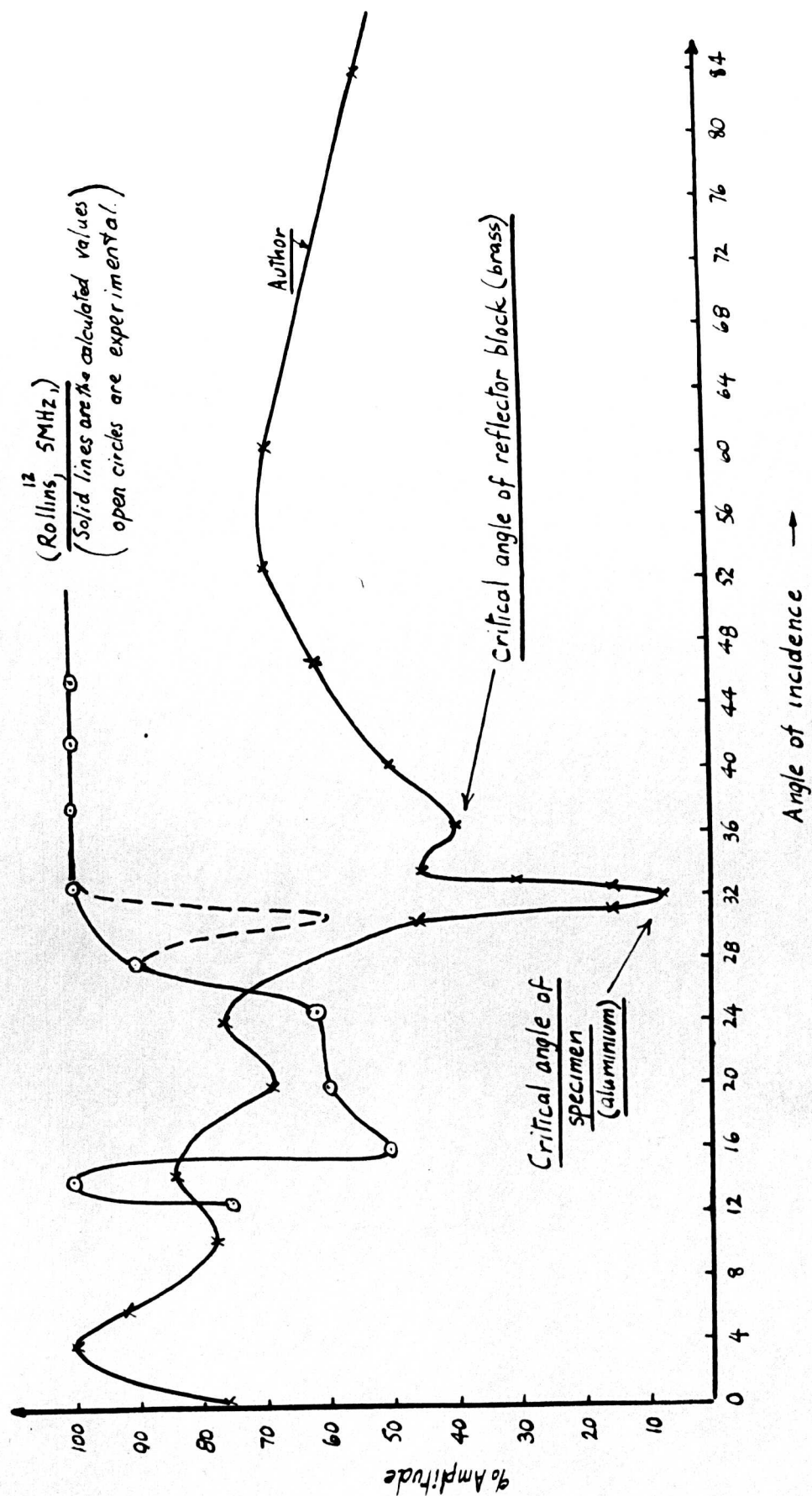


Fig 4-7 Goniogram for a water/aluminium interface (Room temperature) 4.7 MHz



the critical angle for steel ($\approx 32^\circ$). The corresponding value for the critical angle of stainless steel is also about 32° and the complement of this angle is 58° which is far removed from the critical angle of the specimens being tested (See fig.4.8 and 4.9).

The problem of corrosion was solved by using the stainless steel block and by very frequent changing of the water in the tank.

4.2.2 Accuracy

Using the junction of the reflector block and the specimen as centre, a scale marked in degrees was calibrated on the top plate of the goniometer. (see Fig.4.4). A vernier scale was designed to an accuracy of 0.1 degrees. Additionally the digital depth gauge was designed to an accuracy of $\pm 7 \times 10^{-3}$ ins (0.180mm). A position indicator (Fig.4.10), was designed for calibrating the depth gauge, and for setting up the axis of the transducer holder, with the corner of the specimen and reflector block. A 45° "set screw" was used to locate the transducer arm in position. (see Fig.4.4).

4.2.3 Specimen holders

The specimen holders were designed so that they could hold the specimen firmly against the back of the reflector block, and also so that rotation will be possible in the vertical plane. Therefore when the specimens are mounted in the holder, and fastened on to the back of the block, tests could be conducted through 90 degrees on the specimens. Fig.4.11 shows photographs of the specimens mounted in their holders.

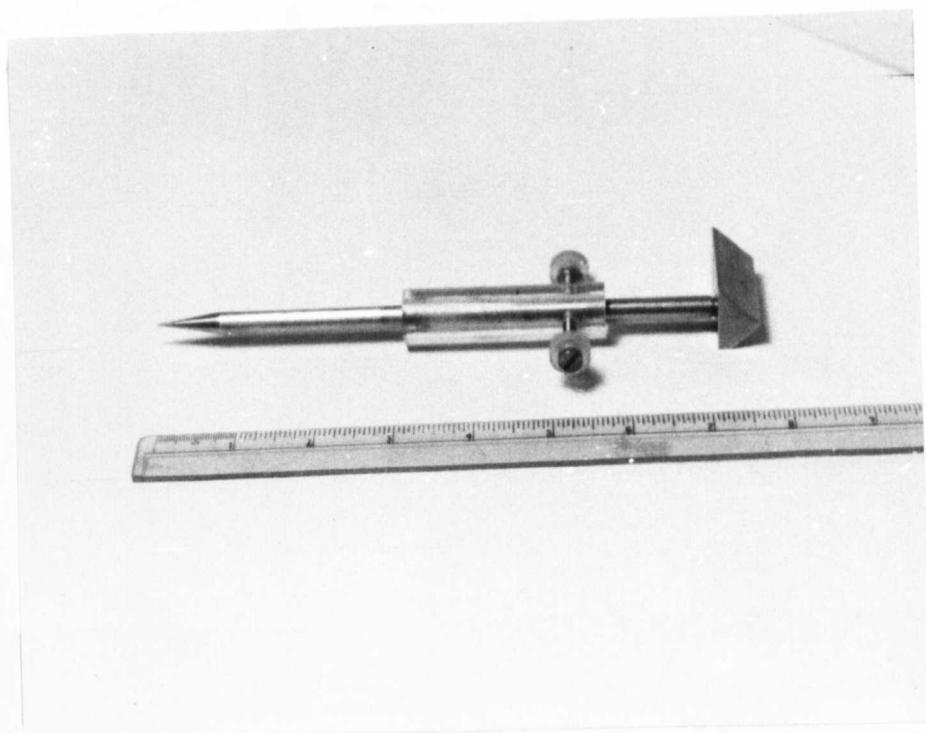


Fig. 4.10 The position indicator.

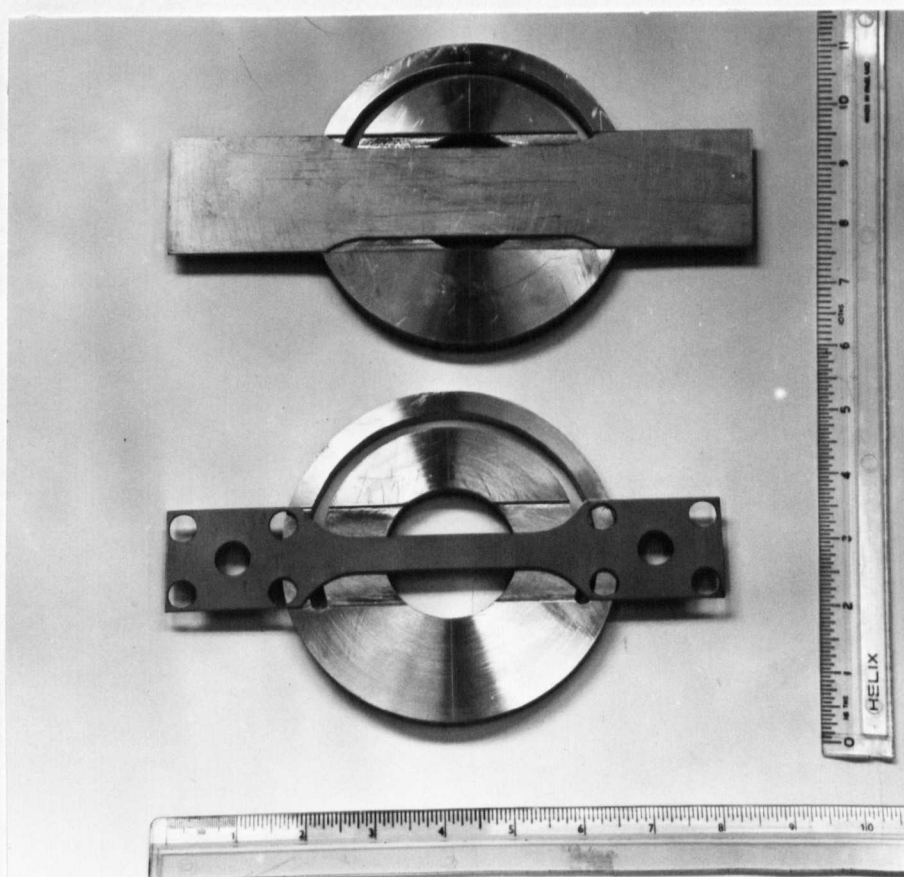


Fig. 4.11 Showing specimens in their respective holders

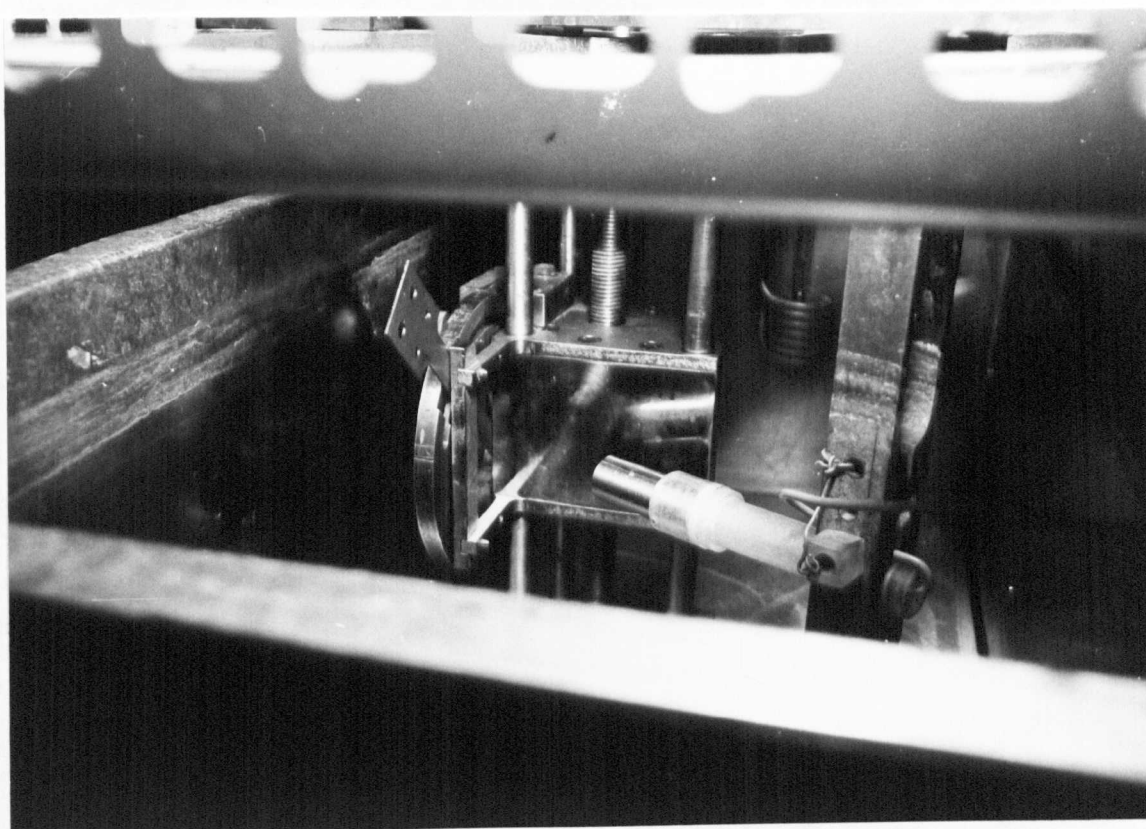


Fig.4.12 Inside view of the Ultrasonic Goniometer.

Specimens of different shapes and thicknesses had to be tested therefore different holders had to be designed for each type of specimen. The holders were all made of brass and their centres of rotation coincided with the centre of the edge of the reflector block. Fig.4.12 shows the inside of the goniometer with a specimen mounted at an angle in its holder. Fig.4.13 shows the rear of the reflector block with a specimen mounted in its holder.

4.3 The medium

The medium used for propagating the dilatational wave was water. This choice was made because:-

- (a) The velocity of the dilatational wave in water is such that when testing most metals, the critical angle of incidence is real and positive. The required condition for mode conversion in immersion testing is that the velocity of waves in the liquid should be very much lower than the shear wave velocity in the solid.
- (b) Water is easy to acquire and deal with.

4.3.1 Temperature considerations

It is well known ¹²⁷ that the velocity of dilatational waves in water changes with temperature. The density also changes with temperature. ¹²⁸ Fig.4.14 shows this velocity varies with temperature. Superimposed on this is a graph showing how the measured critical angle changes with temperature, after the temperature had been controlled to within 0.01 deg.C. Another graph Fig.4.15 shows the change in measured critical angle when

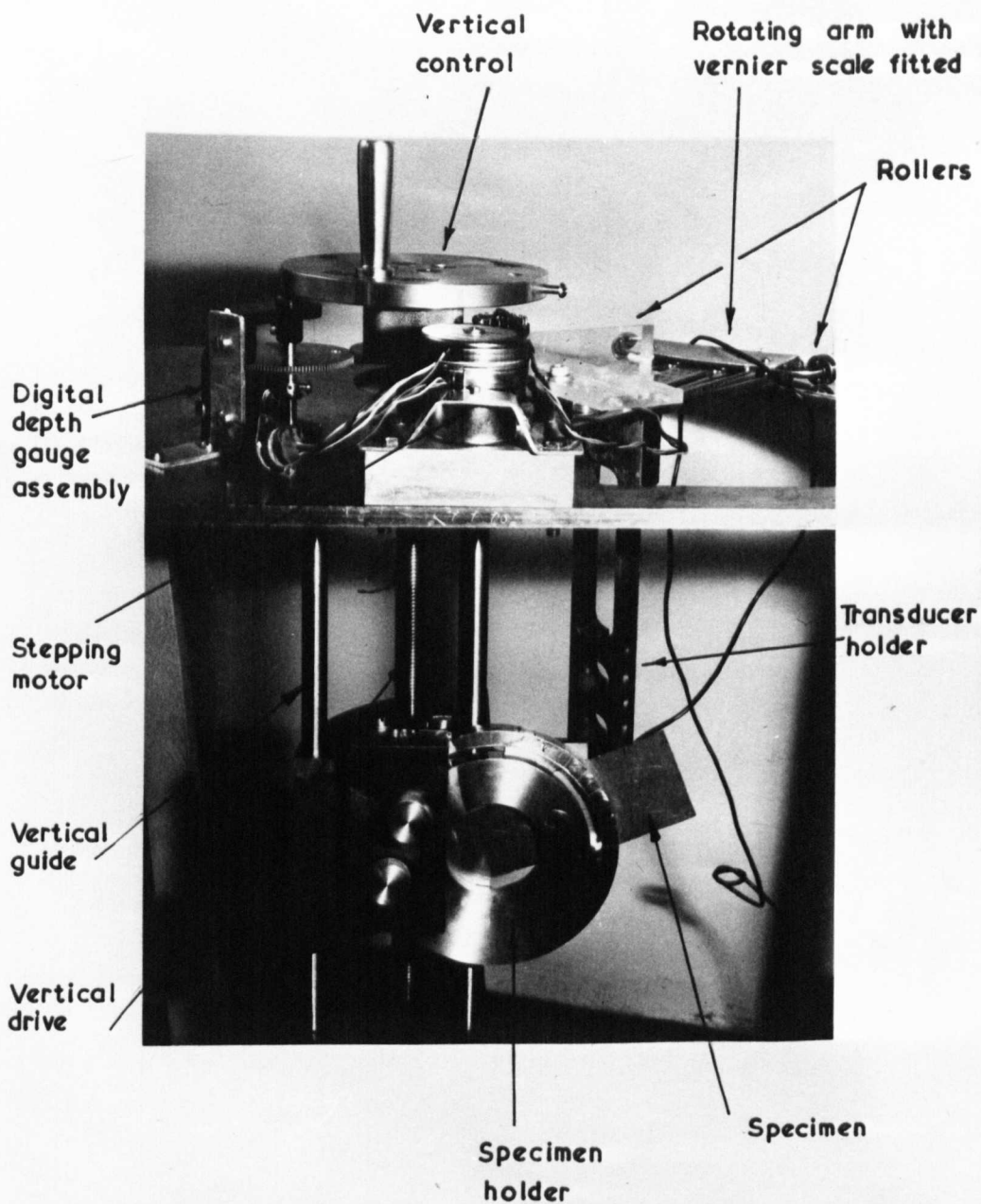


Fig. 4.13.

ULTRASONIC

GONIOMETER (BACK VIEW)

the temperature is controlled to within 0.1 deg.C.

A theoretical analysis was done to ascertain the effect on the measured critical angle due to temperature changes. The result of this analysis is shown below.

Theoretical analysis of the effects on measured critical angle
due to changes in temperature.

Basically from Snell's law (see eqn.3.18),

$$\sin \theta = \frac{C_1}{C_R} \quad \text{where } \theta = \theta_R \text{ the Rayleigh angle.}$$

C_1 = Dilatational wave velocity (C_f).

C_R = Surface wave velocity.

therefore:-

$$-\frac{d\theta}{\theta} = -\frac{C_1}{\theta C_R \cos \theta} \left[\frac{dC_1}{C_1} - \frac{dC_R}{C_R} \right] \dots\dots\dots 4.1$$

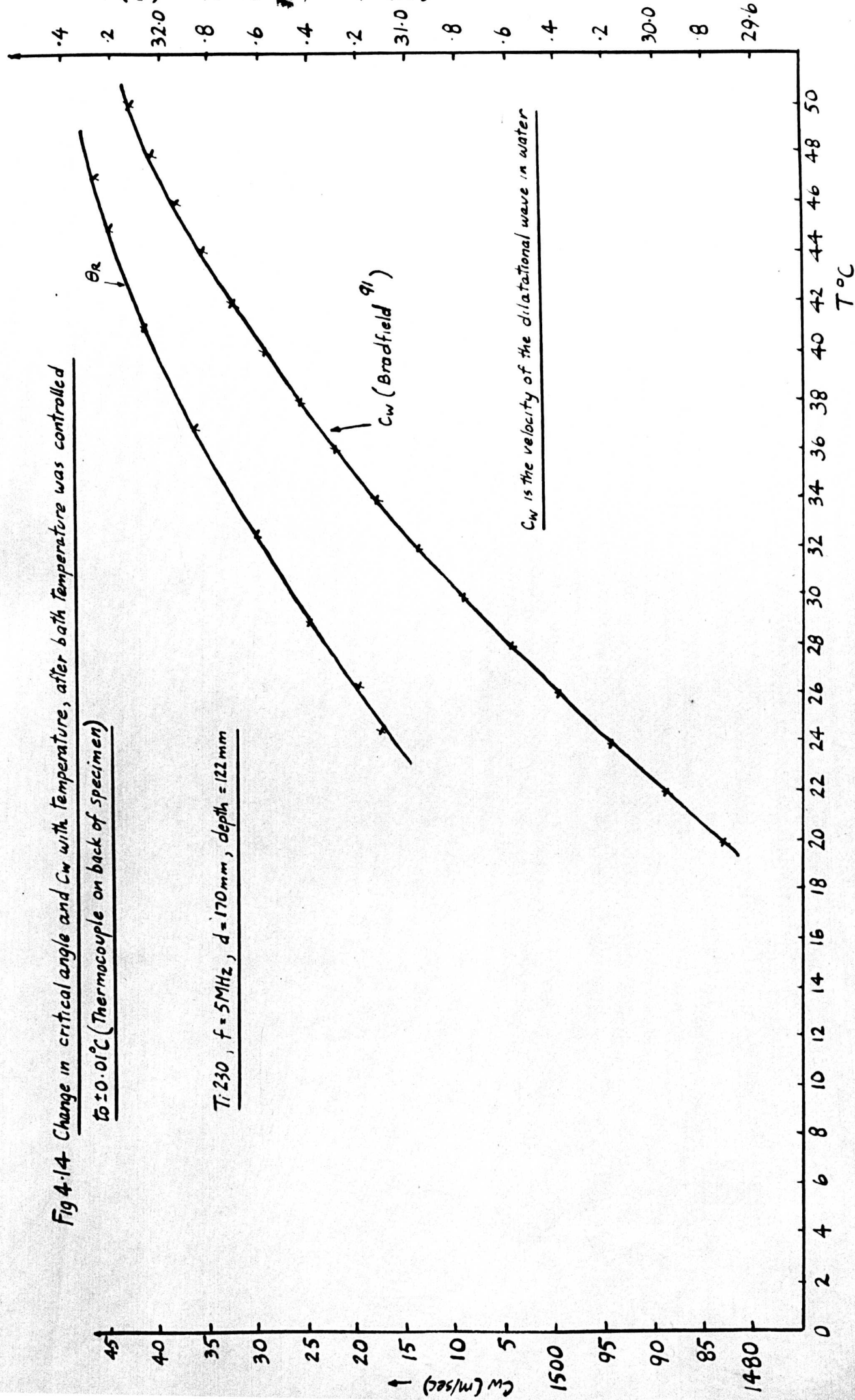
The expression above says that both the changes in C_1 and C_R due to temperature should be taken into account. From Bradfield¹²⁷ $\frac{dC_1}{C_1} = .002$ per deg.C in the region of 20°C.

Also from the same source, for Titanium at 20°C, $C_R = 2958\text{m/sec}$, and θ (calculated) = 30.08 degrees. Additionally the apparent temperature coefficient of elasticity was given as $-0.080/^\circ\text{C}$. This value is dependent upon the extent of preferred orientation and hardness.

Fig 4-14 Change in critical angle and C_w with temperature, after bath temperature was controlled

to $\pm 0.01^\circ\text{C}$ (Thermocouple on back of specimen)

$T: 23.0$, $f = 5\text{MHz}$, $d = 170\text{mm}$, depth = 122mm



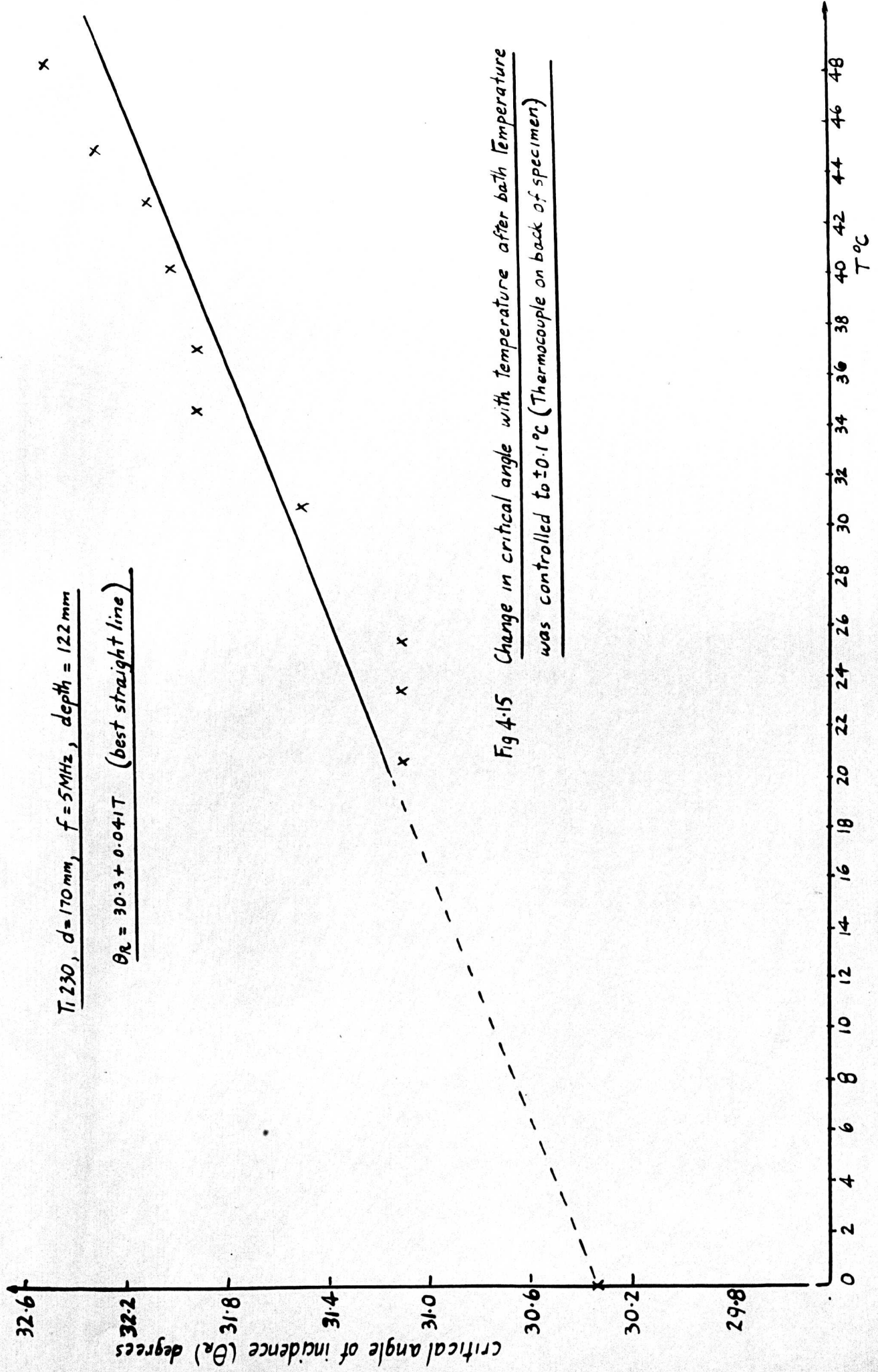


Fig 4-15 Change in critical angle with temperature after bath temperature was controlled to $\pm 0.1^\circ\text{C}$ (Thermocouple on back of specimen)

Assume that the material is nearly isotropic, and neglecting the coefficient of linear expansion, the apparent temperature coefficient will be the same as the true temperature coefficient. The given value of temperature coefficient of elasticity is for the shear modulus and a similar figure is assumed for the bulk modulus. Approximately similar results¹²⁷ were given for the temperature coefficient for the two Moduli for different materials. This value of temperature coefficient is the only one given in the literature.

$$\text{Now since } C_R \approx \sqrt{\frac{\mu}{\rho}} \quad \text{where:- } \mu = \text{shear modulus of the solid.}$$

$$\rho = \text{density of the solid.}$$

$$\text{then } \frac{dC_R}{C_R} \approx \frac{1}{2} \frac{d\mu}{\mu} \quad \text{if the change in density of the}$$

of the material can be neglected.

$$\text{or } \frac{dC_R}{C_R} \approx \frac{1}{2} (-0.080) \approx -0.40 \text{ per deg.C}$$

Substituting these values in equation 4.1 we get:-

$$\frac{d\theta}{\theta} = 0.0463 \text{ per deg.C}$$

θ on the right hand side of the equation was in radians and the value of C_1 was taken as 1482.66m/sec.

In the region of $\theta = 30^\circ$

$$d\theta = 30 \times 0.0463 = 1.4 \text{ degrees per deg.C}$$

$$\text{or } d\theta = 0.14 \text{ degrees per } 0.1 \text{ deg.C}$$

This means that if the bath temperature varies by 0.1°C the error generated in the measuring system is 0.14 angular degrees. The resolution is 0.1 angular degrees, so that temperature control to within $\pm 0.01^\circ\text{C}$ was considered necessary to reduce temperature dependent errors to 0.014 angular degrees.

4.3.2 Depth consideration

Consider the error in θ due to the variations in C_1 with depth of testing.

$$C_1 = \sqrt{\frac{k}{\rho}} \quad \text{where:- } k = \text{the bulk modulus of the liquid.}$$

$$\rho = \text{the density of the liquid.}$$

therefore

$$\frac{dC_1}{C_1} = -\frac{1}{2} \frac{d\rho}{\rho} \quad \dots\dots\dots 4.2$$

since $\rho = \frac{1}{h}$ and $d\rho = -\frac{dh}{h^2}$ therefore eqn.4.2 becomes:-

$$\frac{dC_1}{C_1} = \frac{1}{2\rho} \frac{dh}{h^2} \quad \dots\dots\dots 4.3$$

If we assume a depth of 200mm and a value of dh equal to 100mm the maximum variation in the system, then the change in C_1 will be negligible. Therefore it is thus seen that the error in θ due to finite depth variations can be neglected.

4.3.3 Distance consideration

All ultrasonic probes have a radiation field pattern comprising of two energy zones i.e. (a) the near field (Fraunhofer zone) and (b) the far field (Fresnel zone). Usually in immersion testing the far field region is used where the beam is well defined.

Sometimes however it is not possible to use this region because the acoustic path lengths at high frequencies will be too large thus giving rise to excessive attenuation. Fig 4.16 shows

142

the acoustic pressure versus distance plot for a probe. The expression used for calculating the maxima (Y_m^+) and the minima (Y_m^-) are shown below (see McElroy¹²⁹).

If a = the diameter of the crystal and,

λ = the wavelength, then these intensities can be written as:-

$$Y_m^+ = \frac{4a^2 - \lambda^2 (2m + 1)^2}{4\lambda (2m + 1)} \quad \text{where } m = 0, 1, 2, 3, \dots$$

$$Y_m^- = \frac{a^2 - \lambda^2 m^2}{2m\lambda} \quad \text{where } m = 1, 2, 3, 4, \dots$$

In water $\lambda^2 \ll a$ the equations can be reduced to simpler forms.

The recommended region for immersion testing is the region Y_1^- to Y_0^+ , Although the author was aware of this consideration, it was decided to use a convenient test distance which will give a good reflection. The distances used can be seen in the table below. The nearest maximum and minimum points were calculated to indicate respective positions along the axis of the probe.

| Frequency MHz | Wavelength in water (mm) | Test distance used (mm) | Calculated (mm) | |
|------------------|-----------------------------|----------------------------|--------------------|--------------------|
| | | | Nearest minimum | Nearest maximum |
| 2 | 0.75 | 90 | $Y_1^- = 67$ | $Y_0^+ = 90$ |
| 5 | 0.3 | 60 | $Y_3^- = 56$ | $Y_2^+ = 67$ |
| 10 | 0.15 | 60 | $Y_6^- = 55$ | $Y_5^+ = 61$ |
| 15 | 0.1 | 60 | $Y_9^- = 56$ | $Y_8^+ = 59$ |
| 25 | 0.06 | 40 | $Y_{21}^- = 40$ | $Y_{20}^+ = 42$ |

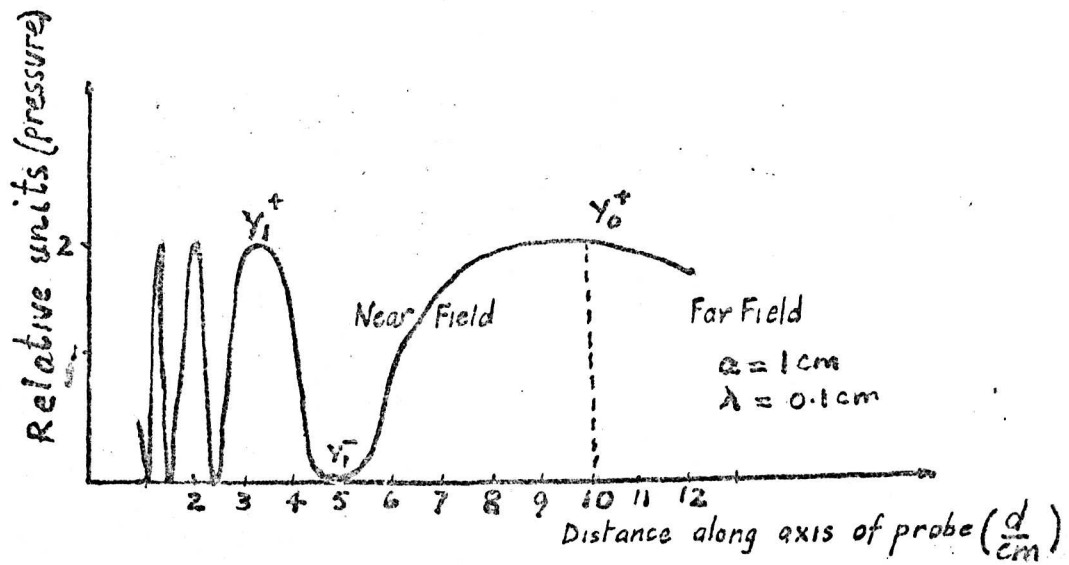


Fig 4.16 Typical theoretical axial pressure distribution curve for a longitudinal probe. (after Blitz¹⁴²)

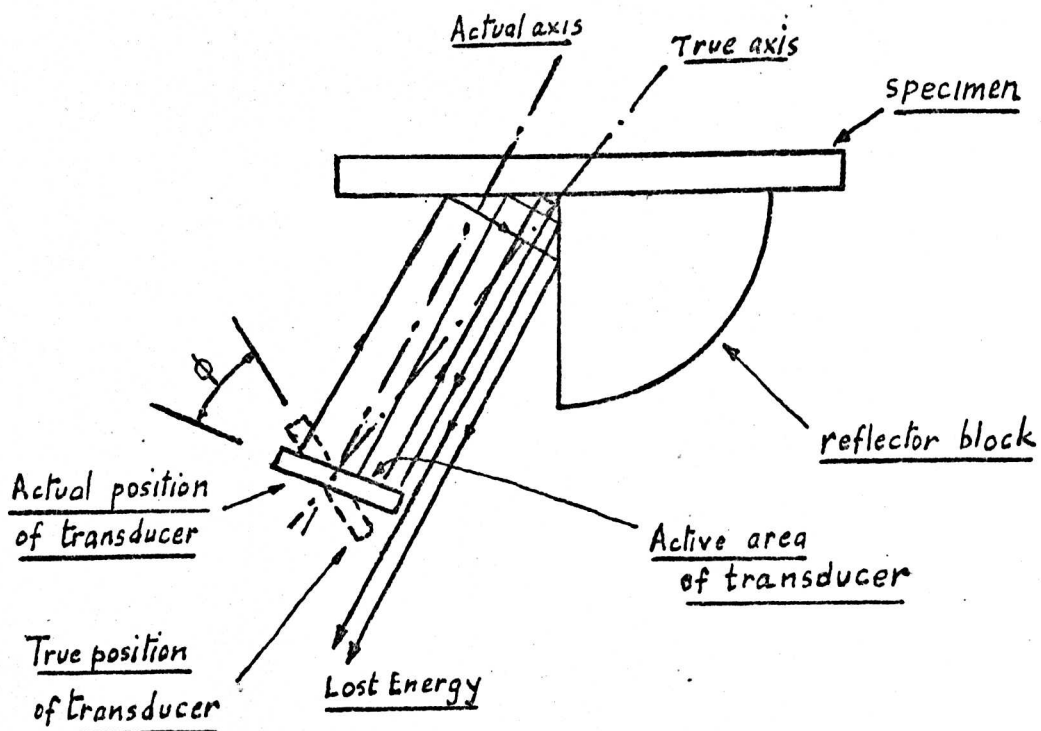


Fig 4.17 Showing the effect on receive signals due to ultrasonic beam deviation

The crystal dismeter used was 10mm. Using these distances the required reflection was obtained. All the probes used throughout the work were acquired commercially, except for the 25MHz probe which was manufactured by the author. Rollins⁹² used a 16mm crystal to generate frequencies from 15 to 85 MHz without changing the test distance.

4.3.4 Beam directivity

For good beam directivity (less than 5° spreading angle) a crystal diameter to frequency ratio is recommended to be 20. The table below shows the actual ratios used in the experiment.

| Frequency(MHz) | 2 | 5 | 10 | 15 | 25 |
|----------------------------------|------|------|----|-----|-----|
| $(\frac{a}{\lambda})$ ratio used | 13.3 | 33.3 | 59 | 100 | 167 |

Although these were not the recommended values, there are no reasons to believe that a large spreading angle will alter the quality of the results obtained.

Many workers^{123,110} have reported on beam spreading at low frequencies. No problems were reported when using higher frequencies.

4.3.5 Beam deviation

If the crystal in the probe is not mounted square with the axis of the transducer, the radiating energy could leave the probe at an angle. Fig.4.17 shows a similar type of beam becoming incident on the corner reflector. Let ϕ be the angle of deviation, then ϕ has a limiting value. If ϕ is large, then no energy will be reflected back into the transducer. For small values of ϕ however, only part of the transducer will be active. The remainder of the reflected signal will be lost in the fluid. Therefore

the problem of beam deviation does not affect the quality of the results obtained. A tool was designed to ensure that during mounting, the axis of the transducer bisects the 90° angle made by the specimen and the reflector block.

4.3.6 Effect of skip distance or interference due to reradiated wave

As mentioned in section 3.2.1, the skip distance is important in the measurement of critical angle. In two-probe testing (Fig. 3.12) the transducer is sometimes shifted laterally a distance Δ given by eqn. 3.22. Richardson and Becker¹¹⁰ displaced the receiving transducer by this value in their experimental work.

Using the corner reflector however, as was used in this work skip distance (beam displacement) has different implications because only one probe was used. Consider the energy leaving the right hand side of the probe. (see fig. 4.18). The waves becoming incident at the reflector block will be reflected 180° out of phase with the incident beam. They then become incident at the specimen where some of the energy is directly reflected. Assuming that the waves skip along the surface by a distance Δ , then it is very likely that it will miss the transducer after leaving the surface. Because the skip distance is proportional to the wavelength, larger skip distances occur at lower frequencies.

Waves leaving the left hand side of the transducer (see fig. 4.19), will become incident on the specimen, and a part of this wave will be directly reflected, via the reflector block. The remainder of the energy will skip the distance Δ then emerge to become incident on the reflector

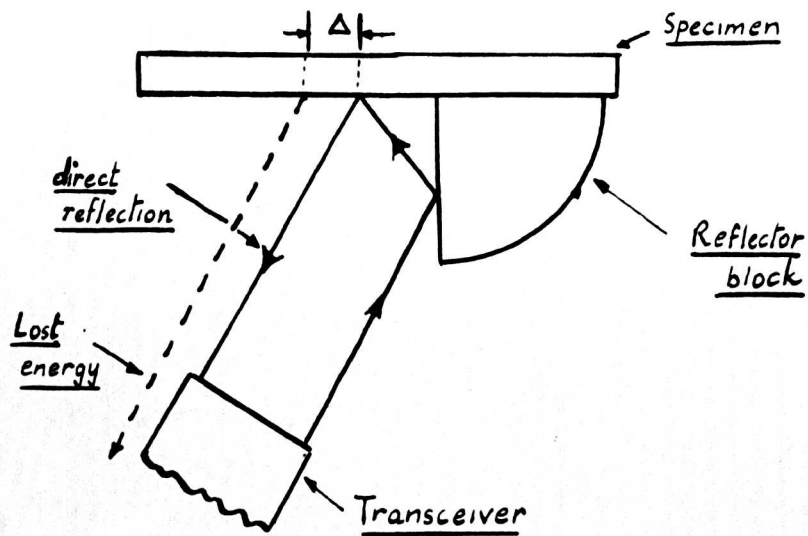


Fig 4-18 Showing the effect of "skip distance" (Δ) on waves leaving the right hand side of the transceiver

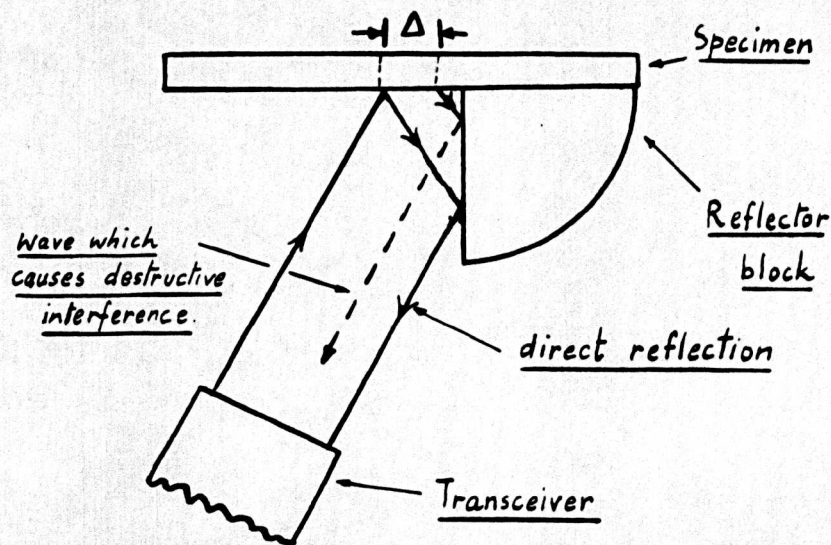


Fig 4-19 Showing the effect of "skip distance" (Δ) on waves leaving the left hand side of the transceiver

71

block. On reflection, this wave will be out of phase with the directly reflected beam. Therefore, destructive interference will take place between the two waves, which will increase the depth of the trough measured at the critical angle, because less reflected energy will reach the transducer.

4.4 The transducers

The transducers used for all frequencies except 25 MHz were commercial immersion type longitudinal probes. The crystals in the probes were acoustically backed with tungsten loaded araldite. The 25 MHz probe was manufactured by the author. Manufacturing details can be seen in Appendix 1. A photograph of the probe can be seen in Fig.4.20.

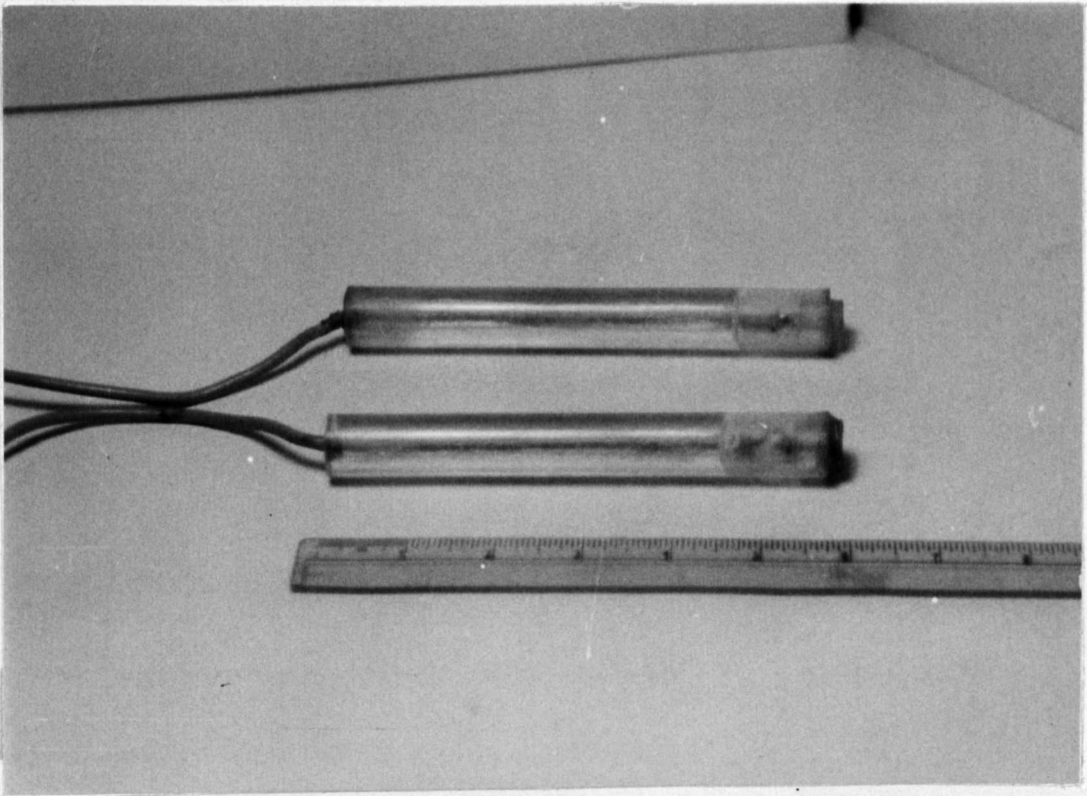


Fig. 4.20 Photograph of manufactured probe.

CHAPTER 5

ELECTRONIC INSTRUMENTATION

Introduction

The block diagram of the electronic system is shown in Fig.5.1. It was decided to use pulsed continuous waves to excite the transducer instead of a pulse which has so many unwanted frequency components. The pulse had to be long enough to simulate quasi-continuous wave conditions.

The astable multivibrator gave a pulse repetition frequency of 1 to 3 kHz. This in turn drove a monostable circuit whose output determined the pulse width of the test signal. Facilities were provided for varying the pulse width from 0.5 to 15 μ s. The output of the monostable pulsed the sinusoidal oscillator, giving the pulsed continuous waves. Additionally the output of this monostable circuit could be used to trigger the first monostable circuit on the receive side. (see appendix 6). The echo received from the surface of the specimen was amplified in the receive amplifier then displayed on the oscilloscope.

5.1 Astable Multivibrator

The circuit diagram of the astable multivibrator can be seen in Fig.5.2. The pulse repetition frequency used was based on the consideration of the test distance used. A range of possible test distances were used to calculate the required pulse repetition frequency (p.r.f). The range selected was 20 to 150mm. The time intervals in water were from 27 to 300 μ s. Therefore the width of the test pulse had to be short compared with the lowest value.

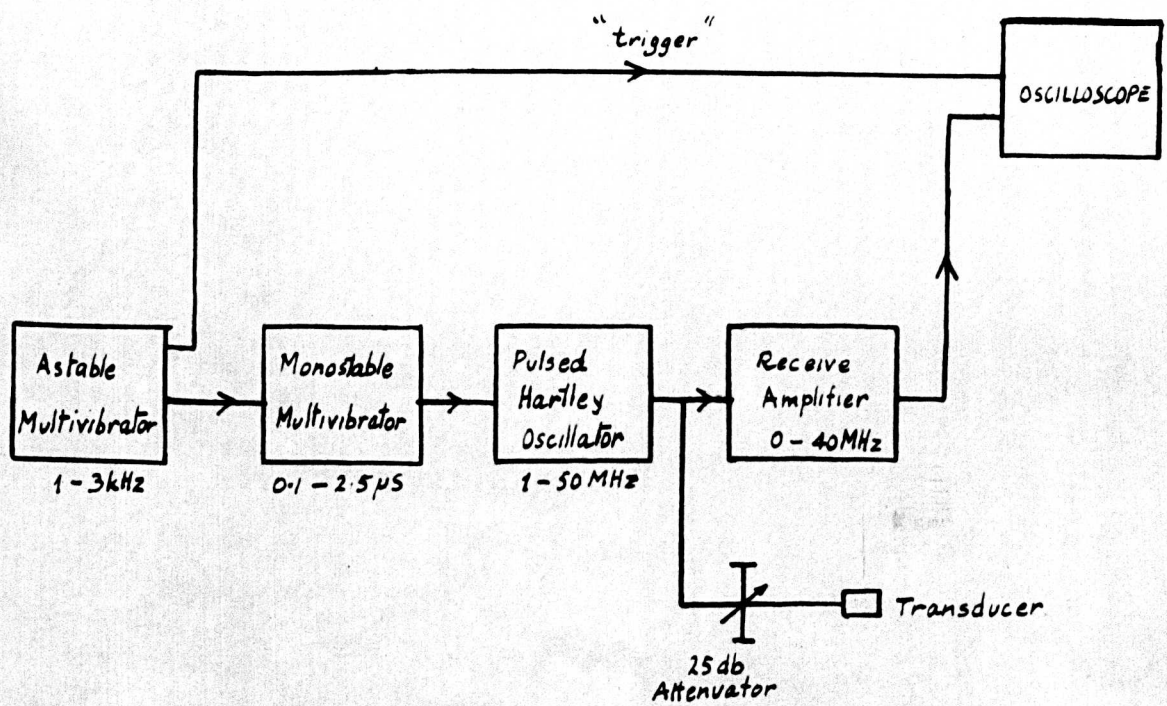


Fig 5.1 Block schematic of electronic system

These values were calculated from $t(\mu s) = \frac{2d}{C_f}$ where d is the test distance in mm, and C_f is the velocity of the dilatational wave in water ($\approx 1.5 \times 10^6$ mm/sec). A p.r.f. of 1.2kHz gave a time repetition cycle of 820 μ s. This is greater than any of the two time intervals given for water. It was therefore decided to use the p.r.f of 1.2kHz.

The mark to space ratio was varied using the 50k Ω variable resistor. The output of the astable was fed to a differentiator with a diode in parallel to prevent any positive going signal from passing to the next stage.

5.2 The Monostable Multivibrator

The monostable multivibrator (Fig.5.2) was used to generate the pulse to "key" the sinusoidal oscillator. The "trigger" pulse from the previous stage was passed on to the first transistor, a PNP, which switches it on and switches the other transistor off, for the period of the monostable circuit, which lay within the range 0.1 to 2.5 μ s.

There were facilities for continuous variations of this period. For the design it was important that the output of this monostable circuit i.e. the gating pulse, had short rise and fall times, since this determined the nature of the signal for exciting the transducer.

The signal from this monostable circuit was passed to a circuit where it was amplified thence to two emitter followers. The emitter followers were necessary to prevent loading of the circuit by the coaxial (75 Ω) cable which was used to pass the gating pulse to the oscillator. The gating pulse had a rise time of 100ns and a fall time of 150ns.

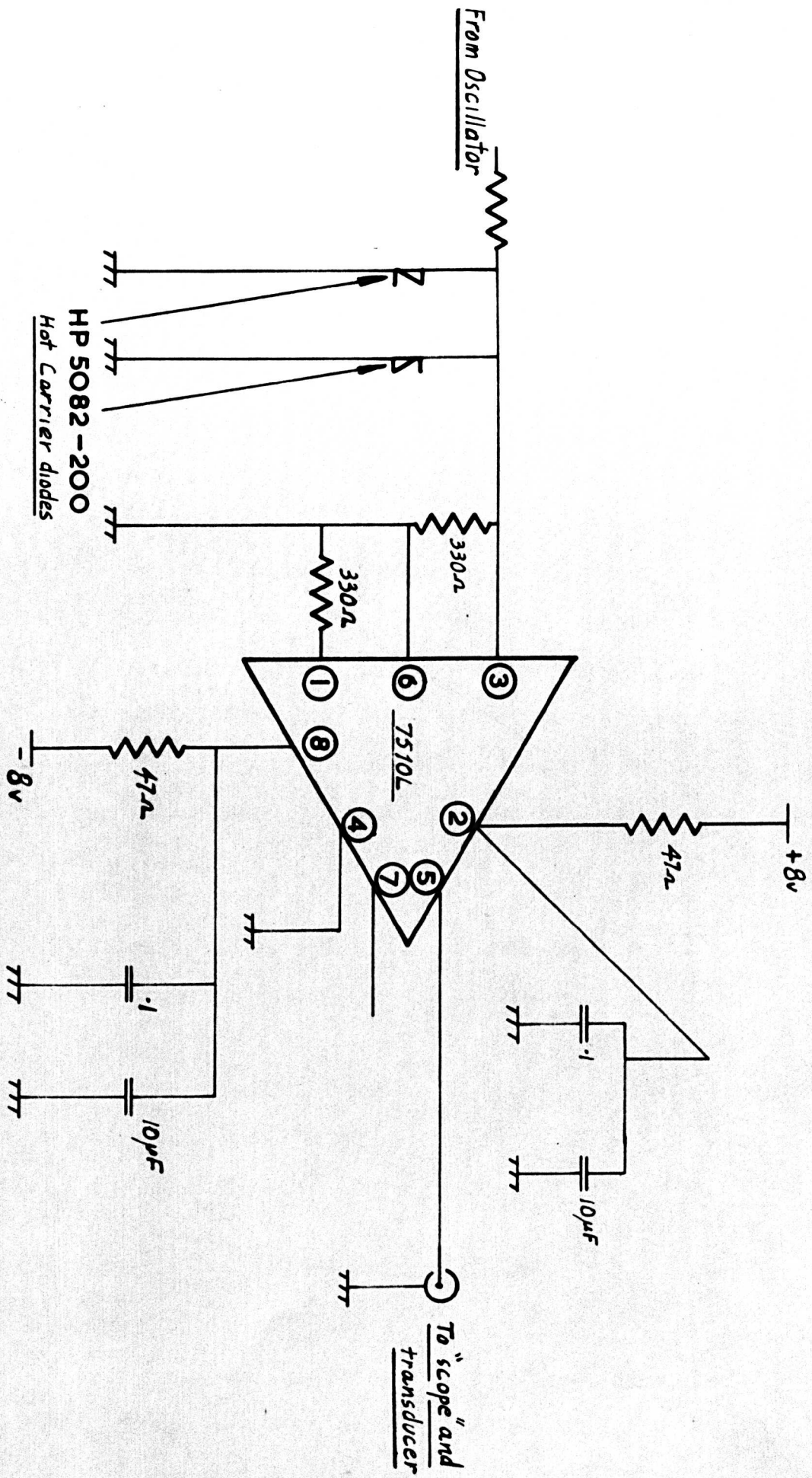


Fig 53-1 Receive Amplifier

5.3 The sinusoidal oscillator

The sinusoidal oscillator can be seen in Fig.5.3. A F.E.T(MPF103) was used in this oscillator. It was a Hartley oscillator and different frequencies were generated by switching ranges. A changeover switch was used to increase the frequency range. Frequency ranges were 1.5 to 3MHz, 3 to 5MHz, 10 to 15MHz, 15 to 20MHz, 25 to 30MHz and 30 to 35MHz. A variable capacitor(18pF) was used to cover the band of frequency in each range. A major problem was encountered when trying to supply the transducer directly from the oscillator, since the output impedance of the F.E.T in this configuration is very high. It therefore was necessary to design a matching circuit for the oscillator. The signal was fed through a 22pF capacitor to a F.E.T amplifier(MPF103). The output of the amplifier was fed to an emitter follower which used an NPN high frequency transistor (BLX67). The coaxial cable was then connected through a 10pF capacitor. There was then no loading of the oscillator.

The keying of the oscillator was done by using the gating pulse to switch "hard on" a PNP transistor(2N3906), when the gating pulse was negative. Then, no output was obtained from the oscillator since the source was at earth potential. For the duration of the gating pulse, when the potential was zero, the PNP transistor was switched off and the oscillator gave an output.

5.4 The signal used

The test method used in this work (ultrasonic reflectometry) was dependent on a reflected pulse reaching a minimum. It was therefore necessary to ensure that all parts of the envelope followed the same

amplitude to angle profile. If the envelope contained too many frequency components then each frequency component *would* have a different minimum. With this criterion under consideration it was decided to use quasi-continuous waves to excite the transducers. Under these conditions the received echo envelope should contain no other frequency but the fundamental.

A theoretical analysis on the frequency components in a 3 cycle sinusoidal pulse was done by Gericke¹³⁰. It was found that the frequency components in the spectrum were as shown in Fig. 5.4. It can be seen that the amplitude of the fundamental (5MHz), is much higher than the amplitude of the other components.

The author did an analysis on a 2 cycle and a 5 cycle pulse and calculated the relative amplitudes of the respective frequency components. (see appendix 2) The results of the analysis can be seen plotted in Figs. 5.5 and 5.6. It can be seen that for the 2 cycle pulse frequency components near the fundamental are very high in amplitude whereas for the 5 cycle pulse this is not the case. In the study reported in this thesis, pulses containing more than 5 cycles were used.

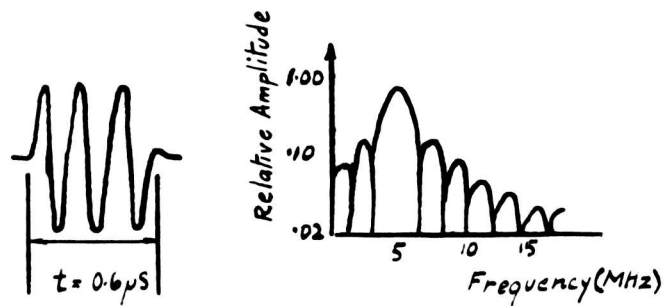


Fig 5.4 Frequency components in a 3 cycle sinusoidal pulse.
(due to Gericke¹³⁰)

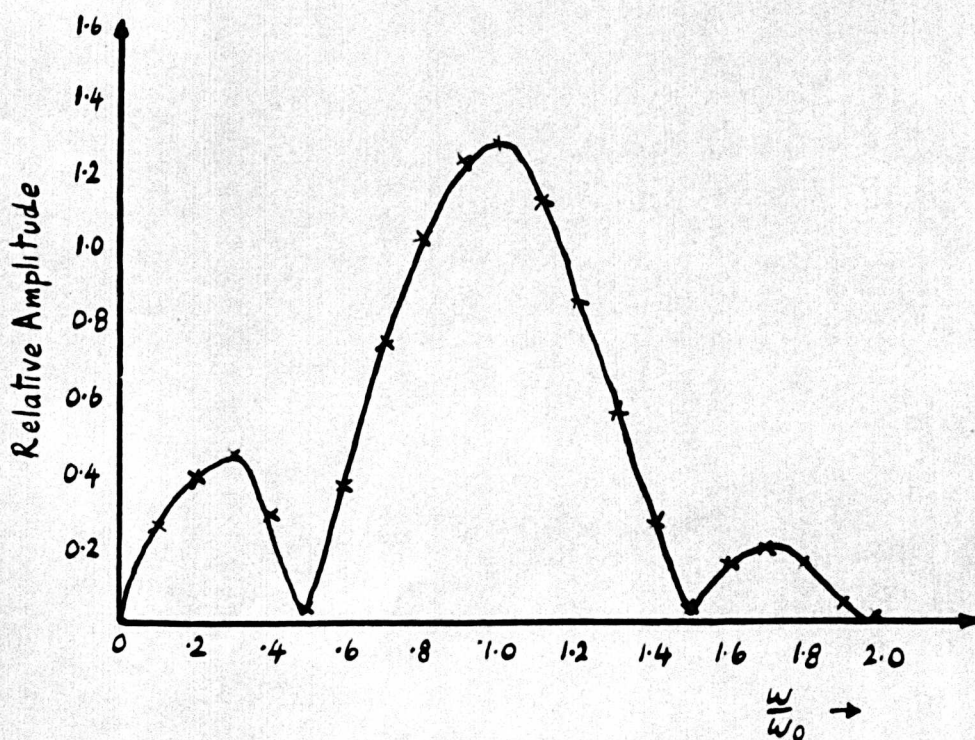


Fig 5.5 Frequency component in a 2 cycle sinusoidal pulse.
(due to Author) see appendix 2

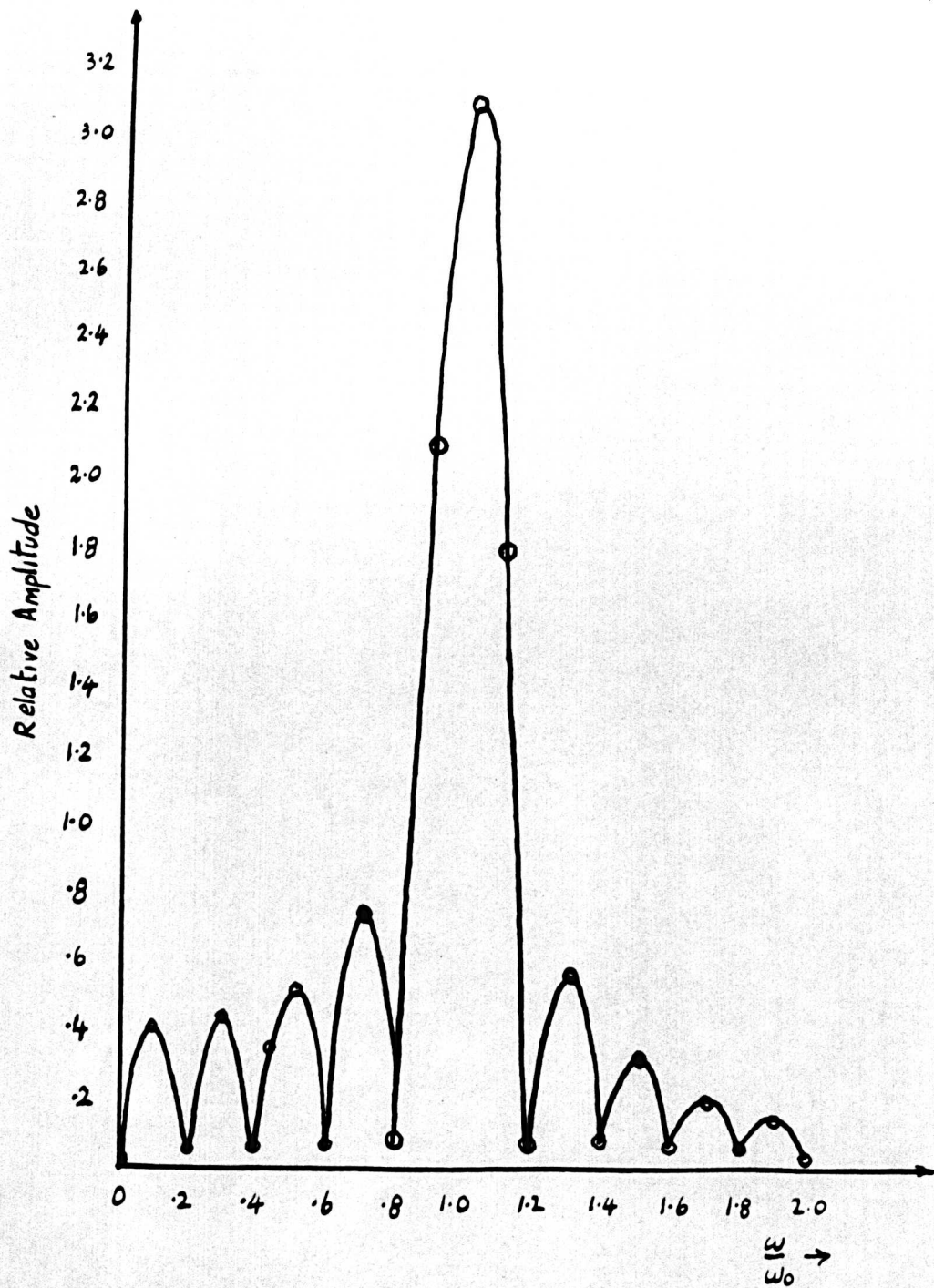


Fig 5-6 Frequency components in a 5 cycle sinusoidal pulse
(due to Author) see appendix 2.

CHAPTER 6

THE SPECIMENS

6.1 Case hardened specimens

The case hardened specimens were steel specimens which were case hardened by carburizing. They were case hardened to various depths of case hardening. Two types of material were used. These were:-

S/ZNC - (0.14 - 0.18)C, (0.10 - 0.3)Si, (0.35 - 0.45)Mn, (0.015max)Ph and Su, (1.0 - 1.3)Cr, (0.15 - 0.35)Mo, (4.0 - 4.5)Ni, bal Fe.

S/ZLN - (0.1 - 0.15)C, (0.10 - 0.35)Si, (0.35 - 0.6)Mn, (2.75 - 3.25)Ni, 0.3max. Cr., 0.02max. Su., 0.25Ph., bal Fe.

The respective case depths were ($\times 10^{-3}$ in .):-

S/ZLN - 15, 25, 30, 35, 40, 50, 60

S/ZNC - 10, 13, 16, 21, 26, 41, 56

Photographs of the casehardened specimens can be seen in Figs. 6.1 and 6.2. All these specimens were supplied by Rolls Royce Ltd, Derby.

6.2 Creep specimens

The creep specimens also were supplied by Rolls Royce Ltd. They were made of two types of materials. These were Nickel alloy and Titanium alloy, both 16 SWG (.048 in .) thick.

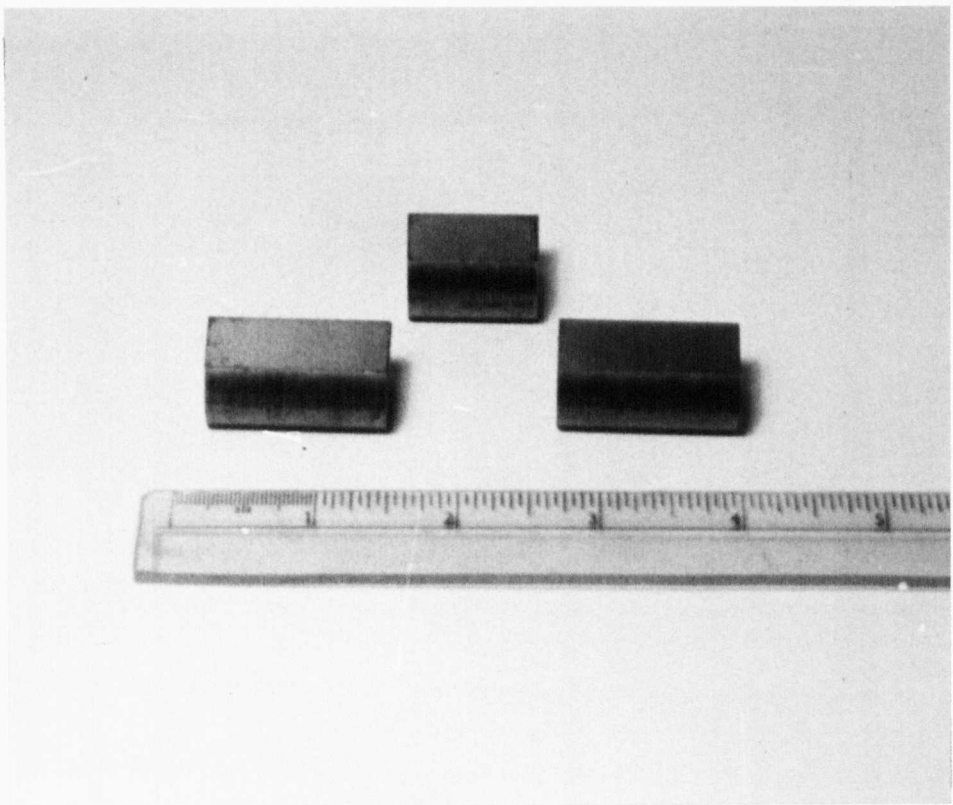


Fig. 6.1 Showing the case hardened specimens used.(S/ZLN).

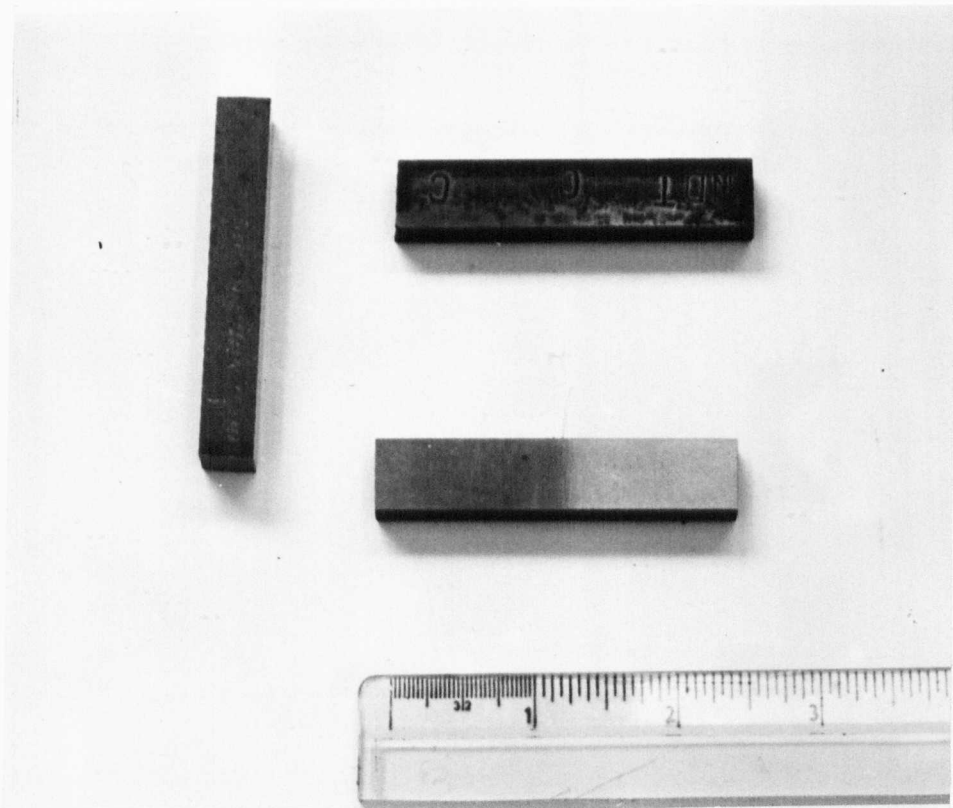


Fig. 6.2 Showing the case hardened specimens used.(S/ZNC).

6.2.1 Nickel alloy

The nickel alloy was C263 Nimonic sheet metal whose chemical composition was:-

0.03C, 0.025Si, 0.2max.Cu, 0.75max.Fe, 0.40Mn, 20Cr, 2.15Ti, 0.45Al, 20Co, 5.9Mo, 0.02max.Zr, 0.001max.B, 0.007max.S, bal.Ni. The crystal structure was h.c.p.

The "as received" state was:- Age hardened at 800°C. The specimens made from this material were subjected to different degrees of creep. These were:- 0, 0.33%, 0.63% and 0.98% Total plastic strain (T.P.S). Details of the creep test for this material are given in Appendix 3.

The specimens were subjected to creep at 780°C with a tensile stress of 170MN/m². They were all chemically cleaned to remove any film on the surface.

6.2.2 Titanium alloy

The titanium alloy used was titanium 230 the composition of which was:- 2.5Cu, 0.2max.Fe, 0.01max.H, bal.Ti.

The "as received" state was:- Solution treated at 805°C and stress relieved. Specimens made from this material were subjected to different degrees of creep. These were:- 0, 0.29, 0.79, and 0.98 Total plastic strain. The creep tests were conducted at static stresses of 18 to 26 Tons/in² (280 to 400MN/m²), at a temperature of 300°C. The stress was varied to get the required extensions. The crystal structure of this material was h.c.p below 882°C and b.c.c above 882°C. The ultimate tensile strength of this material was about 34 Tons/in² (520MN/m²).

All the specimens were heated but only three were loaded so that any oxide skin effect will be also present on the control specimen. All specimens were then chemically cleaned in order to remove any film on the surface.

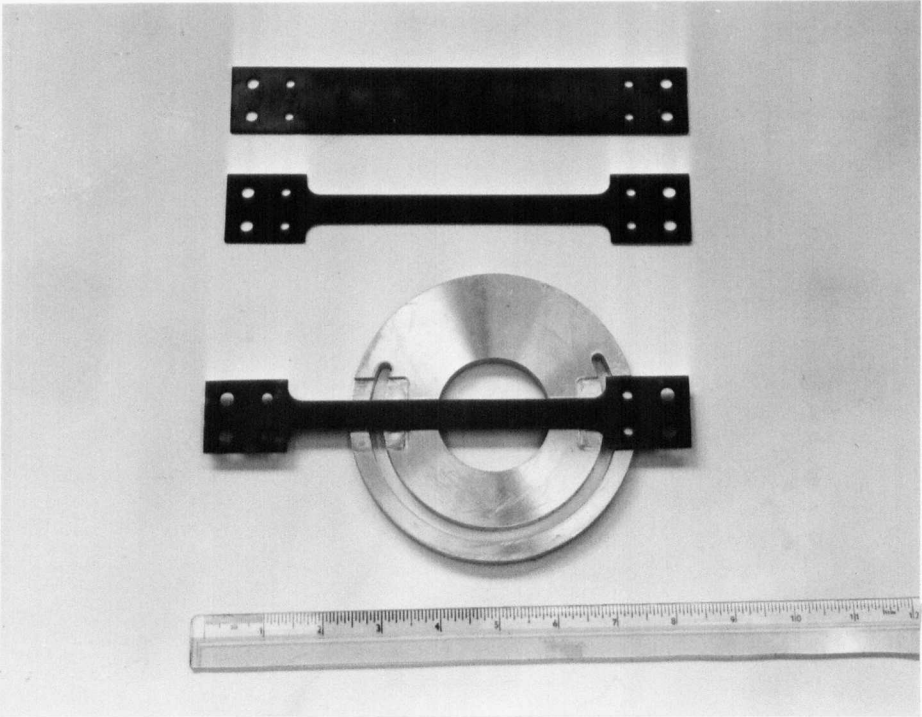


Fig. 6.3 Showing the creep specimens used.

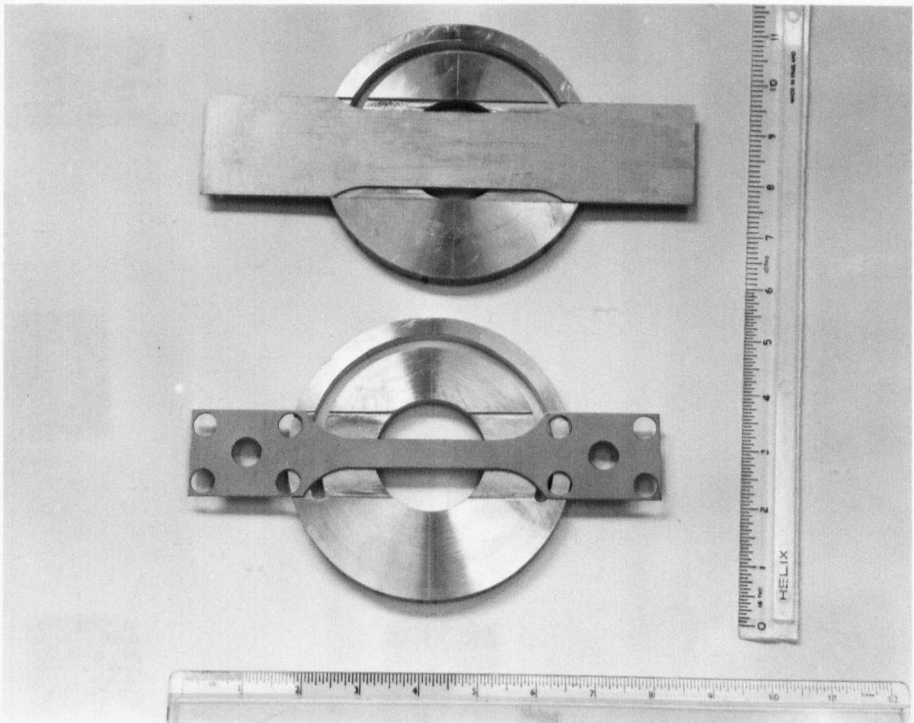


Fig. 6.4 Showing the fatigue specimens used.

6.3 Fatigue specimens

The specimens used for fatigue were IMI Titanium 230 and mild steel. They were 20 SWG and can be seen in Fig.6.4. Some of the titanium specimens were flat rolled specimens designed by Rolls Royce Ltd for fatigue testing. The other titanium specimens and mild steel specimens were designed to BS18 specification and fatigued in the University workshops. The fatiguing was at high stress levels for relatively low numbers of stress cycles.

6.4 Other specimens

Other materials were used for general material evaluation. They were rolled rectangular bars of mild steel, brass, copper, stainless steel and aluminium of thickness $\frac{1}{4}$ in. (6.35mm).

CHAPTER 7

DATA COLLECTION AND EXPERIMENTAL RESULTS

General

The data were collected by varying the angle of incidence and simultaneously observing the reflected envelope on the screen of the oscilloscope. Fig.7.1 shows how this amplitude varies with angle of incidence near the critical angle. When the amplitude of the envelope was a minimum, the angle of incidence was recorded by reading the main and vernier scales (see Fig.4.4), of the goniometer. This gave the critical angle of incidence of the material under test.

The goniograms were plotted by varying the angle of incidence and recording the amplitude of the reflected pulse.

All tests were conducted under controlled temperature conditions, (35 ± 0.01 degrees). The testing depth was kept constant, and the frequency of the test signal was varied. Critical angles and goniograms were measured at different frequencies and for different materials. Care was taken to see that the axis of the transducer bisected the intersection made by the specimen and the reflector block and a "setting up" tool was designed for this purpose (see Fig.4.10). Also, the water in the tank was changed daily to avoid corrosion.

Angle of incidence.

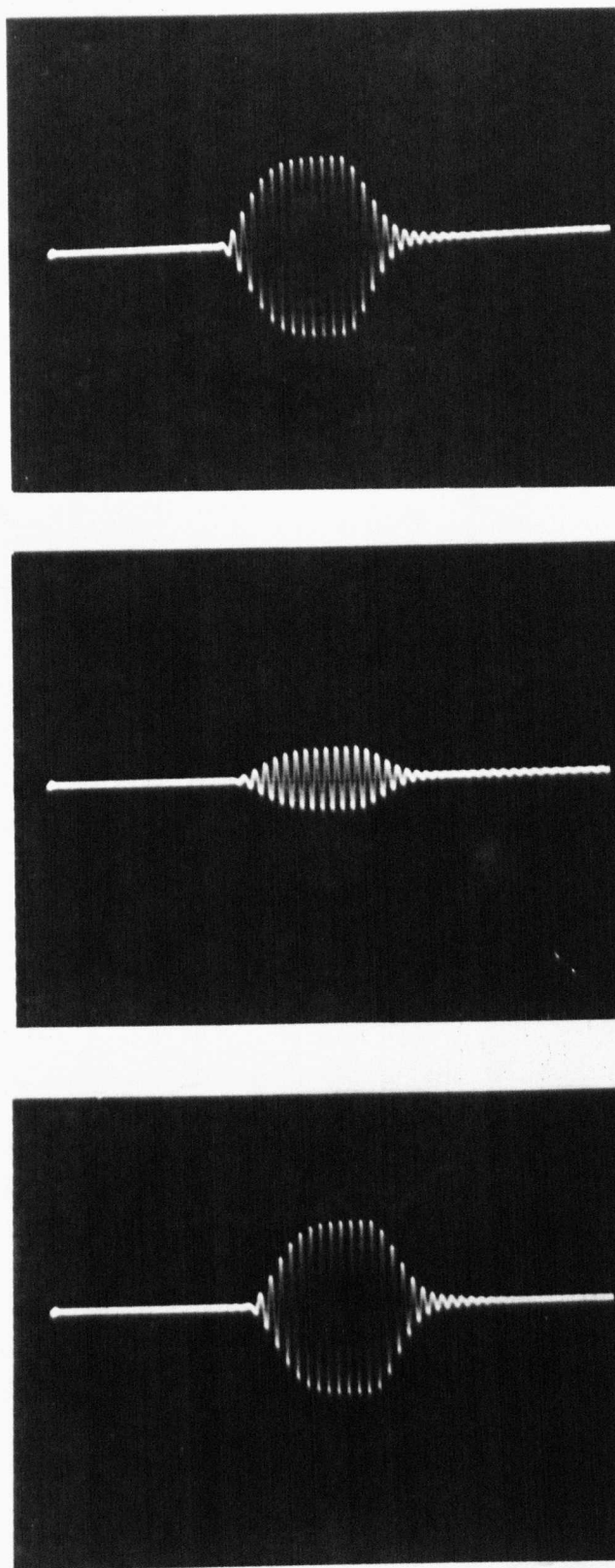


Fig 7.1 Typical reflected pulse for a water/
stainless steel interface at 5MHz.

7.1 CASE DEPTH

7.1.1 Data collection

The data was collected by measuring the critical angles of incidence of different specimens which have been case hardened to various depths of case hardening. The specimens were of the type given in section 6.1. All specimens were tested at 2,4,5,12.5 and 15MHz. The specimens were fastened to the back of the reflector block and the transducer arm rotated, starting from zero angle of incidence, until the critical angle was observed.

Two types of material were tested (see sec. 6.1). Additionally, goniograms were plotted of three specimens of each type in the vicinity of the critical angle. This was done for the 2 and 4MHz test signals.

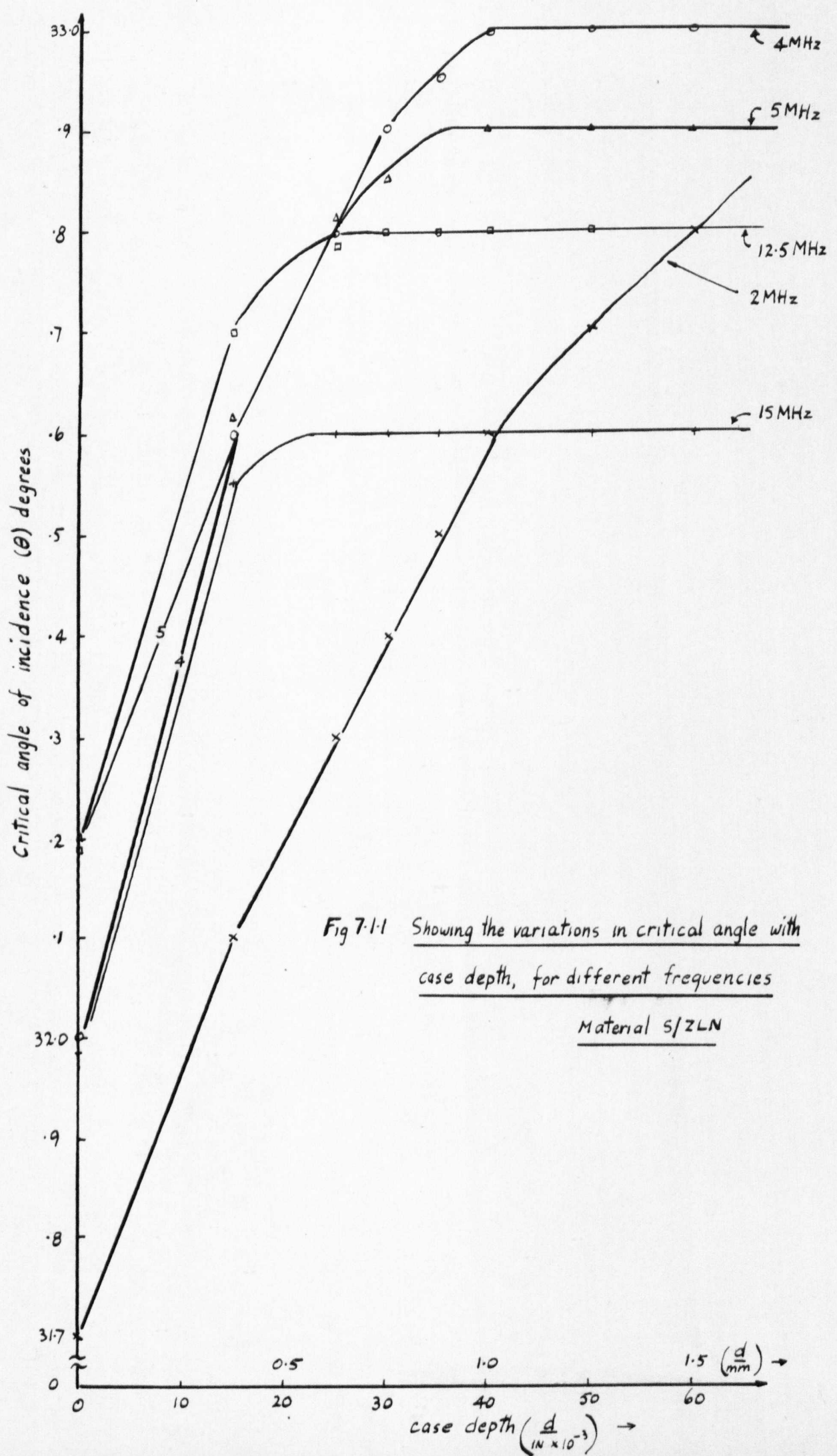
7.1.2 Results and data analysis

The results of the change in critical angle of incidence to case depth(d) can be seen plotted in Fig.7.1.1. (for material S/ZLN) and in Fig.7.1.2 (for material S/ZNC). For both materials the results were plotted for various ultrasonic test frequencies.

Goniograms were also plotted for all specimens at two ultrasonic frequencies, i.e. 2 and 4MHz for different depths of case hardening (see Figs.7.1.3 and 7.1.4).

The data were analysed by calculating the differences in critical angles

RESULTS



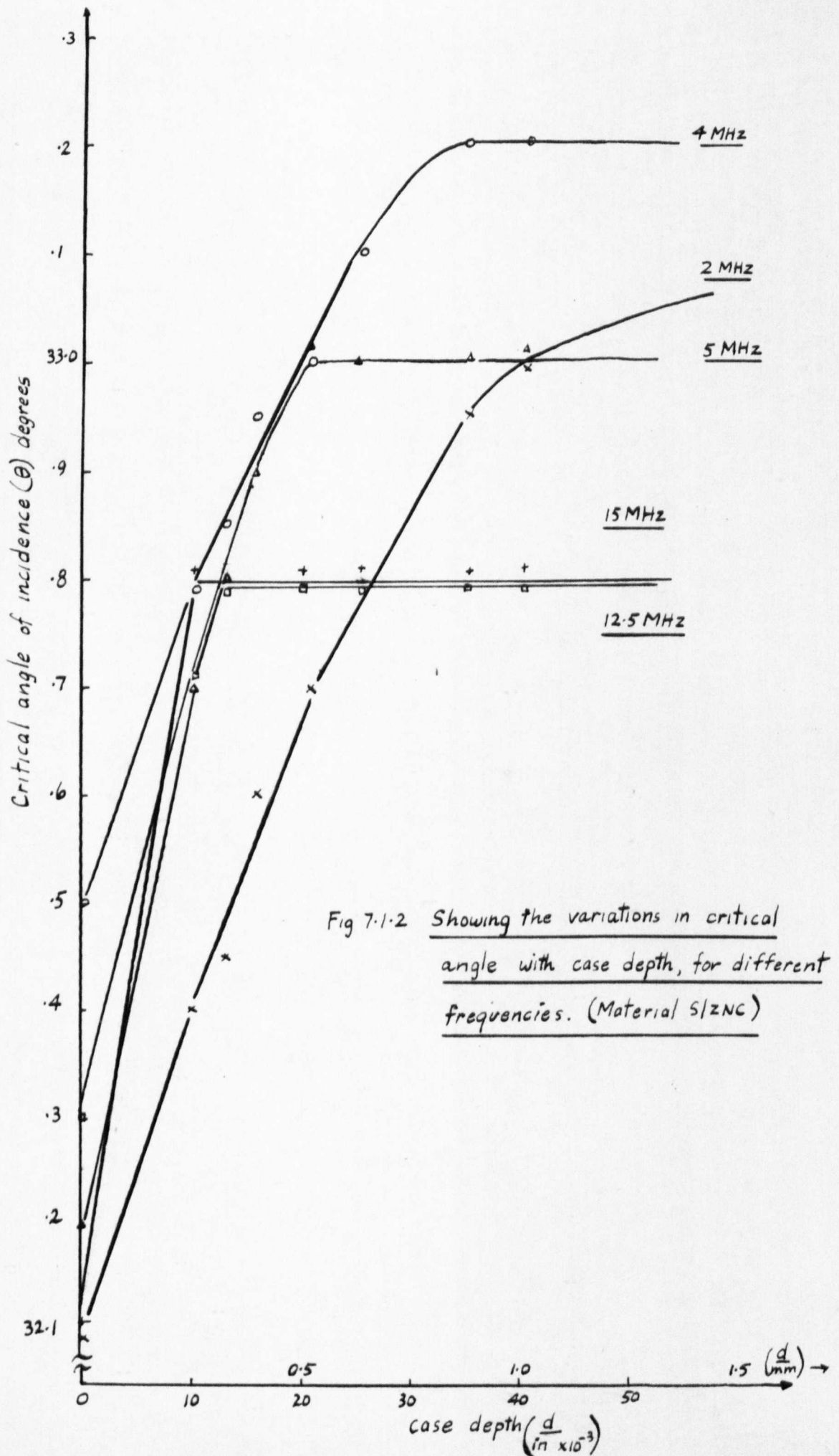


Fig 7.1.3(a) Goniograms for different case depths at 2MHz

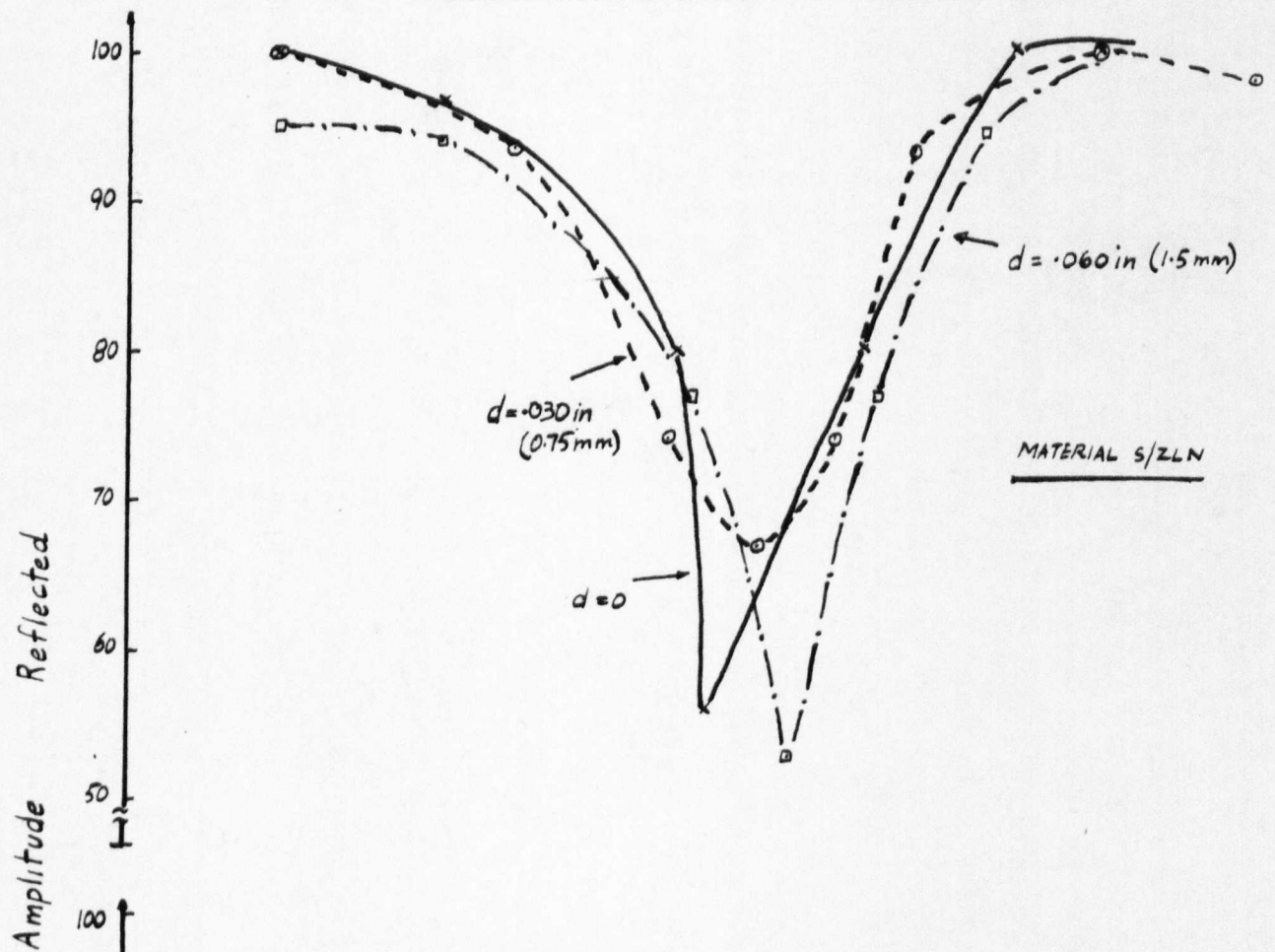
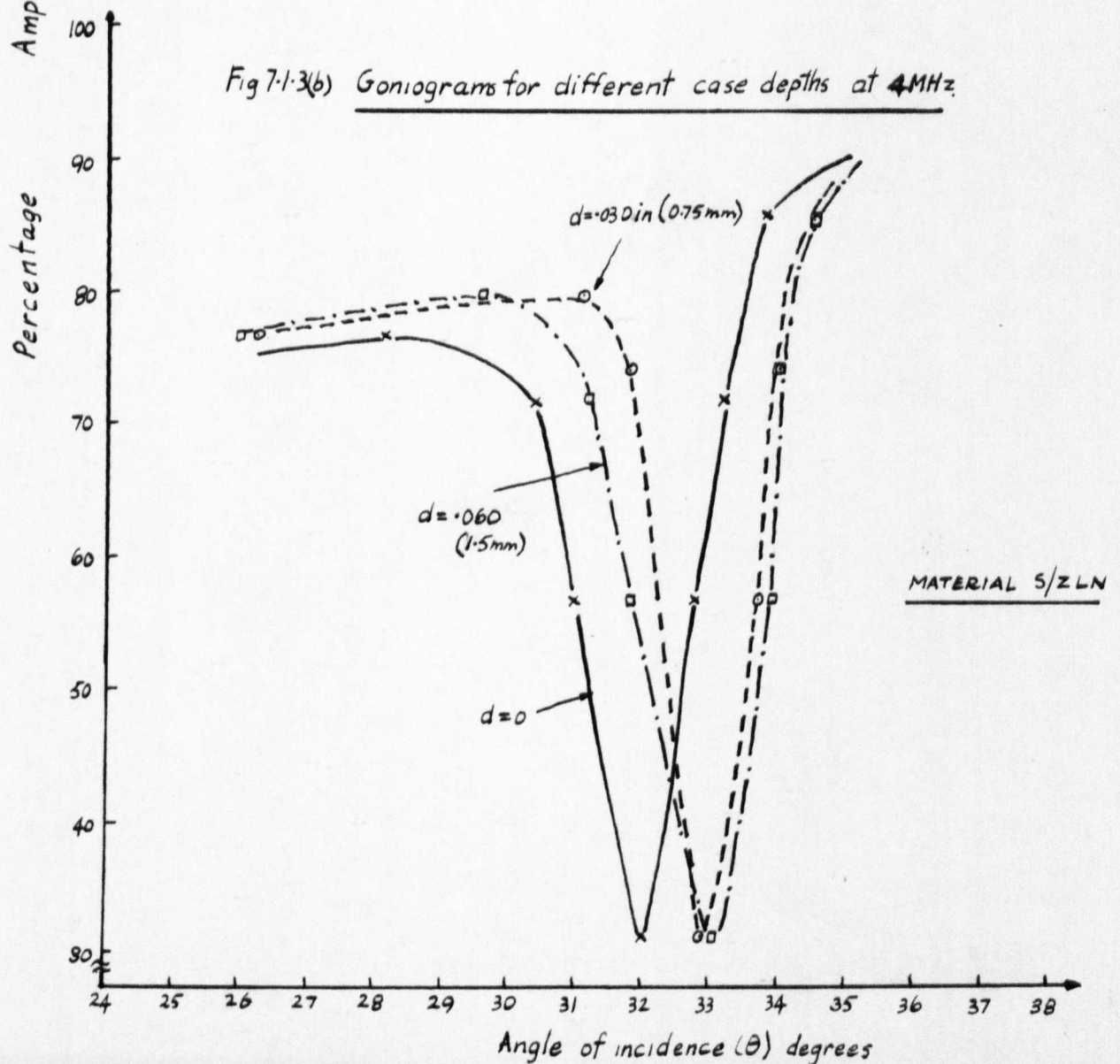


Fig 7.1.3(b) Goniograms for different case depths at 4MHz



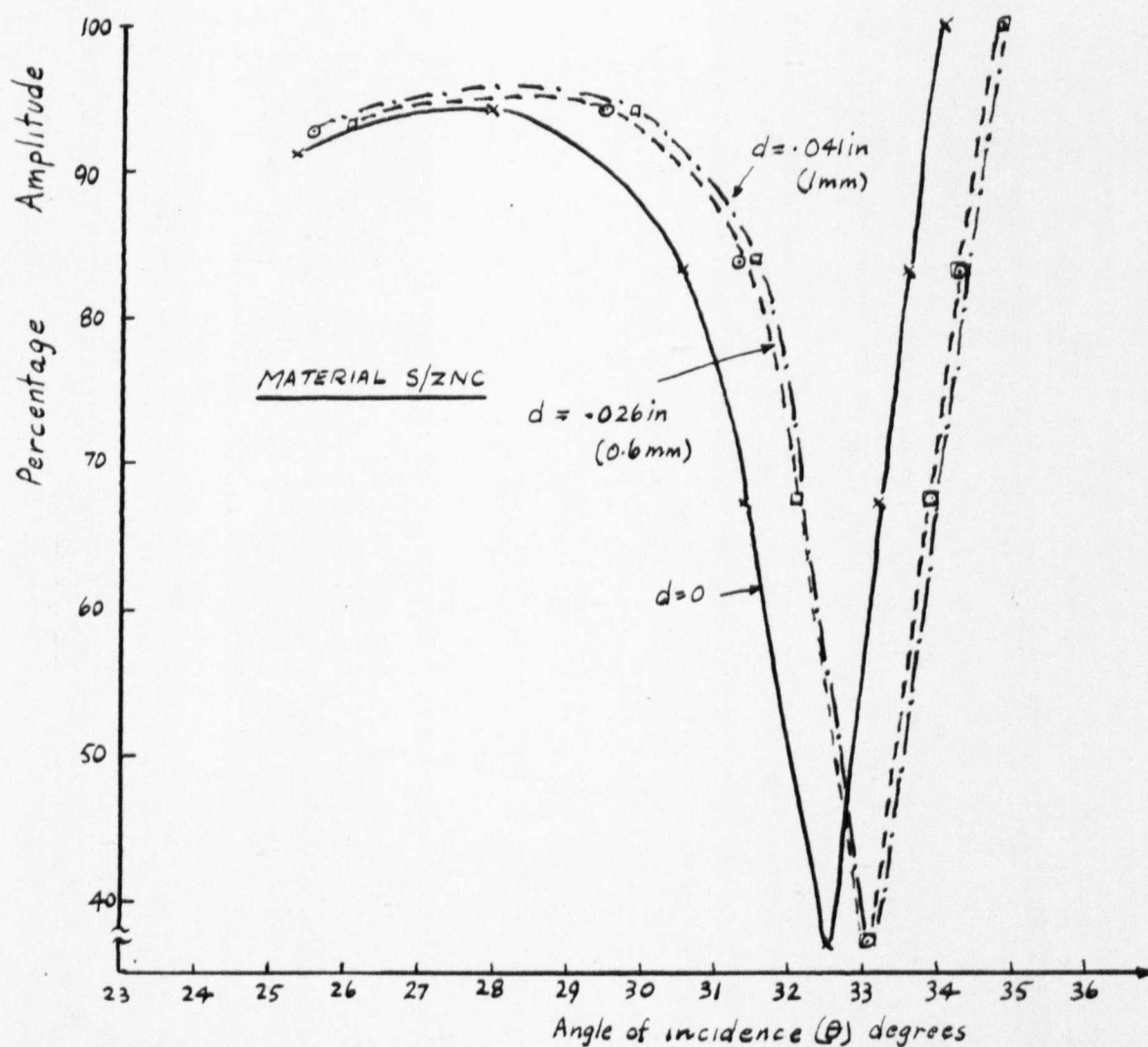
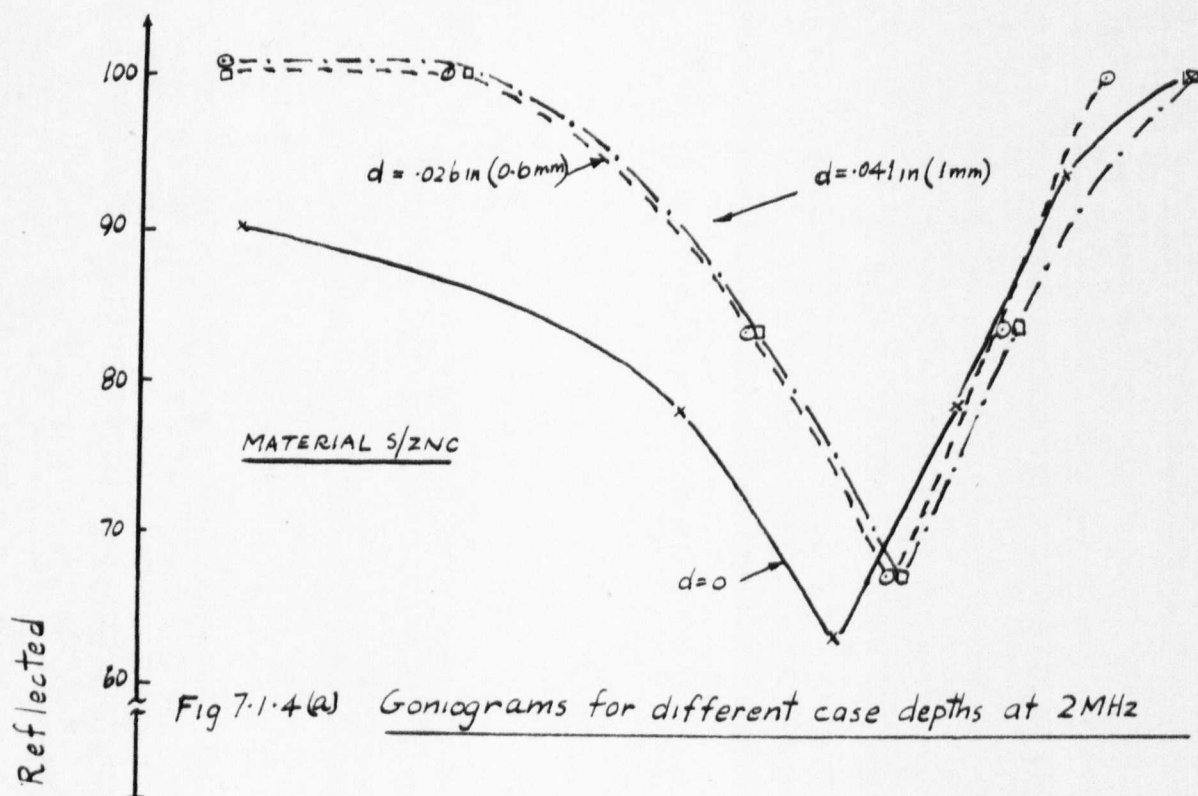


Fig 7.1.4(b) Goniograms for different case depths at 4 MHz

of incidence $(\theta - \theta_0)$, where θ was any measured value of critical angle and θ_0 was the critical angle of the specimen with zero case depth. This was plotted versus the depth of case hardening(d). Plots can be seen in Fig.7.1.6., for both materials.

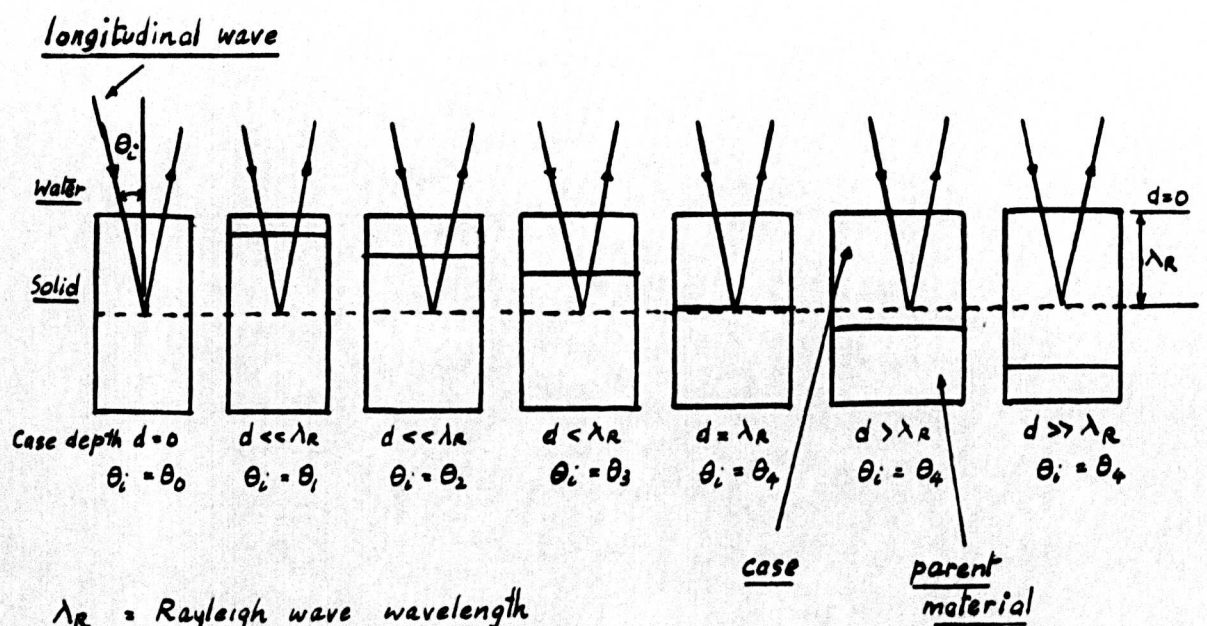
7.1.3 Discussion of results and conclusions

The results for the change in critical angle with case depth as shown in Figs.7.1.1 and 7.1.2, show that lower frequencies can detect greater case depths. This was as expected from theory. It can be seen in Fig.3.8, that the particle displacement is very small for depths below the surface greater than one wavelength. Therefore, when the test frequency is kept constant and the case depth varied, there will be a condition when any further increase in the case depth will give no further change in the measured critical angle.

This condition is when the case depth(d) is approximately equal to the wavelength(λ) of the test signal. If conditions for case depths smaller than λ are considered, then it would be expected that as case depth increases the measured critical angle will change.

Consider Fig.7.1.5. For zero case depth the critical angle will be determined by the elastic property of the parent material.i.e.

$$\theta_R = \sin^{-1} \frac{C_w}{\sqrt{G_{SR}/\rho}} \dots\dots\dots 7.1.1$$



λ_R = Rayleigh wave wavelength
 θ_i = Critical angle of incidence (θ_R)

Fig 7.1.5 Showing the relationship of the change in critical angle to depth of case hardening.

where:- G_{SR} = Elastic modulus of the surface wave.

ρ = the density of the solid.

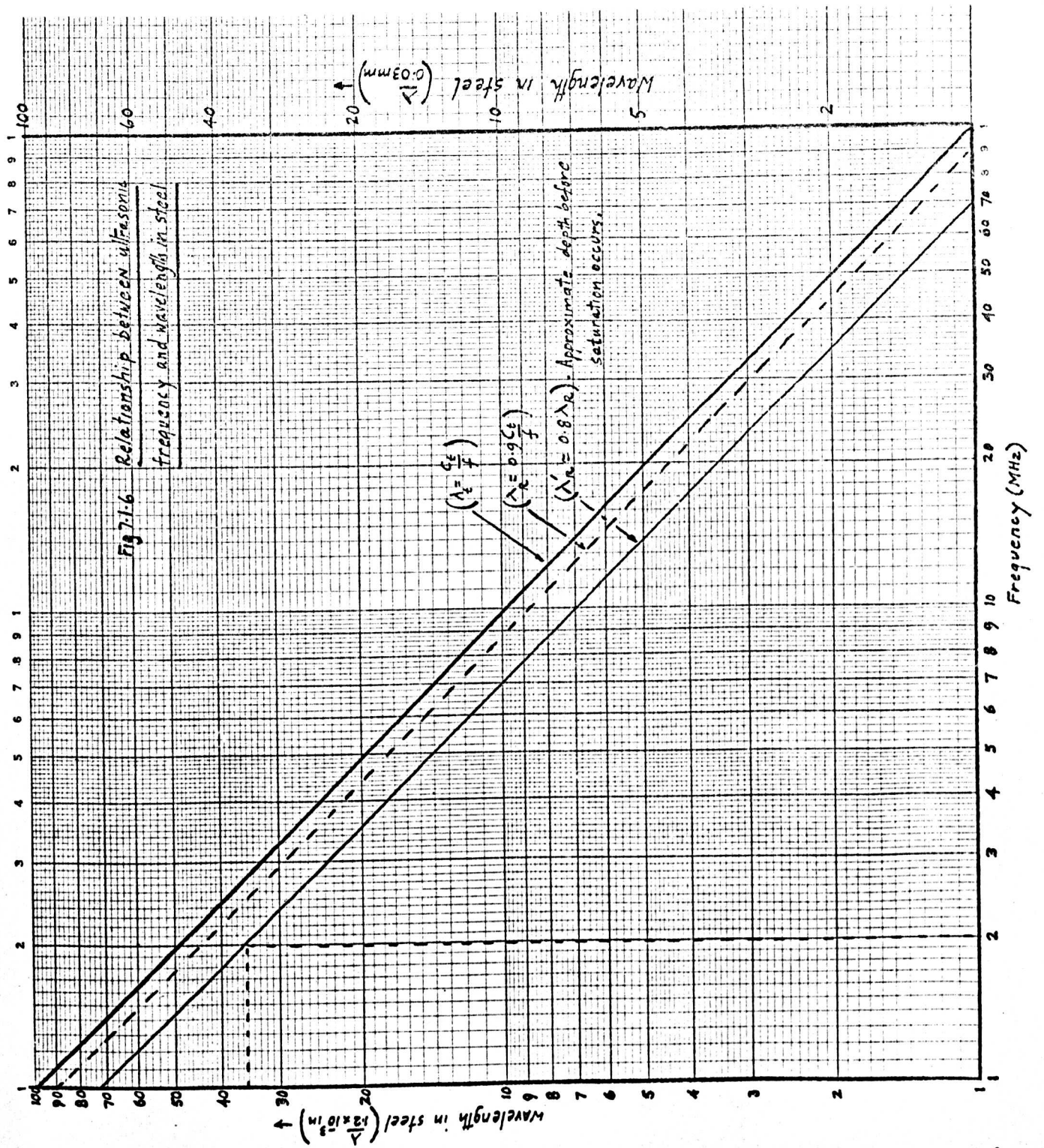
C_w = the velocity of dilatational wave in the water.

When this material is case hardened, to a depth $d < \lambda_R$, the value of G_{SR} changes because the elastic modulus is now made up of the elastic modulus of the hardened layer and the elastic modulus of the parent material.

When $d \gg \lambda_R$ the critical angle is dependent upon the elastic properties of the case material. Also the density of the layer about one wavelength thick will be changed due to the case hardening. Therefore the measured critical angle will be different.

The results plotted in Fig.7.1.1 and Fig.7.1.2 show that the critical angle increases with the case depth. It appears that this increase is due to the increase in density in eqn.7.1.1. As case depth increases, the density also increases and hence the critical angle. For case depths of about one wavelength or greater, the critical angle is the same. This can be seen when the test wavelength is decreased. As the frequency is increased, the point of levelling off in the measured critical angle, is decreased. This demonstrates that lower frequencies can detect larger case depths.

Fig.7.1.6. shows the relationship between frequency and wavelength in steel for the shear ultrasonic bulk waves. It is seen that a 2MHz signal can be used for detecting case hardening up to about 60×10^{-3} ins. (1.5mm). From Fig.3.8 and the corresponding equation 3.12, it shows that at about a depth $d \approx 0.8\lambda_R$ the particle displacements are 10 and 30 percent of their peak values. From the results obtained it appears that for the highest accuracy in determining the case depth, a depth of approximately



$0.8\lambda_R$ should be considered as the surface layer appreciably disturbed.

If the disturbed layer is considered as $d \approx 0.8\lambda_R$, then it follows that a 2MHz test signal can detect a case depth of up to about 48×10^{-3} in. (1.2mm). In the graph of the results Fig.7.1.1, it appears that beyond 50×10^{-3} ins., the critical angle shows a tendency to level off. However, for the other material Fig.7.1.2, this tendency to level off was observed at about 40×10^{-3} in. (1mm).

Considering the other frequencies (see Fig.7.1.1), a 4MHz signal can be used to detect a case depth of 24×10^{-3} in. in steel.

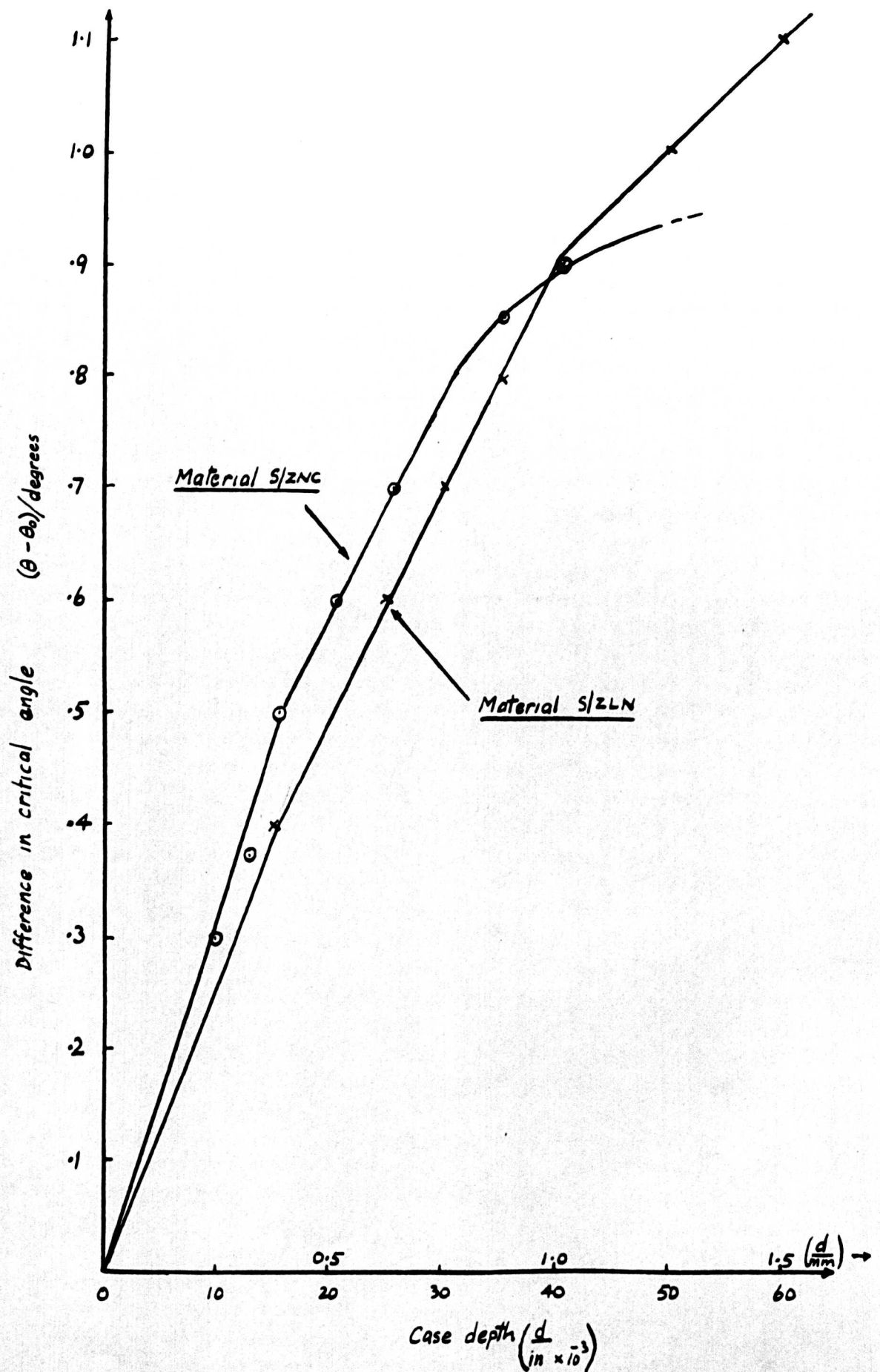
From the graph, a depth of 30×10^{-3} in. was obtained, and about the same value in Fig.7.1.2. Therefore generally it can be said that in steel, for case depths greater than $d \approx 0.8 \frac{C_R}{f}$ (where C_R is approximately equal to the shear wave velocity ($\approx 0.9 C_t$)), i.e. $d \approx \left(\frac{0.8 \times 3000 \times 0.9}{f} \right) \approx 2.16 \text{ mm}$ per MHz., or 86×10^{-3} in. per MHz), the curve begins to saturate.

The table below shows the calculated values for the saturation points at different frequencies.

| Frequency(MHz) | 2 | 4 | 5 | 12.5 | 15 |
|-------------------------------------|----|----|----|------|----|
| Case depth $\times 10^{-3}$ in . | 43 | 22 | 17 | 7 | 6 |

From Figs.7.1.1 and 7.1.2, it can be seen that these figures agree very closely with those in the table with a few exceptions which can be accredited to experimental errors.

Fig 7.1.7 Calibration curve for the change in critical angle
with case depth at 2MHz



A slightly more accurate analysis can be done to determine the depth of case that can be measured before saturation takes place. i.e.

From eqn. 3.18

$$C_R = \frac{C_w}{\sin \theta_R}$$

therefore

$$\lambda_R = \frac{C_w}{\sin \theta_R \times f} \dots \dots \dots 7.1.2$$

where:- θ_R = the measured critical angle.

C_w = the velocity of dilatational waves in water.

f = the ultrasonic test frequency.

$$\text{hence } d = \frac{0.8 C_w}{\sin \theta_R \times f} \dots \dots \dots 7.1.3$$

This is the approximate depth of case that can be measured before saturation takes place.

Fig. 7.1.7 is a plot of $(\theta_i - \theta_o)$ versus case depth for both materials. For the linear regions both curves have approximately the same slope. These curves can be used as calibration curves for the specimens made from a particular material. These curves depend upon the accuracy of measuring θ_o the critical angle of the specimen with zero case depth. Alternatively also, a curve plotted for θ versus d as in figs. 7.1.1 and 7.1.2 can be used as calibration curves for a particular material, at the required frequency.

7.1.4 Application of results on case hardening

The sensitivity of the measuring system was checked by measuring the case depths of specimens supplied by Rolls Royce Ltd. These had case

**PAGE
MISSING
IN
ORIGINAL**

depths which were unknown to the author. The specimens were measured on the goniometer and the results were compared with the known values, which were later supplied by Rolls Royce Ltd. The table below shows the results obtained. Material S/ZNC was used.

| Specimen | Virgin | HF886 | HF881 | HG806 | HF882 | HG805 | HE969 | HF884 |
|---|--------|-------|-------|-------|-------|-------|-------|-------|
| θ_i° (measured) | 32.1 | 32.6 | 32.7 | 32.8 | 32.9 | 32.95 | 33 | 33.05 |
| $(\theta_i - \theta_o)^\circ$ | 0 | 0.5 | 0.6 | 0.7 | 0.8 | 0.85 | 0.9 | 0.95 |
| d (From curve) $\times 10^{-3}$ in. | 0 | 16 | 21 | 26 | 33 | 35 | 40 | 43 |
| d (True value,) $\times 10^{-3}$ in. | 0 | 16 | 22 | 26 | 32 | 36 | 42 | 56 |

The specimen with zero case depth was first measured then all the specimens having unknown case depths were measured. Using the calibration curve Fig.7.1.7 values of case depths were read off for the corresponding values of $(\theta_i - \theta_o)$. As can be seen, from the table the test method used can measure case depth to an accuracy of $\pm 2 \times 10^{-3}$ in. except for specimen HF884. This however can be corrected if the calibration curve is followed around the saturation region. The author initially tried to fit the best straight line through the points. In the upper region of the curve however, there was deviation from the straight line.

For specimen HF884, the value for $(\theta_i - \theta_o)$ was 0.95 degrees. If this value is read off by following the curve around the saturation region, the value of case depth when read off will be 55×10^{-3} in. This

then will be within $\pm 2 \times 10^{-3}$ in. as found with the other specimens.

Thus to draw an accurate calibration curve, specimens of various case depths should be measured and $(\theta_i - \theta_o)$ should be plotted against case depth. Then, the best curve joining all the points should be obtained. Specimens of the same material with unknown case depths can be measured, and the case depth read off for the corresponding values of $(\theta_i - \theta_o)$ from the curve.

This method of testing is suitable for ferrous and nonferrous metals unlike the method used by Blitz et al.³ which is suitable only for ferromagnetic materials. This is because with this method, the specimens are subjected to magnetic hysteresis and the change in electrical conductivity, magnetic permeability and size measured. This method is also easier to apply than that used by Egorov^{2.1}, in which the change in damping of ultrasonic waves was measured. In this present study the changes in critical angle are easily measured.

Care has to be taken however to use a short burst of continuous waves when testing specimens of the same dimensions as used in this study.

7.2 CREEP

7.2.1 Data collection

The critical angles of incidence were measured for all specimens. The specimens used were subjected to various degree of creep, and the two types of materials were used as given in chapter 6. These were C263 Nickel alloy and IMI 230 Titanium alloy. Each specimen was placed in turn in the specimen holder which was fastened to the back of the reflector block(see fig.4.13), and the critical angles measured over the whole area of the specimen. In some cases as many as 20 readings were taken for the Nickel alloy. The titanium alloy was more homogeneous and it was not necessary to take so many readings.

Readings of critical angles were taken along the rolling direction ($\alpha = 0$), 45 degrees to the rolling direction ($\alpha = 45^\circ$), and 90 degrees to the rolling direction ($\alpha = 90$). (see fig.7.2.1), as obtained by rotating the specimen holder in the vertical plane and clamping it in the desired position.

The readings were taken for different frequencies 5, 15 and 25 MHz, and changes in amplitude of the reflected pulse with the angles of incidence were measured.

7.2.2 Results and data analysis

The results obtained from C263 Nickel alloy were analysed by calculating the mean value of the measured critical angles. *This value*

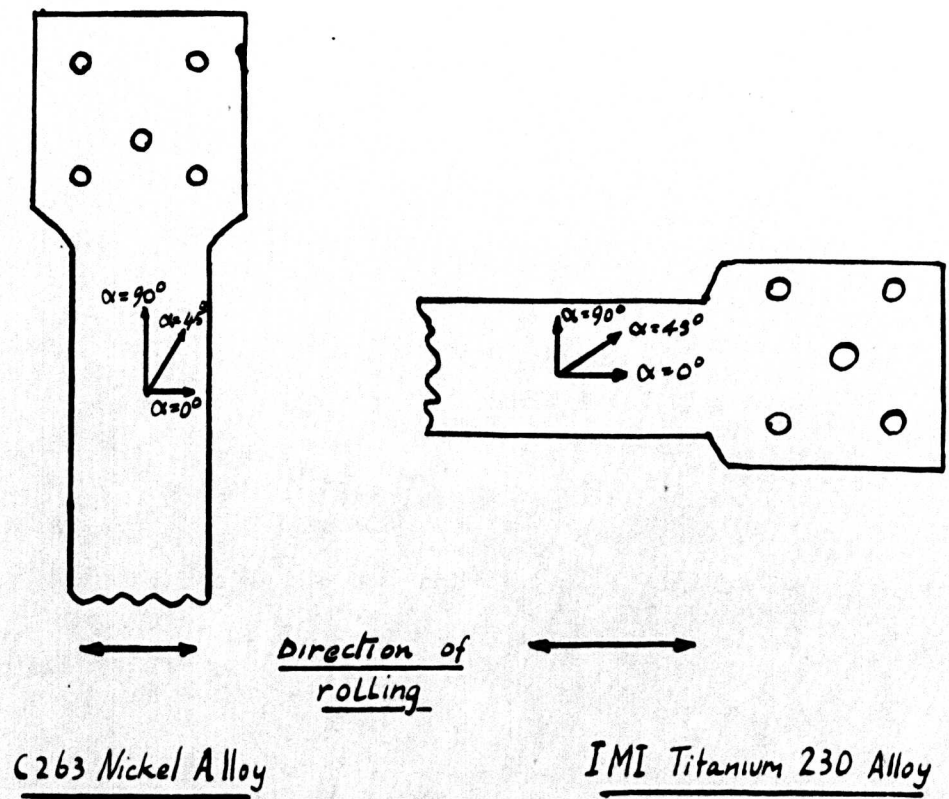


Fig 7-2-1 Showing the different directions of surface wave propagation

was used in all subsequent analysis. A graph of spread was plotted for the nickel alloy (see fig.7.2.2) for each frequency and orientation. The data obtained for the change in critical angle versus reflected amplitude for the titanium alloy was analysed by considering the highest amplitude in the measured range of critical angle as 100% and all other values were normalised to this value.

Goniograms were plotted for the titanium alloy for all three frequencies, and the various states of creep (see Figs.7.2.3, 7.2.4 and 7.2.5).

For both materials the normalised critical angle was calculated for all specimens at each frequency and orientation. Fig.7.2.6 shows how the critical angle changes with the direction of rolling for the nickel alloy and Fig.7.2.7 shows the same for the titanium alloy. For the calculation of the normalised critical angle of incidence, the critical angle of incidence for the direction of rolling was considered as θ_o and all other values were normalised to this value. viz. $\frac{\theta_i}{\theta_o}$ where θ_i is any measured value of critical angle for any orientation or frequency.

Fig.7.2.8 shows how the normalised critical angle changes with creep for the nickel alloy and Fig.7.2.9 shows the same for the titanium alloy. For calculating the normalised critical angle of incidence, the critical angle of the specimen with zero creep was considered as θ_o and all other values of critical angle for any state of creep at any frequency were normalised to this value. Each direction of propagation was taken separately.

Further analysis was done on the raw data to evaluate the normalised surface wave elastic modulus. i.e.

$$\text{From eqn. 3.1} \quad \sin \theta = \frac{C_w}{C_R} \quad \text{where :- } \theta = \theta_R \text{ the critical angle.}$$

C_R = the surface wave velocity.

RESULTS

Fig 7.2.2 Range chart of θ_R v. frequency for C263 creep specimens in various states of creep

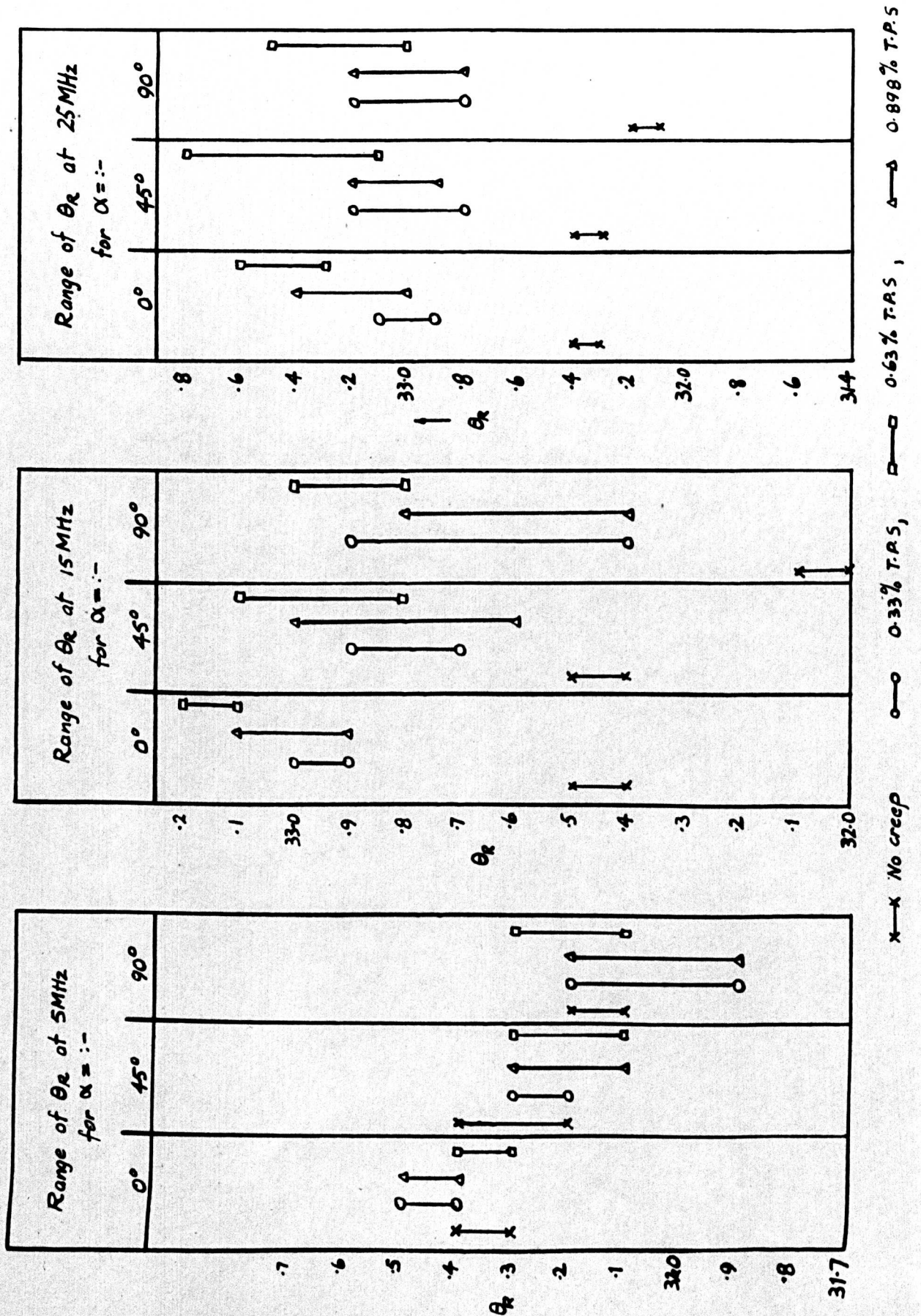


Fig 7.2.3 Goniogram for a water/titanium interface for different states of creep ($\epsilon\%$) T.R.S

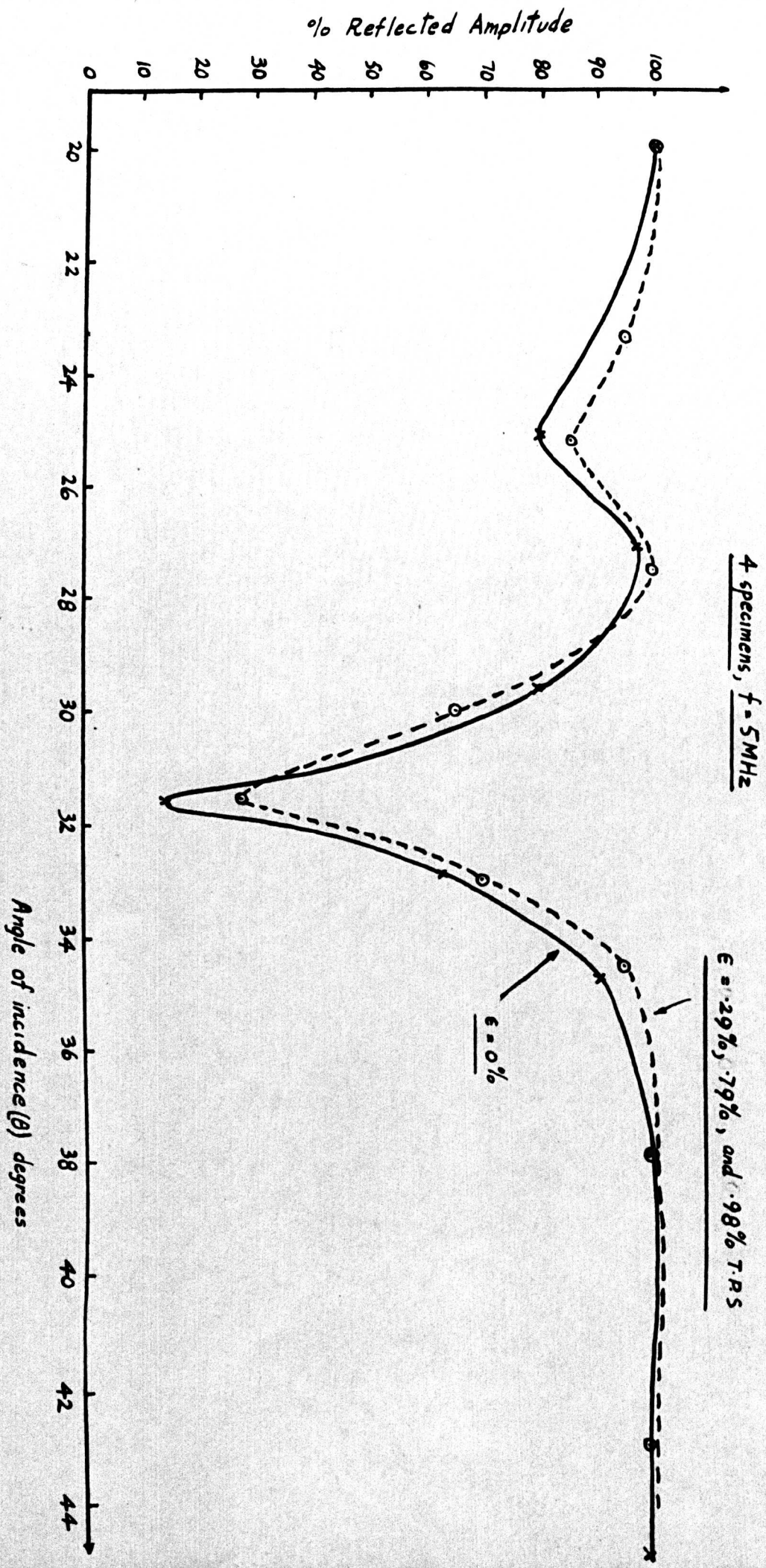


Fig 7.2.4 Goniogram for a water/aluminum interface for different states of creep ($\epsilon\%$) T.P.5

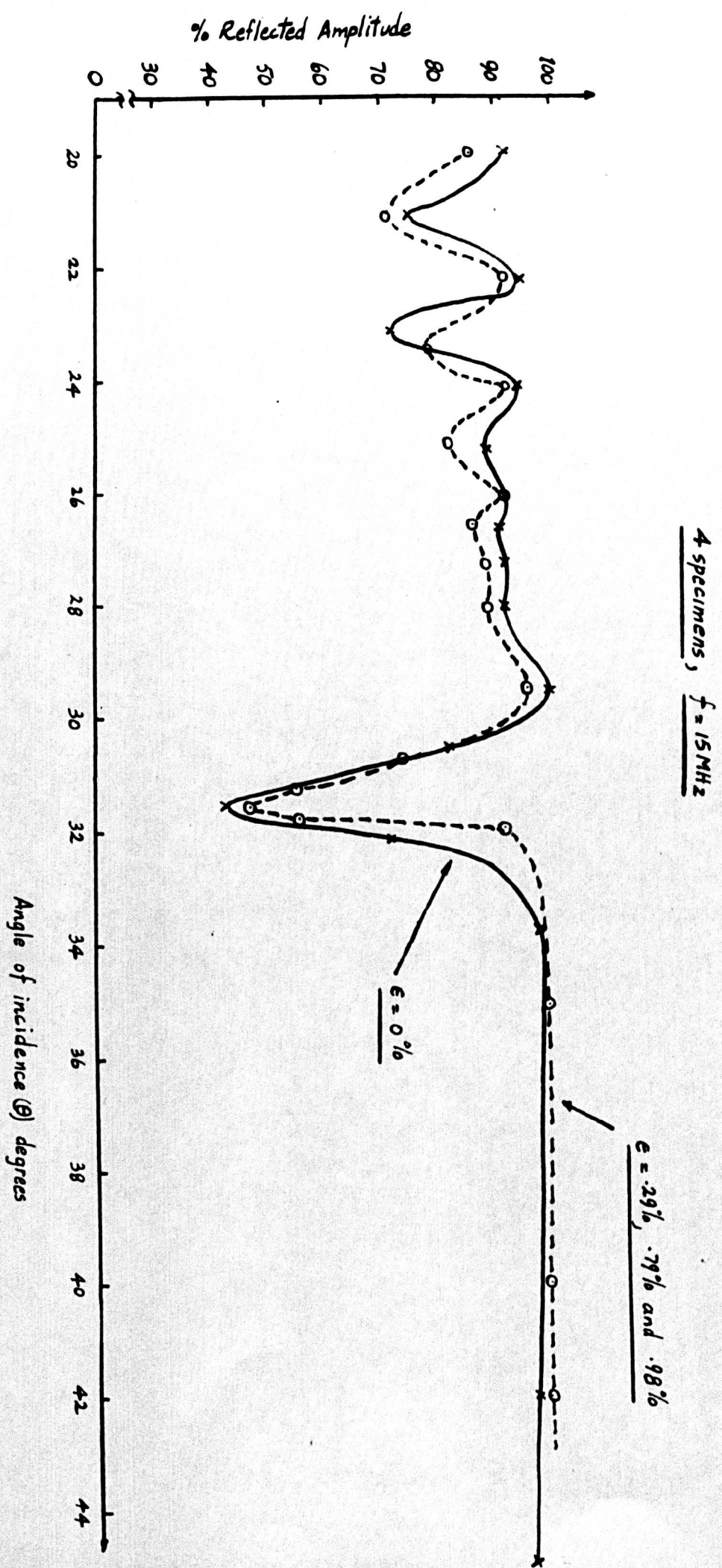


Fig 7.2.5 Goniogram for a water/Titanium interface for different states of creep ($\epsilon\%$) 7.2.5

4 Specimens, $f=25\text{MHz}$

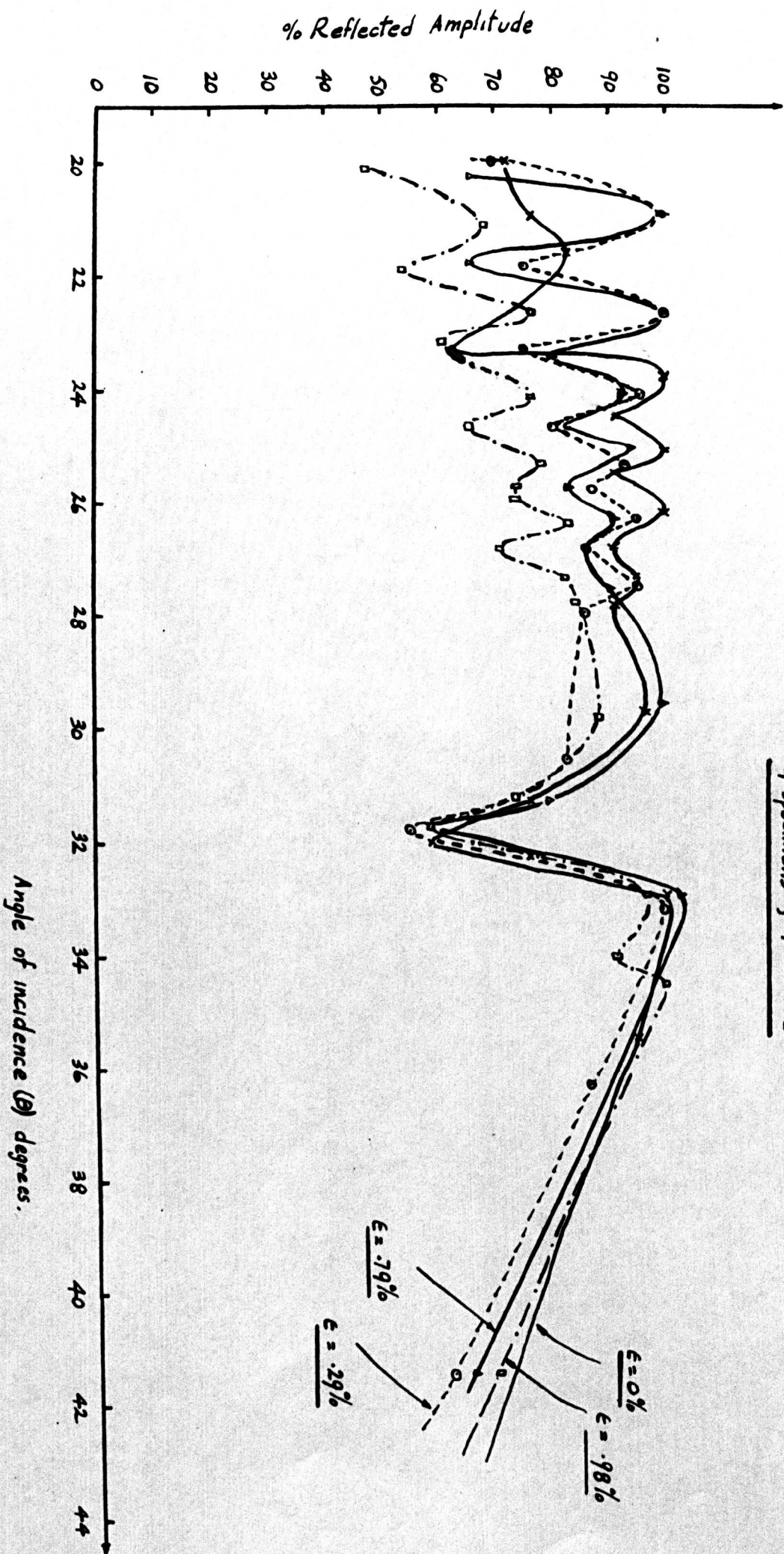


Fig 7.2.6 Showing the change in critical angle with direction from rolling
for different states of creep (C263)

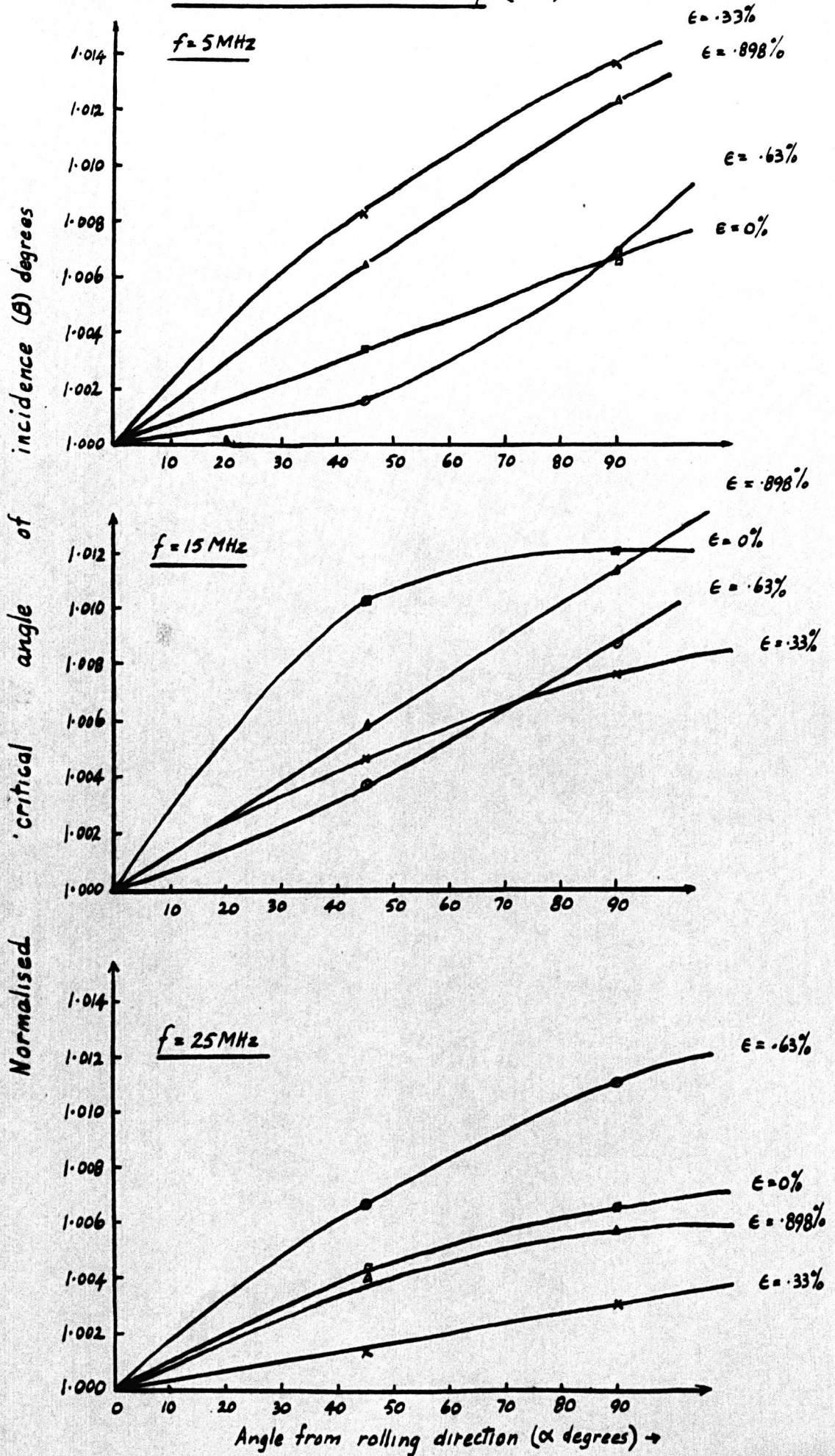
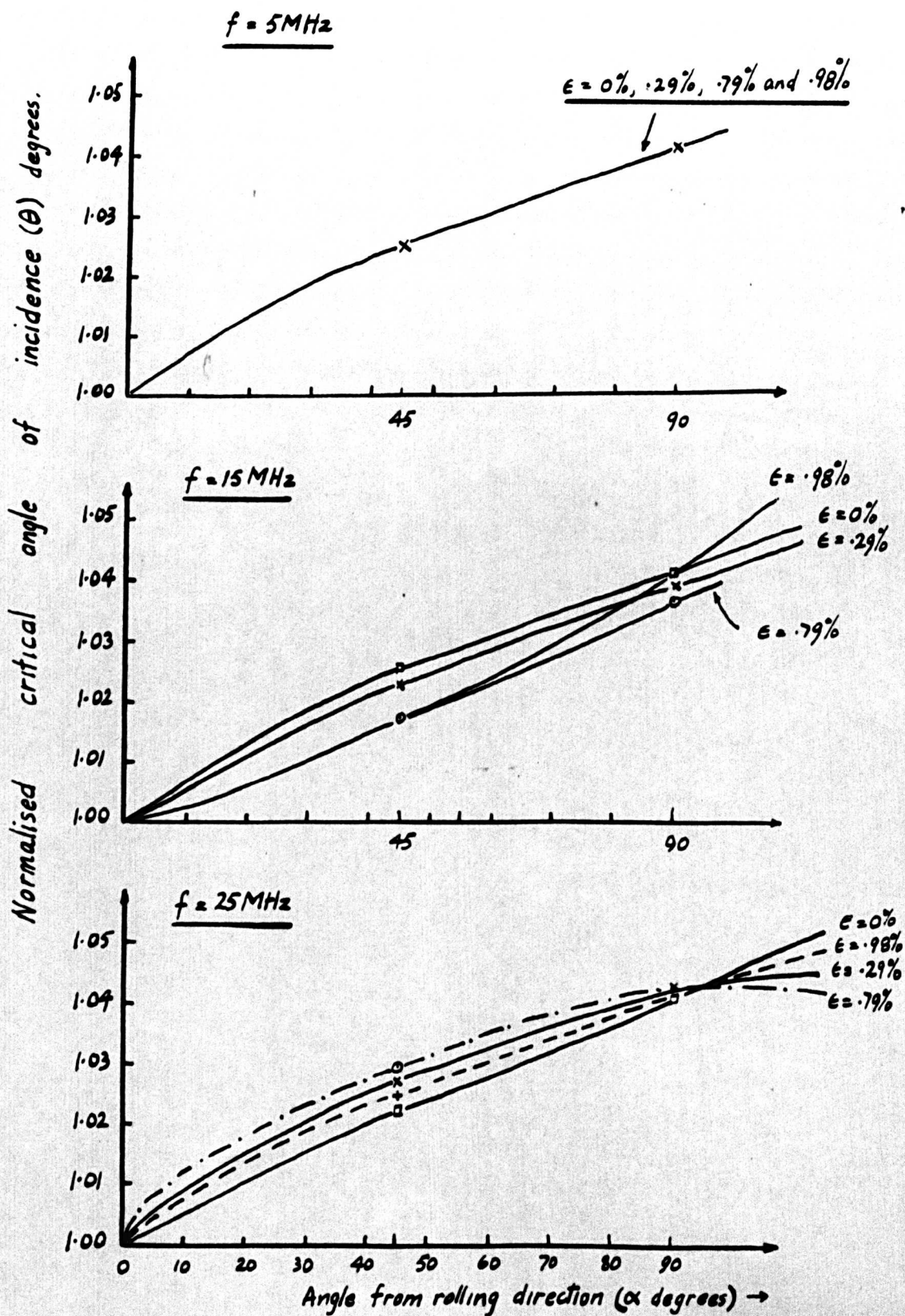


Fig 7.2.7 Showing the changes in critical angle with direction from rolling for different states of creep (Ti 230)



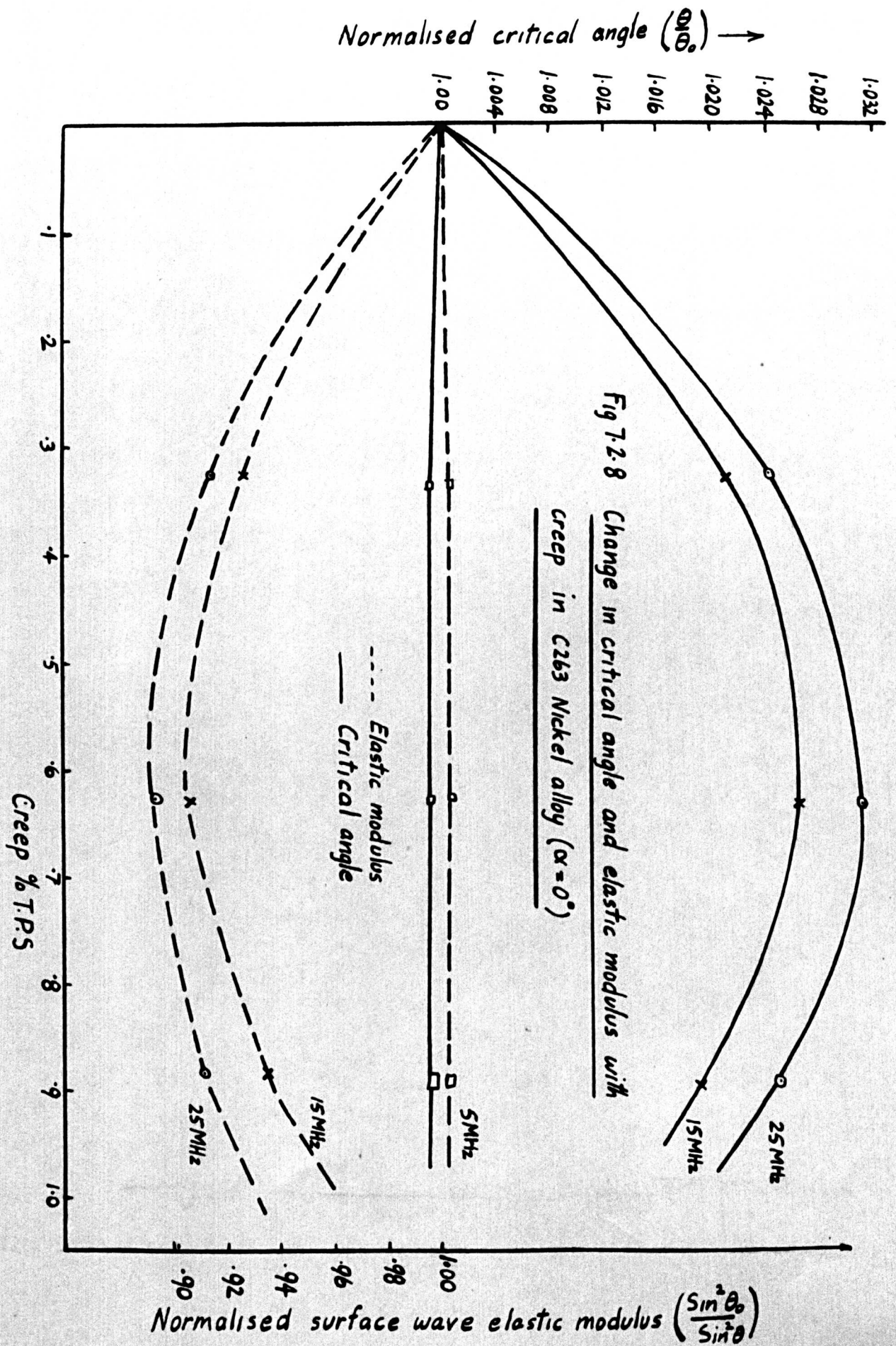


Fig 7.2.9 Change in critical angle and elastic modulus with creep in IMI Ti 230 ($\alpha=0^\circ$)

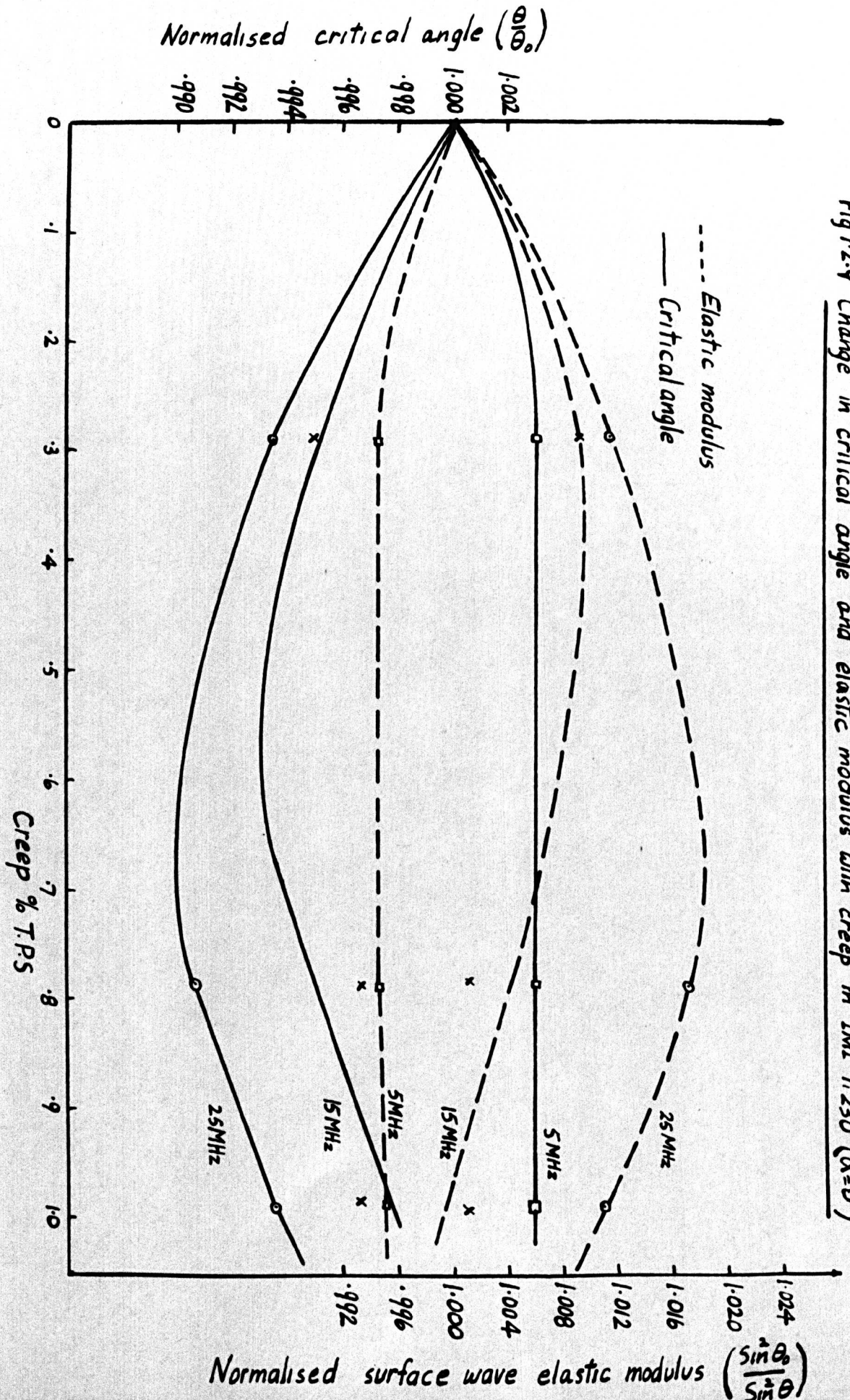
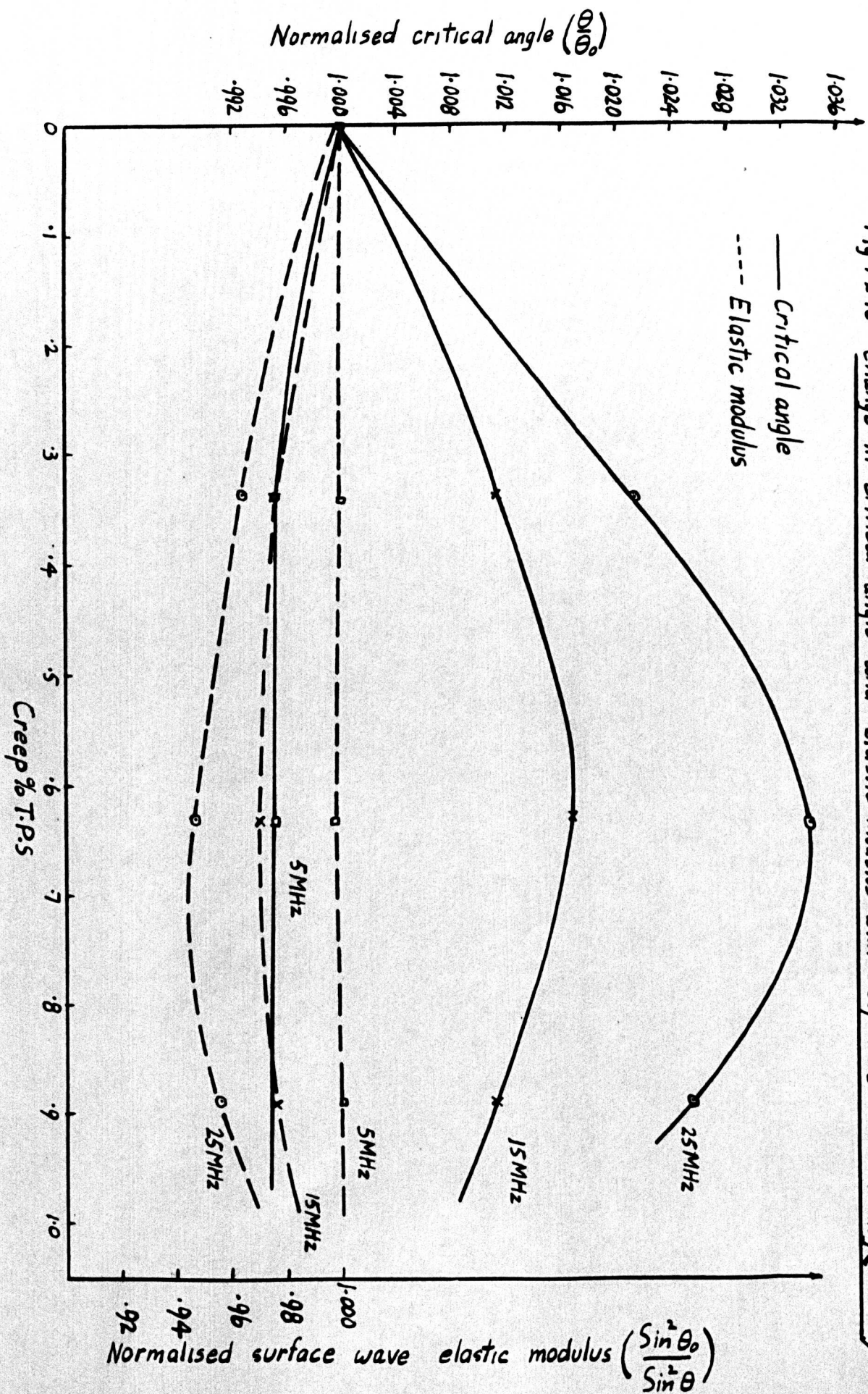
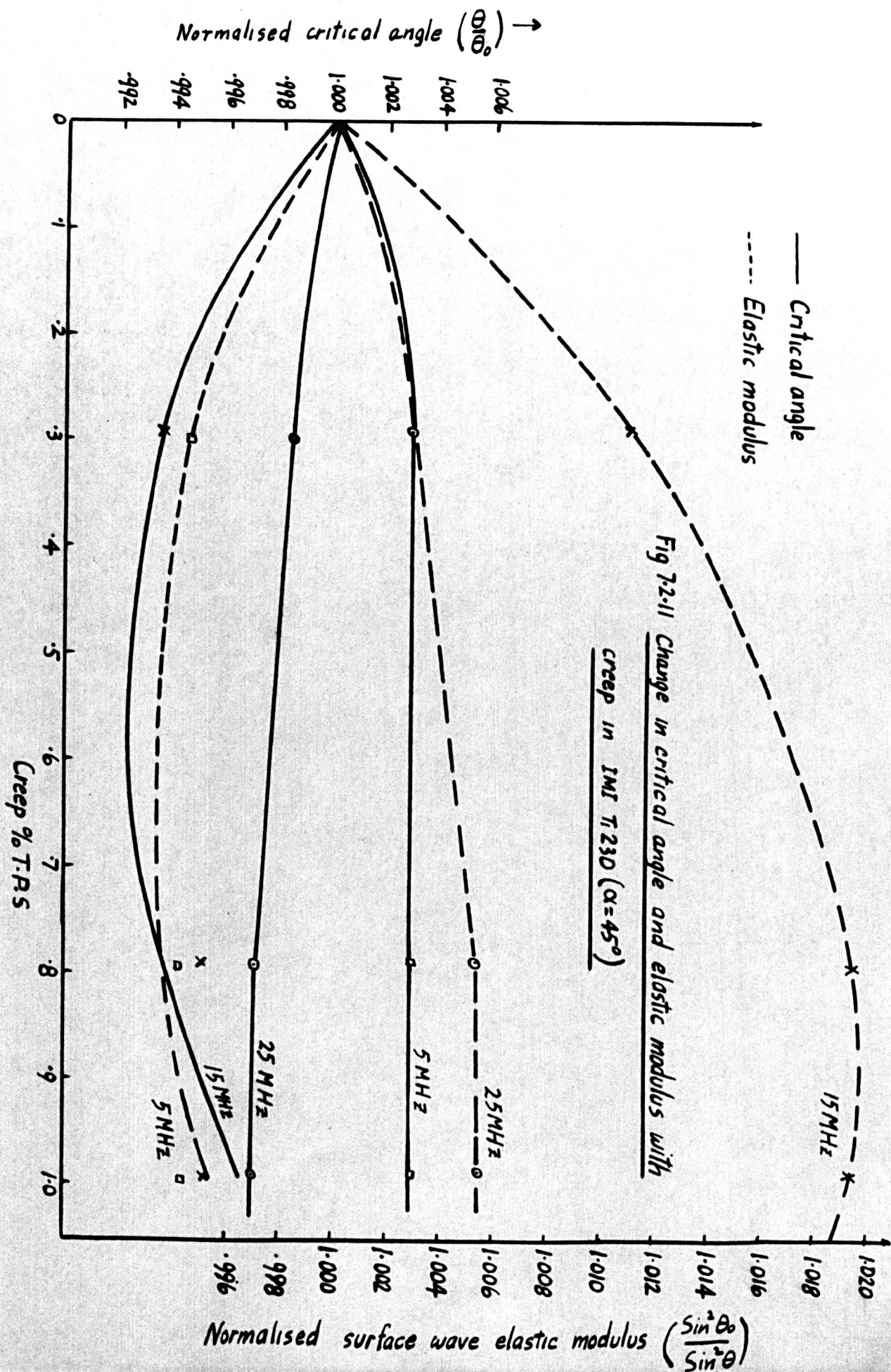
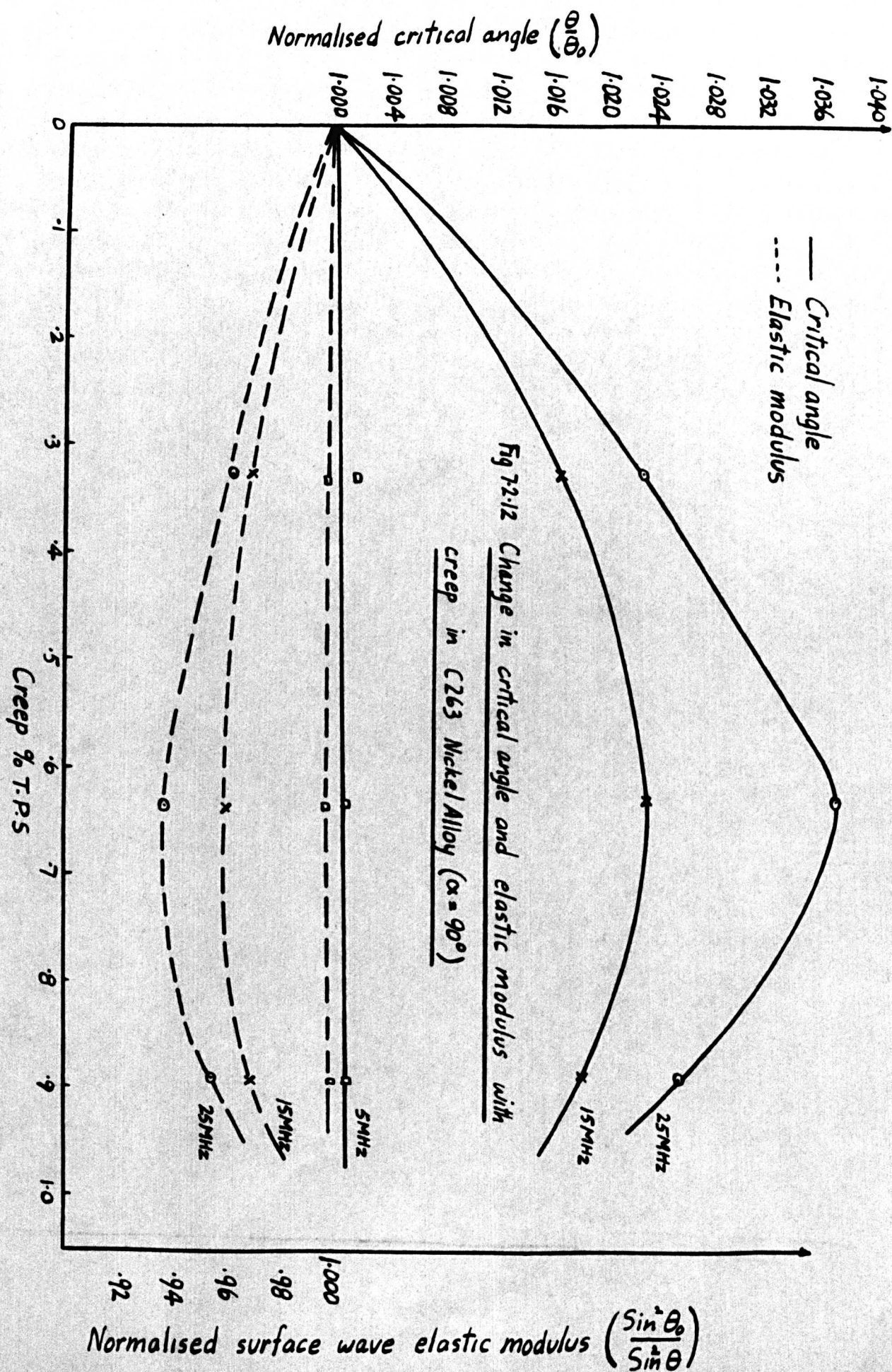
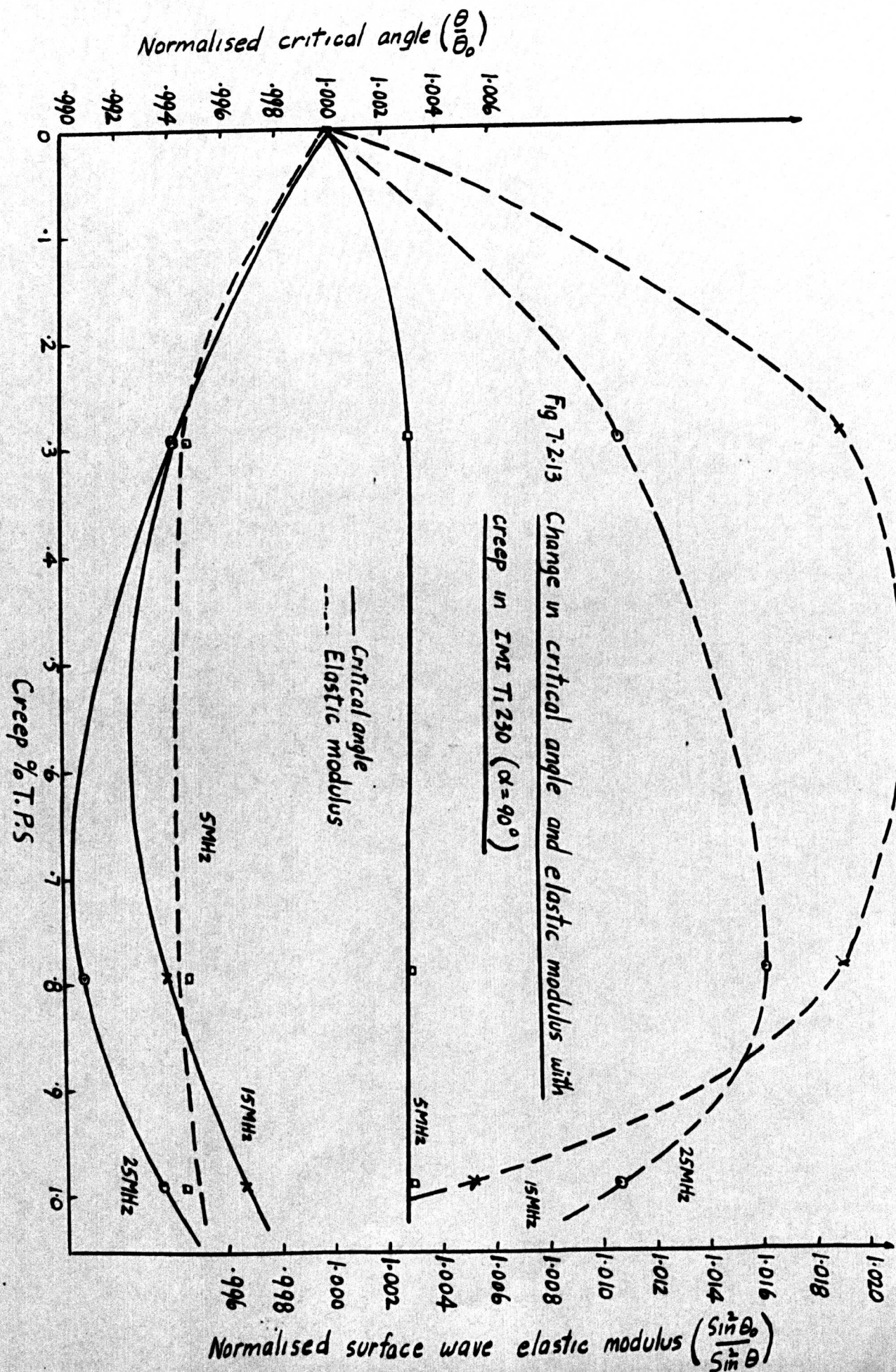


Fig 7.2.10 Change in critical angle and elastic modulus with creep in C263 Nickel Alloy ($\alpha = 45^\circ$)









C_w = the velocity of compressional waves in water.

Therefore:-

$$\sin \theta = \frac{C_w}{\sqrt{\frac{G_{SR}}{\rho}}} \quad \text{where } G_{SR} = \text{the elastic modulus of the surface waves and,}$$

ρ = the density of the solid.

Hence

$$\sin^2 \theta = \frac{\rho C_w^2}{G_{SR}} \dots\dots\dots 7.2.1$$

Now calling $\frac{G_{SR}}{G_{SRO}}$ the normalised surface wave elastic modulus,

where G_{SRO} is the elastic modulus of the specimen that has not been subjected to creep and G_{SR} is any elastic modulus of any crept specimen, equation(7.2.1) becomes:-

$$\frac{G_{SR}}{G_{SRO}} = \frac{\sin^2 \theta}{\sin^2 \theta_o} \dots\dots\dots 7.2.2$$

This is the normalised surface wave elastic modulus and the values for both materials can be seen plotted in Fig.7.2.8 for the nickel alloy and in Fig.7.2.9 for the titanium alloy. These are for *propagation along the rolling direction*. The subsequent figures are for the 45° and 90° from the direction of rolling. (see figs.7.2.10 to 7.2.13)

7.2.3 Discussion of results and conclusions

From the range chart (see fig.7.2.2) for the nickel alloy, it can be seen that its properties vary from point to point on the surface. From the metallographic photograph (Fig.7.2.17), it can be seen that the grain size varies considerably.

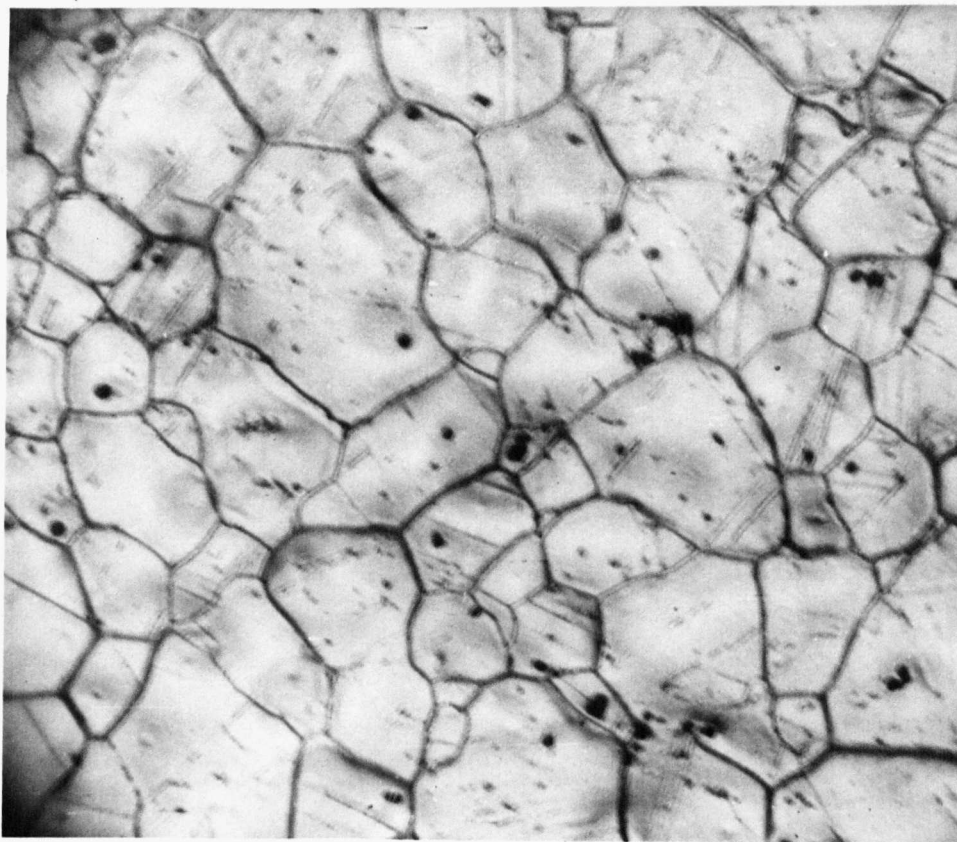


Fig. 7.2.17 Photograph showing the variations in grain sizes
in C263 Nickel Alloy.

It therefore can be said that the ultrasonic goniometer can be a useful tool for quick determination of surface or near surface inhomogeneity in materials.

The goniograms for IMI 230 titanium for 5MHz shows that there is little difference in the angle of incidence versus reflected amplitude response for specimens in different states of creep. The same can be said for the other two ultrasonic test frequencies.(15 and 25MHz). These goniograms can be seen plotted in Figs.7.2.3, 7.2.4, and 7.2.6 respectively. What can be said however is that as frequency increased ~~there~~ was an increase in the number of peaks and troughs observed in the goniogram before the critical angle. A similar observation was made by Rollins⁹² when he measured specimens 10×10^{-3} in. thick. The thickness of the specimen used in this test was 48×10^{-3} in.

From Fig.7.2.6 and 7.2.7 it can be seen that there is an increase in critical angle away from the rolling direction in both materials. There are more variations in critical angle in the nickel alloy.

It follows from eq.3.1 that as θ increases $\sin\theta$ increases. i.e $\sin\theta = \frac{C_w}{C_R}$ where C_w is the velocity of compressional wave in water, and C_R is the velocity of the surface waves. Therefore the surface wave velocity will decrease away from the rolling direction since there will be preferred orientation in the direction of rolling. This will cause anisotropy and the elastic constant will be highest in the rolling direction.

The results show that the ultrasonic goniometer using ultrasonic surface waves can reliably measure preferred orientation. Crecraft¹ reported on similar sensitivity for ultrasonic bulk waves. The elastic modulus is lowest 90° away from the direction of rolling. This can be seen in the

graphs since elastic modulus is inversely proportional to critical angle. Rollins¹²³ results for surface wave velocity in cold rolled copper showed a similar trend.

No significant difference in the variations in critical angle with orientation can be observed between specimens in different states of creep for the IM1230 titanium alloy.(see Fig.7.2.7). Also measurements made at all three ultrasonic frequencies appear to follow the same pattern. At 45° from the rolling direction at 15 and 25MHz(Fig. 7.2.7), a difference in the change of critical angle with different degrees of creep was observed. No pattern was observed however.

For the C263 Nickel alloy (see Fig.7.2.6), the specimen with zero creep showed the greatest variations of critical angle at 15MHz. The specimen in 0.33%T.P.S. state of creep showed the highest variations at 5MHz and the specimen with 0.63%T.P.S state of creep showed similar changes at 5 and 15MHz but slightly greater change at 25MHz. What can generally be said is that the critical angle increases in each case for angles away from the rolling direction. No other distinct pattern was observed.

Considering the change in critical angle with creep for both materials, the graphs showing the changes are presented in such a way that a direct comparison can be made between the two materials. Graphs are shown for all three orientation directions. Graphs for the nickel alloy are followed by the corresponding graph for titanium alloy. These can be seen in Figs.7.2.8. to 7.2.13.

It can be seen that there is a frequency effect in all the graphs.

At low frequencies the change in critical angle is very much smaller *than* at higher frequencies. This demonstrates that higher frequencies can be used to detect early changes in creep.

For the nickel alloy at each orientation the critical angle increases to reach a peak value at about 0.63%T.P.S. The curve then falls off as the creep increases. This means that the velocity of the surface wave decreases to a minimum value at about 0.63%T.P.S., and then increases again at higher creep levels.

For the IMI230 titanium alloy it was found that at 5MHz there was an initial change in critical angle with creep then a levelling off beyond about 0.33%T.P.S. For the higher frequencies however, this was not the case. For the 25MHz test signal at $\alpha = 0$, (see fig.7.2.9), the critical angle decreased to a minimum at about the same value as for the nickel alloy, i.e. about 0.63%T.P.S. After this the critical angle increased again. A similar pattern was observed at each orientation.

The normalised surface wave elastic modulus for both materials can be seen plotted in Figs.7.2.8 to 7.2.13. For the nickel alloy the elastic modulus changed very little at a frequency of 5 MHz. At higher frequencies the elastic modulus decreased to a minimum value at about 0.63%T.P.S. Beyond this point there was an increase in the elastic modulus. In some cases it was difficult to determine the state of creep which gave the minimum value of elastic modulus. For all orientations the trend was the same.

For the IMI230 titanium alloy, the elastic modulus for the 5MHz test signal decreased initially at 0.33%T.P.S. but then levelled off as creep increased. However for the higher frequencies the elastic modulus increased to a peak value at about 0.63%T.P.S. then decreased as creep increased. For the 25MHz signal at the 45° orientation the change in

elastic modulus was very much greater than at 5 or 15MHz. It appeared that there was a steady increase in elastic modulus right up to 0.8%T.P.S.

Comparing the behaviour of the two materials it can be said that with increase in creep the elastic modulus decreased at high frequencies for the nickel alloy but increased for the titanium alloy. Both materials demonstrate that there is a frequency effect in the mechanism due to creep. Lower frequencies are less sensitive detectors of the early changes in creep. Higher frequencies have to be used to detect early changes due to creep.

Considering the results in general, two approaches will be used to attempt an explanation of the mechanism involved which will respond in such a manner to ultrasonic frequencies. The approaches are:-

- (a) An explanation in terms of dislocation theory, and,
- (b) An explanation in terms of hardness and grain size.

7.2.3(1) Explanation in terms of dislocation theory

Before attempting an explanation of the creep mechanism which will respond in such a manner to ultrasonic frequencies, it is appropriate to discuss the basic theory of dislocation.

7.2.3(1.1) Theory of dislocation

The theory of dislocations will be discussed in this section because at least a basic understanding of the mechanism will be necessary in order to interpret the results.

A vibrating string model is considered and the results expected from this model are used to discuss the results of the present study. Dislocations cause changes in ultrasonic wave velocity in metals. Preferred orientation of grains and of dislocations can also change the velocity of these waves. When materials are cold worked, dislocations become oriented in some favourable direction.

7.2.3(1.2) The vibrating string model

This vibrating string model was developed to explain the elastic modulus change in metals. Read¹³¹ suggested that the damping loss and modulus changes observed in metals might arise from the motions of dislocations. Later, calculations of the elastic constant reduction due to dislocations was done by Mott¹³². It was assumed that a dislocation network is contained in a pure crystal, and the dislocation segments between network points bow out in response to an applied oscillatory stress. The results showed that there was a reduction in elastic constant which was proportional to the square of the dislocation segment loop length. This was good for low frequencies. The effects of inertia and viscosity of the dislocation line were considered by Eshelby¹³³. He did not use the vibrating string model.

The vibrating string model was developed by Koehler¹³⁴. He suggested that a dislocation segment can be considered as a string which vibrates under the influence of applied external oscillatory stress. Granato and Lucke¹³⁵ improved the model physically and analytically. Other workers, such as Nowick¹³⁶ and Weertman¹³⁷ made other contributions to the model.

De Witt and Koehler¹³⁸ studied the effect of crystal anisotropy on the interaction of dislocations with applied stress waves as well as

the effect on the elastic constant. The model of dislocations damping developed by Granato and Lucke appears to be the most suitable model available for our purposes.

The vibrating string analogy, including tension, viscous damping and internal forces was introduced by Koehler as early as 1952. He considered a dislocation line pinned with impurities distributed at random. He derived the equation of motion of the dislocation line for low amplitude stresses. He also computed the damping and elastic modulus expected at low frequencies, which agreed with Mott's results. Weertman was the first to give a solution of the Koehler equation for all frequencies, for the case when all the loop lengths are equal. However, with this solution it was difficult to consider the random distribution of dislocation and pinning points or to discuss the effects of various parameters on the loss.

It was Granato and Lucke who connected all the theories to derive a comprehensive quantitative theory of dislocation on the basis of the vibrating string model. This contained both amplitude-independent and amplitude-dependent types of loss. Two types of dislocation lines with two types of pinning points were considered. These were firstly, nodes in the dislocation lines, and secondly impurities and other point defects. In this case the amplitude-dependent loss is negligible.

The damping and modulus change were calculated for all frequencies. This was presented in a form which permitted a distribution of loop lengths to be introduced and an analysis of the dependence of damping on other parameters to be made.

7.2.3(1.3) Dislocation vibration effects on shear wave velocity

The velocity difference between two shear waves polarised parallel and perpendicular to the axis of propagation in metals can be explained

in terms of dislocation vibrations¹³⁹. This difference is called the dispersion of shear wave birefringence. Consider the shear wave velocity dispersion. At the megacycle range of frequencies the dislocation vibrations would be sufficiently damped so that the dislocation would no longer be able to follow in phase with the oscillating stress and that a dispersion will appear.

Dislocations are pinned down by impurities and the portion of the line between two impurity atoms oscillates back and forth on its slip plane like a stretched string. As the ultrasonic shear stresses are very small, it is assumed that the pinning of the dislocation is so strong that no breakaway of the dislocation network lengths occurs. It is assumed that the interactions between the dislocations can be neglected.

Expressions may be derived for the relative change in velocity from the equation of motion for the damped dislocation line. Details are given in appendix 7. Although generally both edge and screw dislocations can be present, the theory of dislocation damping is applicable only to the effects of edge dislocations. The velocity change for pinned dislocation loop theory¹³⁵ as a function of frequency can be written as:-

$$\frac{\Delta V}{V} = \frac{V_0 - V(w)}{V_0} = \frac{\mu N b^2 l^2}{24C} \frac{(1 - \frac{w^2}{w_0^2})}{(1 - \frac{w^2}{w_0^2})^2 + w^2 d^2}$$

where μ is the shear modulus, N is the total length of the dislocation line per unit volume, b is the Burger's vector, l is the dislocation line length and C is the tension in the dislocation line. The term w_0 is the resonant frequency of the dislocation line and $d = \frac{B l^2}{12C}$ where B is the damping constant.

When an alternating stress wave is introduced into the crystal, it is found that the dislocation loops can be set into vibration only when there is a shear component of the stress in the direction of slip in a given slip plane. Therefore it is necessary to resolve the applied alternating stress (which must be transverse), firstly into the given slip plane and then into the slip direction in this slip plane. This process is carried out for all the operative slip systems (combinations of slip planes and slip directions) in order to obtain the orientation factor Ω .

From the above equation the change in shear wave velocity is:-

$$\frac{\Delta V}{V_0} = K \Omega N l^2 \frac{(1 - \frac{w^2}{w_0^2})}{(1 - \frac{w^2}{w_0^2})^2 + w_d^2} \quad (\text{See appendix 7}).$$

Therefore it can be seen that the fractional change in velocity is proportional to the dislocation density N and also the orientation factor Ω . The change in velocity for the fixed orientation depends on the value of the modulus for that polarisation direction, the resolved shear stress on each of the slip systems corresponding to the stress distribution in the system, and on the distribution of the dislocations over the various slip planes. Thus the orientation dependence is in general, different for the different types of wave. The velocity also changes due to a change in the "effective dislocation density".

The effects due to dislocation motion, while directly affecting the attenuation of the ultrasonic wave, produce only second order change in velocities, or difference between the velocities due to elastic strains and velocities due to elastic and dislocation strains. The change in velocity also depends on the nature of the material through the constant

K which includes some physical properties of the material.

The resonant frequency of the dislocation line for most metals would be in the range 200 - 3,000 MHz. At low frequencies, kilocycle range, the change in velocity remains constant with increase in frequency. For the higher frequencies, megahertz range, the expression for the change in shear wave velocity can be written as:-

$$\frac{\Delta V}{V_0} = K_2 N l^2 \left(1 + \frac{w^2}{w_0^2} - w^2 d^2 \right) = K_3 (1 + a w^2) \dots \dots \dots 7.2.2$$

where $a = \left(\frac{1}{w_0^2} - d^2 \right)$ and $K_3 = K_2 N l^2$

From the expression for $\frac{\Delta V}{V_0}$ it can be seen that for a small range of frequencies $\frac{\Delta V}{V_0}$ is linear with frequency. It therefore follows that the fractional change in velocity due to dislocation vibration under the influence of an alternating stress wave of low amplitude remains approximately constant at low frequencies then increases linearly in the megahertz range. Rewriting the equation we get,

$$\frac{\Delta V}{V_0} = \left(\frac{\Delta V}{V_0} \right)_I (1 + a w^2) = K_3 (1 + a w^2) \dots \dots \dots 7.2.3$$

where $\left(\frac{\Delta V}{V_0} \right)_I$ can be called the initial fractional velocity change, and is a parameter dependent upon the nature of the material.

For ultrasonic surface waves the same theory of dispersion and damping due to dislocation loops is applicable, since there is a shear component in the particle displacement vector. Therefore the results of measurements of surface wave velocities will be discussed in the context of the above theory.

7.2.3(1.4) Creep in C263 Nickel alloy

It can be seen in all the curves Figs. 7.2.8, 7.2.10 and 7.2.12, that higher frequencies were better for detecting changes due to creep.

This implies that there was more ultrasonic damping at high frequencies, because the change in critical angle was greatest at the highest ultrasonic test frequency.

In the context of the theory, of dislocation, the change in velocity is a function of frequency, the dislocation density, and the dislocation loop length. It appears therefore that in this material, as creep increases, either the dislocation density or the dislocation loop length or both increases initially and then decreases during the later stages of creep.

This is deduced from the response of the critical angle to creep curves for one orientation and considering either the 15 or 25 MHz test frequency. The increase in dislocation density with creep has been reported by e.g. Granato and DeRosset.⁴⁰ Measuring the changes in dislocation density with creep in sodium chloride crystals they found that the dislocation density increased in a similar manner to the increase in creep. Gilman and Johnston³⁸ reported on similar findings.

If it is assumed that in the Nickel alloy the dislocation density increases with creep, then the curves for critical angle versus creep should increase continually as creep increases. As can be seen this was not the case. Possibly there was an initial increase in dislocation density, then during the later stages of creep there was annihilation of dislocations. No work has been reported on the change in dislocation density with creep for this material.

Consider now the change in dislocation loop length. Assume that the loop length increases with creep, then falls off during later stages of creep. (This was found to be the case in sodium chloride by Granato and De Rosset)⁴⁰. Then the curve of critical angle to creep should increase during early stages of creep then fall off as creep increases.

In our case it can be seen that this was the manner in which the critical angle changed with creep. No work has been reported on how loop length varies with creep for this C263 nickel alloy. From the experimental results it is suggested that during the early stages of creep both mechanisms i.e. increase in dislocation density and loop length, are active in causing an increase in critical angle. Beyond some value of creep, about 0.6%T.P.S., there is levelling off in the dislocation density and a shortening of the loop lengths. This appears to be the case since it can be seen that at higher values of creep the decrease in critical angle i.e. increase in surface wave velocity is greatest at 25MHz the highest test frequency. This will be the case if the dislocation segments were shortening with increase in creep. The curves for 45 degrees and 90 degrees from the direction of rolling Figs.7.2.10 and 7.2.12 demonstrate this clearly.

Maybe the shortening of the dislocation segments for this material can be attributed to the fact that the creep test was conducted at 780°C. It has been reported¹⁴⁰ that beyond 750°C for this material appreciable ageing and precipitation take place. There is a phase transformation and probably these new particles contribute to pinning and therefore shortening of the dislocation segments.

7.2.3(1.5) Creep in IMI230 Titanium

As can be seen in Figs.7.2.9, 7.2.11 and 7.2.13 are the results of

of the change in critical angle with creep for IMI230 titanium. It will be observed that the results are different from that for the nickel alloy. If the same reasoning⁴⁰ is used to interpret the results it will mean that the dislocation density and loop length decreases initially with creep instead of the increase as in the other material. Next, beyond some value of creep, again about 0.6%T.P.S., the dislocation density levels off and the loop length increases.

No work has been reported on the change in dislocation density or loop length with creep for this material. However as reported by Kornilov et al²⁸ the mechanism of plastic deformation in titanium and its alloys considerably differs from that of the metals belonging to the VIth and VIIIth group of the periodic system. For example alloying of nickel leads to the pinning down of part of the slip planes and the blocking of dislocations. Alloying of titanium however leads to a decrease in the number of active plastic deformation centres.

It would be argued that the dislocation mechanism in the IMI230 titanium is opposite to the mechanism active in the C263 Nickel alloy. Maybe the dislocation loop length increases beyond about 0.6%T.P.S. This appears to be the case because beyond this point there is an increase in critical angle i.e. a decrease in velocity. This means that there is less dislocation damping beyond this point for higher frequencies.

7.2.3(2) Explanation in terms of grain size and hardness

7.2.3(2.1) Creep in C263 Nickel alloy

The calculated results obtained for the surface wave elastic modulus can be seen plotted in Figs.7.2.8, 7.2.10 and 7.2.12. since the

grain size increases with creep¹⁴⁰ it will be expected that the elastic modulus will decrease. In the results obtained it can be seen that the elastic modulus has decreased.

A plot of hardness for a plain sheet as a function of ageing time shows that the hardness for around 780°C falls off beyond about 32 hours of ageing time¹⁴⁰. In the creep test on this material the times taken for the three stages of creep were all greater than this value (see app.3).

No figures of hardness are given for beyond 128 hours of ageing time but it would be assumed that the falling trend in hardness will continue beyond this point. This means that the material is becoming softer with creep. The curve of the elastic modulus shows this to be the case.

There are no indications in the plots for grain size or hardness that beyond a certain time the hardness increases as was obtained in the present study. However this might be due to the fact that during the ageing time for the curves of hardness and grain size, there was no tensile stress applied. These specimens were not subjected to creep. In the present study, however, the specimens were crept, and it is very likely that different mechanisms were active. These mechanisms might have been responsible for causing an increase in hardness and resulting in an increase in surface wave elastic modulus.

7.2.3(2.2) Creep in IMI230 titanium

It has been reported¹⁴¹ that the hardness level was unlikely to change significantly after creep testing this material at 300°C. This was the temperature at which the material was subjected to creep. Also¹⁴¹ that at this temperature recrystallization will not occur.

What can occur at this temperature is age hardening. Blenkinsop and Goosey²⁹ showed how the hardness of this material varies with time at a temperature of 400°C. This was above the temperature used in the present study, but possibly a similar trend in hardness will occur at 300°C.

Measurements showed that hardness increased with time, reaching a peak value then falling off with time. The curves of elastic modulus versus creep (Figs. 7.2.9, 7.2.11, 7.2.13.) show that the elastic modulus follows a similar pattern for all measured directions along the surface.

7.2.4 Possible application of the results on creep

Considering the results for both materials i.e C263 Nickel alloy and IMI230 Titanium alloy, it can be said that by the use of ultrasonic critical angle reflectometry early stages in creep can be detected. In both cases it appears that it could be possible to measure up to 0.6% T.P.S. state of creep. Beyond this point the curve turns over, and the curve for critical angle versus creep become double valued.

In most industrial situations there will be a tolerance limit on the extension of components or machine parts, when subjected to tensile stress at high temperatures. It will be the decision of engineers to consider whether the technique reported in this present study is suitable for industrial application.

Maybe the tolerance limits on extensions is far less than 0.6% T.P.S. This quite likely is the case for components such as turbine blades used in jet engines. The author suspects that there are many more

possible areas with tolerance limits lower than this figure. Therefore with careful and detail development this method of testing could be very useful to industry.

7.3 FATIGUE

7.3.1 Data collection

The critical angle of incidence was measured for all specimens at three angles of orientation. These were along the rolling direction ($\alpha = 0$), 45 degrees from the rolling direction ($\alpha = 45$), and 90 degrees from the rolling direction ($\alpha = 90$). All specimens were measured in the unfatigued state in order to determine their "as received" state.

Consider one specimen. This specimen was measured in its "as received" state for all three directions as given above. It was then fatigued to N_1 cycles at a stress level S_1 and the critical angle again measured in all directions.

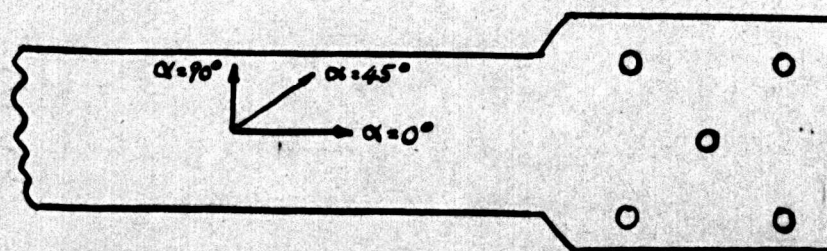
After this, a further cycling was done to N_2 cycles, at the same stress level S_1 . The critical angle of incidence was again measured for all directions. The specimen was then cycled to N_3 cycles at the same stress level S_1 and the critical angle again measured for all directions.

Further cycling at the same stress level was done and after each cycling the critical angle measured. This procedure was continued until failure of the specimen.

Three specimens were used at most stress levels and two types of material were used. These were mild steel and titanium alloy (see ch.6).

The stress levels used were $19.5 \text{ Ton/in}^2 (300 \text{ MN/m}^2)$ and $22.5 \text{ Ton/in}^2 (350 \text{ MN/m}^2)$ for the mild steel and $16.8 \text{ Ton/in}^2 (260 \text{ MN/m}^2)$, $21 \text{ Ton/in}^2 (325 \text{ MN/m}^2)$ and $29.5 \text{ Ton/in}^2 (455 \text{ MN/m}^2)$ for the titanium specimens. Tests were done at 5, 15, and 25 MHz. (ultrasonic frequencies)

Fig 7.3.1(a) shows the type of fatigue loading used for this high stress level low cycle fatigue program.



← direction of rolling

Specimen for fatigue testing

Fig 7.3.1 Showing the different directions of surface wave propagation

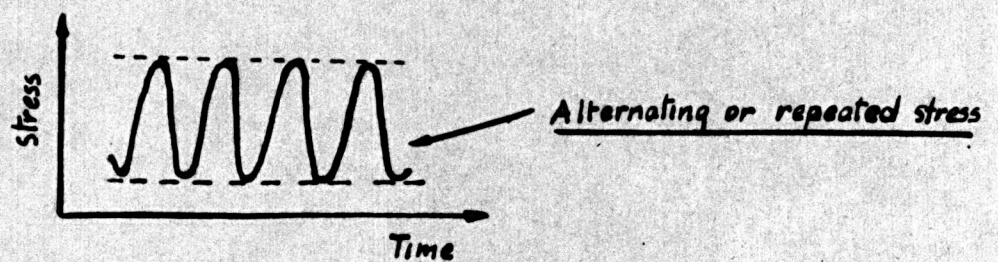


Fig 7.3.1(a) Showing the type of loading used for fatigue tests.

7.3.2 Results and data analysis

The mean value of the critical angle of incidence was calculated from the results obtained for each frequency and direction of propagation, on each specimen. The mean value of the critical angle was used for the plotting of all graphs. The normalised critical angle of incidence was plotted versus the number of fatigue cycles(N), or the ultrasonic test frequency(f).

For the first case the critical angle was normalised to the critical angle of the unfatigued specimen. Figs.7.3.2, 7.3.3 and 7.3.4 are plots of this normalised critical angle versus fatigue cycles for mild steel at different frequencies and orientations.

For the second case the critical angle was normalised to the critical angle of incidence of the specimen at the 5MHz ultrasonic test frequency. Graphs of critical angle versus the ultrasonic test frequency can be seen plotted in Figs.7.3.5 and 7.3.6. They are plotted for the two stress levels used for the mild steel.

Graphs of the normalised critical angle versus the stage of fatigue life can be seen plotted for the titanium alloy in Figs.7.3.7 and 7.3.8. The plots are for different orientation and for the stress levels used.

The corresponding graphs for the change in normalised critical angle versus frequency for the titanium alloy can be seen plotted in Fig.7.3.9. This was plotted as before for various stages in fatigue life.

Two further graphs were plotted. These were for different stress levels. Fig.7.3.10 is the plot for the 16.8Ton /in² stress level, and Fig.7.3.11 is the plot for the 21Ton /in² stress level. Both graphs were for the titanium specimens.

RESULTS FOR MILD STEEL

Fig 7.3.2 Showing the change in critical angle with number of fatigue cycles at two stress levels (average of 3 specimens)

$f = 5\text{MHz}$, Mild steel

$$S_1 = 19.5 \text{ Ton} \cdot \text{in}^2 (300 \text{ MN/m}^2) = 65\% \text{ U.T.S}$$

$$S_2 = 22.5 \text{ Ton} \cdot \text{in}^2 (350 \text{ MN/m}^2) = 75\% \text{ U.T.S}$$

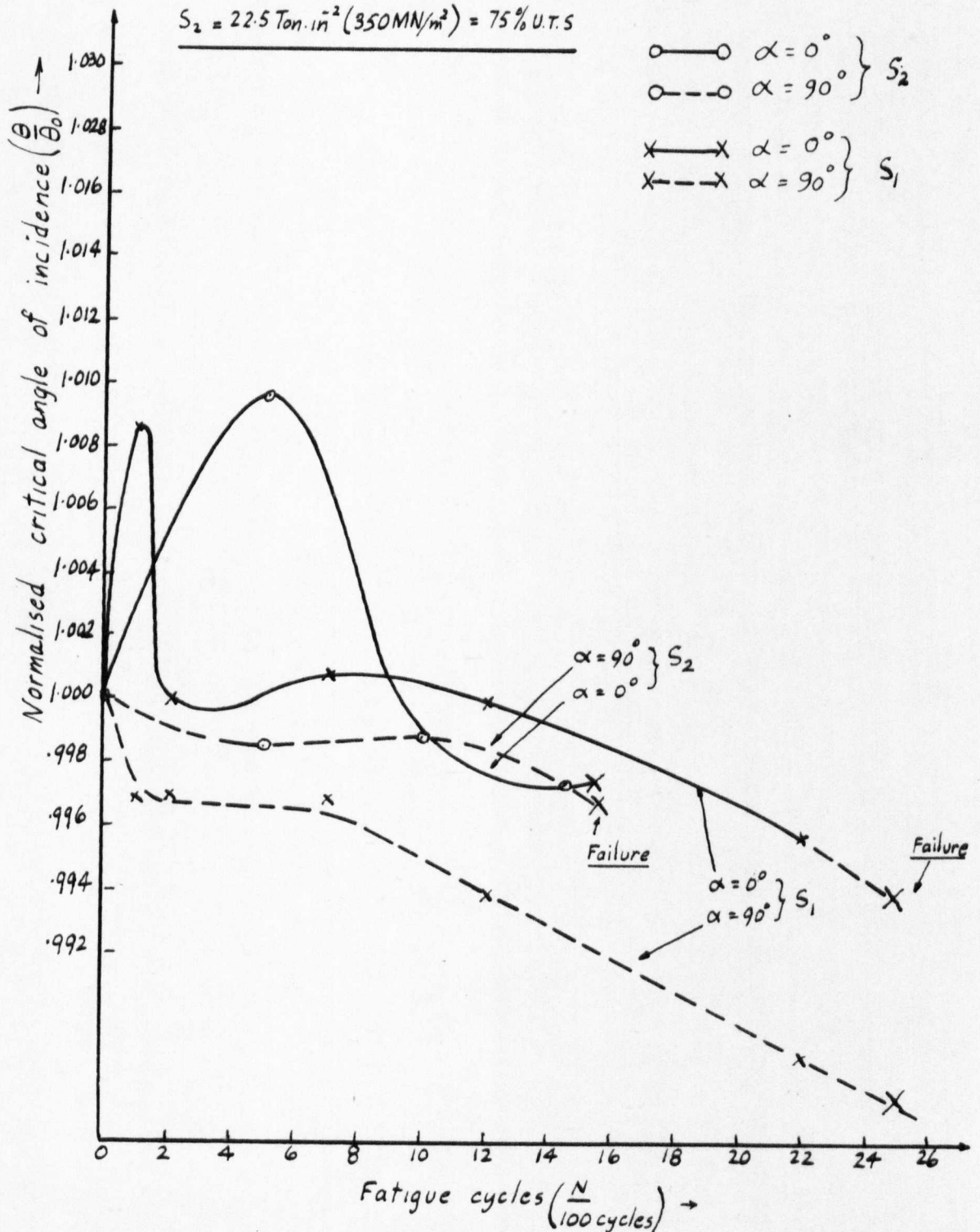


Fig 7.3.3 Showing the change in critical angle with number of fatigue cycles at two stress levels (average of 3 specimens)

$f = 15 \text{ MHz}$, Mild steel,

$$S_1 = 19.5 \text{ Ton. in}^{-2} (300 \text{ MN/m}^2) = 65\% \text{ U.T.S}$$

$$S_2 = 22.5 \text{ Ton. in}^{-2} (350 \text{ MN/m}^2) = 75\% \text{ U.T.S}$$

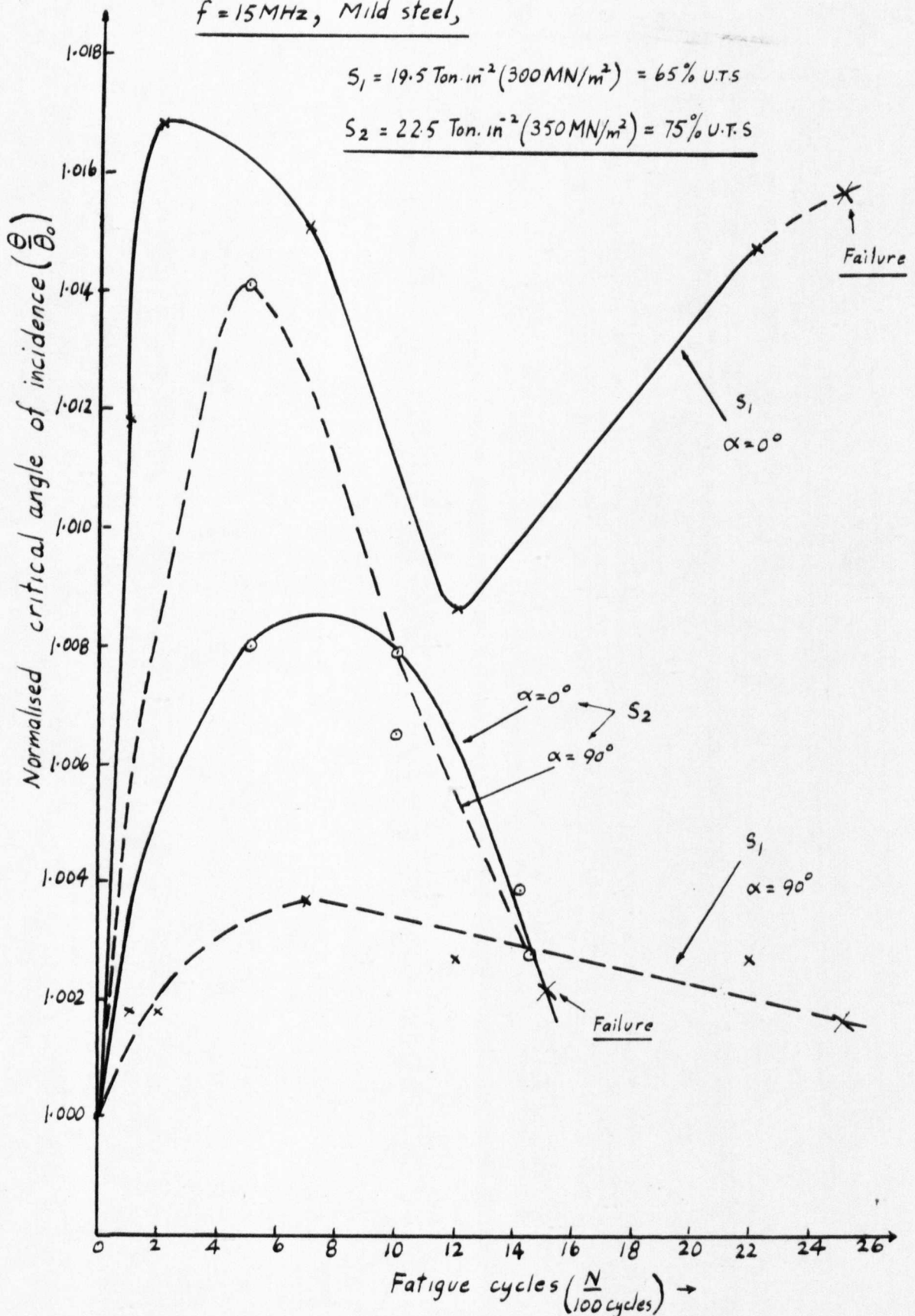


Fig 7.3.4 Showing the change in critical angle with number of fatigue cycles at two stress levels (average of 3 specimens)

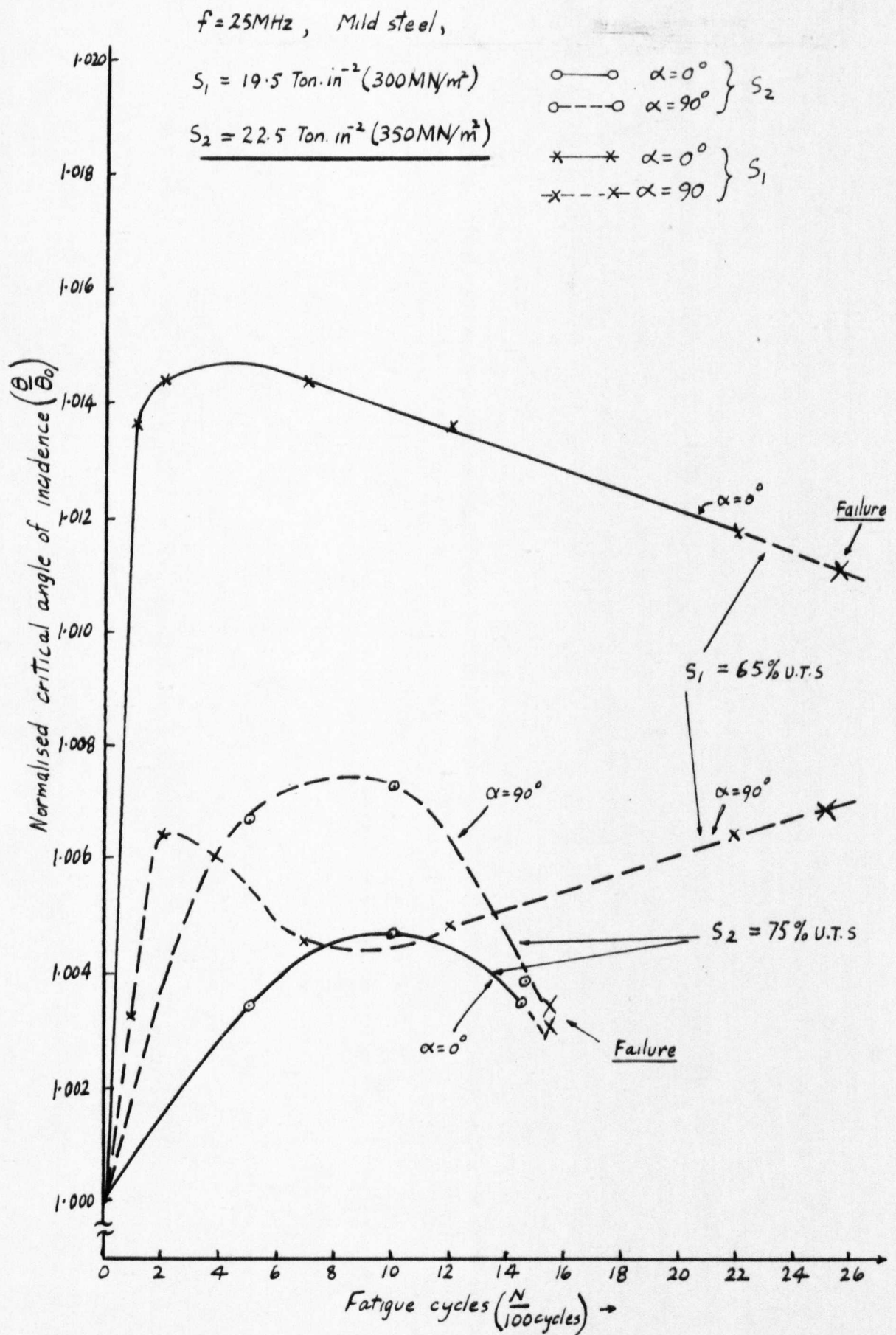


Fig 7.3.5 Showing the change in critical angle with frequency
at various stages in fatigue life

Mild Steel, $\alpha = 0^\circ$, $S = 19.5 \text{ Ton.in}^{-2}$ (300 MN/m^2)
 $= 65\% \text{ U.T.S}$

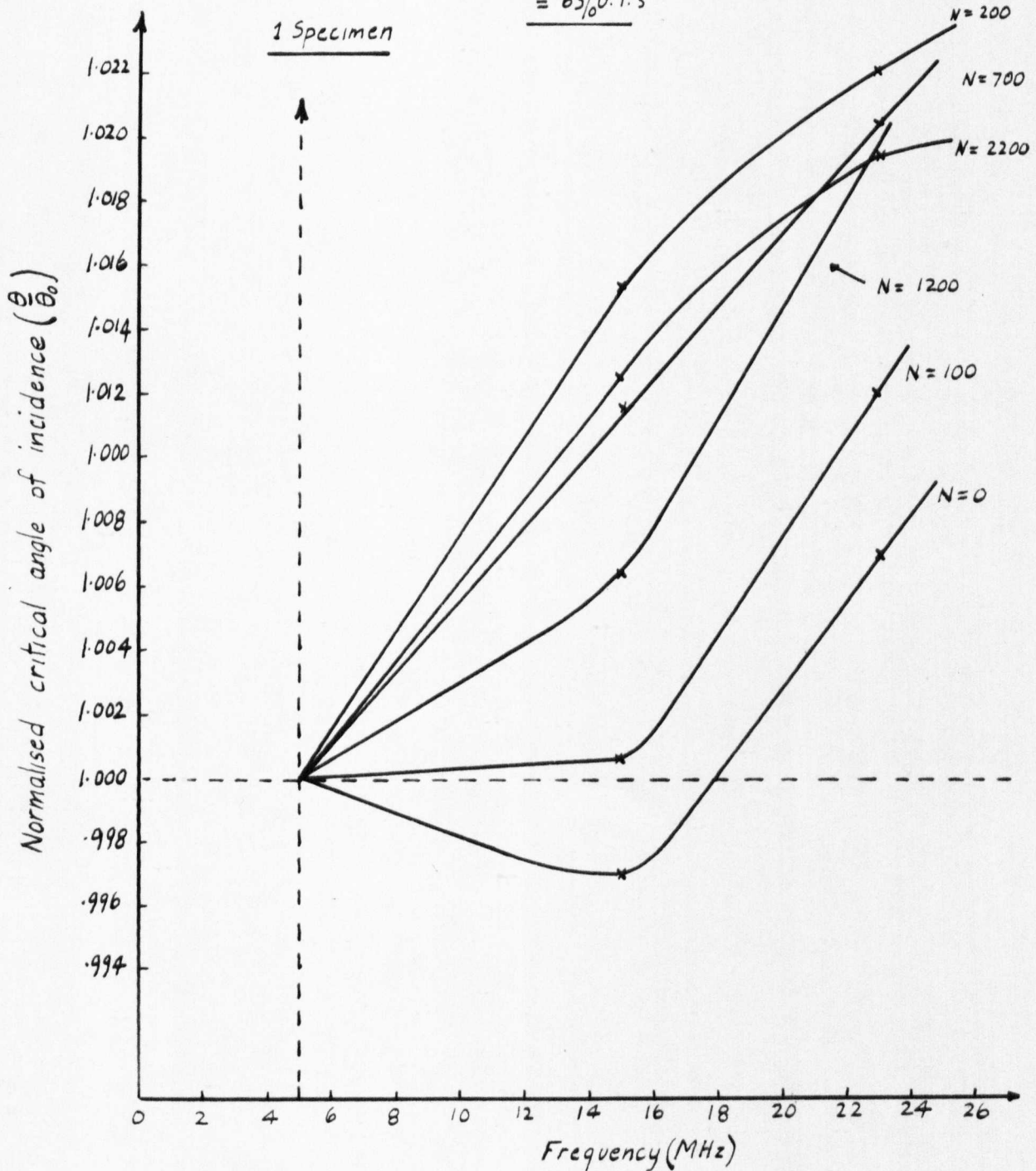
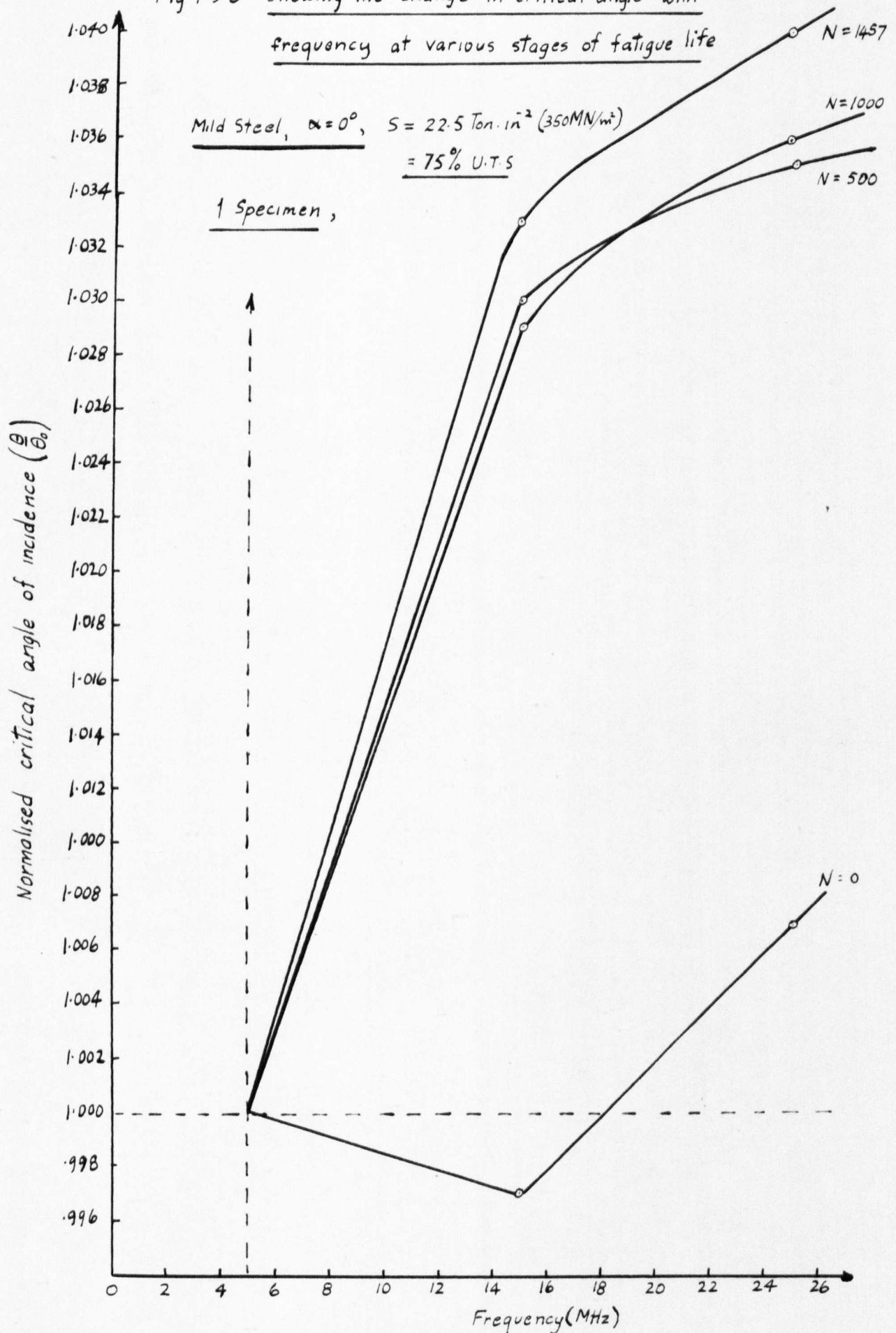


Fig 7.3.6 Showing the change in critical angle with frequency at various stages of fatigue life



RESULTS FOR TITANIUM (Ti 230)

Fig 7.3.7 Showing the change in critical angle with number of fatigue cycles. (Average of 3 specimens)

$T, 230, \alpha = 0^\circ \quad S = 29.5 \text{ Ton. in}^2 \text{ (455 MN/m}^2\text{)}$

$= 84\% \text{ U.T.S}$

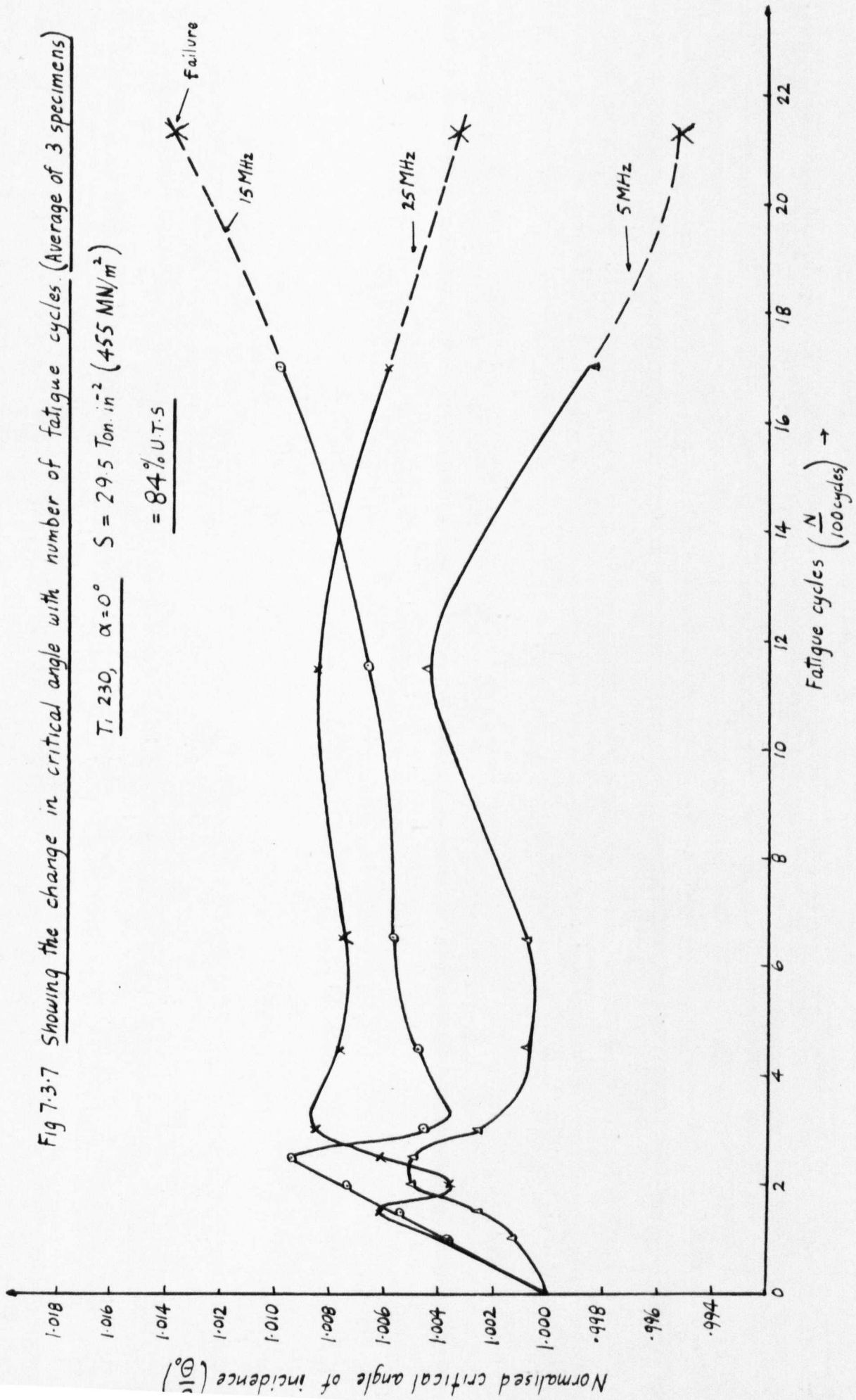


Fig 7.3.8 Showing the changes in critical angle with number of fatigue cycles (average of 3 specimens)

$$\begin{aligned} \text{Ti 230, } \alpha = 90^\circ, S &= 29.5 \text{ Ton. in}^{-2} (455 \text{ MN/m}^2) \\ &= 84\% \text{ U.T.S.} \end{aligned}$$

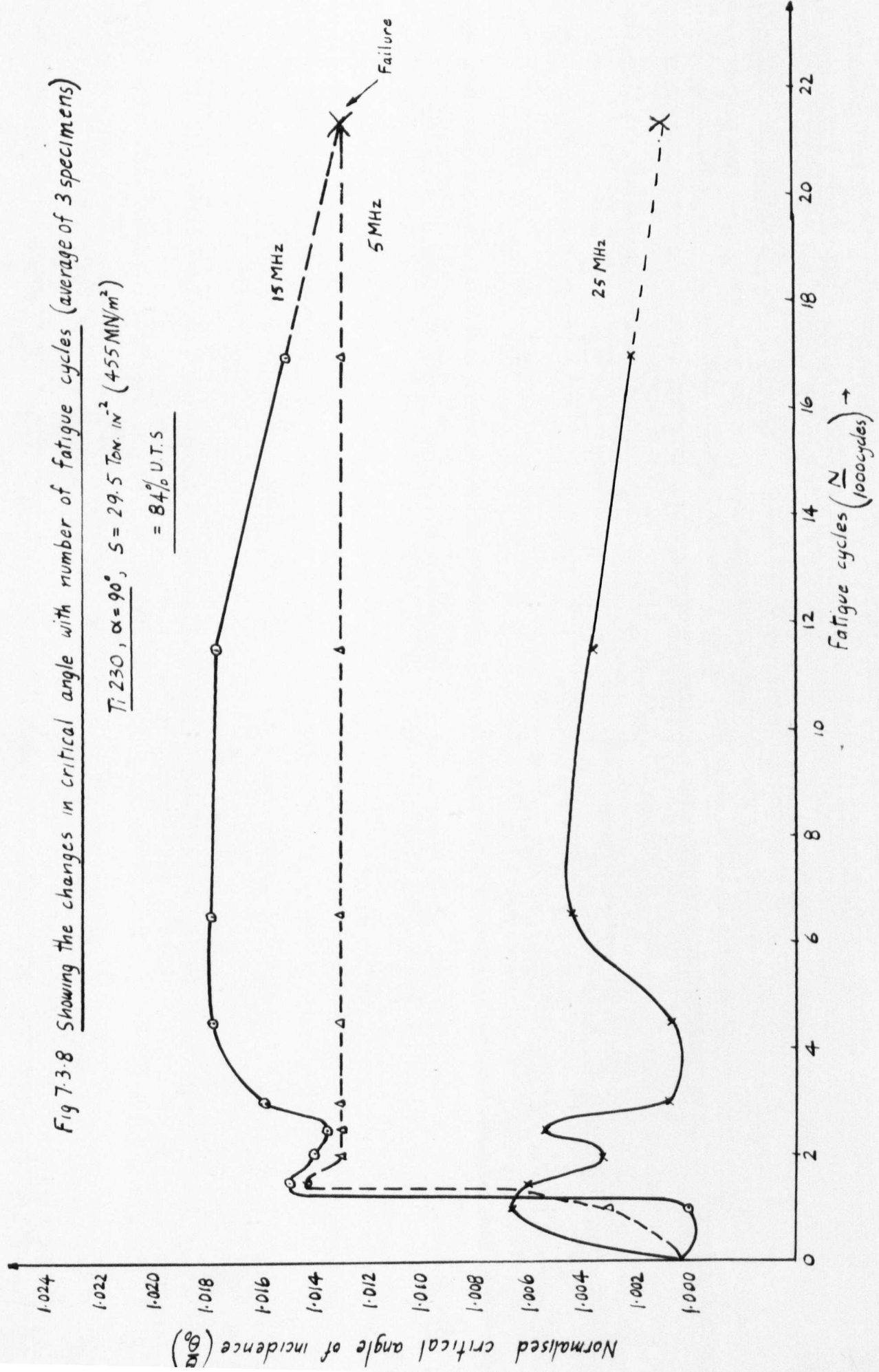


Fig 7.3.9 Showing the change in critical angle with frequency
at various stages in fatigue life

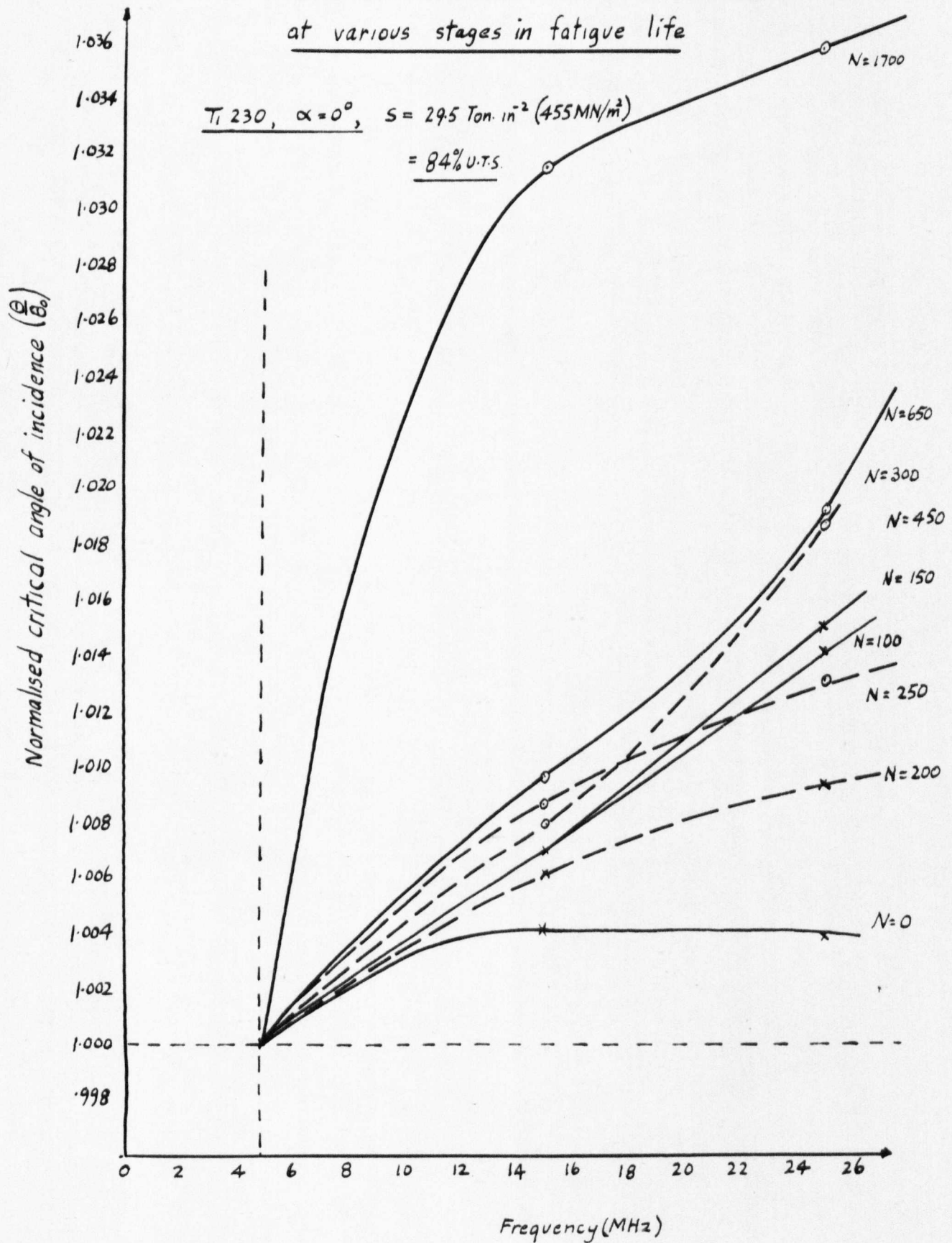


Fig 7.3.10 Showing the change in critical angle with number of fatigue cycles.

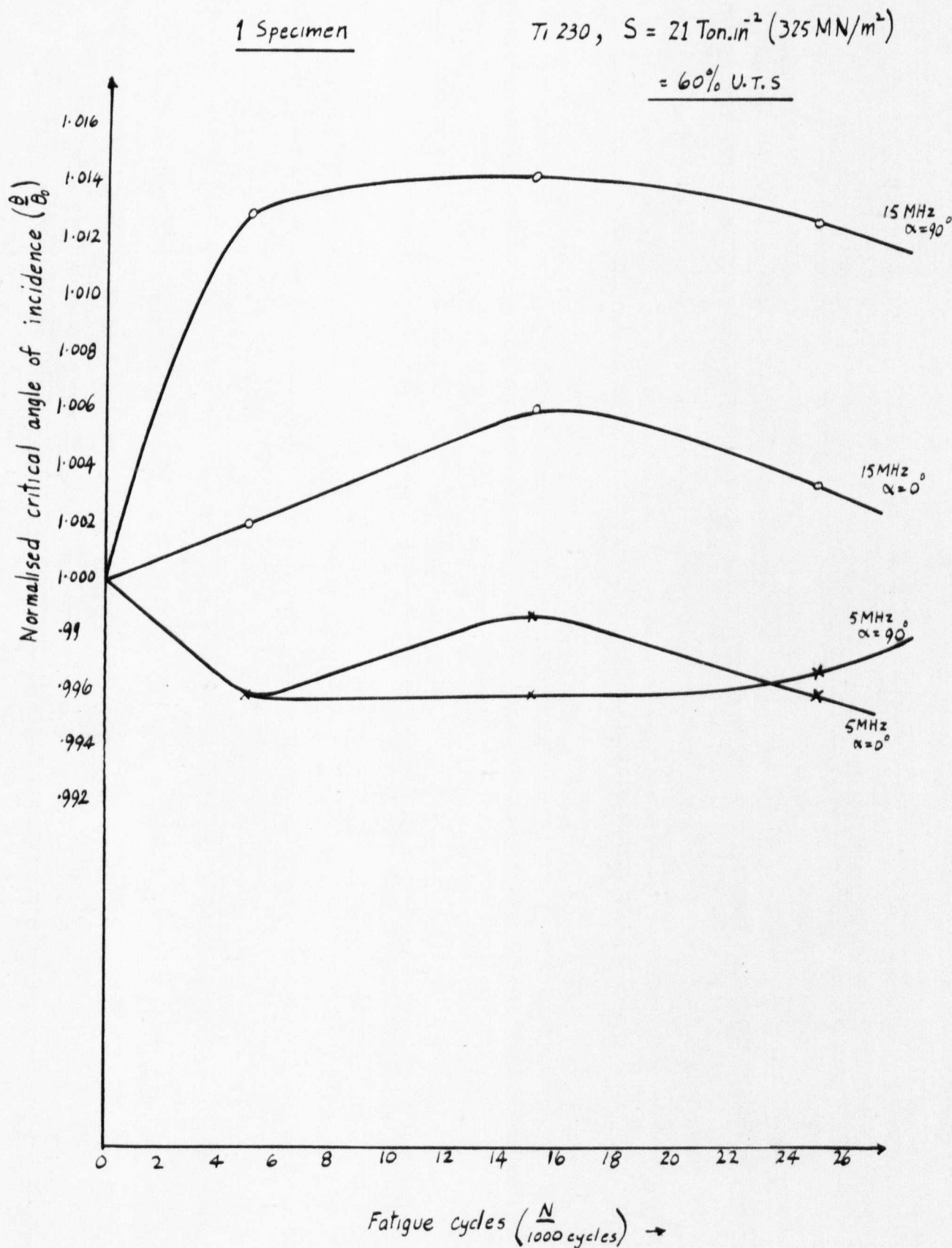
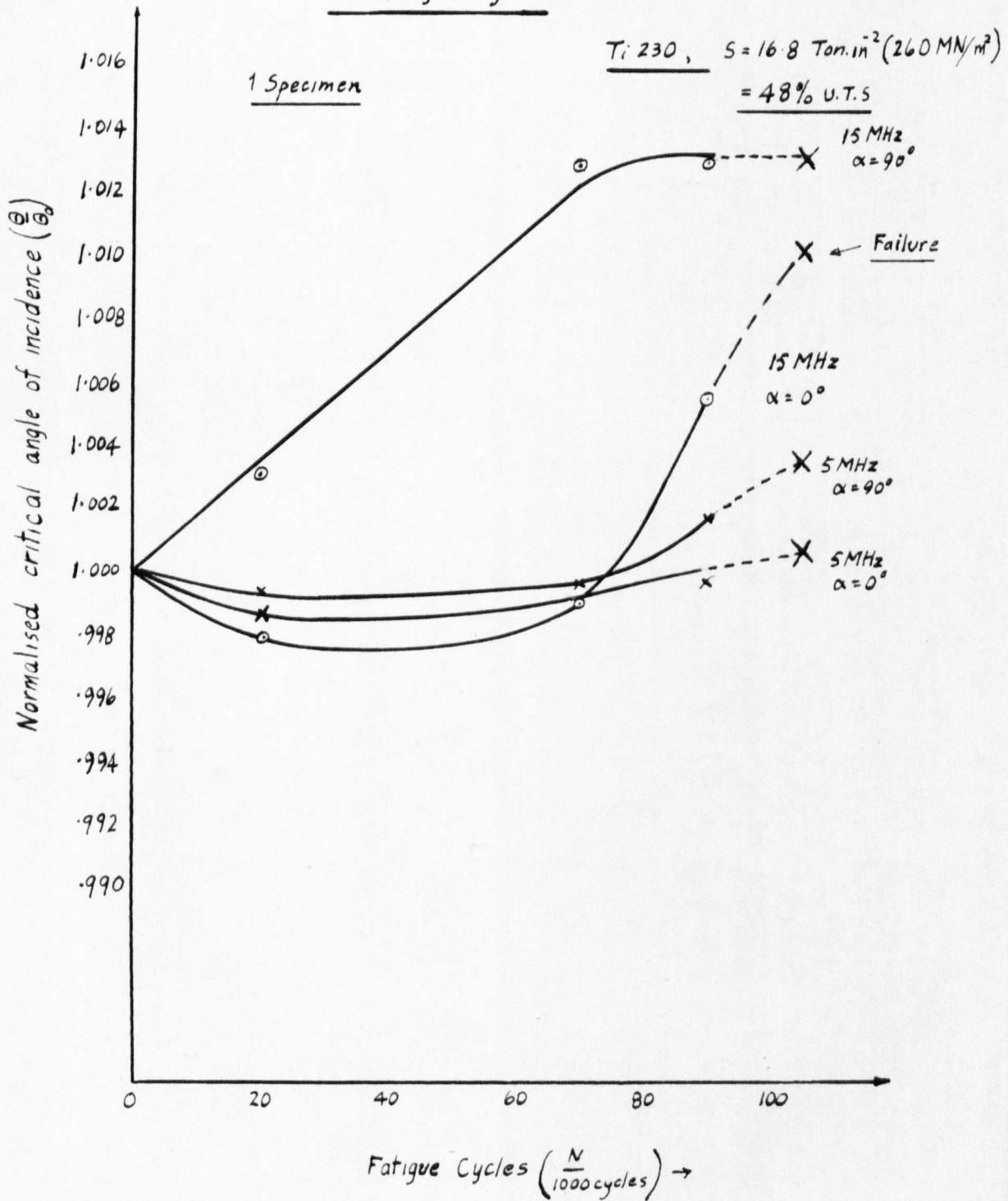


Fig 7.3.11 Showing the change in critical angle with number of fatigue cycles



7.3.3 Discussion of results and conclusions

The results obtained for both materials show that during the very early stages of fatigue life there is a large increase in the critical angle, which reaches a peak value then falls off with increase in fatigue stress cycles. For the mild steel (Figs. 7.3.2, 7.3.3, and 7.3.4) at all frequencies for $\alpha = 0$, the lower stress level showed a more rapid rise to this peak value. This was especially the case at 25MHz. In this case the fall off in critical angle was very gradual with the number of cycles

With the 15MHz test signal the fall off was rather more rapid, passing through a minimum point then rising to a high value before failure. At 5MHz there was a rapid rise in the critical angle then a rapid fall followed essentially by a slow fall off with number of fatigue cycles.

For the higher stress level at each frequency the critical angle increased to a peak value then fell off. The magnitude of the increase in critical angle was less in each case than that due to the lower stress level. Interpreting the results in terms of surface wave velocity and elastic modulus, it can be seen that the velocity decreases rapidly at early stages of fatigue. i.e. there is a softening of the material initially followed by a hardening. Sometimes the hardening is rapid for higher stresses and less rapid for lower stresses.

This is different to the type of response of ductile material as tested by Bullen et al.⁴². They found that for stress levels well below the yield stress, the hardness of copper increased rapidly with the number of fatigue cycles, then levelled off to a constant value. However, as reported by many workers, the present study seem to confirm that there is strain hardening before fracture. This can be seen in all the graphs for mild steel. The results

of Palakowski and Palchouduri⁴³ showed that for certain cold worked materials, e.g. copper, aluminium, nickel and steel, there was a distinct strain softening with cyclic loading. This can be used to partially explain the decrease in surface wave velocity during the early stages of fatigue, i.e. there is an increase in critical angle.

The results from the study did not agree completely with the results of Lazan and Wu⁵⁸. They found that when measuring damping during fatigue, the damping increased and then suddenly levelled off. This was more marked for high stress levels than for low stress levels. From the present results it can be seen that there is a sudden increase in critical angle during the early stages of fatigue life. Measurements using magnetic hysteresis⁶² and eddy currents⁶³ showed a similar type of response.

As reported by Rasmussen,^{64,65} cracks appear on the surface of high stress level low cycle fatigue specimens early in fatigue life. Cracks were observed at about 60 percent of fatigue life when measuring the specimen "off machine". This was independent of stress level. Therefore if this is considered as a basis to explain the results for the specimens tested, it would appear that before the crack formation stage using ultrasonic surface waves the change in critical angle can be measured. The change then is due to strain softening⁴³. When cracks begin to form, there is a slow down in this change in elastic properties. Eventually a large number of cracks are formed which are accompanied by strain hardening. The elastic modulus then increases showing a fall in the measured critical angle of incidence leading to failure.

Figs. 7.3.5 and 7.3.6 are plots of the change in critical angle with ultrasonic test frequency for the two stress levels in mild steel. It appears that this type of plot can indicate the best test frequency

for the material used. However since the critical angle is normalised, at 5MHz, the results may be inconclusive. In both graphs there is a sudden increase in critical angle at 15 and 25MHz during the early stages in fatigue life.

The titanium specimens for high stress level appear to behave in a rather different way from the mild steel specimens. For the very early stages of fatigue life there was a sudden increase in the measured critical angle just as for the mild steel (see fig. 7.3.7). This occurred for all ultrasonic test frequencies. Again the critical angle reached a peak, but then fell off to a minimum value, this peak being reached early in fatigue life.

The minimum value reached was very sharp in the case of the 15 and 25MHz test signal but broad in the case of the 5MHz test signal. In all cases beyond this minimum the critical angle increased to another peak then fell off for the 5 and 25MHz, but increased for the 15MHz signal. The graph for the change in critical angle versus the number of fatigue cycles for 90 degrees from the rolling direction (Fig. 7.3.8), shows a similar type of response to Fig. 7.3.7 discussed before, except that there are more peaks and troughs in early fatigue life for the 5MHz ultrasonic signal.

The type of curve obtained is somewhat similar to that given by Shagaev⁶⁶ when measuring magnetic permeability. He mentioned peculiar types of peaks and troughs similar to those obtained in this study during the early stages of fatigue life. Also the characteristic gradual falling off in permeability with increase in fatigue cycles was observed.

If an attempt is made to explain the response of the change in critical angle versus fatigue cycles in terms of dislocation theory,

a similar type of reasoning⁶⁶ can be used. If there was an initial increase in dislocation density, during early stages of fatigue, it will be expected that the surface wave velocity will decrease due to dislocation damping. This can be seen in the graphs at all frequencies. As the number of stress cycles increase, dislocations move creating vacancies around obstacles and the ultrasonic damping decreases. i.e velocity increases.

More dislocations are then created and the velocity decreases. Finally, the dislocations come up against pinning points which eventually leads to strain hardening. The surface wave velocity then increases because the damping is decreased. Most curves seem to follow this pattern. i.e. increase in critical angle.

For the lower stress levels in titanium (see figs. 7.3.10 and 7.3.11), the curves of changes in critical angle versus the number of fatigue cycles, are different ~~from~~ those for the higher stress levels. Measurements were done at 5 and 15 MHz test frequencies only. Readings were not taken during the early stages of fatigue life so it is difficult to make any direct comparison with the curves given in Figs. 7.3.7 and 7.3.8.

For the 21 Ton / in^2 (260 MN/m^2) stress level however the same type of falling off in critical angle occurred as that obtained for higher stress levels in both types of specimens. The 15 MHz signal showed that the critical angle increased with the number of cycles, then fell off with fatigue cycles. The 5 MHz signal however showed a fall in the critical angle initially.

For the 16.8 Ton / in^2 stress level (see fig. 7.3.11), the result shows an initial change in critical angle at 15 MHz ($\alpha = 90$ degrees), then a levelling off in critical angle. For $\alpha = 0$ degrees, at the same frequency, the critical angle decreased initially, then rose to a high value later in fatigue life.

These results show how difficult it is to correlate information obtained from fatigue tests. The author cannot see any pattern in the results obtained that will be directly useful to engineers in the study of fatigue.

Brook and Parry⁵⁷ reported that the fatigue life of a specimen can be predicted by measuring the apparent dynamic Young's modulus and the damping. In the present study there was no direct correlation between measured critical angle and fatigue life for either material at any stress level. What can be said is that there was an initial change in the critical angle during the very early stage in fatigue life for both materials. This was followed by a decrease in critical angle at about 60 percent or less of fatigue life.

The author concludes that in this form the results indicate that it will not be possible to predict fatigue life by measuring the change in critical angle.(i.e. the change in ultrasonic surface wave velocity). This is similar to a conclusion arrived at by Mitchell and Frederick⁶⁸ in their study of acoustic emission versus fatigue life. They found that no parameter in the emission significantly correlated with fatigue.

However the author will not recommend a discontinuity of research in this area since all possibilities should be exhausted before such a decision can be taken. Therefore a few recommendations are made on the possibilities of future work. This can be seen in Chapter (8).

7.4 MEASUREMENTS OF CRITICAL ANGLE IN SOME OTHER MATERIALS

7.4.1 Data collection

In this section the data was collected by measuring the critical angles of incidence in different materials at 5, 10, 15 and 25 MHz. Additionally the peak amplitudes of the reflected pulse, at and in the neighbourhood of the critical angle were recorded for each material at each frequency. These specimens were cut from rolled rectangular bar stock and the critical angle of incidence was measured for the direction of rolling. The materials used were mild steel, stainless steel, copper, brass and aluminium.

A further test was done on a mild steel sheet specimen. The critical angle of incidence was measured along the rolling direction and 90 degrees from the rolling direction on the specimen before and after being statically stressed well above the yield stress. This was done for the three ultrasonic test frequencies, 5, 15, and 25 MHz.

7.4.2 Results and data analysis

The variations in critical angle with the test frequency were plotted for each material. This can be seen in Figs. 7.4.1 to 7.4.5 for the materials tested. On the same graphs the variation of the pseudo-reflection factor with frequency was plotted for the respective material.

The pseudo-reflection factor was calculated from the recorded amplitude. The peak amplitude of the reflected pulse immediately before the critical angle was used as reference. The reflected amplitude at the critical angle was expressed as a percentage of this value.

For the mild steel specimen(sheet), the results of the change in critical angle with frequency for two directions of surface wave propagation was measured, and the results used to plot a graph of $-(\sin\theta_{II} - \sin\theta_I)$ versus the ultrasonic test frequency(See fig.7.4.6).

RESULTS

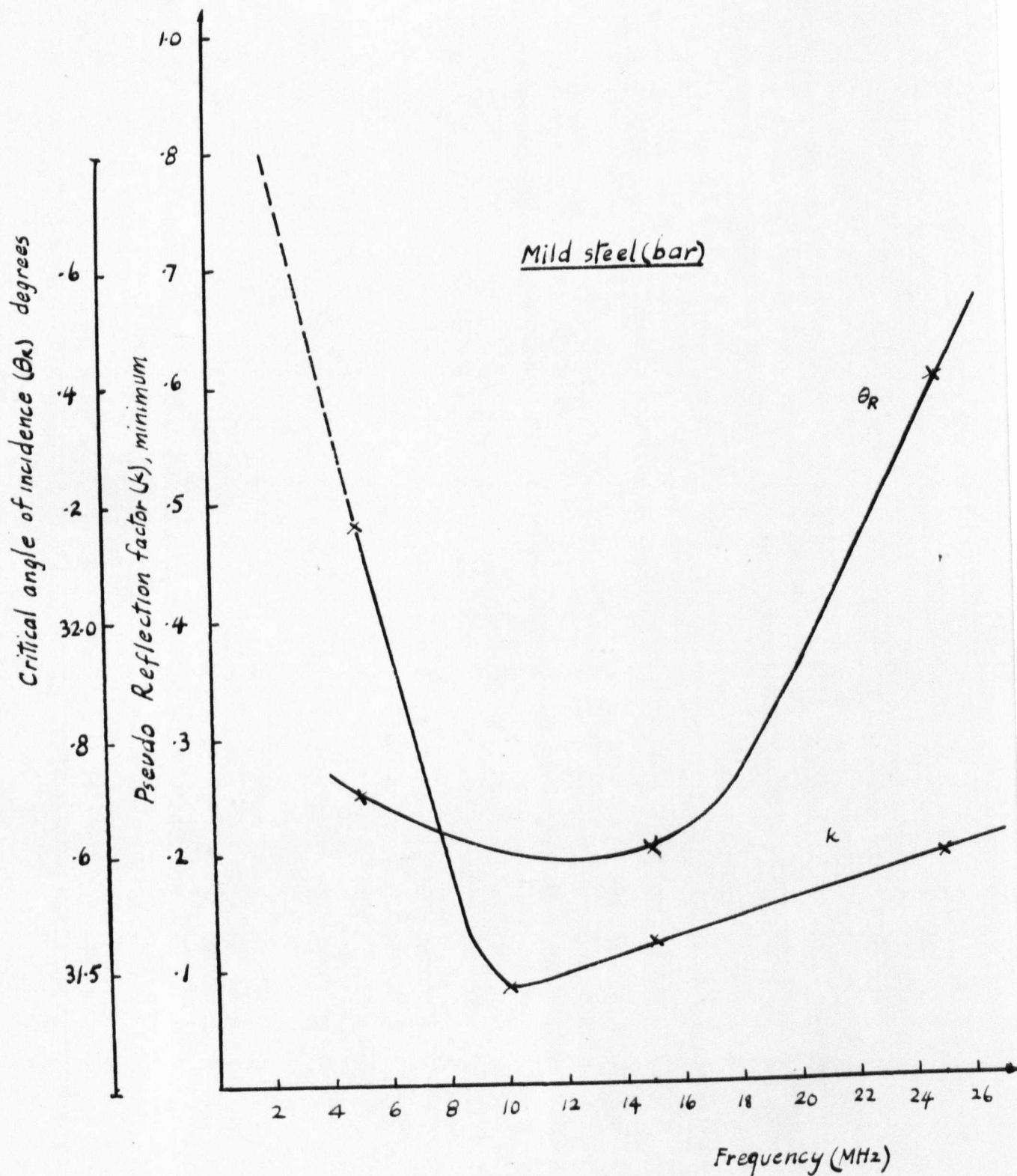


Fig 7.4.1 Showing the changes in critical angle and reflected amplitude with frequency at critical angle.

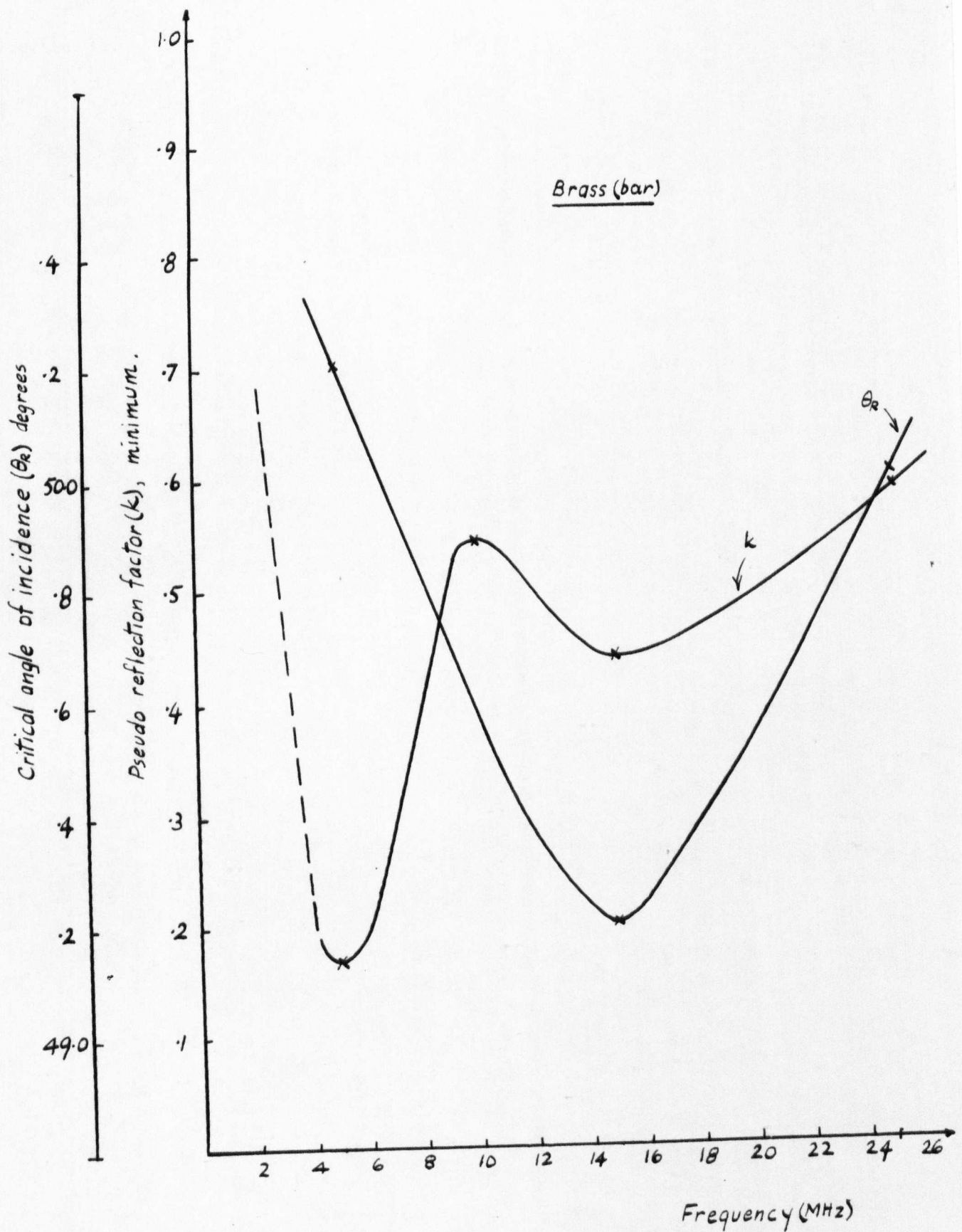


Fig 7.4.2 Showing the changes in critical angle and reflected amplitude at critical angle, with frequency.

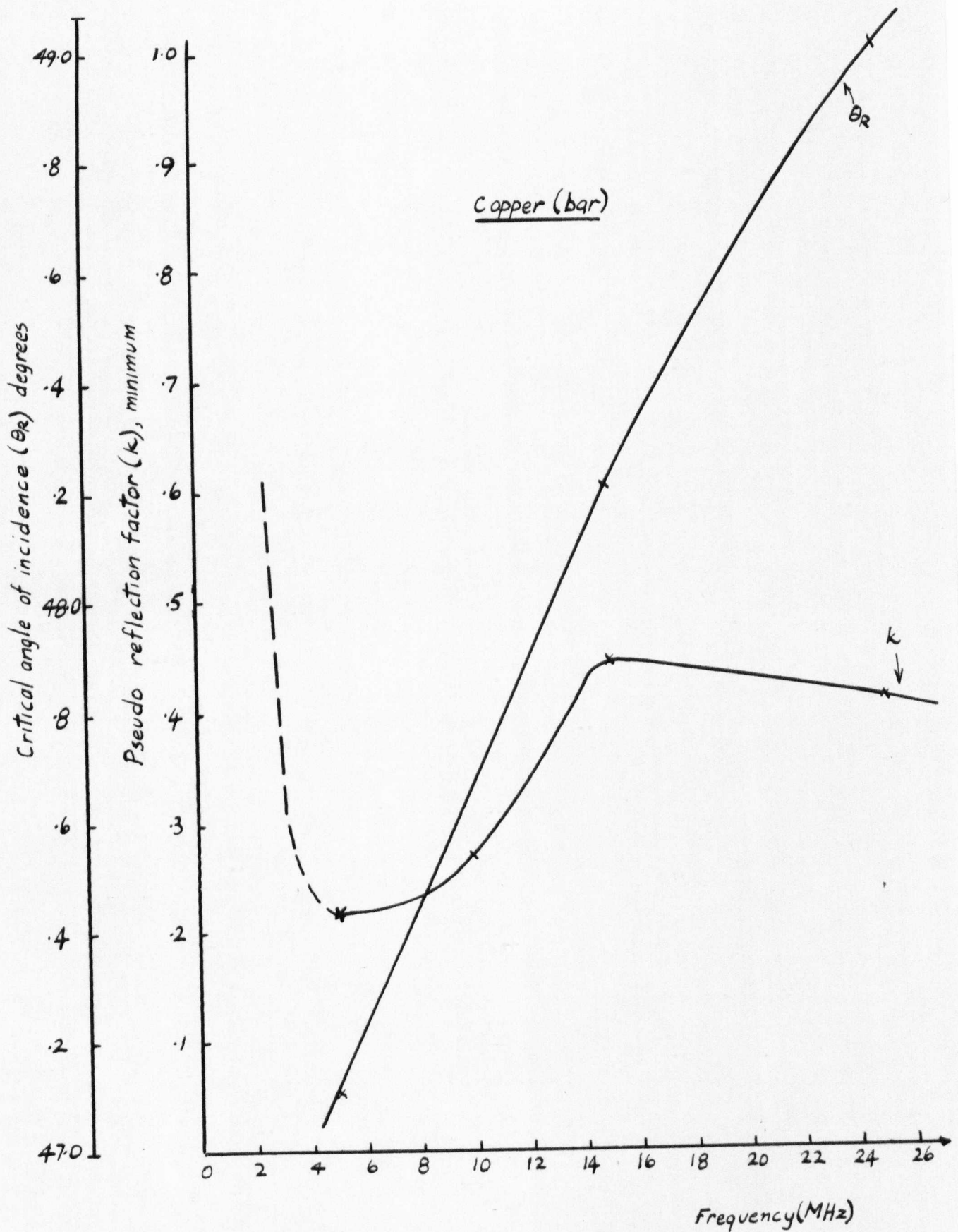


Fig 7.4.3 Showing the changes in critical angle and reflected amplitude with frequency at critical angle.

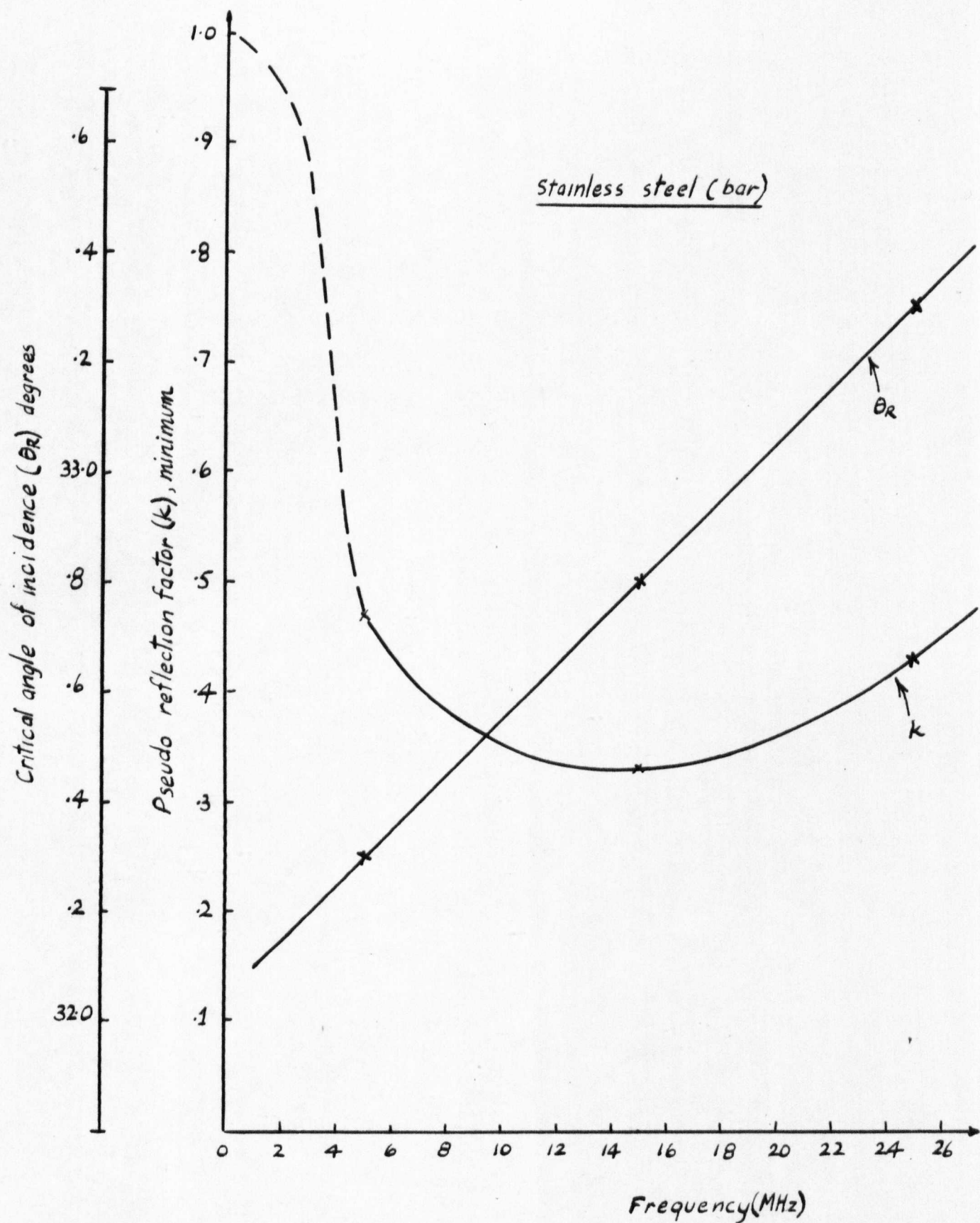


Fig 7.4.4 Showing the changes in critical angle and reflected amplitude with frequency at critical angle

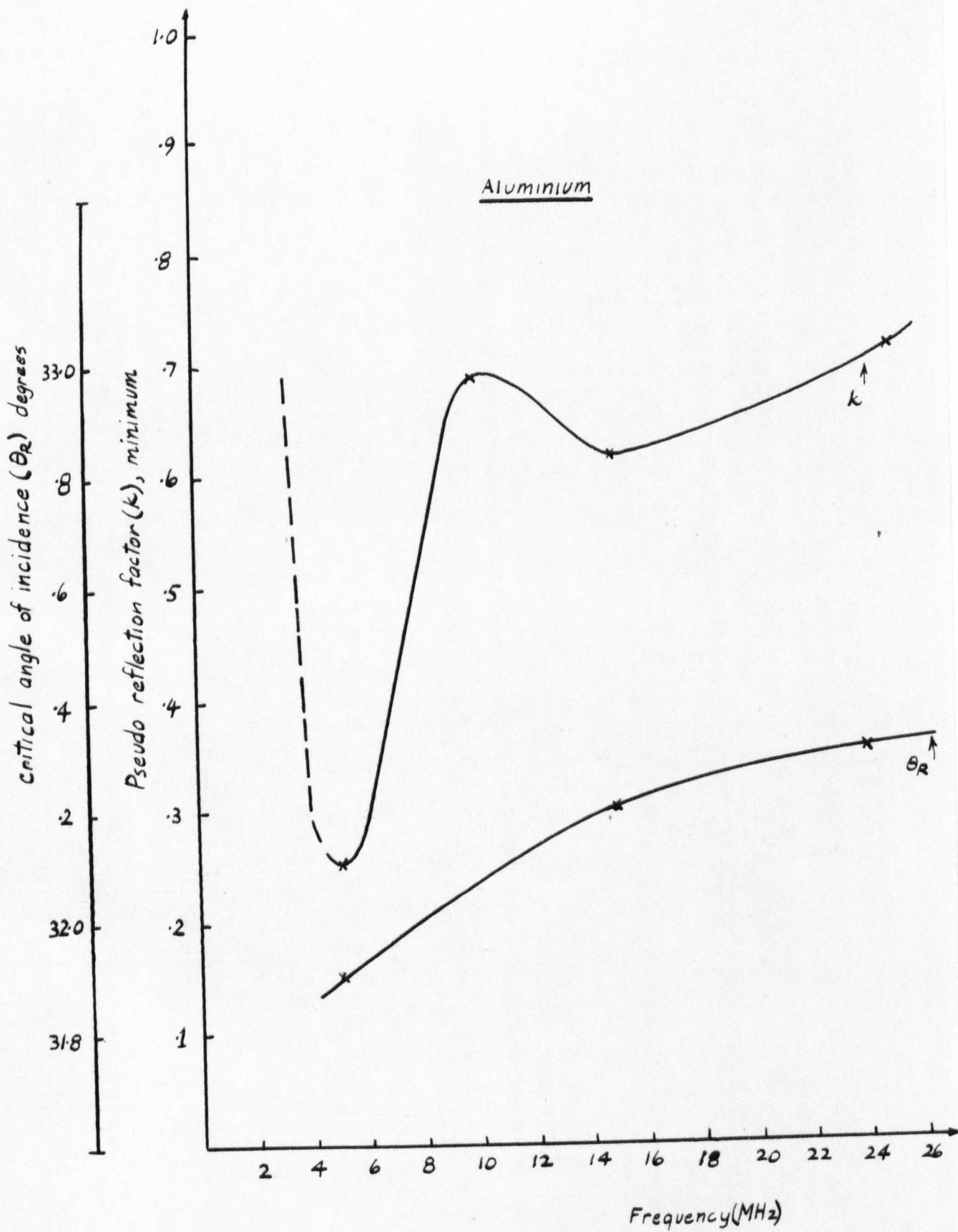


Fig 7.4.5 Showing the changes in critical angle and reflected amplitude with frequency at critical angle

7.4.3 Discussion of results and conclusions

The results of the change in critical angle with frequency for each material demonstrate that the critical angle of incidence is a function of frequency. For the aluminium, stainless steel and copper bars, the critical angle increased with frequency. (see figs. 7.4.3, 7.4.4 and 7.4.5). For the aluminium specimen the increase was not so great but for the other two materials especially copper, the change was very large. Numerically this was 47.1° at 5 MHz to 49° at 25 MHz.

For the brass and mild steel specimens the critical angle of incidence went through a minimum between 5 and 25 MHz. For the brass specimen the critical angle appeared to have a minimum value at about 15 MHz. For the mild steel specimen it was not so easy to decide on the minimum critical angle.

The pseudo-reflection factor for mild steel showed a minimum at some particular frequency. This can possibly be explained by considering the reflection factor as a measure of the energy absorbed at the critical angle for each frequency.

The reflection factor for the brass specimen had two minima. No attempt will be made to explain this phenomenon.

For the copper and aluminium specimens the pseudo-reflection had a minimum value at about 5 MHz. This was the frequency at which the highest surface wave velocity was recorded (minimum critical angle).

Frequency of least reflection (FLR)

The frequency at which the reflection factor as defined by Richardson and Becker¹¹⁰ reach a minimum was called the frequency of least

reflection (FLR). The author believes that the minimum frequency of the graph of the pseudo reflection factor is that of the least reflection, since the graph for the pseudo-reflection factor for stainless steel (see Fig. 7.4.4), was similar to that obtained for the reflection factor, minimum by Richardson and Becker.¹¹⁰ They calculated (see eqn. 3.20), and measured the reflection factor and compared the two values. They got a figure of 15 MHz for the frequency of least reflection which was similar to that measured by the author.

7.4.3(1) Dispersion of "Birefringence"

The term "birefringence" is used in a different context to that applied to light or ultrasonic bulk shear waves.¹³⁹ In both these cases birefringence is the difference between the velocities of the waves polarised along and normal to the principal axis. The dispersion is the way in which this difference changes with frequency.

For surface waves the dispersion of the "birefringence" is the manner in which the difference in the surface wave velocities, $C_{R//}$ and C_R varies with frequency.

It is reasonable to assume that there are more dislocations oriented along the direction of preferred grain orientation. This means, that along this direction, there are a greater number of slip planes or components of dislocations than normal to it. It follows therefore that more dislocation vibrations will be generated by waves parallel to the preferred axis than normal to it. Therefore these parallel polarised waves will suffer greater dispersion. Hence there will be a negative slope for the birefringence, when a plot of $C_{R//} - C_{R\perp}$ versus frequency is made.

Since the critical angle of incidence is inversely proportional to the surface wave velocity, the slope of a plot of $-(\sin\theta_{R//} - \sin\theta_{R\perp})$ will be positive for the linear region when plotted to frequency.

Considering the equation for the fractional velocity change as given in eqn.7.2.3, we have:-

$$\frac{c_{//}}{c_o} = K_{//} (1 + aw^2) \quad \text{for the surface waves parallel to the principal axis, and,}$$

$$\frac{c_{\perp}}{c_o} = K_{\perp} (1 + aw^2) \quad \text{for the surface waves perpendicular to the principal axis.}$$

Therefore the surface wave "birefringence" can be written as:-

$$\frac{c_{//} - c_{\perp}}{c_o} = B = B_o (1 + aw^2) \quad \dots\dots\dots 7.4.1$$

where B is the birefringence at frequency f and B_o is the low frequency birefringence.

7.4.3(1.1) Effect of preferred orientation

From the above theory it can be seen that the linear part of the birefringence curve is dependent upon dislocation density. Also, it is expected that a large degree of preferred orientation of dislocations would be accompanied by a large degree of preferred orientation of grains, giving rise to a steep slope in the birefringence graph.

Conversely, it is expected that random orientation of dislocations will be accompanied by random grain orientation.

7.4.3(1.2) Effect of static stress

The elastic constant of a material is altered very slightly when subjected to static stress below the elastic limit. As a consequence, there is a small change in the atomic binding energy. Hence the elastic constants change slightly, leading to a change in the wave velocity which is independent of frequency. The effect of the dislocations is negligible, and they vibrate in an identical manner to that without applied stress. Thus the birefringence due to the applied stress is the same at all ultrasonic frequencies,^{1,139} and is added algebraically to that due to dislocation vibration which is frequency dependent. A similar situation arises when residual stresses are present on cold worked materials, which have preferred orientation.

7.4.3(1.3) Effect of plastic strain

When a material is subjected to stress above its elastic limits plastic strain is produced.

This was the case when a mild steel specimen was clamped between the jaws of a tensile testing machine and a static load applied. The intensity of the load was such as to cause severe deformation of the specimen. i.e. large plastic strain.

For large plastic strains there will be strain hardening in the bulk of the material. Many dislocations will be created by dislocation sources but most of them will either be annihilated or come up against pinning points.

7.4.3(1.4) Prediction of surface residual stress from measurements of frequency variations of surface wave birefringence

We may express the surface wave birefringence at frequency f as:-

$$B = \frac{\Delta c}{c_0} = B_0(1 + mf^2) \quad \text{where } B_0 \text{ is dependent on dislocation density,}$$

and $m = 4\pi a^2$. (a is a constant for any material undergoing the same cold working process (See appendix.7) Mahadevan¹³⁹ called B the shear wave birefringence.

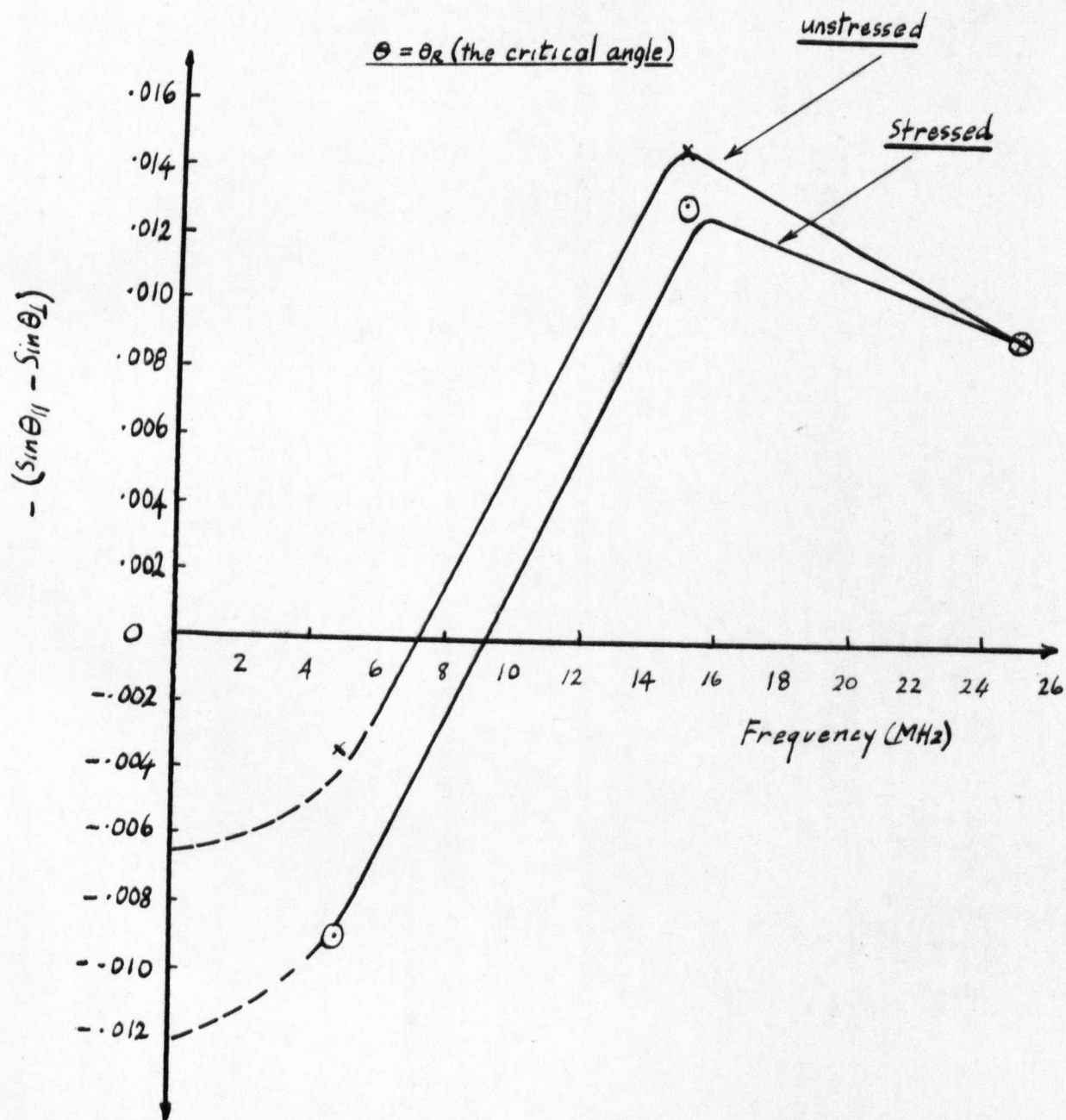
For any material, to evaluate m , measurements of critical angles should be made on the unstressed specimen at various frequencies. These should be made along and across the rolling directions. If the sine of the difference of these critical angles is related to B then using these values in the above equation the value of m can be calculated.

The curve plotted from these points will be a curve for the birefringence due to texture only. If measurements are made on a specimen which has been stressed another curve can be plotted. The difference between the intercepts of the y axis for the two curves is then a measure of the birefringence due to stress.

A curve (Fig.7.4.6) was plotted from the measurements obtained on an unstressed specimen and on the same specimen after it had been statically stressed and as a consequence severely deformed; it appears that both curves have the same slope.

From the equation above the value of m was calculated. i.e.

Fig 7.4.6 Plot of birefringence v. frequency for unstressed and severely statically stressed mild steel specimens



$$-.0035 = B_0(1 + 25m), \text{ and,}$$

$$+.015 = B_0(1 + 225m)$$

The two points used were 5 and 15 MHz.

$$\text{The calculated value for } m \text{ was } m = -\frac{1}{60}$$

Mahadevan¹³⁹ measured the shear wave birefringence in stainless steel and calculated for this material $m = -\frac{1}{24}$. Measurements were not made below 5 MHz in the present study hence a direct comparison with Mahadevan's work cannot be made. However it appears that at high ultrasonic frequencies the curves falls off. This was not observed by Mahadevan since he did not use so high a frequency(15 MHz). His maximum frequency was 5 MHz.

Maybe if measurements were done in the low frequency region as was done by Mahadevan a similar type of response will be obtained. Then the difference of the intercepts of the y axis for the two curves will be a measure of the surface wave birefringence and as a consequence, a measure of the surface residual stress on the specimen.

CHAPTER 8

SUGGESTIONS FOR FURTHER WORK

Further work is suggested in the area of using ultrasonic surface waves generated by critical angle reflectometry to measure changes in elastic properties due to creep.

In the study reported in this thesis two types of material were used. The author suggests that it will be useful if other materials can be studied and some work conducted in the area of creep greater than 1% T.P.S. It will be advisable that in such studies the intervals in the degree of creep chosen should be relatively small so that a curve plotted for the surface wave velocity versus creep will be continuous hence the results will be easy to interpret.

In this study of fatigue again two materials were studied, using one type of loading program i.e. constant amplitude alternating or repeated stress remaining in tension for the whole program. The author suggests that more work can be done using different materials and different loading programs.

The goniometer to be used in these recommended studies should be very sensitive.. The angular position should be very accurately read.. It may be possible that using the correct types of instrumentation the angular settings can be digitised. Appendix 6 shows a possible way of improving the sensitivity of the receive side so that the minimum signal reflected can be accurately monitored.

The ultrasonic transducer should be of the focus type so that very

localised elastic properties can be measured and if possible the data collecting and processing sides should be automated.

In the area of case depth it may be possible to do some work on the measuring of very thin coatings e.g. electroplated coatings, on different substrate materials to ascertain the exact limitations of the measuring technique. High frequency transducers will have to be used. It is suggested that focussed probes be used.

Finally, the results for the other materials studied shows that there are many more questions to be answered about the manner in which metals behave at the ultrasonic critical angle. More work is suggested in this area. Also from the study of the difference in the response to ultrasonic surface waves, for the unstressed and severely deformed mild steel specimens, it appears that it may be possible to detect surface residual stresses using critical angle reflectometry. If a focussed probe is used at each ultrasonic frequency it can be used to measure localised surface residual stresses. This is a far better method than measuring the average residual stress which is done when the through transmission type of test is employed.

CHAPTER 9

PAPERS

Two papers were submitted for publication during the course of this work. One was to the Journal of Nondestructive Testing which gave the preliminary results of the findings, and the second paper was to the journal "Ultrasonic". This second paper is a theoretical paper, but some results are included. A possible application of the results of the analysis was suggested by the author.

In the remaining pages of this chapter further information of these papers is presented.

To be published in the
"International Journal of Nondestructive Testing"

December 1972

Some Results Using the Ultrasonic Goniometer (The Corner Reflector Method)

W. WESTON-BARTHOLOMEW

Department of Engineering
University of Warwick
Coventry, England

Abstract—The ultrasonic goniometer is a tool for the use in nondestructive testing. Its use is increasing. There are many problems that are to be solved in trying to interpret the results. The amplitude of the reflected signal from the specimen at the critical angle is a function of the elastic property of the specimen, and the exciting frequency.

This paper gives the results of experiments conducted on materials in various mechanical states and at different frequencies. The change of critical angle was measured.

The results show that the corner reflection method could be used to investigate surface-hardened specimens using the frequency effect to measure the case depth. Specimens in different state of creep were also examined and a frequency dependence effect was observed. A bar of mild steel was stressed and the critical angle before and after stressing was measured. An inverse frequency was observed.

The ultrasonic goniometer⁽¹⁾ was used to measure case depth in case-hardened materials and the state of creep.

The principle of operation of the goniometer is as follows: Water is used as a medium. Dilatational waves are propagated in this medium becoming incident on the solid surface (see Fig. 1). Using Snell's law as in optics $\sin \theta_1 = (C_1/C_2) \sin \theta_2$ where C_1 and C_2 are velocities in the liquid and solid respectively. As the angle of incidence is increased in dilatational wave in the solid becomes critical, then the shear wave becomes critical. Immediately beyond this point there is an angle where most of the energy is converted into a surface wave which propagates along the surface of the solid. The perturbation is confined to a layer of approximately one wavelength thick. The wave amplitude dies away in both the x and z directions.

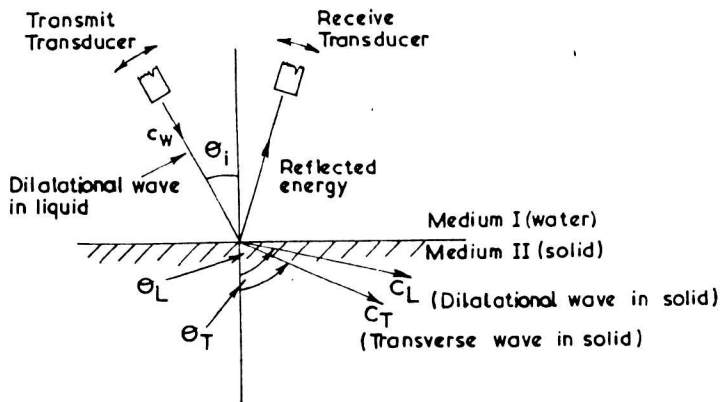


Figure 1. A liquid-solid interface.

At this angle

$$\sin \theta_s = \frac{C'_w}{C'_s}$$

where θ_s is the critical angle

C_w is the velocity of dilatational wave in water, and

C_s is the surface wave velocity.

In this experiment the water temperature was kept constant within 0.01°C , since the velocity of the dilatational wave changes with temperature. The critical angle was measured for specimens with various state of creep. The velocity C_s can be calculated from the above expression and checked from the expression

$$C_s = n_R C_t \quad \text{where} \quad n_R = \frac{0.87 + 1.12\nu}{1 + \nu}$$

where ν is Poisson's ratio

C_t is the shear wave velocity in the solid.

The corner reflection method⁽²⁾ uses one transducer and relies on an acoustic reflector to return the signal reflected from the specimen (see Fig. 2).

This was the method used in the experiment. The reflector was highly polished to reduce scattering of the incident wave. Caburised and case-hardened steel specimens were tested. The change in the critical angle was measured, for different case depths and at different

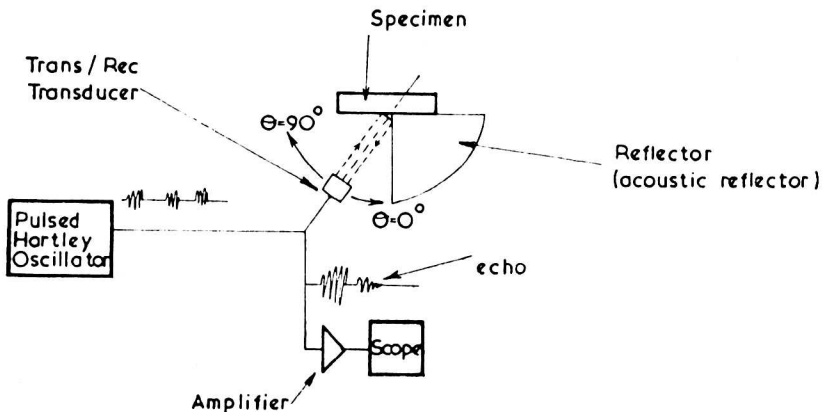


Figure 2. Drawing of system used.

frequencies. It will be seen that there is some correlation between case depth and frequency (see Graph 1).

The theory will not be gone into in this paper but it is well known that the surface wave perturbation is confined to a layer of approximately one wavelength thick. The critical angle is inversely proportional to the surface wave velocity, which is a function of the elastic property of this layer. Hence as d the case depth changes the elastic property of the layer changes and the critical angle changes. For $d > \lambda_s$ the elastic property of the layer is the same and the angle remains constant. To obtain any more information from the specimen the interrogating frequency has to be lowered making $d < \lambda_s$.

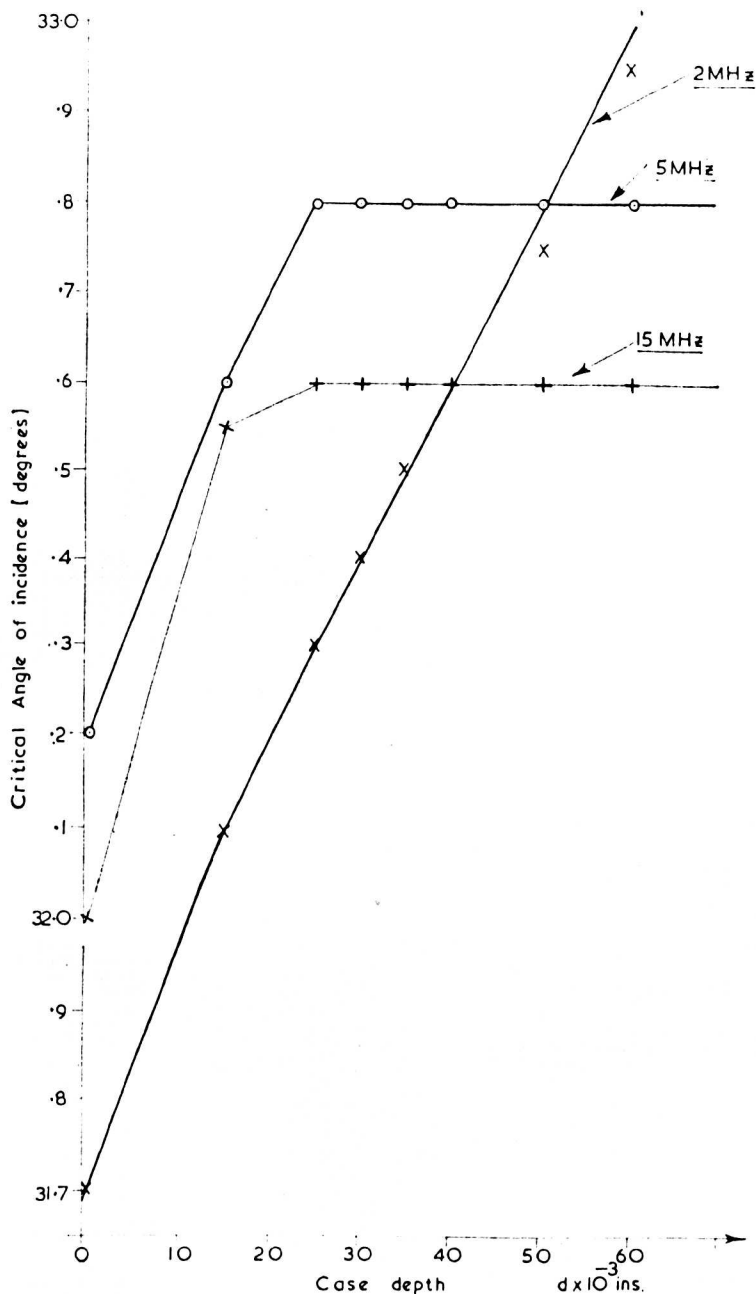
Since the surface wave velocity is given by:

$$C_s = n_R C_t$$

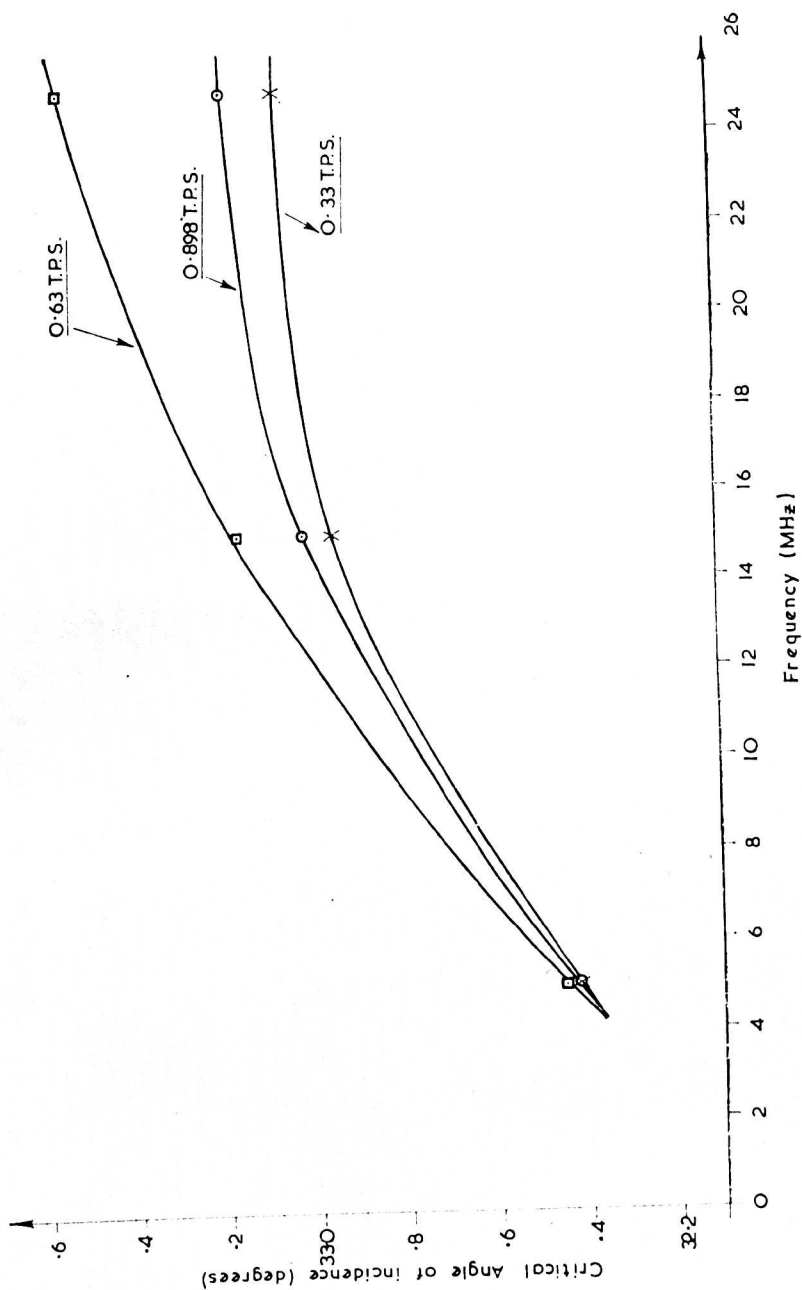
where $n_R = 0.94$ for steel, and $C_t = 3200$ m/sec, therefore $C_s = 3000$ m/sec. and the wavelength $\lambda_s = C_s/f$.

It follows that a 2 MHz interrogating signal can detect a case depth of approximately 1.5 mm (60×10^{-3} in.) in steel. Graph 1 shows that lower frequencies can detect larger case depths.

It was found also that for C263 Ni. that specimens which were subjected to creep at varying degrees, there was a frequency dependence effect. Graph 2 shows this. A possible explanation is as follows.



Graph 1. Changes in the critical angle for different case depth at different frequencies.



Graph 2. Changes in critical angle for different state of creep at different frequencies. (T.P.S. is total plastic strain).

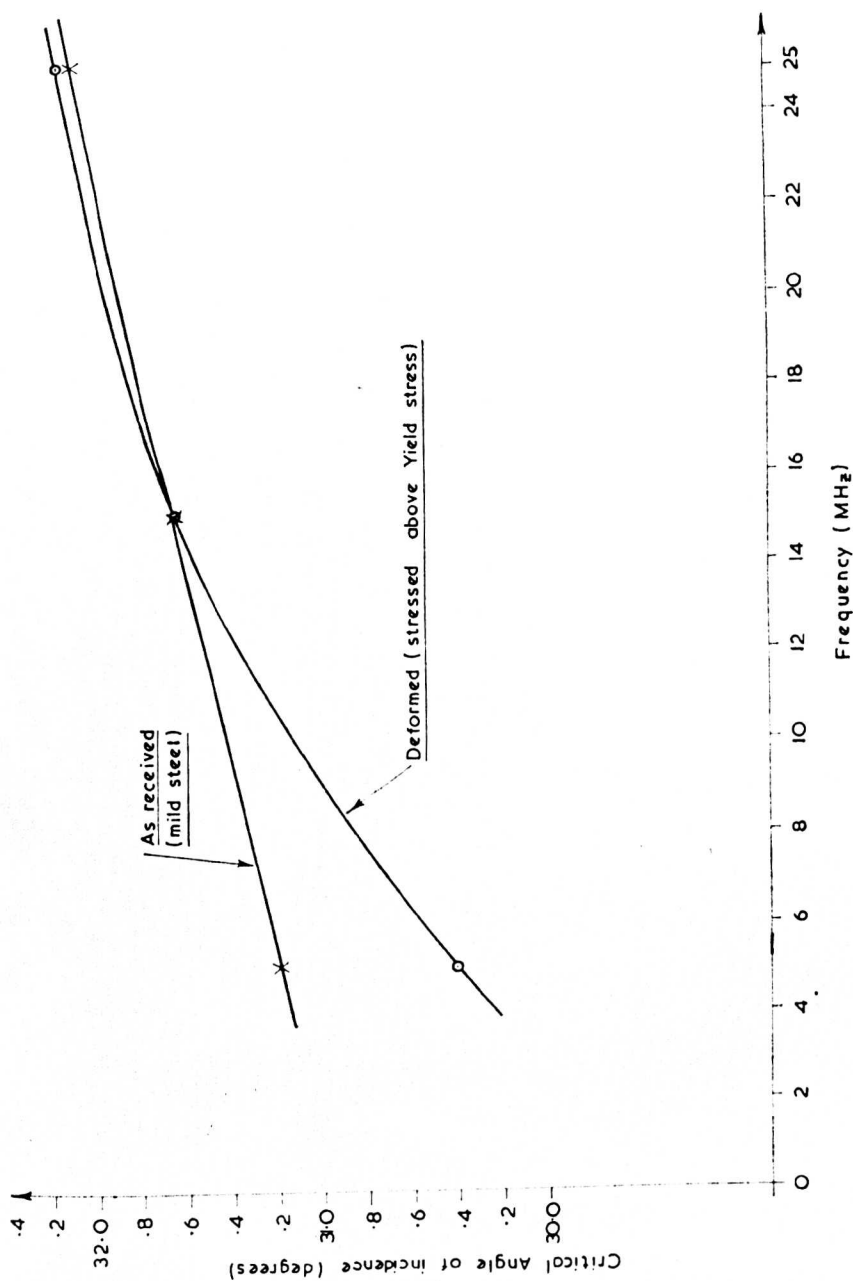
If the critical angle is considered as a resonance of the amplitude of the dislocation displacement, then as the dislocation density increases the critical angle will increase, i.e. the surface wave velocity will decrease. Furthermore, at low frequencies the frequency of the exciting signal is very much lower than that of the resonant frequency of the dislocation in all three states of creep. Hence there is very little difference in the measured critical angle. When the frequency is increased becoming nearer to the resonant frequency of the dislocations the difference in the critical angle is evident. It shows that the surface wave velocity decreases for increasing creep. It is possible that at much higher frequencies very early changes in elastic properties due to creep can be measured. It appears that the elastic modulus of the surface wave has a frequency dependent part which increases with the state of creep.

For fatigued specimens it appears that there is an inverse frequency effect. It appears that for the measuring of the change in elastic properties during the early stages of fatigue, a low frequency has to be used. Work is still in progress in this area.

A test was done on a mild steel specimen, which was stressed in a static tension above its yield stress to such an extent as to cause severe deformation. In order of magnitude, this was approximately 22% elongation and a 15% reduction in area. Graph 3 shows an inverse frequency effect. A possible explanation is that due to this deformation, there is an increase in the dislocation density in the bulk of the material, and also a very high incidence of pinning. This will make the metal more brittle, hence an increase in the elastic modulus. The specimen was stressed by clamping it between the jaws of a tensile testing machine. From the graph it appears that the surface properties before and after stressing are only marginally different. There is only marginal change in critical angle at high frequencies. The lower frequency monitors the change in elastic properties in the bulk of the material. This shows that the critical angle is lower in the stressed material, which means that the surface wave velocity has increased.

Conclusion

The results presented in this paper show that the reflection method



Graph 3. Changes in critical angle for mild steel specimen before and after severe stressing, at different frequencies.

can be very useful. The corner reflector type goniometer is easier to construct, and accurate and repeatable results can be obtained.

The frequency dependence effect found when interrogating creep specimens means that with high frequencies, it will be possible to detect changes in elastic properties in very early stages of creep.

Again with careful measurements, the method can be used as a sensitive detector of case depth.

The author found that specimens which were fatigued when measured showed an inverse frequency effect.

Acknowledgements

This work is supported by a Ministry of Technology contract and the author wishes to thank the Ministry for permission to publish this paper. The author wishes to thank Dr. D. I. Crecraft for his helpful suggestions.

REFERENCES

1. Bradfield, G. E., Notes on Applied Sciences No. 30, National Physical Laboratory, p. 21.
2. Rollins, F. R. Jr., *J. Acoust. Soc. Amer.* **44**, No. 2, 431 (1968).

To be published in "Ultrasonics"

March 1973

Temperature considerations when evaluating materials using the Ultrasonic
Goniometer(Critical angle reflectometry)

by W. Weston-Bartholomew*

Abstract

The ultrasonic goniometer is a new tool for use in non destructive testing.

To obtain repeatable results the temperature of the coupling media (usually water) has to be controlled. This paper represents a theoretical analysis of the dependence of the measured angle on temperature. Additionally, if the temperature is controlled, using the results of the same analysis an expression for the temperature coefficient of elasticity can be obtained.

Some experimental work was done and the results presented.

* Department of Engineering, University of Warwick, Coventry.

Introduction

In immersion testing the temperature of the fluid has to be controlled, since the velocity of the dilatational wave changes with temperature. This change is due to the change in density and bulk modulus of the fluid.

The general expression relating velocity to density and modulus is:-

$$C_1 = \sqrt{\frac{k}{\rho}} \quad \text{where} \quad \begin{array}{l} k = \text{the bulk modulus} \\ \rho = \text{density of the fluid} \end{array}$$

therefore the change in velocity with temperature can be written as:-

$$\frac{1}{C_1} \frac{dC_1}{dT} = \frac{1}{2k} \frac{dk}{dT} - \frac{1}{2\rho} \frac{d\rho}{dT}$$

If water is used as a fluid, then the change due to density can be neglected. The velocity change is due mainly to the change in bulk modulus with temperature. For some fluids e.g. volatile liquids, the change in density cannot be neglected. The curve giving changes in dilatational wave velocity with temperature for water can be plotted from the table given in Bradfield². The curve is plotted on graphs 1 and 2.

Theoretical analysis of the effects of temperature
on measured critical angle.

Basically from Snells law (see fig. 1)

$$\sin \theta = \frac{C_1}{C_R} \text{ where } C_1 = \text{dilatational wave in water (m/sec)}$$

$$C_R = \text{surface wave on the solid (m/sec).}$$

$$\theta = \theta_R \text{ the critical angle.}$$

$$\text{Therefore } d\theta = \frac{1}{C_R \cos \theta} \left[dC_1 - \frac{C_1}{C_R} dC_R \right]$$

dividing thro by $C_1 \theta$ we get:-

$$\frac{d\theta}{\theta} = \frac{C_1}{\theta C_R \cos \theta} \left[\frac{dC_1}{C_1} - \frac{dC_R}{C_R} \right]$$

$$\text{and } \frac{1}{\theta} \frac{d\theta}{dT} = \frac{C_1}{\theta C_R \cos \theta} \left[\frac{1}{C_1} \frac{dC_1}{dT} - \frac{1}{C_R} \frac{dC_R}{dT} \right] \dots\dots\dots(1)$$

Now $C_R = \eta_R C_T = \eta_R \sqrt{\frac{\mu}{\rho}}$ where $\eta_R = \frac{0.87 + 1.12\nu}{1 + \nu}$ is an approximate equation due to Bergmann³. ν = Poissons ratio and μ = shear modulus of the solid.

Then differentiating and dividing through by $\frac{1}{dT}$ we get:-

$$\frac{1}{C_R} \frac{dC_R}{dT} = \frac{1}{2} \left[\frac{1}{\mu} \frac{d\mu}{dT} - \frac{1}{\rho} \frac{d\rho}{dT} \right] + \frac{1}{\eta_R} \frac{d\eta_R}{dT} \dots\dots\dots (2)$$

Substituting (2) in eqn. (1) we get:-

$$\frac{1}{\theta} \frac{d\theta}{dT} = \frac{C_1}{\theta C_R \cos \theta} \left[\frac{1}{C_1} \frac{dC_1}{dT} - \frac{1}{2\mu} \frac{d\mu}{dT} - \frac{1}{\eta_R} \frac{d\eta_R}{dT} \right] \dots\dots\dots (3)$$

This is the root equation from which certain practical forms can be derived. Using Bergman's approximation relating η_R and ν the generalisation can however be taken one step further.

$$d\eta_R = \frac{d\nu}{4(1+\nu)^2}$$

and

$$\frac{d\eta_R}{\eta_R} = \frac{1}{4(1+\nu)(0.87 + 1.12\nu)} d\nu \dots\dots\dots (3.1)$$

Substituting this into eqn.(3) a general expression is obtained showing the changes in θ with temperature.

$$\frac{1}{\theta} \frac{d\theta}{dT} = \frac{C_1}{\theta C_R \cos \theta} \left[\frac{1}{C_1} \frac{dC_1}{dT} - \frac{1}{2\mu} \frac{d\mu}{dT} + \frac{1}{2\rho} \frac{d\rho}{dT} - \frac{1}{4(1+\nu)(0.87 + 1.12\nu)} \frac{d\nu}{dT} \right] \dots\dots\dots (4)$$

In cases where; the specimen density does not vary greatly over the range of temperatures considered this reduces to:-

$$\frac{1}{\theta} \frac{d\theta}{dT} = \frac{C_1}{\theta C_R \cos \theta} \left[\frac{1}{C_1} \frac{dC_1}{dT} - \frac{1}{2\mu} \frac{d\mu}{dT} - \frac{1}{4(1+\nu)(0.87+1.12\nu)} \frac{d\nu}{dT} \right] \dots\dots (4.1)$$

In cases where; Poissons ratio does not vary greatly over the range of temperature considered, this reduces to:-

$$\frac{1}{\theta} \frac{d\theta}{dT} = \frac{C_1}{\theta C_R \cos \theta} \left[\frac{1}{C_1} \frac{dC_1}{dT} - \frac{1}{2\mu} \frac{d\mu}{dT} + \frac{1}{2\rho} \frac{d\rho}{dT} \right] \dots \dots \dots (4.2)$$

As can be seen it is important to know $\frac{1}{\mu} \frac{d\mu}{dT}$ and $\frac{1}{C_1} \frac{dC_1}{dT}$. All the values can be obtained from Bradfield², for most materials at 20°C. Note that θ on the right hand side of the equation is in radians.

If the change in ν due to temperature is not known, then it may be useful to express $\frac{1}{\eta_R} \frac{d\eta_R}{dT}$ in terms of the change in elastic moduli with temperature. For an isotropic solid (see Gooberman⁴), λ and μ are Lamé's constants and are the only two constants necessary for the elastic constant matrix for an isotropic solid.

$$\begin{aligned} \nu &= \frac{C_{11} - 2C_{44}}{2C_{11} - 2C_{44}} \text{ in terms of elastic moduli where } C_{11} = \lambda + 2\mu \\ &\quad \text{and } C_{44} = \mu \\ \therefore d\nu &= \frac{C_{44} dC_{11} - C_{11} dC_{44}}{2(C_{11} - C_{44})^2} \end{aligned}$$

$$\begin{aligned} \eta_R &= \frac{2.86C_{11} - 3.98C_{44}}{3C_{11} - 4C_{44}} \text{ in terms of elastic moduli.} \\ d\eta_R &= \frac{d\nu}{4(1+\nu)^2} = \frac{(2C_{11} - 2C_{44})^2}{4(3C_{11} - 4C_{44})^2} d\nu \end{aligned}$$

Equation (3.1) then becomes:-

$$\frac{d\eta_R}{\eta_R} = \frac{C_{44} dC_{11} - C_{11} dC_{44}}{2(2.86 C_{11} - 3.98 C_{44})(3 C_{11} - 4 C_{44})}$$

This can be reduced to:-

$$\frac{d\eta_R}{\eta_R} = \frac{c_{44} \left[\frac{1}{c_{11}} \frac{dc_{11}}{dT} - \frac{1}{c_{44}} \frac{dc_{44}}{dT} \right]}{2c_{11} \left[8.58 - 23.38 \left(\frac{c_{44}}{c_{11}} \right) + 15.92 \left(\frac{c_{44}}{c_{11}} \right)^2 \right]} \dots\dots\dots (4.3)$$

This can now be substituted into eqn.(3) to get:-

$$\frac{1}{\theta} \frac{d\theta}{dT} = \frac{c_1}{\theta c_R \cos \theta} \left[\frac{1}{c_1} \frac{dc_1}{dT} - \frac{1}{2c_{44}} \frac{dc_{44}}{dT} + \frac{1}{2\rho} \frac{d\rho}{dT} - \frac{c_{44} \left(\frac{1}{c_{11}} \frac{dc_{11}}{dT} - \frac{1}{c_{44}} \frac{dc_{44}}{dT} \right)}{2c_{11} \left(8.58 - 23.38 \left(\frac{c_{44}}{c_{11}} \right) + 15.92 \left(\frac{c_{44}}{c_{11}} \right)^2 \right)} \right] \dots\dots\dots (4.4)$$

This is the general expression relating the change in critical angle to temperature for any material.

It may be useful also to express eqn.(3) in terms of Lamé's constants. Therefore:-

$$\frac{1}{\theta} \frac{d\theta}{dT} = \frac{c_1}{\theta c_R \cos \theta} \left[\frac{1}{c_1} \frac{dc_1}{dT} - \frac{1}{2\mu} \frac{d\mu}{dT} + \frac{1}{2\rho} \frac{d\rho}{dT} - \frac{\mu \left(\frac{1}{\lambda} \frac{d\lambda}{dT} - \frac{1}{\mu} \frac{d\mu}{dT} \right)}{2\lambda \left((8.58 + 10.94 \left(\frac{\mu}{\lambda} \right) + 3.48 \left(\frac{\mu}{\lambda} \right)^2 \right)} \right] \dots (4.5)$$

Graphs 1 and 2 are results for θ (critical angle for different materials at different temperatures after the temperature of the water was controlled to $\pm 0.01^\circ\text{C}$. A corner reflector technique¹ was used.

Now rearranging eqn(1) we get an equation that should give the temperature coefficient of elasticity for the surface wave in any material.

$$\text{i.e. } \frac{1}{C_R} \frac{dC_R}{dT} = -\left(\frac{\theta C_R \cos \theta}{C_1}\right) \frac{1}{\theta} \frac{d\theta}{dT} + \frac{1}{C_1} \frac{dC_1}{dT} \dots\dots\dots (5)$$

$$\text{But } C_R = \frac{C_1}{\sin \theta} \text{ (see fig.1)}$$

Substituting this in equation 4 we get :-

$$\frac{1}{C_R} \frac{dC_R}{dT} = -\frac{\theta}{\tan \theta} \left(\frac{1}{\theta} \frac{d\theta}{dT} \right) + \frac{1}{C_1} \frac{dC_1}{dT} \dots\dots\dots (5.1)$$

where θ outside the bracket is in radians. Therefore,

$$\frac{1}{C_R} \frac{dC_R}{dT} = -\left(\frac{\pi}{180 \tan \theta}\right) \frac{d\theta}{dT} + \frac{1}{C_1} \frac{dC_1}{dT} \dots\dots\dots (5.2)$$

All the values can be obtained from carefully plotted graphs of θ and C_1 to temperature.

$$\text{But } C_R = \sqrt{\frac{G_{SR}}{\rho}} \text{ where } G_{SR} \text{ is the elastic modulus of the surface wave.}$$

therefore

$$\frac{1}{C_R} \frac{dC_R}{dT} = \frac{1}{2G_{SR}} \frac{dG_{SR}}{dT} - \frac{1}{2\rho} \frac{d\rho}{dT}$$

$$\text{i.e. } \frac{1}{G_{SR}} \frac{dG_{SR}}{dT} \approx \frac{2}{C_R} \frac{dC_R}{dT} \dots\dots\dots (6)$$

This is the expression for the temperature coefficient of elastic modulus for the surface waves. The temperature coefficient of linear expansion is neglected, and so is the temperature coefficient of density.

Below are some results for different materials at 20°C.

| Material | θ_R degrees | $d\theta_R$ degrees | From Bradfield ² | | Calculated | |
|-----------------|-----------------------|------------------------|-----------------------------|-----------------|---------------------------------|--|
| | | | C_1 m/sec | dC_1 m/sec | $\frac{1}{C_R} \frac{dC_R}{dT}$ | $\frac{1}{G_{SR}} \frac{dG_{SR}}{dT} \times 100$ |
| Titanium | 30.7 | .09 | 1482.66 | 3.02 | -.000678 | -0.1356 |
| Mild steel | 30.5 | .08 | " | " | -.000398 | -0.0796 |
| Stainless steel | 31.5 | .1 | " | " | -.00878 | -0.1756 |
| Copper | 45.24 | .11 | " | " | +.000125 | +0.0250 |
| Brass | 47.88 | .12 | " | " | +.000134 | +0.0268 |
| Aluminium | 30.8 | .12 | " | " | -.001541 | -0.382 |

Conclusion:-

The goniometer used was the corner reflector type. The system is a relative one, but with careful construction and measurements, consistent and repeatable results can be obtained. The exciting frequency was 5 MHz and the sensitivity of the measuring system was $\pm .1$ degree.

The temperature coefficient of elasticity for the surface wave can be calculated using the given expression and the results of very carefully controlled experiments relating θ to temperature. It should also be possible to evaluate the temperature coefficient of the shear modulus in a similar way, given the temperature coefficient of the Poisson ratio.

References

- 1 - Rollins F.R. - Journal of the Acoustical Society of America.
Vol. 44, No. 2, 1968, pp 431-434.
- 2 - Bradfield G.E. - Notes on Applied Sciences No. 30.
National Physical Laboratory.
- 3 - Bergmann L - Ultraschall und Seine Anwendung in
Wissenschaft und Technik, Edwards,
Ann Arbor, Mich.
- 4 - Goobermann G.L. - Ultrasonic theory and applications.,
English University Press Ltd.

Acknowledgements

This work is supported by a Ministry of Technology Contract. The author wishes to thank the Ministry for permission to publish this paper. Thanks also to Dr. D.I. Crecraft for his useful suggestions.

- (1) Figure showing critical angle, for surface wave generation.
- (2) Variation of critical angle for different materials at different temperatures.
- (3) Variation of critical angle for different materials at different temperatures.

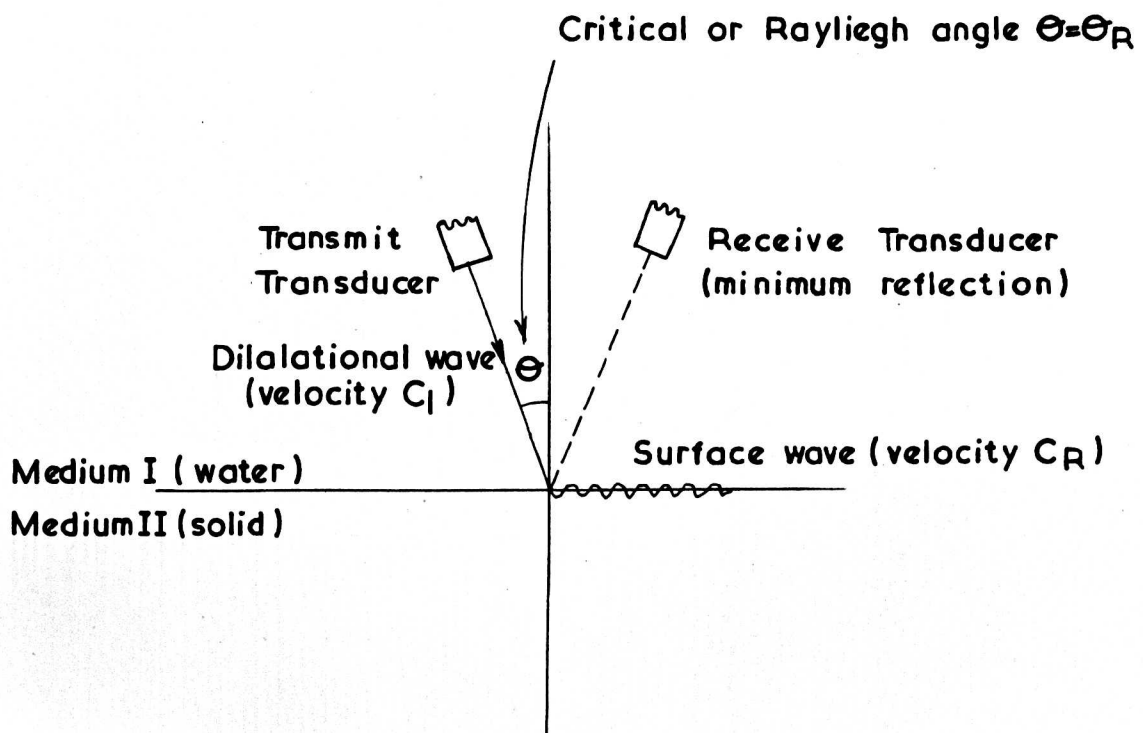


Fig. I

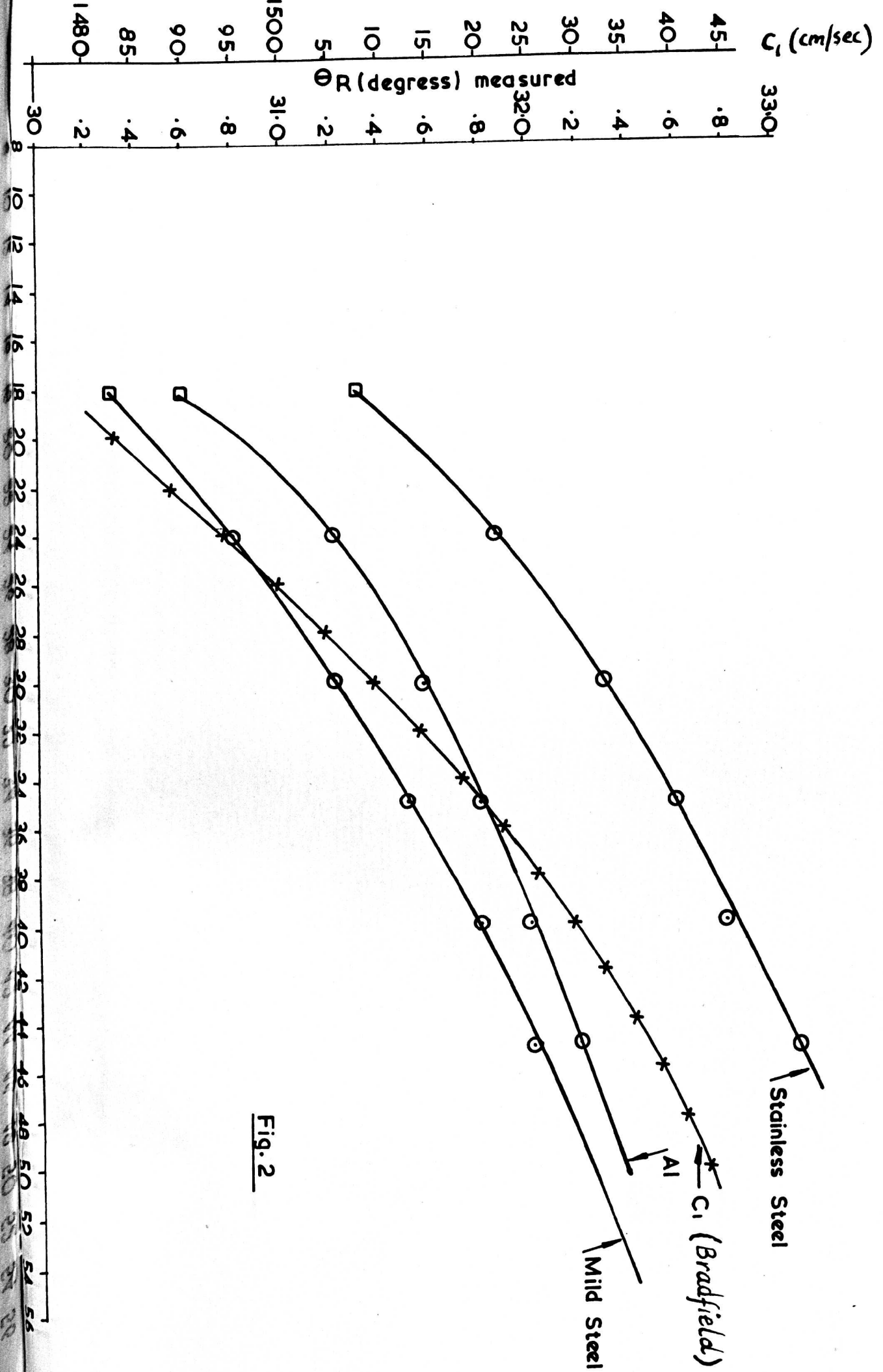


Fig. 2

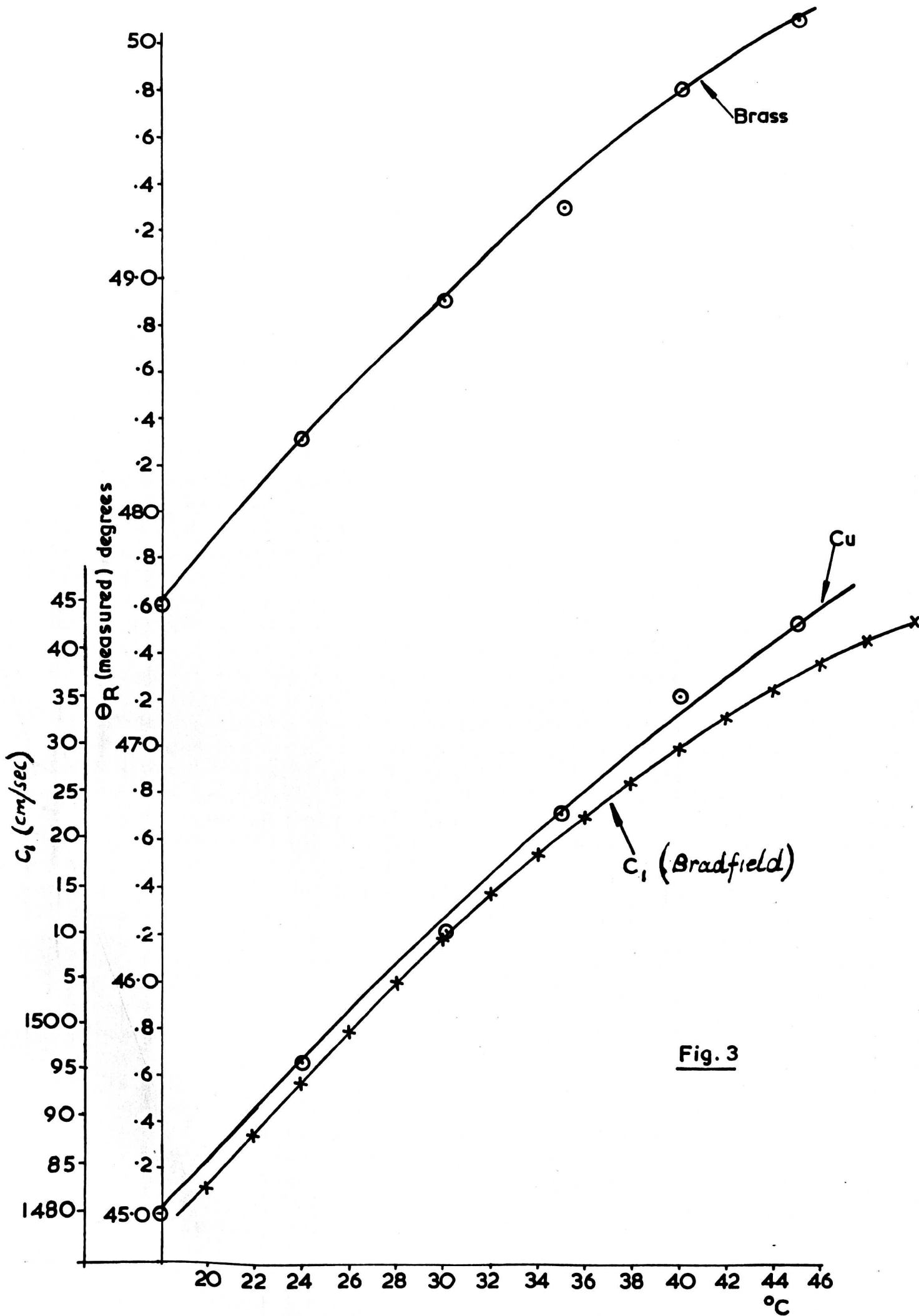


Fig. 3

CHAPTER 10

REFERENCES

1. Crecraft D.I., PhD thesis, Birmingham University, 1964.
2. Clark D.S. and W.R. Varney., Physical Mett. for Engineers, D. Van Nostrand 1969, p262.
- 2.1 Egorov N.N., Study of the elastic properties of some surface consolidated layers., Moskva, no.14, 1961, p185 -195.
3. Blitz J., W.G. King and D.C. Rogers., Electrical, Magnetic and Visual methods of testing materials., Butterworth (1969) p50.
4. Vicat L.J., Note sur l'allongement progressif du fil de fer soumis a diverses tensions, Ann. ponts et chausees, Mem. et Doc., 7(1):40 (1834).
5. Weber W., Uber die Elasticitat der Seidenfasen, Ann. Phys. Chem. (Poggendorf) 34(2):247 (1835).
6. Boltzman L., Zur Theorie der elastischen Nachwirkung, Ann. Phys. Chem. (Poggendorf) Ergeb. 7:624 (1878).
7. Tresca H., On the flow of solids with practical applications in forgings., Proc. Inst. Mech. Engrs. p114 (1867).
8. Fairbairn W., On the tensile strength of wrought iron at various temperatures., Brit. Assoc. Adv. Sci. Rept., 1878, p405.
9. Kirkaldy D., Experiments in wrought iron and steel., Glassgow, Scotland., p65 (1862).
10. Le Chatelier A., Les Lois du recuit et leurs consequences au point de vue des proprietes mecaniques des metaux, Compt. rend., 110:705 (1890).
11. Thurston R.H., Materials of construction, 5th ed. John Wiley and Sons, New York (1955).
12. Hopkinson B. and F. Rogers, The elastic properties of steel at high temperatures., Proc. Roy. Soc. (London), A76:419 (1905).

13. Phillips F., The slow stretch of india rubber, glass and metal wire when subjected to a constant pull., *Phil. Mag.*, 9:513(1905).
14. Andrade E.N.da C., The viscous flow of metals and allied phenomena., *Proc. Roy. Soc. (London)*, A84:1(1910).
15. Dickenson J.H.S., Experiments on the flow of steel at a low red heat, with a note on the scaling of heated steels., *J. Iron Steel Inst.*, 106:103(1922).
16. ASTM-ASME Symposium on the effect of temperature upon the properties of metals., *Trans. ASME*, 46:349 (1924).
17. Prandtl L., Ein Gedankenmodell zur Kinetischen theorie der festen Korper, *Z. angew. Math. Mech.*, 8:85 (1928).
18. Becker R., Uber die plastizitat amorpher und kristalliner fester korper., *Physik. Z.*, 26:919 (1925).
19. Orowan E., Zur Kristallplastizitat, *Z. Physik.*, 89:601 (1934).
20. Taylor G., The mechanism of plastic deformation in crystals., *Proc. Roy. Soc. (London)*, 145:362, 388(1934).
21. Carpenter H.C.H., The production of single metallic crystals and some of their properties., *J. Iron Steel Inst.*, 107:175(1923).
22. Andrade E.N.da C., The flow in metals under large constant stresses., *Proc. Roy. Soc. (London)*, A90:329 (1914).
23. Sully A.H., *Metallic creep and creep resistant alloys*, Butterworth 1949, ch.4.
24. Kanter J.J., Interpretation and use of creep results., *J. Am. Soc. Metals*, 24:870(1936).
25. Kennedy A.J., *Processes of creep and fatigue in metals.*, Oliver and Boyd(1962), p148.
26. Dorn J.E., *Creep recovery.*, *Am. Soc. Metals*, (1957) p255.
27. Chaudhuri A., Stress and temperature-dependence of creep in a nickel-base high-temperature alloy., *J. Inst. Metals.*, Vol. 98(1970), p114.
28. Kornilov I.I., A.Ya Shinyaev and O.N. Andreev., The activation energy of

- creep and the mechanism of plastic deformation of titanium alloys.,
Titaniums and its alloys. Publication 10, I.I.Kornilov,ed. p268.
29. Blenkinsopp P.A., and R.E.Goosey., A study of the age hardening reaction in titanium-2 $\frac{1}{2}$ %Cu., Proc. Inter. Conference on titanium., Pergamon Press, (1970)., R.E.Jaffe,ed. p783.
 30. Goosey R.E., The effect of fabrication variables on the properties of age-hardened titanium-2 $\frac{1}{2}$ %Cu., Proc. Inter. Conference on titanium., Pergamon Press(1970), R.E.Jaffe,ed. p901.
 31. Guiner A., X-ray crystallographic technology., A.Higler and Co.(1952).
 32. Barret C.S., A new microscopy and its potentials., AIME tech. publ. (1865).
 33. Ancker B., T.H.Hazlett and E.R.Parker., Relationship between small-angle dislocation boundaries and creep., J.Appl.Phys. 27:333(1956).
 34. Weissman S., Method of the study of lattice inhomogenieties combining x-ray microscopy and diffraction analysis., J.Appl.Phys., 27:389(1956).
 35. Broom T., Lattice defects and the electrical resistivity of metals., Adv. in Phys., 3:26(1954).
 36. Nowick A.S., Internal friction in metals., Prog. in Metal Phys., 4:1 (1953).
 37. Seigel S., Radiation damage as a metallurgical research technique., Am.Soc.Metals(1953), p312.
 38. Johnstone W.G. and J.J.Gilman., Dislocation and the mechanical properties of crystals., John Wiley and Sons (1957).
 39. Heslop J., Creep fracture in Nickel-Chrome base creep-resistant alloys. J.Inst.Metals., Vol.91(1962), p28.
 40. De Rosset W.S. and A.V.Granato., Ultrasonic study of creep in sodium chloride., J.Appl.Phys. Vol.41, no.10., Sept.1970, p4105.
 41. Hikata A., and M.Tutumi., J.Phys.Soc. Japan., 14, 687(1959).
 42. Bullen F.P., A.K.Head and W.A.Wood., Proc.Roy.Soc.(London), A216(1953) 332.

43. Polakowski N.H. and A.Palchoudhuri., Softening of certain cold worked metals under action of fatigue loads., Proc.ASTM., Vol.54(1954), p701.
44. Marsh K.J. and J.A.Mackinnon., Random-loading and block loading fatigue tests on sharply notched mild steel specimens., J.Mech.Eng.Sci., Vol 10(1)1968.
45. Fisher B.F., PhD thesis, Warwick University, 1971.
46. Miner M.A., Cumulative damage in fatigue., J.App.Mech., 12, A159(1945).
47. Palmgren A., V.D.I. ForschHft, 68(1924), 339.
48. Serensen S., Vest Mashinost., N7-8(1944).
49. Swanson S.R., An improved law of cumulative damage in metal fatigue., Rep.Coll.Aeronaut.Cranfield. N0148(1961).
50. Marsh K.J., Cumulative damage under a symmetrical loading program., J.Mech.Eng.Sci., 1965, 7, no2, 138.
51. Corten H.T. and T.J.Dolan., Cumulative fatigue damage., Proc.Int.Conf. Fatigue Metals 1956, 235.(Inst.Mech.Eng.).
52. Henry D.L., A theory of fatigue damage accumulation in steel., Trans. Am.Soc.Mech.Eng.(1955), 77, 913.
53. Richart F.E. and N.M.Newmark., An hypothesis for the determination of cumulative damage in fatigue., Proc.Am.Soc.Test.Mat.(1948) 48, 767.
54. Grover H.J., S.M.Bishop, and L.R.Jackson., Axial loading fatigue test on unnotched specimens., Tech.notes nat. adv. Comm. Aero. Wash.No2324(1951)
55. Rey W.K., Cumulative damage at elevated temperatures., Tech.notes. nat. adv. Comm. Aero. Wash.No4284(1958).
56. Erickson W.H. and C.E.Work., A study of the accumulation damage in steel., Proc. A.S.T.M.(1961) 61, 704.
57. Brook R.H.W. and J.S.C.Parry., Cumulative damage in fatigue a step towards its understanding., J.Mech.Eng.Sci. Vol.11, no3(1969).
58. Lazan B.J. and T.Wu., Damping fatigue and dynamic stress-strain properties of mild steel., Proc.A.S.T.M.(1951), 51, 649.

59. Lazan B.J. and T.Wu., Damping, elasticity, and fatigue properties of temperature resistant materials., Proc. A.S.T.M., (1951), 51, 611.
60. Morrow J.D., Cyclic plastic strain energy and fatigue of metals., A.S.T.M. Spec. Tech. Publ. 378 (1965).
61. Thompson N., C.K. Coogan and J.R. Rider., J. Inst. Metals, 84, 75 (1955).
62. Ueda T. and M. Tanaka., J. Mat. Test. Japan (1953) 2, 354.
63. Nyukhalov V.V, T Ya Gorazdovskii and P.G. Guzenkov., Translated from Defektoskopiya no2, p9, March-April 1970.
64. Rasmussen J.G., Prediction of fatigue using ultrasonic surface waves. N.D.T. March 1962, p103.
65. Rasmussen J.G., Ultrasonic inspection of turbine and compressor rotor blades for cracks and early flaws., N.D.T. May-June (1958) p228.
66. Shagaev Yu P., Laws governing fatigue failures of steel parts as studied by electromagnetic methods., Translated from Defektoskopiya no5, Sept-Oct (1970), p115.
67. Mitchell L.D., PhD thesis, University of Michigan 1965 c/o G. Curtis, NDT Centre, AERE Harwell internal memorandum. Private communication.
68. Mitchell L.D. and J.R. Frederick., Plastic stress and acoustic emission as predictors of fatigue life., Exp. Mechanics. 10(8) Aug 1970 p323.,
69. Macherauch E., X-ray stress analysis., Proc. 2nd SESA Inter. Congress on Experimental Mechanics., Sept-Oct 1965, Washington D.C.
70. Minton C., Inspection of metals with ultrasonic surface waves. NDT 12(4) p13, 1954.
71. Firestone F. and I. Frederick., Refinements in supersonic reflectoscopy., J. Ac. Soc. Am. 18(1) p200, 1954.
72. Vinogradov K.N. and G.K. Ul'yanov., Measurements of the velocity and attenuation of ultrasonic waves on hard materials., Akust. Zh. 5(3) p290, 1959.

73. Shraiber D.S., Flaw detection in metals (collection), Gos.Izd.Oboron. Prom., Moscow(1959) p241.
74. Sokolonskii A.G., Technique for the excitation and reception of surface waves., Author's Certificate no19297(1958).
75. Bommel H. and K.Dransfield., Excitation of hypersonic waves on quartz., Phys.Rev. Vol 117(1960), p1245.
76. deKlerk J., Ultrasonic transducers., Ultrasonic, Jan 1971 p35.
77. Coquin G.A. and H.F.Tiersten., Analysis of the excitation and detection of piezoelectric surface wave in quartz by means of surface electrodes., J.Ac.Soc.Am. Vol41, no4,pt2,1967.
78. Mayer W.G. and G.B.Lamers., Calculation of acoustic surface wave velocity. Ultrasonic. 1967, 5, p167.
79. Artz R.M., E.Salzman and K.Dransfield., Elastic surface waves in quartz at 316 MHz.
80. Voltmer F.W., R.M.White and C.W.Turner., Magnetostrictive generation of elastic surface waves., Appl.Phys.Lett., Vol 15 (1969), p153.
81. Evans D.R., M.F.Lewis and E.Patterson., Sputtered ZnO surface wave transducers., Electronic Lett., 9 Sept.1971, Vol 7 no 18.
82. Bradfield G., Surface wave velocity measurements., Nature, Aug 20, 1966, Vol 211 p480.
83. Daniel M.R. and J.deKlerk., Velocity measurements of elastic surface waves in layered systems of ZnS on Al_2O_3 , App.Phys.Lett., Vol16 no9 1 May 1970, p331.
84. Bagdanov S.V., M.D.Levina and I.B.Yakovkin., Existence of a surface wave in a system comprising a layer and a half space., Sov.Phys.Ac., 15(10)1969.
85. Brekhovskikh L.M., The propagation of surface Rayleigh waves along an uneven surface of an elastic solid., Akust.Zh. 5(3) p282 (1959).
86. Viktorov I. and T.M.Kaekina., The scattering of ultrasonic Rayleigh waves at models of surface defects., Sov.Phys.Ac. Vol 6 p500, 6(4)1960.

87. Sabine P.V.H., Rayleigh wave propagation on a periodically roughened surface., Electronic Lett. 19Mar.1970, Vol 6,no6, p149.
88. Humphreys R.F. and E.A.Ash., Electronic Lett. 1May 1969., Vol 5 no9 p175, Acoustic Bulk-Surface wave transducer.
89. Kao K.C., Approximate solutions of the H-plane right angle corner in overmoded rectangular waveguides operating in the H_{10} mode., Electronic Lett. 1964, 111, p624.
90. Bykov N.S. and Yu G. Shnieder., An experimental investigation of the effect of surface quality on attenuation of surface waves., Sov. Phys. Ac. Vol 6, 6(4)1960, p500.
91. Bradfield G.E., Notes on Applied Sciences. no 30, NPL(1964),p31.
92. Rollins F.R., Ultrasonic examination of liquid-solid boundaries using a right-angle reflector technique., J.Ac.Soc.Am. Vol 44, no2(1968) p431.
93. Lord Rayleigh., On waves propagated along the plane surface of an elastic solid., Proc.Lond.Math.Soc.XVII ,p4, 1885.
94. Lamb G., On the vibration of an elastic sphere., Proc.Lond.Math.Soc. May 1882.
95. Ewing W.M., W.S.Jardetzky and F.Press., Elastic waves in layered media., McGraw-Hill, 1957.
97. Viktorov I.A., Rayleigh and Lamb waves., Plenum Press, New York(1967) p4.
98. Tursanov D.A., Generalized surface waves in cubic crystals., Sov.Phys. Ac., Vol 13, no1, July-Sept 1967.
99. Stoneley R., The propagation of elastic surface waves in a cubic crystal., Proc.Roy.Soc.(London) A232, 447(1955).
100. Lim T.C. and G.W.Farnell., Character of pseudo surface waves on anisotropic crystals., J.Ac.Soc.Am., Vol 45 no4(1969), p845.

101. Love A.E.H., Some problems in geodynamics., Cambridge University Press, London (1911). Also Dover Publications, Inc., New York (1967).
102. Smith H.I., The physics and the Technology of Surface Elastic waves., Int.J.N.D.T. 1970. Vol 2 p31.
103. Synge J.L., Elastic waves in anisotropic media., J.Math.and Phys. 35, 323(1967).
104. Gazis D.C., R.Herman and R.F.Wallis., Surface elastic waves in cubic crystals., Phys.Rev. 119, 533(1960).
105. Büchwald V.T. and A.Davis., Nature 191, 889(1961).
106. Verivkina L.V., L.G.Merkulov and D.A.Tursunov., Surface waves in quartz crystals., Sov.Phys.Ac. Vol. 12, no3, Jan-Mar 1967.
107. Bergmann L., Ultraschall und seine Anwendung in Wissenschaft und Technik, Edwards, Ann Arbor, Mich.
108. Viktorov I.A., Rayleigh and Lamb waves, Plenum Press, New York (1967) p3.
109. Oliner A.A., Microwave network methods for guided elastic waves., IEEE Trans. on Microwave theory and techniques., MTT-17, no 11, Nov 1969, p812.
110. Becker F.L. and L.Richardson., Research Techniques in nondestructive testing., Academic press (1970), p108., R.S.Sharpe, editor.
111. Schoch von A., Seitliche versetzung eines total reflektierten strahls bei ultraschallwellen., Acustica 952 Vol 2 pt 1, p18.
112. Curtis G., Fresh approach to NDT techniques 1971/72., Colloquim, IEE Electronics division, and private communications.
113. Becker F.L., Phase measurements of ultrasonic waves near the critical angle., J.Appl.Phys., 42(1) Jan 1971, p199.
114. Brekhovskikh L.M., Waves in Layered Media., Academic Press, New York (1960), p32 -34.
115. Fitch Jr.C.E., New methods of measuring ultrasonic attenuation., J.Ac.Soc.Am., 40(5), 1966 p989.

116. Dixon N.E., Proc.Sixth Symp. on NDT of Aerospace and Weapons systems components and materials (1967)..,pl6.
117. Hunter D.O., Ultrasonic velocity and critical angle changes in irradiated A302B and A542-B steel, BNWL-998, AEC Research and development report.
118. Rollins F.R., Critical angle reflectivity - A neglected tool for material evaluation., Mat. Eval. Dec.1966, p683.
119. Rollins F.R., Report, Midwest Research Institute,Kansas, Missouri.
120. Bradfield G., The ultrasonic goniometer and its applications., Non destructive Testing, Feb. 1968, pl65.
121. Papadakis E.P., Ultrasonic attenuation and velocity in three transformation products in steel., J.App.Phys. Vol 35, 1964, pl474.
122. Papadakis E.P., Ultrasonic nondestructive testing for the detection of improper heat treatment of steel., Mat.Eval., Vol XXIII, 1965,pl36.
123. Rollins F.R., Ultrasonic reflectivity of single and polycrystalline copper., Int.J.N.D.T.(1969) Vol 1, pl27.
124. Alers G.A. and Y.C.Lim., Calculation of the elastic anisotropy in rolled sheets.,Trans.Metall.Soc. of AIME, 236(482) 1966.
125. Rollins F.R., Evaluation of elastic constants from ultrasonic reflection measurements., Int.J.N.D.T. (1970), Vol 2 p81.
126. Rollins F.R., Ultrasonic reflectivity. Report, Midwest Research Institute, Kansas, Missouri.
127. Bradfield G., Notes on Applied Sciences. no 30 (1964) NPL, pl47.
128. Watson W., A texbook in Physics., Logmans Green and Co.(1907), pl67.
129. McElroy J.T., Focused ultrasonic beams., Int.J.N.D.T.,(1971), Vol 3 p27.
130. Gericke O.R., Determination of the geometry of hidden defects by ultrasonic pulse analysis testing., J.Ac.Soc.Am. Vol 35 no3 , March 1963, p364.

131. Read T.A., Internal friction of single crystals of copper and zinc., Trans.Am.Inst.Min.Metallurg.Engrs., 143 ,(30),1941
132. Mott N.F., Imperfection in Nearly Perfect Crystals., John Wiley and Sons,Inc. New York,(1953) p 173.
133. Eshelby J.D., Proc Roy.Soc. (London), A197, 396, 1949.
134. Koehler J.S., Imperfections in nearly perfect crystals.,John Wiley and Sons,Inc. New York,(1953) p197.
135. Granato A. and R.Lucke., Theory of mechanical damping due to dislocations., J.Appl.Phys., 27, 583 (1956).
136. Nowick A.S., Internal friction in metals., Prog.Metal Phys.,4, 1(1954).
137. Weertman J., Internal friction in metals of single crystals., J. Appl. Phys., 26, 202, (1955).
138. DeWitt G. and J.S.Koehler., Interaction of dislocations with an applied stress in anisotropic crystals., Phys.Rev., 116, 1113(1959).
139. Mahadevan P., PhD Thesis, Lanchester College of Technology, 1969.
140. White C., Private communication.
141. Blenkinsopp P.A., Private communication.
142. Blitz J., Fundamentals of acoustics, 2nd edition, p35, Butterworth.

APPENDIX 1

MANUFACTURING DETAILS OF TRANSDUCER

The material used was PXE 11 (PSN). i.e Potassium Sodium Niobate. Details of this material is given in Mullards Handbook "Piezoelectric ceramics". This material was chosen because of its high frequency constant and low dielectric constant, which means that at any given frequency a transducer made from this material will be thicker than an equivalent transducer made from any other ferroelectric material. Comparable figures are:-

PXE 5 ... Frequency constant (longitudinal mode) = 1390m/sec.

PXE 11 .. Frequency constant (longitudinal mode) = 2500m/sec.

Therefore at 1 MHz say, the respective thicknesses (t) of transducers made from these materials will be:-

$$\text{PXE 5 ... } t = \frac{1390\text{m/sec}}{1\text{MHz}} = 1390\mu\text{m}$$

$$\text{PXE 11 .. } t = \frac{2500\text{m/sec}}{1\text{MHz}} = 2500\mu\text{m}$$

The material was received in block form from Mullards Ltd. This was then sliced by the author on a diamond saw, then an ultrasonic drill was used to cut them into discs. For slicing the material was mounted on substrate wax and for drilling the sliced pieces were placed flat on a brass plate and surrounded by adhesive.

Thin films of copper were deposited on both sides of the discs. To prevent the sides from becoming coated a jig with thimbles was

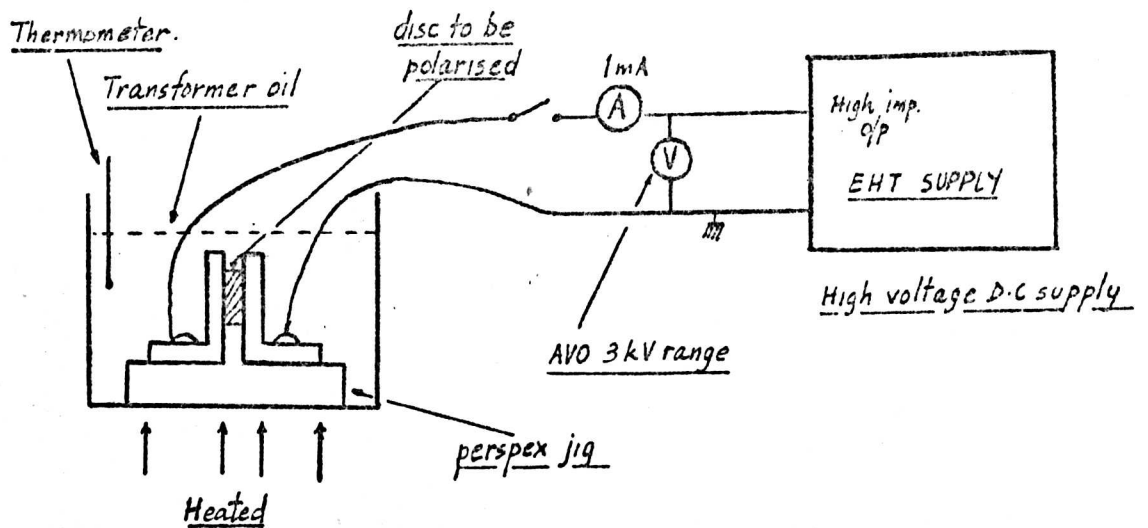


Fig A1.1 Set-up used for crystal polarization

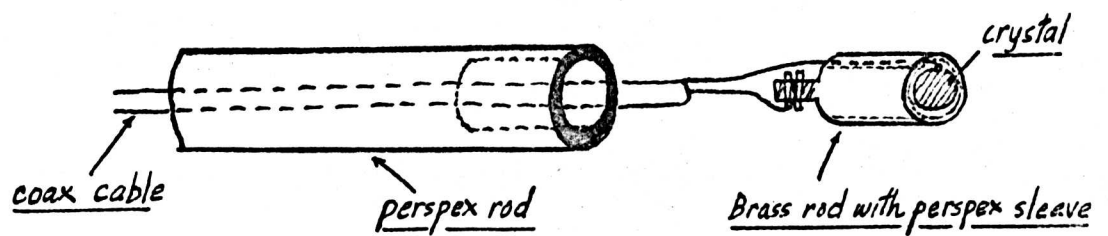


Fig A1.2 Exploded view of transducer

designed to cover the sides of the discs. The coating was done in a vacuum unit, and to get the copper to adhere to the surface a thin coat of nichrome was deposited before depositing the copper.

Polarising the discs.

The polarising of the discs was done with the discs immersed in transformer oil (Silicone oil was recommended.) The discs were placed between two brass plates of a jig and the assembly immersed in the oil. The ~~system~~ used can be seen in Fig. A1.1.

For this material the polarising voltage is 2 to 3 volts, per μm , and depending on the thickness of the discs the open circuit voltage was set up. The oil in the bath was heated to 180°C , then the voltage was switched on for 1 min., then switched off making sure that the current ~~did~~ not exceed $20\mu\text{A}/\text{mm}^2$. The bath (with the discs) was allowed to cool down to 100°C then the discs were taken from the bath. They were then checked for activity on a flaw detector. The thicknesses of the discs were in the range 500 to $800\mu\text{m}$, and the diameter was 10mm.

Thickness-Frequency relationship

As mentioned before the thickness (t) of a crystal made from this material for longitudinal mode vibration is calculated from:-

$$t = \frac{2500\text{m/sec}}{f \text{ MHz}} = 2500\mu\text{m per MHz.}$$

Therefore for a 25 MHz crystal $t = 100\mu\text{m}$.

The discs were then mounted on brass rods using conducting araldite as adhesive and back electrode connecting. A perspex sleeve was then placed over the brass rods so as to facilitate easier machining of the

crystals. The crystals were then machined down to the required thickness on a lathe, at a low speed and cooling continually.

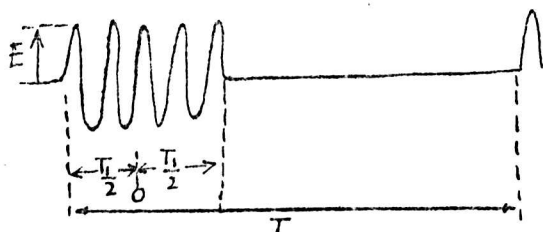
After this a front electrode was deposited as before. The crystal on its brass rod was mounted in a perspex rod and the necessary connections made via coaxial cable. (see Fig. A1.2).

Another type of crystal was found to be equally useful. An X-cut crystal (quartz) coaxially coated so as to facilitate easy connections to the cable was used in the same type of assembly as used above. This transducer (25 MHz) was used also during the course of this work.

The author acknowledges the very helpful and useful information given by Mullards Research Laboratories through Mr. J. S. Wright and Mr. G. Palfreeman.

APPENDIX 2

FREQUENCY COMPONENTS OF A PULSED CONTINUOUS WAVE



Let the continuous wave pulse be on for a duration - $\frac{T_1}{2}$ and $+\frac{T_1}{2}$, and the time repetition of the pulse is T . Then the Fourier integral is of the form:-

$$F(j\omega) = \frac{1}{T} \int_{-\frac{T_1}{2}}^{+\frac{T_1}{2}} f(t) e^{j\omega t} dt \quad \text{where } f(t) = E \sin \omega_0 t \text{ for } -\frac{T_1}{2} \leq t \leq +\frac{T_1}{2}$$

$$= 0 \text{ for } +\frac{T_1}{2} \leq t \leq T$$

$$\begin{aligned} F(j\omega) &= \frac{1}{T} \int_{-\frac{T_1}{2}}^{+\frac{T_1}{2}} E \sin \omega_0 t e^{j\omega t} dt = \frac{E}{2jT} \int_{-\frac{T_1}{2}}^{+\frac{T_1}{2}} (e^{j(\omega+\omega_0)t} - e^{j(\omega-\omega_0)t}) dt \\ &= \frac{E}{2jT} \left[\frac{e^{j(\omega+\omega_0)t}}{j(\omega+\omega_0)} - \frac{e^{j(\omega-\omega_0)t}}{j(\omega-\omega_0)} \right]_{-\frac{T_1}{2}}^{+\frac{T_1}{2}} \\ &= \frac{E}{2jT} \left[\frac{e^{j(\omega+\omega_0)\frac{T_1}{2}}}{j(\omega+\omega_0)} - \frac{e^{j(\omega-\omega_0)\frac{T_1}{2}}}{j(\omega-\omega_0)} \right]_{-\frac{T_1}{2}}^{+\frac{T_1}{2}} \\ &= \frac{E}{jT} \left[\frac{e^{j(\omega+\omega_0)\frac{T_1}{2}}}{2j(\omega+\omega_0)} - \frac{e^{-j(\omega-\omega_0)\frac{T_1}{2}}}{2j(\omega-\omega_0)} \right]_{-\frac{T_1}{2}}^{+\frac{T_1}{2}} \\ &= \frac{E}{T} \left[\frac{1}{j(\omega+\omega_0)} \sin(\omega+\omega_0) \frac{T_1}{2} - \frac{1}{j(\omega-\omega_0)} \sin(\omega-\omega_0) \frac{T_1}{2} \right] \end{aligned}$$

putting $\frac{T_1}{2} = \frac{n\pi}{\omega_0}$ then:-

$$\sin(\omega \pm \omega_0) \frac{T_1}{2} = \cos(n\pi) \sin\left(\frac{\omega}{\omega_0} n\pi\right) \pm \sin(n\pi) \cos\left(\frac{\omega}{\omega_0} n\pi\right)$$

Therefore:-

$$F(j\omega) = \frac{2E}{(\omega^2 - \omega_0^2)} \omega \sin(n\pi) \cos\left(\frac{\omega}{\omega_0} n\pi\right) - \omega_0 \cos(n\pi) \sin\left(\frac{\omega}{\omega_0} n\pi\right)$$

This is the expression which was used to plot the relative amplitudes of the frequency components in the test signal. A fundamental frequency ω_0 of 5 MHz was used, and n the number of cycles in the "on" period in the pulse was varied. A computer was used to tabulate the results for the response.

The bandwidth considered was $0.1\omega_0$ to $2\omega_0$ in steps of 0.1 MHz. Two conditions were considered. i.e.

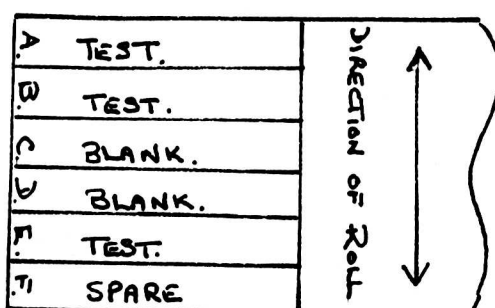
- (a) When there are only two cycles in the pulse, and,
- (b) When there are five cycles only in the pulse.

APPENDIX 3

CREEP TESTING OF C 263 SHEET MATERIAL

Herewith, the results of creep tests carried out on C 263 sheet material, with the object of introducing a known amount of extension into the specimen.

Testpieces were removed from the sheet as indicated in the diagram below.



Cast No. HTS 6193 - 16 SWG.

Test Temperature - 780°C.

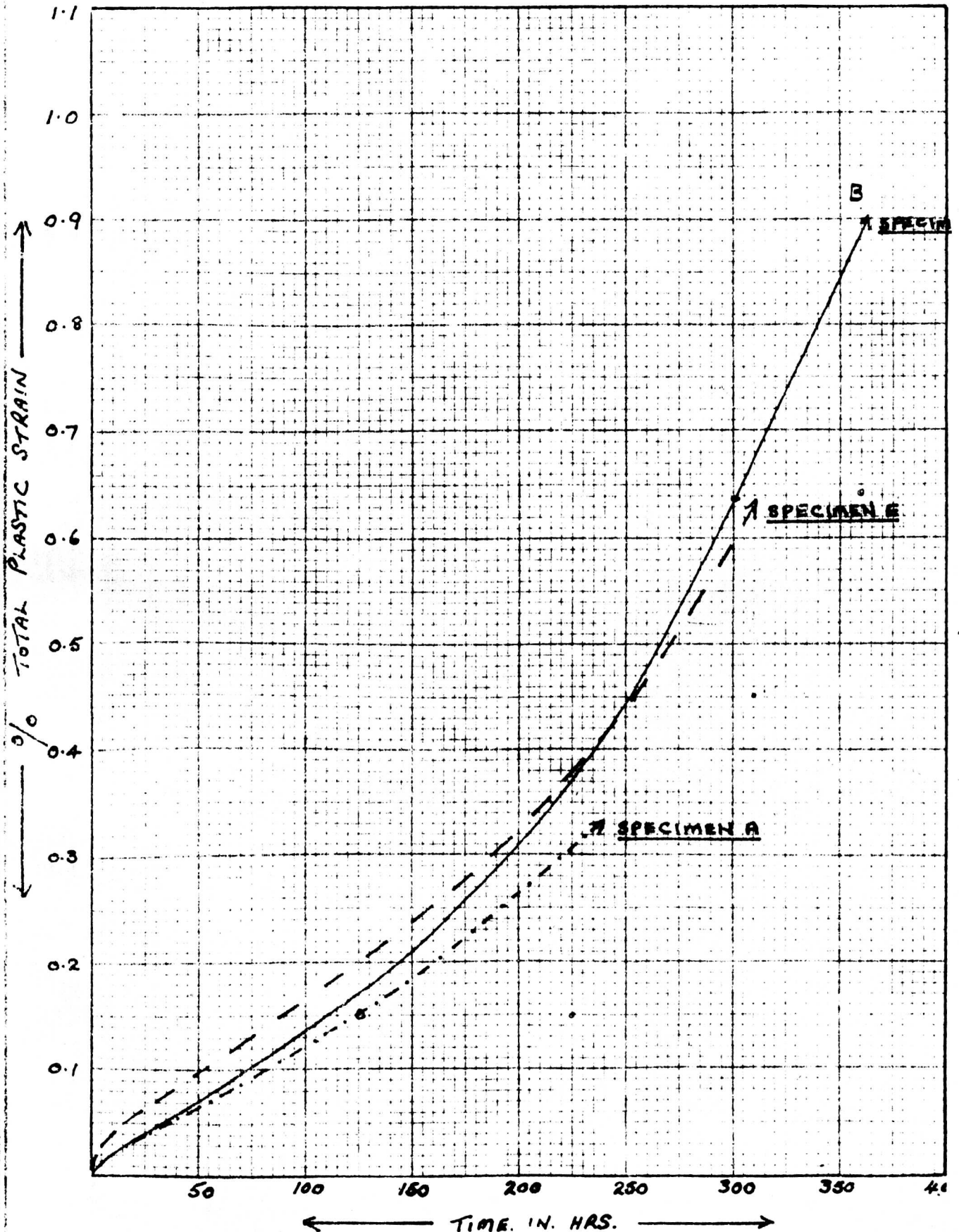
Stress - 170 MN/M².

% Total Plastic Strain in each specimen when removed.

Specimen A 0.33% T.P.S. at 238hrs.

Specimen B 0.898% T.P.S. at 359hrs.

Specimen E 0.63% T.P.S. at 310hrs.

CREEP TESTING OF C263 SHEET MATERIALCAST NO HTS 6193 - 16 SWGTEST TEMPERATURE 780°STRESS 170 MN/m²

2022 2021 2020 2019 2018 2017 2016 2015 2014 2013 2012 2011 2010 2009 2008 2007 2006 2005 2004 2003 2002 2001 2000 1999 1998 1997 1996 1995 1994 1993 1992 1991 1990 1989 1988 1987 1986 1985 1984 1983 1982 1981 1980 1979 1978 1977 1976 1975 1974 1973 1972 1971 1970 1969 1968 1967 1966 1965 1964 1963 1962 1961 1960 1959 1958 1957 1956 1955 1954 1953 1952 1951 1950 1949 1948 1947 1946 1945 1944 1943 1942 1941 1940 1939 1938 1937 1936 1935 1934 1933 1932 1931 1930 1929 1928 1927 1926 1925 1924 1923 1922 1921 1920 1919 1918 1917 1916 1915 1914 1913 1912 1911 1910 1909 1908 1907 1906 1905 1904 1903 1902 1901 1900 1899 1898 1897 1896 1895 1894 1893 1892 1891 1890 1889 1888 1887 1886 1885 1884 1883 1882 1881 1880 1879 1878 1877 1876 1875 1874 1873 1872 1871 1870 1869 1868 1867 1866 1865 1864 1863 1862 1861 1860 1859 1858 1857 1856 1855 1854 1853 1852 1851 1850 1849 1848 1847 1846 1845 1844 1843 1842 1841 1840 1839 1838 1837 1836 1835 1834 1833 1832 1831 1830 1829 1828 1827 1826 1825 1824 1823 1822 1821 1820 1819 1818 1817 1816 1815 1814 1813 1812 1811 1810 1809 1808 1807 1806 1805 1804 1803 1802 1801 1800 1799 1798 1797 1796 1795 1794 1793 1792 1791 1790 1789 1788 1787 1786 1785 1784 1783 1782 1781 1780 1779 1778 1777 1776 1775 1774 1773 1772 1771 1770 1769 1768 1767 1766 1765 1764 1763 1762 1761 1760 1759 1758 1757 1756 1755 1754 1753 1752 1751 1750 1749 1748 1747 1746 1745 1744 1743 1742 1741 1740 1739 1738 1737 1736 1735 1734 1733 1732 1731 1730 1729 1728 1727 1726 1725 1724 1723 1722 1721 1720 1719 1718 1717 1716 1715 1714 1713 1712 1711 1710 1709 1708 1707 1706 1705 1704 1703 1702 1701 1700 1699 1698 1697 1696 1695 1694 1693 1692 1691 1690 1689 1688 1687 1686 1685 1684 1683 1682 1681 1680 1679 1678 1677 1676 1675 1674 1673 1672 1671 1670 1669 1668 1667 1666 1665 1664 1663 1662 1661 1660 1659 1658 1657 1656 1655 1654 1653 1652 1651 1650 1649 1648 1647 1646 1645 1644 1643 1642 1641 1640 1639 1638 1637 1636 1635 1634 1633 1632 1631 1630 1629 1628 1627 1626 1625 1624 1623 1622 1621 1620 1619 1618 1617 1616 1615 1614 1613 1612 1611 1610 1609 1608 1607 1606 1605 1604 1603 1602 1601 1600 1599 1598 1597 1596 1595 1594 1593 1592 1591 1590 1589 1588 1587 1586 1585 1584 1583 1582 1581 1580 1579 1578 1577 1576 1575 1574 1573 1572 1571 1570 1569 1568 1567 1566 1565 1564 1563 1562 1561 1560 1559 1558 1557 1556 1555 1554 1553 1552 1551 1550 1549 1548 1547 1546 1545 1544 1543 1542 1541 1540 1539 1538 1537 1536 1535 1534 1533 1532 1531 1530 1529 1528 1527 1526 1525 1524 1523 1522 1521 1520 1519 1518 1517 1516 1515 1514 1513 1512 1511 1510 1509 1508 1507 1506 1505 1504 1503 1502 1501 1500 1499 1498 1497 1496 1495 1494 1493 1492 1491 1490 1489 1488 1487 1486 1485 1484 1483 1482 1481 1480 1479 1478 1477 1476 1475 1474 1473 1472 1471 1470 1469 1468 1467 1466 1465 1464 1463 1462 1461 1460 1459 1458 1457 1456 1455 1454 1453 1452 1451 1450 1449 1448 1447 1446 1445 1444 1443 1442 1441 1440 1439 1438 1437 1436 1435 1434 1433 1432 1431 1430 1429 1428 1427 1426 1425 1424 1423 1422 1421 1420 1419 1418 1417 1416 1415 1414 1413 1412 1411 1410 1409 1408 1407 1406 1405 1404 1403 1402 1401 1400 1399 1398 1397 1396 1395 1394 1393 1392 1391 1390 1389 1388 1387 1386 1385 1384 1383 1382 1381 1380 1379 1378 1377 1376 1375 1374 1373 1372 1371 1370 1369 1368 1367 1366 1365 1364 1363 1362 1361 1360 1359 1358 1357 1356 1355 1354 1353 1352 1351 1350 1349 1348 1347 1346 1345 1344 1343 1342 1341 1340 1339 1338 1337 1336 1335 1334 1333 1332 1331 1330 1329 1328 1327 1326 1325 1324 1323 1322 1321 1320 1319 1318 1317 1316 1315 1314 1313 1312 1311 1310 1309 1308 1307 1306 1305 1304 1303 1302 1301 1300 1299 1298 1297 1296 1295 1294 1293 1292 1291 1290 1289 1288 1287 1286 1285 1284 1283 1282 1281 1280 1279 1278 1277 1276 1275 1274 1273 1272 1271 1270 1269 1268 1267 1266 1265 1264 1263 1262 1261 1260 1259 1258 1257 1256 1255 1254 1253 1252 1251 1250 1249 1248 1247 1246 1245 1244 1243 1242 1241 1240 1239 1238 1237 1236 1235 1234 1233 1232 1231 1230 1229 1228 1227 1226 1225 1224 1223 1222 1221 1220 1219 1218 1217 1216 1215 1214 1213 1212 1211 1210 1209 1208 1207 1206 1205 1204

**DO NOT SCALE DRAWING
IF IN DOUBT—ASK**

[illegible]

THREADED. TO DRIVE SPECIMEN
HOLDER M-16

57

SLIDE
FIT IN
HOLES IN SPECIMEN HOLDER

SHAFT

12.7

30.0

32.5

⑤

K. NURLED

1-OFF STAINLESS STEEL

CONTROL KNOB (OFF) (ALUMINIUM)

NOTE: This drawing is a private and confidential communication and the property of the University of Warwick. It must not be copied or loaned without the written consent of the University and must be returned immediately on completion of tender or contract.

ALL DIMENSIONS IN MILLIMETERS UNLESS OTHERWISE STATED

MACHINE SYMBOLS MARKED THUS:-

- ✓ MACHINE
- ✗ ROUGH MACHINE
- ✓ SMOOTH MACHINE
- ✗ GROUND FINISH

| SIZE mm | TOLERANCE mm |
|--------------------|--------------|
| UP TO 75 | ± 0.2 |
| OVER 75 UP TO 300 | ± 0.3 |
| OVER 300 UP TO 600 | ± 0.4 |
| OVER 600 | ± 0.6 |

Scale: _____

| | |
|-------------|----------|
| Project No. | ESW/1389 |
|-------------|----------|

| | |
|----------|----------|
| Cost No. | Drawn By |
|----------|----------|

Traced By

Checked By:

Approved E

Date Drawn _____

| | |
|---------------|-----------|
| No. Of Sheets | Sheet No. |
|---------------|-----------|

UNIVERSITY OF WARWICK

TITLE OF DRAWING:

TITLE OF PROJECT:

DEPARTMENT:

Project No.

Cost No.

Drawn By _____
Traced By _____

Checked By _____

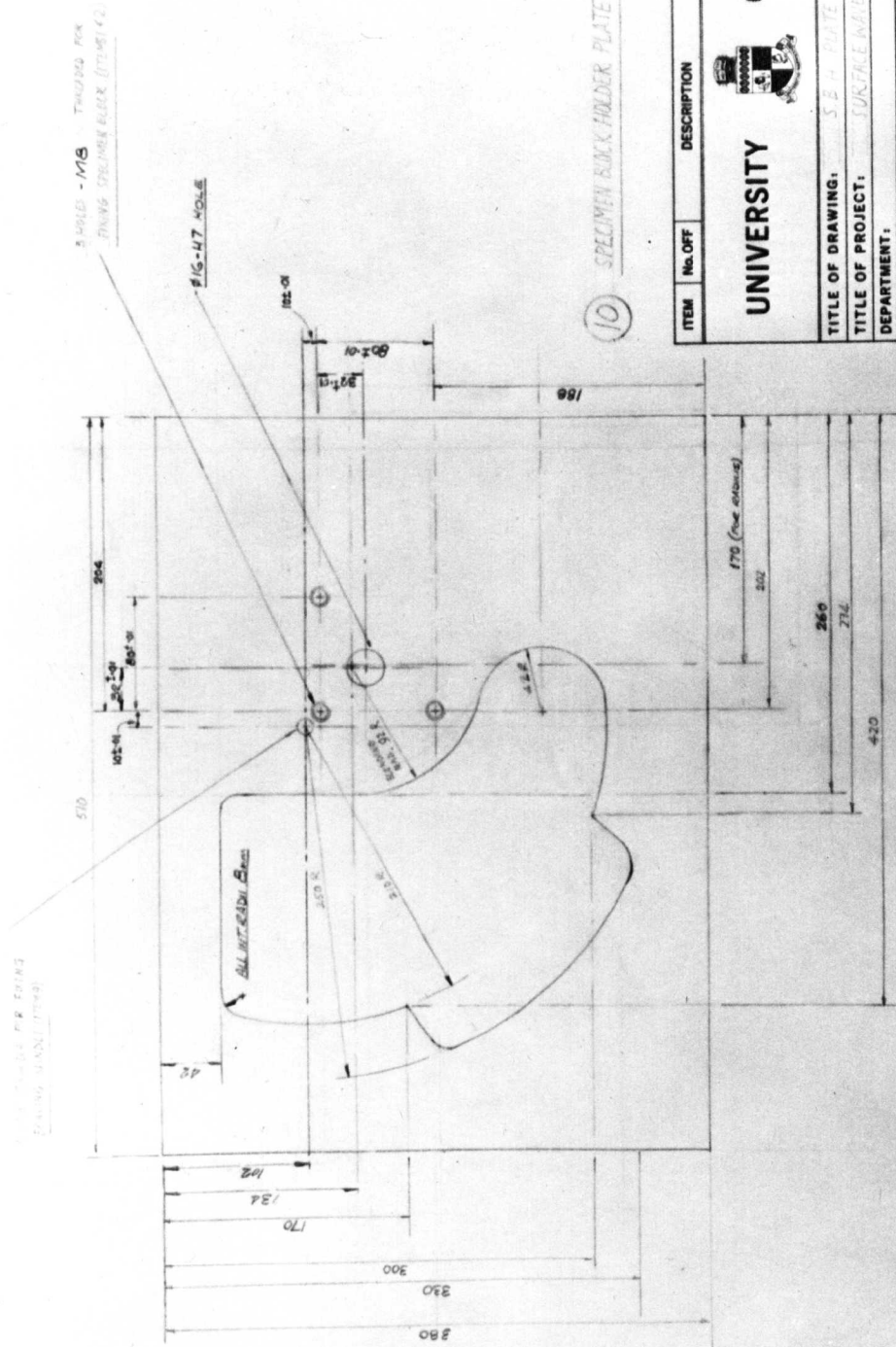
Approved E

Date Drawn _____

| | |
|---------------|-----------|
| No. Of Sheets | Sheet No. |
|---------------|-----------|

DO NOT SCALE DRAWING
IF IN DOUBT-ASK

| REVISIONS | |
|-----------|--|
| | |

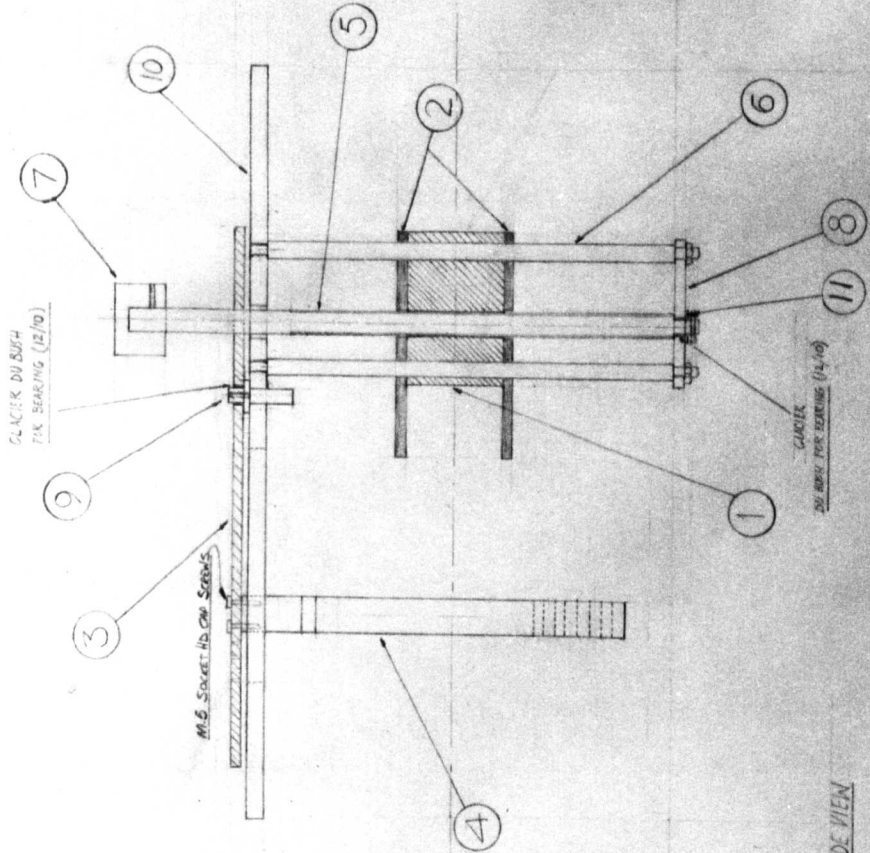


| | | | | |
|---------------------------------------|---------|-------------|----------|---------|
| ITEM | No. OFF | DESCRIPTION | MATERIAL | REMARKS |
| UNIVERSITY OF WARWICK | | | | |
| TITLE OF DRAWING: 5 B H PLATE | | | | |
| TITLE OF PROJECT: SURFACE WAVE | | | | |
| DEPARTMENT: ESW/389 | | | | |
| Scale: HALF FULL SIZE | | | | |
| ES2/243 | | | | |
| Project No. ESW/389 | | | | |
| Cost No. W R E | | | | |
| Drawn By W R E | | | | |
| Tread By W R E | | | | |
| Checked By W R E | | | | |
| Approved By W R E | | | | |
| Date Drawn 10-1-70 | | | | |
| No. Of Sheets 5 | | | | |
| Sheet No. 5 | | | | |


| | | | | | | | | | | | | |
|---|---|---|---|---|---|---|---|---|----|----|----|----|
| 1 | 2 | 3 | 4 | 5 | 6 | 7 | 8 | 9 | 10 | 11 | 12 | 13 |
|---|---|---|---|---|---|---|---|---|----|----|----|----|

DO NOT SCALE DRAWING
IF IN DOUBT—ASK

REVISIONS



SIDE VIEW

| ITEM | No. OFF | DESCRIPTION | MATERIAL | REMARKS |
|---|-----------|-------------|-----------|---------|
| UNIVERSITY OF WARWICK | | | | |
|  | | | | |
| TITLE OF DRAWING: ASSEMBLY (SEE SHEETS 1, 2, 3, & 4, 5) | | | | |
| TITLE OF PROJECT: SURFACE WAVES | | | | |
| DEPARTMENT: ENG. SCIENCE | | | | |
| Project No. | ESN/389 | Scale: | HALF SIZE | |
| Cost No. | 841340/20 | Drawn By | H. H.S. | |
| Traced By | | Checked By | D. J. L. | |
| Approved By | | Date Drawn | 12.3.70 | |
| No. Of Sheets 6 Sheet No. 6 | | | | |

ES2/243

NOTE: This drawing is a private and confidential communication and the property of the University of Warwick. It must not be copied or loaned without the written consent of the University and must be returned immediately on completion of tender or contract.

| ALL DIMENSIONS IN MILLIMETERS UNLESS OTHERWISE STATED | | | |
|---|----------------|---|--------|
| MACHINE SYMBOLS MARKED TRUE— | | | |
| ✓ | MACHINE | ALL UNFINISHED DIMENSIONS GIVEN TO BE WITHIN THE FOLLOWING LIMITS | |
| ✓ | ROUGH MACHINE | 0.13 mm | 100 mm |
| ✓ | SMOOTH MACHINE | 0.075 mm | 100 mm |
| ✓ | GROUND FINISH | 0.05 mm | 100 mm |

| | | | | | | | | | | | | |
|---|---|---|---|---|---|---|---|---|----|----|----|----|
| 1 | 2 | 3 | 4 | 5 | 6 | 7 | 8 | 9 | 10 | 11 | 12 | 13 |
|---|---|---|---|---|---|---|---|---|----|----|----|----|

APPENDIX 5

THEORY OF SKIP DISTANCE

Let $V(\theta)$ be the reflection coefficient of a plane wave incident on a reflecting boundary at angle θ . (See Fig.A5.1.). Then:-

$$V(\theta) = (\rho)e^{j\phi(\rho)} \quad \text{where } \rho \text{ and } \phi \text{ are f(p) hence f}(\theta).$$

Upon reflection the wave undergoes a phase change.

Physical meaning of Δ (Brekhovskikh¹¹⁴)

If a plane wave becomes incident upon the boundary of a perfect reflector(see fig.A5.2), the reflection factor will be unity. Then the incident and reflected waves can be written as:-

$$\psi_{\text{inc}} = \phi \exp[j(\alpha x - \gamma z) - j\omega t] \quad \text{and,}$$

$$\psi_{\text{ref}} = \phi \exp[j(\alpha x + \gamma z) - j\omega t]$$

where $\alpha = k \sin \theta$ and $\gamma = k \cos \theta$ which are both attenuation factors for the horizontal and vertical directions respectively.

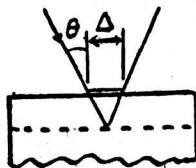


Fig A5.1

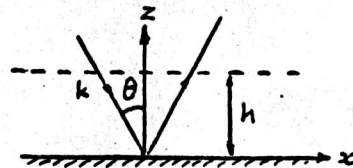


Fig A5.2

At $z = 0$ both waves have the same amplitude and phase. At a plane $z = h$, if we substitute in equations given above, we get:-

$$\frac{\psi_{\text{inc}}}{\psi_{\text{ref}}} = V(\theta) = e^{j2\gamma h} = |\rho| e^{j\phi}$$

This is the therefore the reflection coefficient at $z = h$, where $|V| = 1$, is the modulus and the phase $\phi = 2\gamma h$. is the phase change for the wave as it travels from the plane $z = h$ to $z = 0$ and back.

Generally $\phi = 2\gamma h$ where $\gamma = \sqrt{k^2 - p^2}$ and $p = k \sin \theta$ which is the projection of the wave vector on the x axis.

The skip distance can be written as:-

$$\Delta = - \left(\frac{\partial \phi}{\partial p} \right)_{p \rightarrow \alpha} \dots\dots\dots A5.1$$

This skip distance is the horizontal displacement of the ray, and it follows that the rate of phase change when greatest will give the largest Δ . In the region when the phase changes most rapidly with angle the beam displacement will be the greatest. One of these conditions is when the beam become incident on a boundary between two media, at an angle just beyond the angle of total internal reflection. In this case it is assumed that the velocity in the reflecting media is greater than the wave velocity in the coupling media. This condition is discussed below.

Conditions at critical angle for a liquid-solid interface

For the liquid-solid interface the condition for total internal reflection is when $\sin \theta > \frac{C_w}{C_t}$ where C_w is the velocity of the dilatational wave in water, and C_t is the velocity of the shear wave in the solid. Near this angle beam displacement will occur.

Under these conditions the reflection coefficient can be written as:-

$$V = \frac{Z_1 \cos 2\gamma_l + Z_t \sin 2\gamma_l - Z}{Z \cos 2\gamma_l + Z \sin 2\gamma_l + Z} = V_{\phi}$$

where $Z_1 = \frac{\rho C_1}{\cos \gamma_l}$, $Z_t = \frac{\rho C_t}{\cos \gamma_l}$, $Z = \frac{\rho C_w}{\cos \theta}$ and are the impedances for

the longitudinal and shear waves in the solid respectively, and Z is the impedance for the longitudinal wave in the fluid.

Also γ_c is the critical angle for the shear wave in the solid. By putting $\sin\theta = \frac{c_w}{c_t} \sin\gamma_c$, $s = \sin^2\gamma_c = \left(\frac{c_t}{c_R}\right)^2$, $q = \left(\frac{c_t}{c_l}\right)^2$ and $r = \left(\frac{c_t}{c_w}\right)^2$,

the phase angle can be calculated. It should be noted that since

$c_t > c_R$ then $\sqrt{1-s} = j\sqrt{s-1}$. also from the previous section $p = k\sin\theta$

hence the skip distance can be calculated from:-

$$= -\left(\frac{\partial\phi}{\partial p}\right)_{p \rightarrow \alpha} = -\frac{c_R}{w} \frac{\partial\phi}{\partial(\sin\theta)} = -\frac{\lambda}{2\pi} \left(\frac{\partial\phi}{\partial(\sin\theta)}\right)$$

The result of this analysis is given in equation 3.22.

APPENDIX 6

Suggested Receive Side Circuits

The system diagram Fig.A6.1 is a general system drawing of the transmit side used and a possible receive side. The switching-pulse generator should control the gate so as to pass only the receive echo pulse which will be detected then displayed on a digital voltmeter.

It will be possible then, to increase the accuracy of the measuring system considerably, since the minimum voltage i.e the voltage at the critical angle of incidence will be easily read off.

A possible circuit for the switching-pulse generator can be seen in Fig.A6.2.

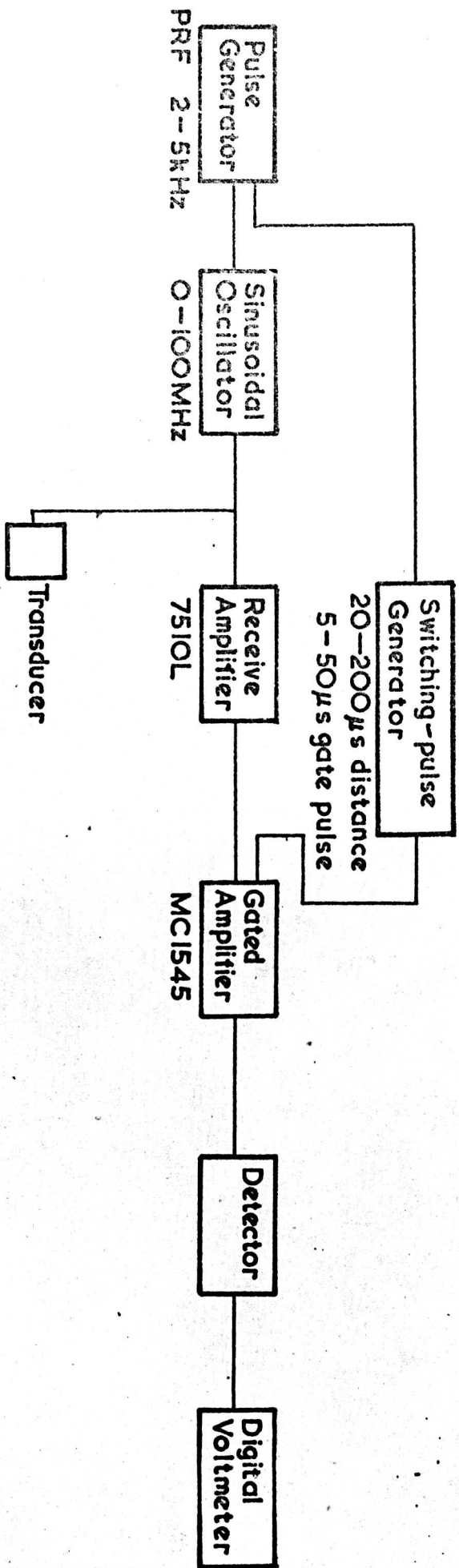


Fig. A6/ Electronic System.

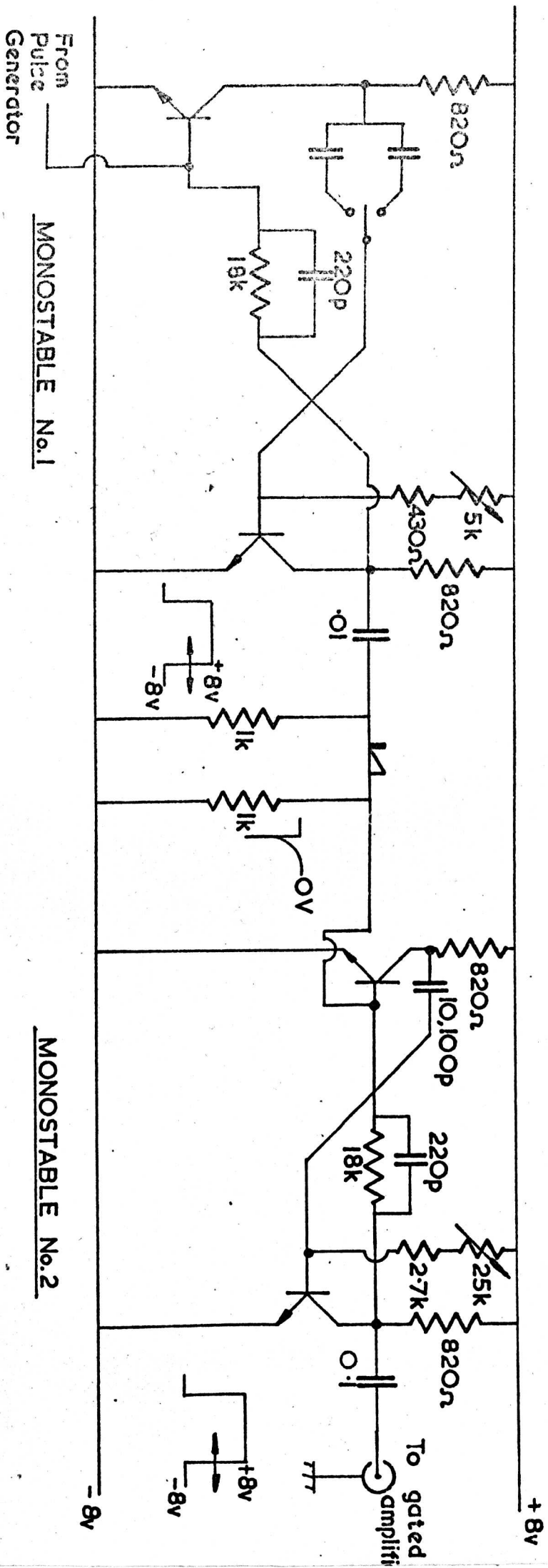


Fig. A6.2 SWITCHING - PULSE GENERATOR (RECEIVE SIDE).

APPENDIX 7

THE GRANATO-LUCKE THEORY OF DISLOCATION

The equation for an oscillating dislocation line can be written as:-

$$A \frac{\partial^2 x}{\partial t^2} + B \frac{\partial x}{\partial t} - C \frac{\partial^2 x}{\partial y^2} = b\sigma \quad (\text{due to Koehler})$$

where A is the effective mass per unit length of the dislocation line, B is the damping per unit length, C is the effective line tension, b is the Burger's vector, and $b\sigma$ is the force exerted on the dislocation line by the external stresses. The displacement x is the lateral displacement of an element of the dislocation line from its equilibrium position at distance y from one end. ($A = \pi \rho b^2$, $C = \frac{2\mu b^2}{\pi(1-\nu)}$ where ν is poisson's ratio)

The Granato-Lucke model for dislocation damping of a plane harmonic wave propagating normal to the dislocation line leads to an expression for the modulus defect which depends upon the frequency of the wave(ω) This expression is :-

$$\frac{\Delta\mu}{\mu} = \frac{\mu N b^2 l^2}{12C} \left[\frac{\left(1 - \frac{\omega^2}{\omega_0^2}\right)}{\left(1 - \frac{\omega^2}{\omega_0^2}\right)^2 + \omega^2 d^2} \right] \dots\dots\dots A7.1$$

Where ω_0 is the resonant frequency of the dislocation line ($\omega_0^2 = \frac{12C}{Al^2}$), l is the length of the dislocation line, and d is $\frac{Bl^2}{C}$. also N is the dislocation density.

Since the shear wave velocity can be written as $V = \sqrt{\frac{\mu}{\rho}}$ where ρ is the density it follows that $\frac{\Delta V}{V_0} = \frac{\Delta\mu}{\mu}$ which is a function of frequency.

Since the resonant frequency f_0 is very high ($\approx 2000\text{MHz}$), $\frac{w^2}{w_0^2}$ will be very small and equation A7.1 becomes:-

$$\frac{\Delta E}{\mu} = \frac{\Delta V}{V_0} = KNl^2 \left(1 - \frac{w^2}{w_0^2}\right) \left[\left(1 - \frac{2w^2}{w_0^2} + \dots\right) + w^2 d^2 \right]^{-1}$$

$$\frac{\Delta V}{V_0} = \frac{V - V(w)}{V_0} \approx KNl^2 \left(1 - \frac{w^2}{w_0^2}\right) \left(1 + w^2 d^2 + \frac{2w^2}{w_0^2}\right)$$

$$\text{therefore } \frac{\Delta V}{V_0} \approx KNl^2 \left[\left(1 + \frac{w^2}{w_0^2} - w^2 d^2\right) \right] \dots\dots\dots \text{A7.2}$$

If we call Ω the "orientation factor" of the dislocation orientation then equation A7.2 can be written as:-

$$\frac{\Delta V}{V_0} \approx K_1 (1 + aw^2) \dots\dots\dots \text{A7.3}$$

where:-

$$K_1 = KNl^2 \Omega = \left(\frac{\mu b^2}{24C}\right) Nl^2 \Omega \text{ and,}$$

$$a = \left(\frac{1}{2} - d^2\right) \text{ a constant for any material.}$$